## REPORT DOCUMENTATION PAGE

READ INSTRUCTIONS BEFORE COMPLETING FORM

| | |
|---|---|
| 1. REPORT NUMBER: AFFDL-TR-75-90 | 2. GOVT ACCESSION NO. |
| 3. RECIPIENT'S CATALOG NUMBER | |
| 4. TITLE (and Subtitle): EXPERIMENTAL AND THEORETICAL CONTROL SURFACE CHARACTERISTICS ON LOW ASPECT RATIO DELTA WING VEHICLES AT SUBSONIC MACH NUMBERS | 5. TYPE OF REPORT & PERIOD COVERED: Final Report May 1973 to February 1975 |
| | 6. PERFORMING ORG. REPORT NUMBER |
| 7. AUTHOR(s): Peter R. Gord | 8. CONTRACT OR GRANT NUMBER(s) |
| 9. PERFORMING ORGANIZATION NAME AND ADDRESS: High Speed Aero Performance Branch (AFFDL/FXG) Air Force Flight Dynamics Laboratory Wright-Patterson Air Force Base, Ohio 45433 | 10. PROGRAM ELEMENT, PROJECT, TASK AREA & WORK UNIT NUMBERS: Project 1366 Task 136601 Work Unit 13660124 |
| 11. CONTROLLING OFFICE NAME AND ADDRESS: Air Force Flight Dynamics Laboratory, Wright-Patterson Air Force Base, Ohio 45433 | 12. REPORT DATE: December 1975 |
| | 13. NUMBER OF PAGES: 146 |
| 14. MONITORING AGENCY NAME & ADDRESS (if different from Controlling Office) | 15. SECURITY CLASS. (of this report): UNCLASSIFIED |
| | 15a. DECLASSIFICATION/DOWNGRADING SCHEDULE |

16. DISTRIBUTION STATEMENT (of this Report)

Approved for public release; distribution unlimited

17. DISTRIBUTION STATEMENT (of the abstract entered in Block 20, if different from Report)

18. SUPPLEMENTARY NOTES

19. KEY WORDS (Continue on reverse side if necessary and identify by block number)

Subsonic Aerodynamic
Control Surfaces
Low-Aspect-Ratio Wings
Vortex Lattice

20. ABSTRACT (Continue on reverse side if necessary and identify by block number)

An experimental study was conducted to determine the characteristics of control surfaces on low aspect ratio delta wings at subsonic Mach numbers. Included were parametric studies on control surface span, chord, and position, all of which were shown to have a significant effect on control surface performance.

Comparisons were made with several low speed theories and it was demonstrated that the vortex lattice theoretical approach provided an effective means

Abstract continued:

of calculating control surface characteristics on both the study models and on several realistic configurations, including the X-24B and two early advanced air defense interceptor concepts.

# FOREWORD

This report was prepared by the High Speed Aero Performance Branch, Aeromechanics Division, Air Force Flight Dynamics Laboratory, Wright-Patterson Air Force Base, Ohio, Peter R. Gord (AFFDL/FXG) Engineer. The work was accomplished under Project Nr. 1366 "Aeroperformance and Aeroheating Technology", Task Nr. 136601 "Aerodynamic Analysis and Evaluation Techniques", Work Unit Nr. 13660124 "Aerodynamics of Control Surfaces on High Speed Advanced Military Flight Vehicles".

The report covers work conducted during the period from May 1973 to Feb 1975. The report was submitted by the author in Feb 1975.

The author wishes to express his appreciation to Mr. Anthony J. Brigalli who assisted in the experimental program and in the data reduction.

TABLE OF CONTENTS

# LIST OF ILLUSTRATIONS

LIST OF ILLUSTRATIONS (CONTD)

LIST OF ILLUSTRATIONS (CONTD)

## LIST OF ILLUSTRATIONS (CONCLUDED)



## LIST OF TABLES

## LIST OF SYMBOLS

| | |
|---|---|
| $b$ | Basic wing maximum span, 12.62 in |
| $C_D$ | Drag coefficient $\left(\frac{\text{Drag}}{q\ S_R}\right)$ |
| $C_L$ | Lift coefficient $\left(\frac{\text{Lift}}{q\ S_R}\right)$ |
| $C_{L_\alpha}$ | Lift curve slope $\frac{\partial C_L}{\partial \alpha}$ |
| $C_M$ | Pitching moment coefficient $\left(\frac{\text{Moment}}{q\ S_R\ C_R}\right)$ |
| $C_{M_\alpha}$ | Slope of $C_M$ vs. $\alpha$ curve $\frac{\partial C_M}{\partial \alpha}$ |
| $C_R$ | Basic wing root chord, 29.92 in |
| $M$ | Mach number |
| $q$ | Free stream dynamic pressure, PSF |
| $R_e$ | Reynolds number |
| $S_R$ | Reference area (basic wing planform area), 188.79 $in^2$ |
| $V_\infty$ | Freestream Velocity, $\frac{\text{Ft}}{\text{Sec}}$ |
| $\alpha$ | Angle of attack, deg, measured with respect to the free stream velocity vector and the basic wing center line. Nose up positive. |
| $\delta$ | Control surface deflection angle, deg, measured with respect to the basic wing center line. Trailing edge down positive. |
| $\Delta C_L$ | Incremental lift coefficient due to control surface deflection, $C_{L_\delta} - C_{L_{\delta=0}}$ |
| $\Delta C_M$ | Incremental pitching moment coefficient due to control surface deflection, $C_{M_\delta} - C_{M_{\delta=0}}$ |

# SECTION I
# INTRODUCTION

Many of the advanced aircraft concepts currently under investigation have aerodynamic shapes with highly swept delta wing planforms. These vehicles, with design speeds in excess of Mach 3, must also have acceptable subsonic performance, including the capability to perform conventional take-offs and landings. The ability to satisy these requirements depends to a high degree on the adequacy of the control surfaces in maintaining trim and stability at widely varying conditions.

Considerable work has been done in previous studies, such as Popinski and Ehrlich (Reference 1) on analytic methods to calculate control surface characteristics at hypersonic speeds. However, at low subsonic speeds most of the work has been of a purely experimental nature.

This study had as its main objectives the generation of a complete set of subsonic control surface parametric data on low aspect ratio delta wings and a comparison with low speed theory. The experimental study included the effects of control surface chord, span, arrangement, and deflection. The theoretical study considered two approaches; one based on a simple engineering solution; and one utilizing a currently available sophisticated low speed theory.

# SECTION II
# FACILITY DESCRIPTION, MOUNTING PROCEDURE, AND TEST CONDITIONS

## 1. FACILITY DESCRIPTION

The Air Force Institute of Technology (AFIT) Five Foot Wind Tunnel is an open return subsonic facility with a circular test section 5 feet in diameter and 18 feet long. Power is supplied by four 400 H.P. D-C electric motors driving counterrotating fan sections. Maximum test section velocities of up to 375 mph have been obtained. However, in practice velocities in excess of 200 mph, corresponding to $R_e/Ft = 1.9 \times 10^6$ and M=0.25, are seldom exceeded. The tunnel turbulence factor has been established at 1.5. A drawing of the facility is presented in Figure 1.

## 2. MOUNTING PROCEDURE

Models can be mounted in the tunnel using either an internal strain-gage balance or an external wire balance system. The wire balance was selected for this test series since its use left the base of the model free for installation of the control surfaces.

The use of wire balance system requires a front mounting bar to attach to the forward lift and drag lines, and a rear bracket to attach to the rear lift line (Figure 2). Model pitch is controlled by displacing the rear lift line, with rotation about the front mounting bar.

The aerodynamic forces experienced by the model are transferred through the lift and drag lines to a system of external scales, where they are recorded. Tare measurements for the wire and mounting bar drag are subtracted, with final data reduction accomplished using a CDC 6600 computer system.

## 3 TEST CONDITIONS

Test conditions included a free stream dynamic pressure (q) of 40 PSF, with a Reynolds number based on model length of $2.9 \times 10^6$. The free stream velocity, $V_\infty$ , was approximately 183 Ft/Sec, corresponding to a free stream Mach number of 0.16.

# SECTION III
# MODEL DESCRIPTION

A drawing of the basic wing model (wing $W_1$ of Reference 2) used as a baseline configuration for this test series is presented in Figure 3. Constructed of laminated poplar wood, the model featured a conventional delta wing planform with rounded leading edges, a blunt trailing edge, and an overall thickness of 0.685 inches. The leading edges were swept at 78° with a constant leading edge radius of 0.343 inches. Pertinent model dimensions included a planform area ($S_R$) of 188.79 $in^2$, a root chord ($C_R$) and span (b) of 29.92 inches and 12.62 inches, respectively, and an aspect ratio of 0.84.

The basic wing model was designed to accept a series of control surfaces which could be mounted at various positions along the trailing edge. All of these were rectangular in planform with a constant thickness equal to the model thickness and were constructed of laminated mohogany. The leading edges (i.e. at the hinge lines) and the outboard side edges were rounded with a radius of 0.343 inches. All of the control surfaces terminated with a blunt trailing edge. Mounting brackets were available for deflection angles of 10°, 0°, -10°, and -20°, with the conventional - trailing edge down for positive deflection - sign convention used (Figure 3). Pertinent control surface dimensions, expressed in percentages of the basic wing span, chord, and area, are presented in Table I.

Two types of control surfaces were available for testing, single flap systems (Figures 4 and 5), and dual flap systems (Figure 6). The single flap systems were further subdivided into continuous span systems and separated span systems. The continuous span systems featured a one piece flap with spans ranging from 50%b to 100%b, while the separated span systems were composed of two elements, both of which were deflected as a single unit. The total spans for these systems ranged from 50%b to 75%b with separation distances of up to 50%b. The dual flap systems consisted of two distinct control surface configurations, either of which could be deflected independent of the other. The inner side edges

of the separated span systems and the interface edges of the dual flap systems were not rounded, but were instead simple cuts normal to the upper and lower surfaces of the flap. Photographs of several typical model configurations are presented in Figure 7.

The model identification scheme used was based on the type of control surface and the parameters involved (See Table I), examples of which are as follows:

Configuration S/50/10/50

S/ - denotes a single flap system
50/ - total span of all elements of the system, in % b
10/ - chord, in % $C_R$
50 - separation distance between elements of the system, in % b

Configuration D/50/50/10

D/ - denotes dual flap system
50/ - total span of all elements of the outboard system, in % b
50/ - span of the inboard system, in % b
10/ - chord, in % $C_R$

On all of the dual flap systems, the separation between the elements of the outboard flap system was equal to the span of the inboard flap system, with the total span of both systems equal to 100%b.

# SECTION IV
# EXPERIMENTAL RESULTS

The data obtained during the parametric studies conducted during this test series are presented in Figures 8 to 26. The force and moment coefficients are referenced to the basic wing area and length

$$S_R = 188.79 \text{ IN}^2$$

$$C_R = 29.92 \text{ in,}$$

with the moment reference center located at 50% $C_R$. Standard wing tunnel corrections for model blockage as developed in Reference 3 were applied to the data. In all cases the control surface hinge lines were sealed to preclude air passage.

## 1. DATA REPEATABILITY

Several repeat runs were made throughout the experimental program using the basic wing model with all control surfaces removed. The results of four such runs are presented in Figure 8, and in general the data repeatability was very good.

## 2. EFFECTS OF CONTROL SURFACE DEFLECTION ANGLE

All of the data for the individual control surface configurations as functions of angle of attack ($\alpha$), with deflection angle ($\delta$) as a parameter, are presented in Figures 9 to 19. For the cases where a dual flap system was concerned, one system was varied through the standard deflection sequence while the other was held constant at $\delta = 0°$.

Most of the data presented in these figures are self explanatory, hence no detailed discussion is included. However, several generalized observations can be made. With regards to the lift and pitching moment coefficients, the control surface effects appear to be a nearly linear function of deflection angle. The effects of angle of attack were not so well defined with no consistent trend applicable to all of the data. For most of the configurations the minimum value of control authority (defined as the absolute value of the incremental lift coefficient ($\Delta C_L$) and incremental pitching moment coefficient ($\Delta C_M$) produced by the control

surface at a given deflection angle) occurred at or very near $\alpha = 0°$, and tended to increase as the angle of attack diverged from 0°. The effects of control surface deflection on the drag coefficient were more complex, due in part to (1) changes in the angle of zero lift with subsequent changes in the induced drag which are nonlinear with lift and (2) variations in the base area (and base drag) which can be presumed to change with deflection angle. This latter effect is supported by the fact that the minimum drag observed for each of the configurations tested occurred when the control surfaces were not deflected.

## 3. RESULTS OF CONTROL SURFACE PARAMETRIC STUDIES

Figures 20 to 26 present a series of summary comparison plots showing some of the results obtained from the parametric studies conducted during this test series. For simplicity, data are shown only for deflection angles of 0° and -20°. Included are figures showing the effects of changes in chord at constant span, changes in span at constant chord, the effects of separation distance on a single flap system, the effects of a fixed center flap on a separated flap system, and an investigation of a dual flap system.

### a. Control Surface Chord and Span Effects

Figure 20 presents data showing the effects of increasing the control surface chord at constant span. The chord was increased from 5% $C_R$ to 15% $C_R$ in increments of 5% $C_R$, resulting in control surface planform areas of from 10% $S_R$ to 30% $S_R$. The span was held constant at 100%b.

For the undeflected flap configuration, the increased area of the larger flap systems produced small increases in $C_{L_\alpha}$ at high angles of attack, with corresponding increases in drag coefficient ($C_D$) and the absolute value of $C_{M_\alpha}$. When deflected, the larger flap systems consistently exhibited more control authority than the smaller systems. However, the efficiency of the larger systems was not in proportion to their area increase. Considering configurations S/100/15/0 and S/100/5/0,

the former had three times the planform area of the latter, but at $\alpha$ =0°, produced a $|\Delta C_L|$ only 1.66 times larger.

Figure 21 presents data from a study on control surface span effects at constant chord. The span was increased in increments of 25%b from 50%b to 100%b, with the chord constant at 10% $C_R$. The resulting control surface planform areas ranged from 10% $S_R$ to 20% $S_R$.

Again the larger flap systems consistently demonstrated more control authority than the smaller systems. In this study, however, the efficiency of the control surfaces was in direct proportion to their area. Considering configurations S/100/10/0 and S/50/10/0, the former had twice the planform area of the latter, and at $\alpha$ =0, produced a $|\Delta C_L|$ 2.26 larger.

The chord and span effects discussed here are in complete agreement with even the most simple theory, and will be discussed in more depth in Section V.

b. Control Surface Separation Gap Effects

The effects of separation distance on single flap systems are presented in Figures 22 and 23. Included are data for configurations with spans of 50%b and 75%b, and control surface planform areas of 10% $S_R$ and 15% $S_R$, respectively. The separation distance between the elements of the systems was varied in increments of 25%b, ranged from 0 to 50%b on the smaller flap systems and from 0 to 25%b on the larger. The chord was constant at 10% $C_R$ for both of the configurations used in this study.

When the control surfaces were undeflected, the effects of separation distance on the longitudinal aerodynamic characteristics were negligible for all of the configurations. When deflected, however, the control authority increased as the separation distance decreased, reaching a maximum for the continuous span systems (i.e. separation distance equal to zero). For example, on the 50%b span configurations at $\alpha$ = 0°, the

$\Delta C_L$'s between the deflected and undeflected cases ranged from -0.0932 for a separation distance of 50%b, to -0.1276 for the continuous span case. This represents an increase in control authority of about 37% achieved with no change in control surface span or area.

c. Effects of a Fixed Center Flap on Separated Flap System

Figures 24 and 25 present data from a study to determine the effects of filling the gap between the elements of a separated single flap system. Two configurations with spans of 50%b and 75%b and separation distances of 50%b and 25%b, respectively, were used. A chord of 10% $C_R$ resulted in control surface planform areas of 10% $S_R$ for the former and 15% $S_R$ for the latter. The separation gap was filled by the addition of an undeflected second flap system, which in effect converted each configuration to a dual flap system. The total control surface planform area with the added flap was increased to 20% $S_R$ for both configurations.

When undeflected the increased planform area produced the same type of results as discussed in Section IV-3a. For the deflected case, however, the addition of the undeflected center flap produced a significant increase in the efficiency of the outer flaps at all angles of attack. For example, when operated as part of a dual flap system (at $\alpha = 0°$), an increase of approximately 20% was noted in the $|\Delta C_L$'s$|$ for both configurations, as compared to the corresponding separated single flap systems.

d. Dual Flap Systems

In this section data are presented showing a comparison of the two flap systems on a dual flap configuration. The projected planform area, span, and chord of both control surfaces were identical at 10% $S_R$, 50%b, and 10% $C_R$, respectively. The outer flap represents a separated single flap system with the gap filled as discussed in Section IV-3c and the inner flap a simple continuous span configuration as described in Section IV-3a. Each flap system was deflected independent of the other.

The data as presented in Figure 26 clearly show the inner flap to be the most effective control surface at all angles of attack. At $\alpha = 0°$, the inner control surface produced a $|\Delta C_L|$ 48% greater than the similarly deflected outer flap.

In Section IV-3c it was noted that by filling in the gap between the elements of a separated flap system, the effectiveness of the control surface was considerably increased. Comparing the control authority of the inner flap of configuration D/50/50/10 with configuration S/50/10/0 shows that a similar effect results from filling in the planform around the flap, in this case by the outer flap. Examining Figures 21 and 26 shows that the identically same control surface when operated as part of a dual flap system produced (at $\alpha = 0°$) a $|\Delta C_L|$ 33% larger than when operated as a single flap system.

# SECTION V
# THEORETICAL ANALYSIS

The theoretical analysis considered only the incremental changes in the lift and pitching moment coefficients ($\Delta C_L$, $\Delta C_M$) due to control surface deflections, and was approached from two viewpoints; one treating the control surface as an isolated wing and the other using a vortex lattice to represent the complete wing-control surface configuration. Both theoretical approaches produced only linear results (i.e. potential flow solutions). The use of a linear theory seemed apropos since most of the incremental effects data exhibited basically linear characteristics with changes in control surface deflection. Because no consistent trend for angle of attack effects was apparent, all of the results were calculated at an angle of attack of zero degrees only. No attempt was made to calculate the effects of control surface deflection on the drag characteristics, since previous experience with lifting body configurations had shown that the effective base area was strongly influenced by the deflection angle. Thus, any drag prediction routine would require an analysis of the base drag, which at subsonic speeds constitutes a considerable problem in itself and is beyond the scope of this report.

## 1. ISOLATED WING APPROACH

This approach utilized the theoretical lift curve slopes for unswept rectangular wings as presented in Reference 4, and treated the control surfaces as an isolated wing with an angle of attack equal to the deflection angle. The calculation procedure involved only four steps: (1) determine the aspect ratio of the control surface based on its area and span, (2) determine the appropriate lift curve slope, (3) calculate the lift based on the control surface deflection, and (4) refer the lift back to the basic wing reference conditions.

The results obtained using this method are presented in Figures 27 and 28 for the control surface chord and span studies, respectively. In general the theory provided reasonably good results, accurately predicting the trends in the data, but slightly underpredicting the magnitude of the experimental results.

Using the isolated wing approach, the reason for the improved control surface efficiency achieved through increasing the span at constant chord (Section IV-3a) becomes apparent. As the span is increased, the control surface aspect ratio increases in direct proportion to the span, which results in not only a larger lifting surface but an improved lift curve slope as well. For the case where the chord is increased while holding the span constant, the control surface aspect ratio decreases inversely proportional to the chord. Thus, even though the area is increased, the lift curve slope based on that area is decreased.

Since reasonable agreement was achieved for the simple shapes tested, an attempt was made to extend the theory to some of the more complicated control configurations. Stone suggested in Reference 5 that if the results where known for full span and partial span inboard flaps, as typically represented by configurations S/100/10/0 and S/50/10/0, respectively, then the principle of superposition could be used to extend the method to separated flap systems. Thus, for example, the control surface lift for configuration S/50/10/50 would be simply the control surface lift for S/100/10/0 - S/50/10/0, etc. Using this approach did not, however, produce the degree of correlation with experiment achieved on the more simple configurations previously discussed. Figure 29 presents data-theory comparison for a parametric study on separated flap systems with span as the parameter. It is evident that although the theory predicted the trends correctly, it considerably overpredicted the magnitude of the experimental results for the separated configurations. Even poorer correlation was experienced for the study on constant span configurations with separation distance as the parameter (Figure 30). For this study the theory did not even predict the correct trends in the data with changes in separation distance. From this analysis it appears that the principle of superposition is not applicable to control surface effects on low aspect ratio delta wing configurations. This limits the usefulness of the isolated wing concept to only the most simple control surface configurations.

## 2. VORTEX LATTICE APPROACH

### a. Program Description

The sophisticated analytic approach utilized the vortex lattice program developed by NASA Langley, which in turn was an extension of the finite step lifting-line method suggested by Glauert (Reference 6) and applied by Campbell (Reference 7). A description of the program, including theory, user's manual, and sample cases, is presented in Reference 8. However, for entirety a brief description is included below.

The vortex lattice program was developed to estimate the linear aerodynamics of complex shapes at subsonic Mach numbers. In the analytic simulation the lifting surface is represented by series of horseshoe vortex systems, hence the name vortex lattice (these vortices should not be confused with the leading edge vortex cores usually associated with low aspect ratio wings at high angles of attack). The basic assumptions are that the flow is attached, incompressible, irrotational, inviscid, and steady. Although thickness effects are ignored, dihedral and camber may be introduced when appropriate. The effects of compressibility are considered through an application of the Prandtl-Glauert similarity rule.

A given planform is divided into a series of elemental panels such that each panel can be replaced by a horseshoe vortex system. The leading filament of the vortex is placed at the quarter-chord of its respective panel and is swept at the quarter-chord sweep angle. The outer filaments begin at the quarter-chord and extend parallel, downstream to infinity (Figure 31). The boundary conditions are met by requiring the inclination of the fluid streamlines to match the angle of attack at the three-quarter-chord point of the panel. After determining the circulation by solution of a matrix equation, the Kutta - Joukowski theorem for lift from a vortex filament is used to determine the lift for each panel. The summation of the individual panel lifts then provides the total lift, pitching moment, etc.

The program has the option of considering one or two separate planforms. For this study it was advantageous to use the two planform option where one planform was used to represent the basic wing surface and the other the control surface. In the analytic representation the trailing edge of the wing planform was coincident with the leading edge of the control surface planform. As shown in Figure 32 for a typical configuration, the elemental panels on the two planforms were arranged in constant span rows such that the vortex filaments from the wing panels trailed over their respective span panels on the control surface. Deflection of the control surface was accomplished by changing the angle of attack of the elemental panels on the control surface planform.

The one planform option could also have been used to represent the complete wing/control surface configuration. This would, however, have had the disadvantage of having some of the elemental panels partially located on both surfaces, which in turn would have considerably complicated the procedure for deflecting the control surface.

b. Application to Study Models

The results obtained using the vortex lattice program applied to the control surface configuration investigated during this study are presented in Figures 33 to 38. At low angles of attack the study models conform closely to the limitations imposed by the theory, and as such represent optimum configurations for evaluating its adequacy. As can be seen in the figures the data-theory correlations were in very good agreement for all of the configurations.

c. Application to Realistic Configurations

The high degree of correlation achieved on the simple shapes tested provided the impetus to extend the evaluation of the vortex lattice approach to realistic configurations. Three typical high speed shapes chosen for data-theory comparisons included the X-24B (Ref. 9) and two early advanced air defense concepts (Ref. 10). Since the theory did not include thickness effects, only those control surfaces preceded by a relatively thin wing section were considered in the

analysis. On the X-24B this included the outboard ailerons as shown in Figure 39. These are used primarily for roll control but can be biased symmetrically for additional pitch authority. The air defense wing-body configuration (Figure 40) had conventional elevons mounted near midspan along the swept trailing edges, while the blended body shape (Figure 41) featured rotating outboard wing tips bounded on the inner body lines by swept vertical tails. The engine nacelles shown on these configurations were removable and could be replaced with smooth fairing blocks. The incremental control surface effects data presented in this report were acquired with the fairing blocks in place.

The results obtained on these configurations are presented in Figures 42 to 44 for several control surface deflections. In all cases the control surfaces were used as elevators with each surface deflected symmetrically in the same direction. As in the previous cases, the data-theory comparisons are presented for $\Delta C_L$ and $\Delta C_M$ at a basic vehicle angle of attack of 0°.

The X-24B calculations were made at a Mach number of 0.60 and for bias angles from 0° to 17°. The theory provided reasonable agreement with the data at the larger deflection angles but tended to overpredict the absolute magnitude of the experimental results, particularly at the lower deflection angles. A possible explanation for the poorer agreement experienced at the lower deflection angles lies in the control surface reference scheme used on the X-24B vehicle. At 0° deflection the ailerons conform to the basic vehicle mold lines, which in effect puts them at a large negative angle of attack (-16°) for a vehicle angle of attack of 0°. Because of this and the complex flow field induced by the body thickness and fin-strake interaction, a distinct possibility exists for incipient flow separation on the leeward surfaces, which is not accounted for by the theory. As the deflection angle is increased, the local angle of attack of the ailerons is decreased until at $\delta$ = 16°, they are aligned with the free stream velocity vector. If this explanation is correct, better agreement would be expected at the larger deflection angles where separation would not be expected to occur, which is the case.

Data for the two air defense configurations were acquired at a nominal Mach number of 0.20 and for deflection angles ranging from -10° to +10°. These slender shapes conform more closely to the limitations imposed by the theory than does the X-24B. As can be seen in Figures 43 and 44, the correlation between data and theory is somewhat better for the air defense shapes.

# SECTION VI
# CONCLUSIONS

The following conclusions are noted:

1. The efficiency of the control surface is strongly influenced by its geometry (aspect ratio).

2. For separated flap systems, control surface efficiency increases as the separation distance decreases, reaching a maximum for continuous span configuration.

3. Control surface efficiency for partial span or separated span systems is enhanced when the control surface is an integral part of the planform, as opposed to simply extending from the planform.

4. The vortex lattice theoretical approach provided good data-theory correlation when applied to the study models.

5. When applied to realistic configurations, the vortex lattice approach provided good data-theory correlation for those configurations conforming to the limitations of the theory.

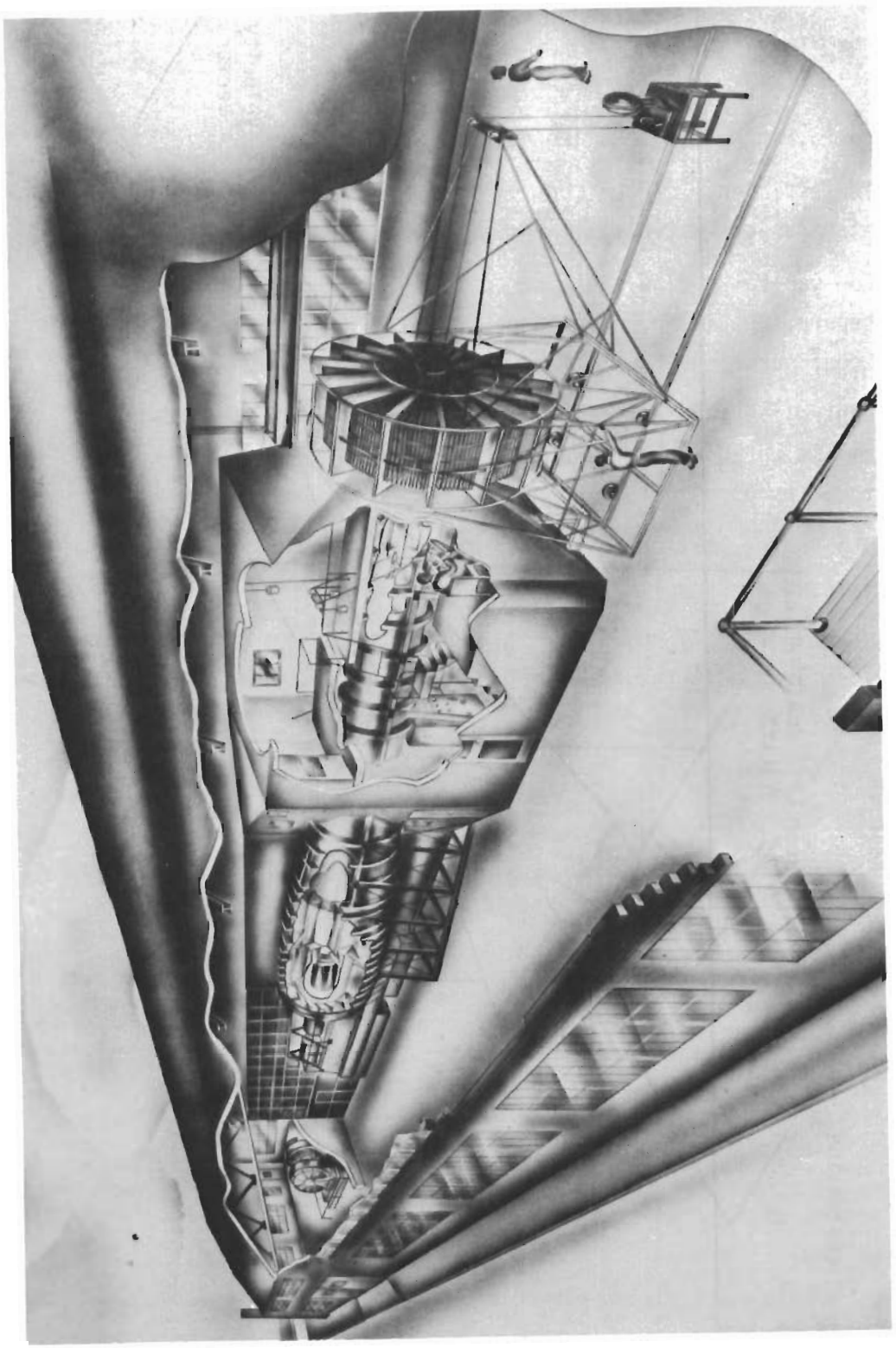

Figure 1. Schematic Drawing of the AFIT 5 Foot Wind Tunnel

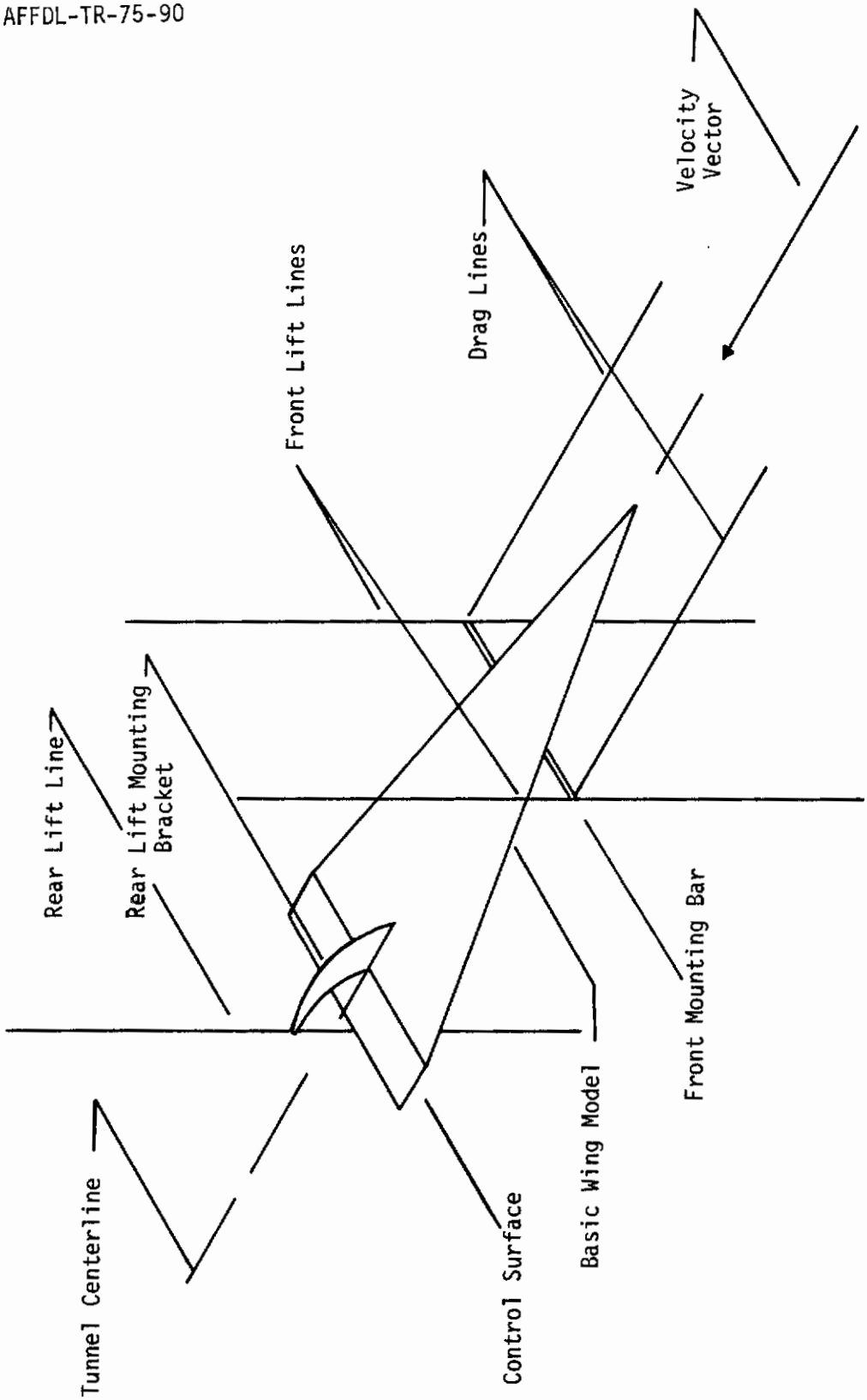


Figure 2. Model Mounting Procedure Using the Wire Balance Assembly

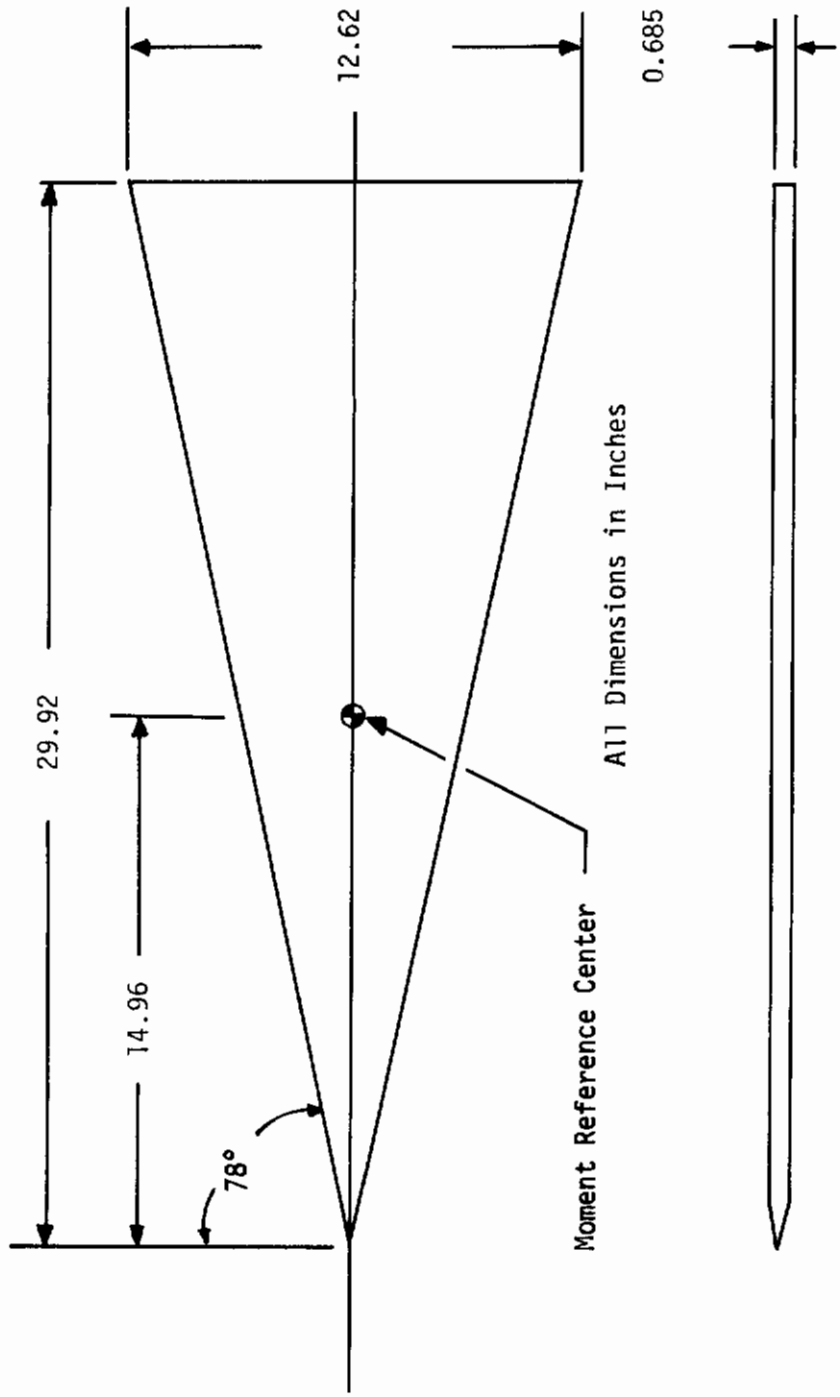


Figure 3. Basic Wing Model Description and Sign Convention

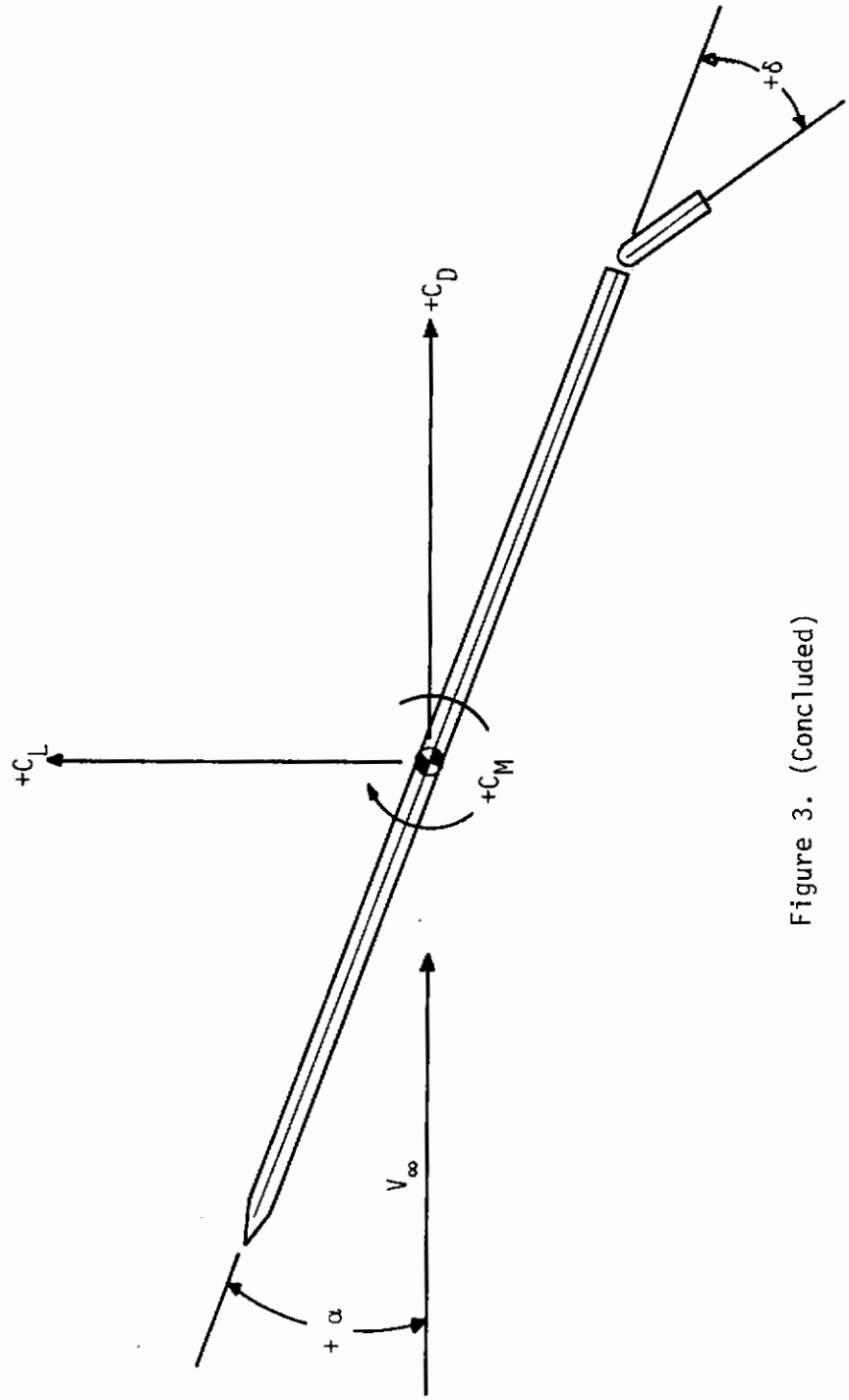


Figure 3. (Concluded)

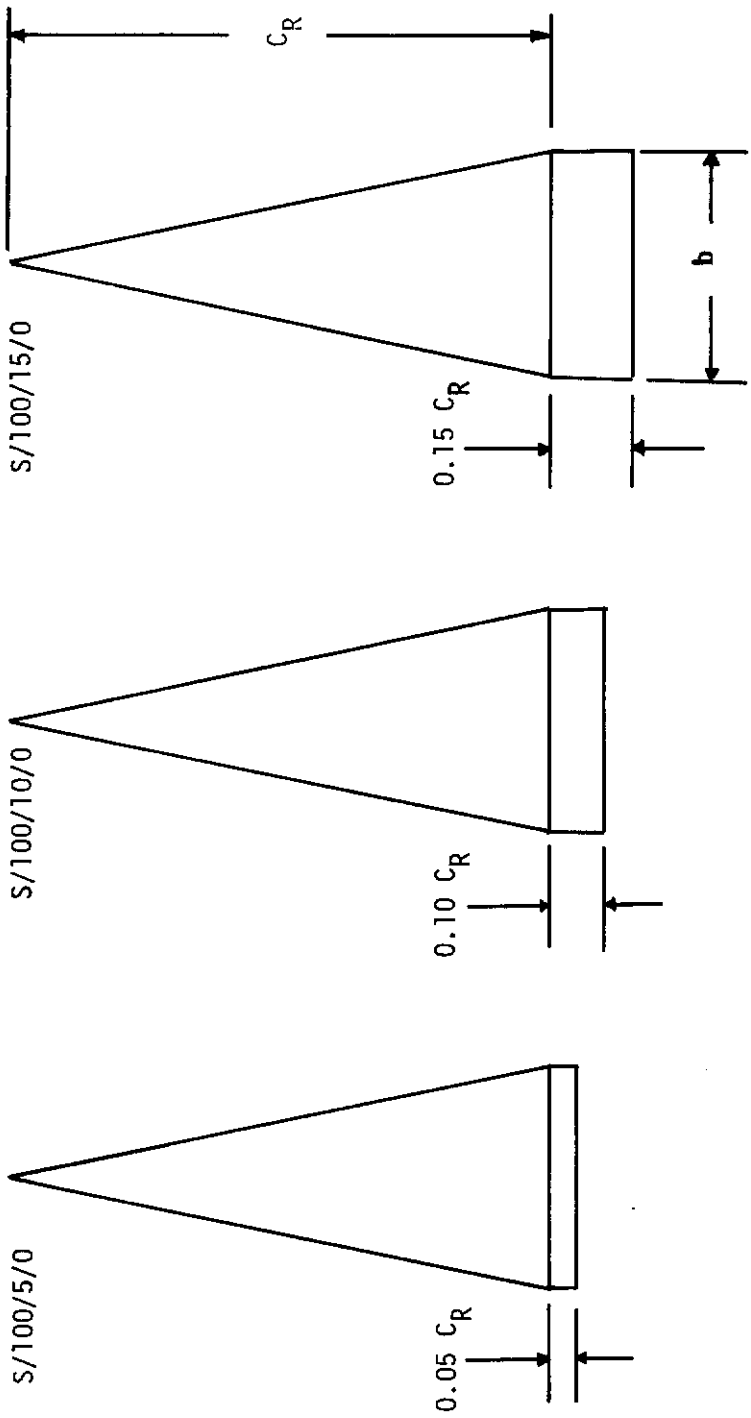


Figure 4. Control Surface Chord Effects Study Models

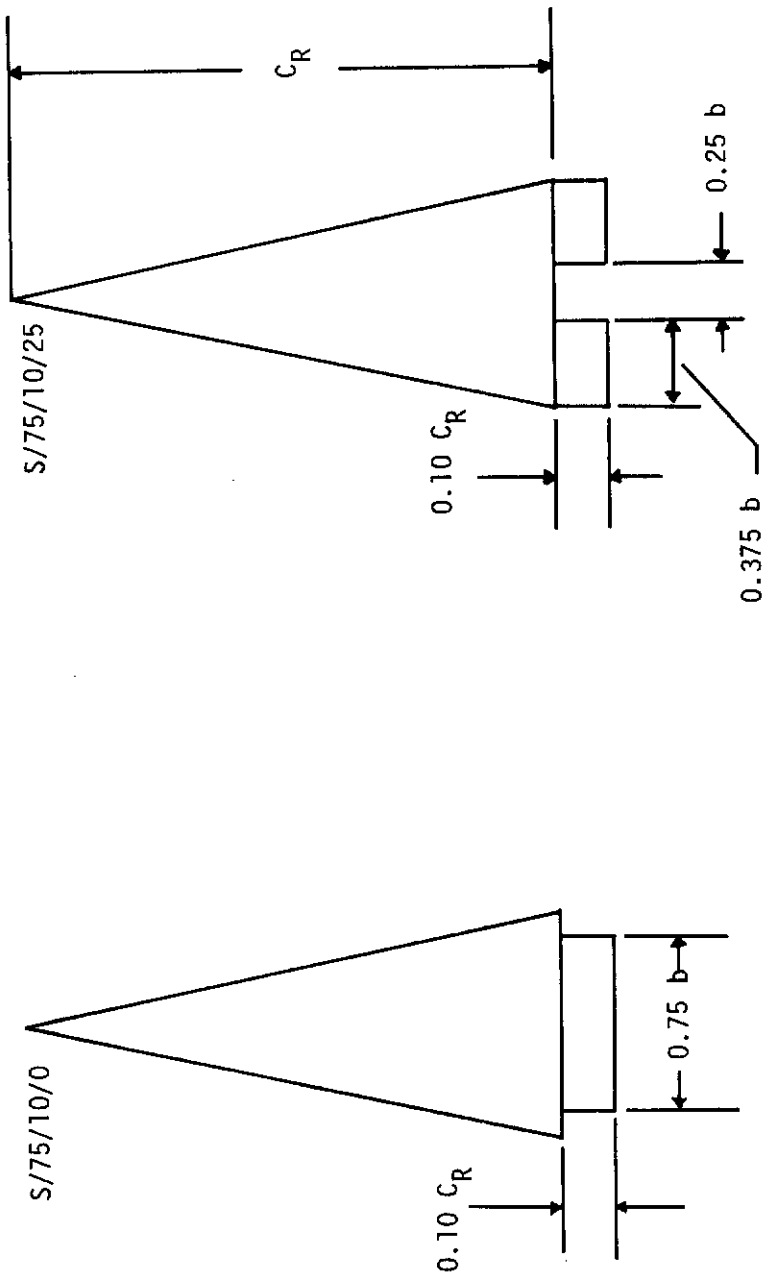


Figure 5. Control Surface Spacing Effects Study Models

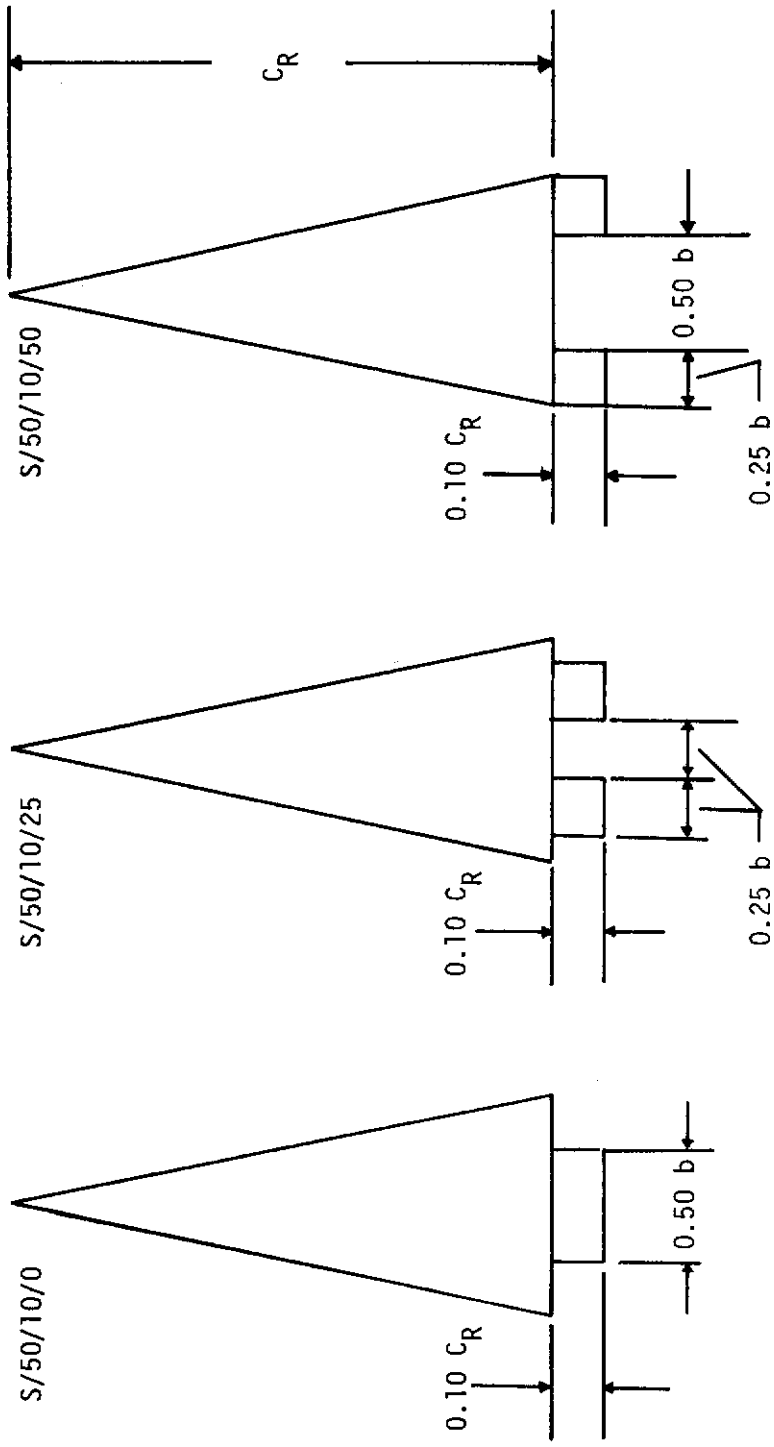


Figure 5. (Concluded)

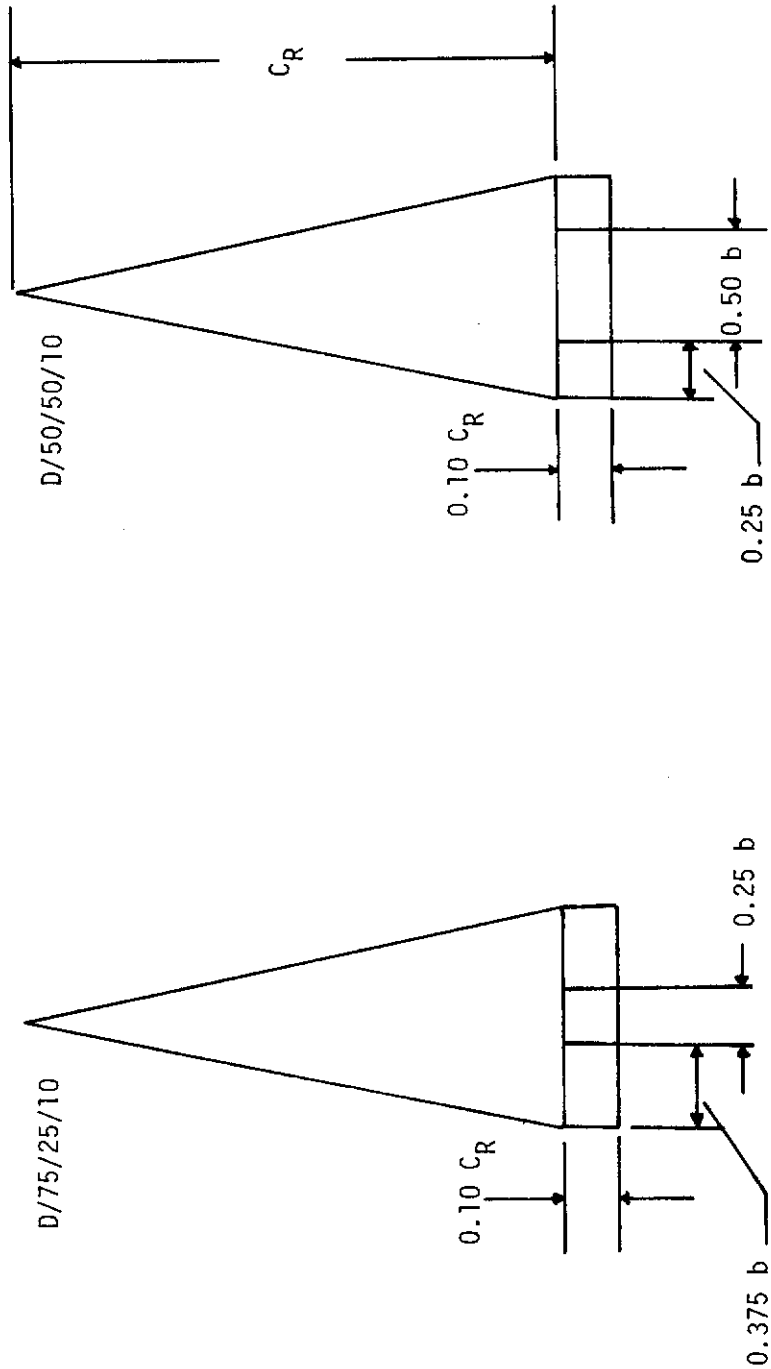


Figure 6. Dual Control Surface Study Models

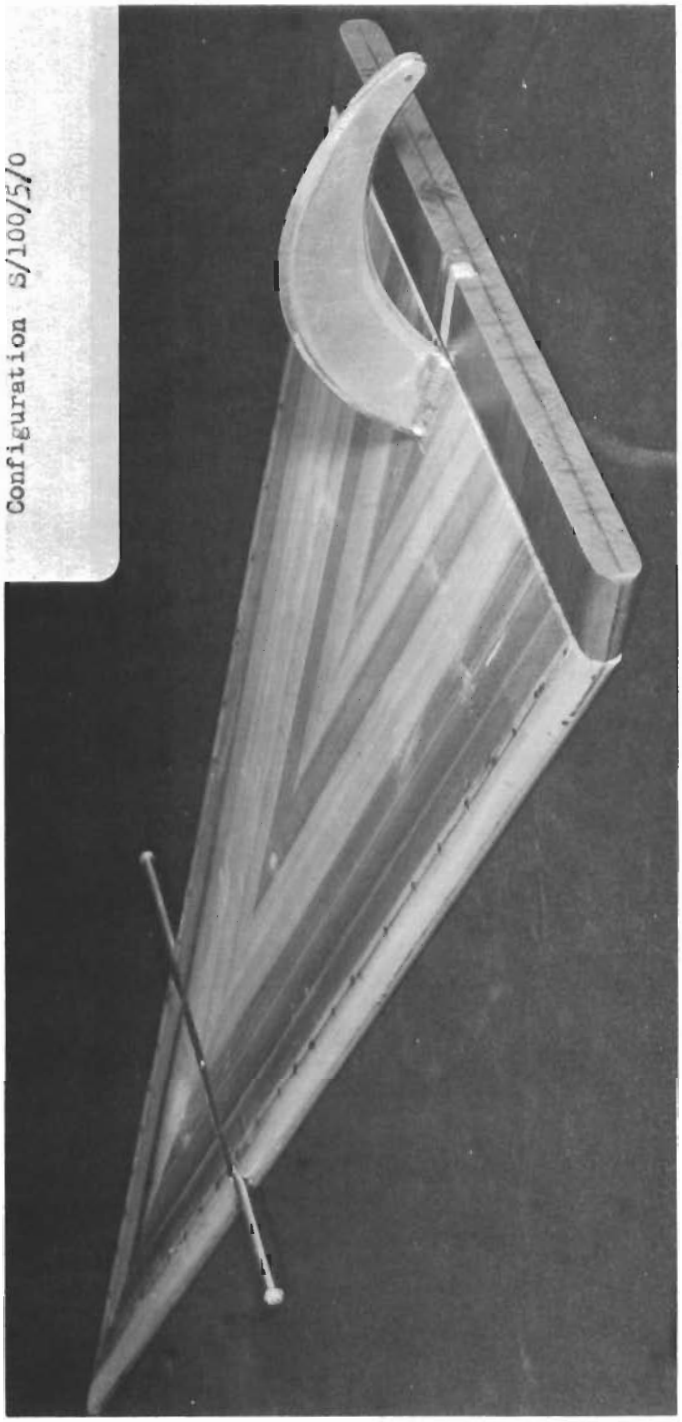


Figure 7. Photographs of Typical Control Surface Configurations

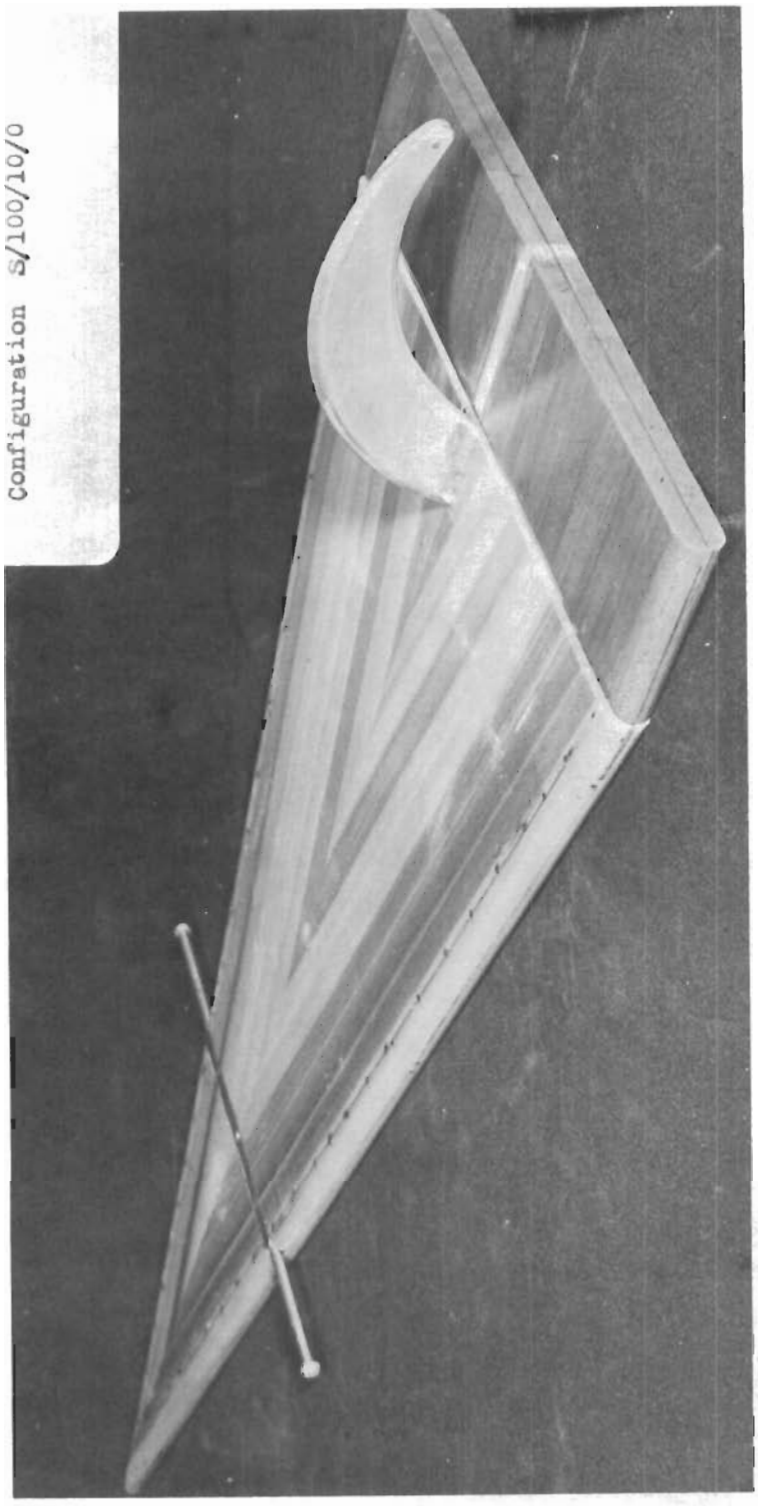


Figure 7. (Continued)

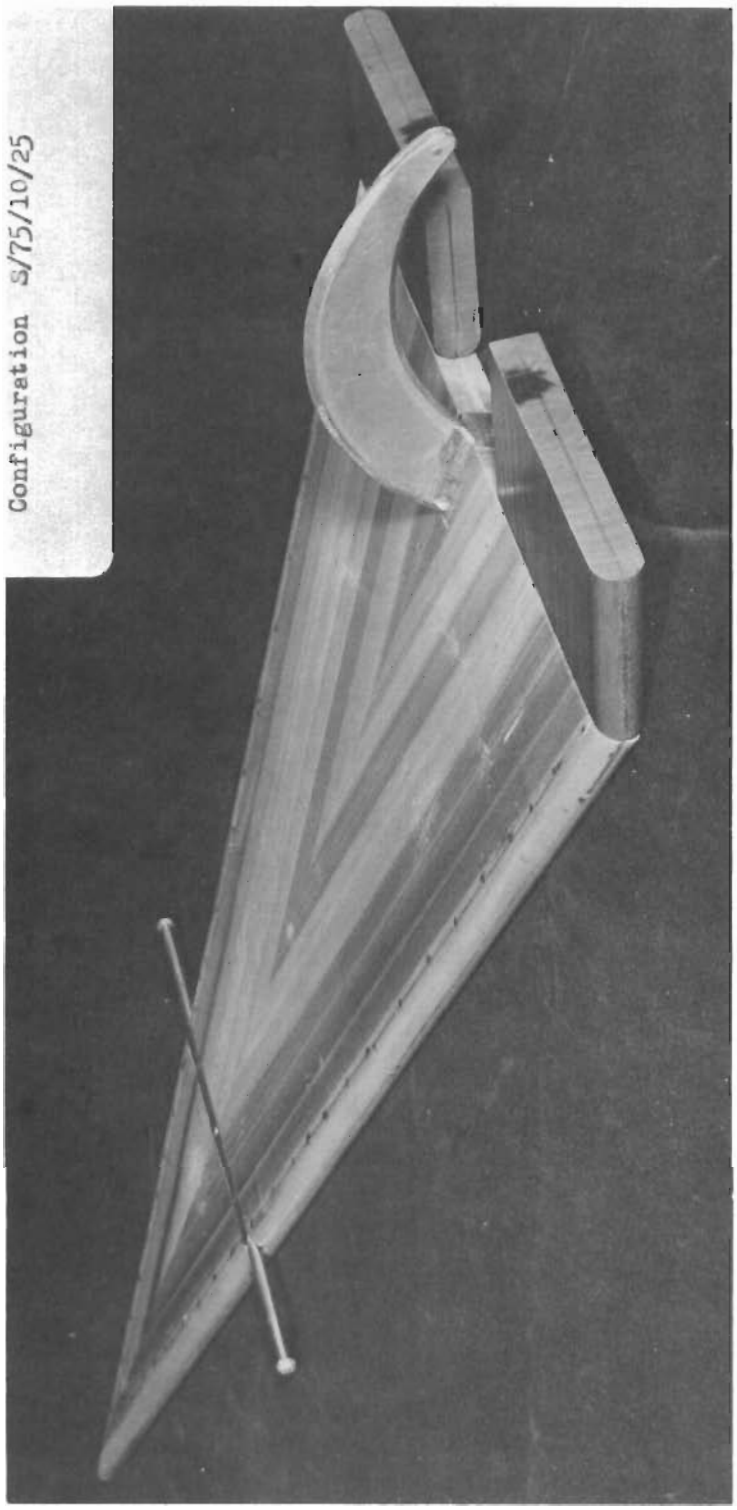


Figure 7. (Continued)

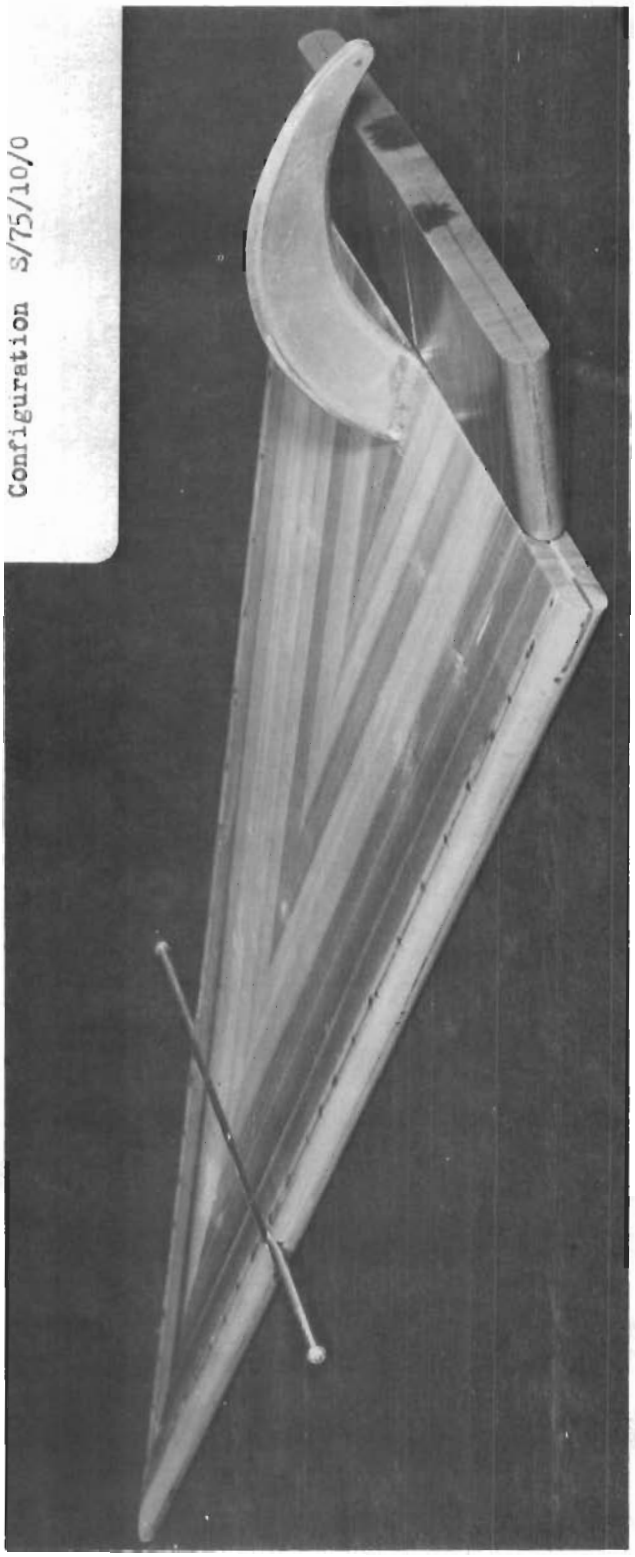


Figure 7. (Continued)

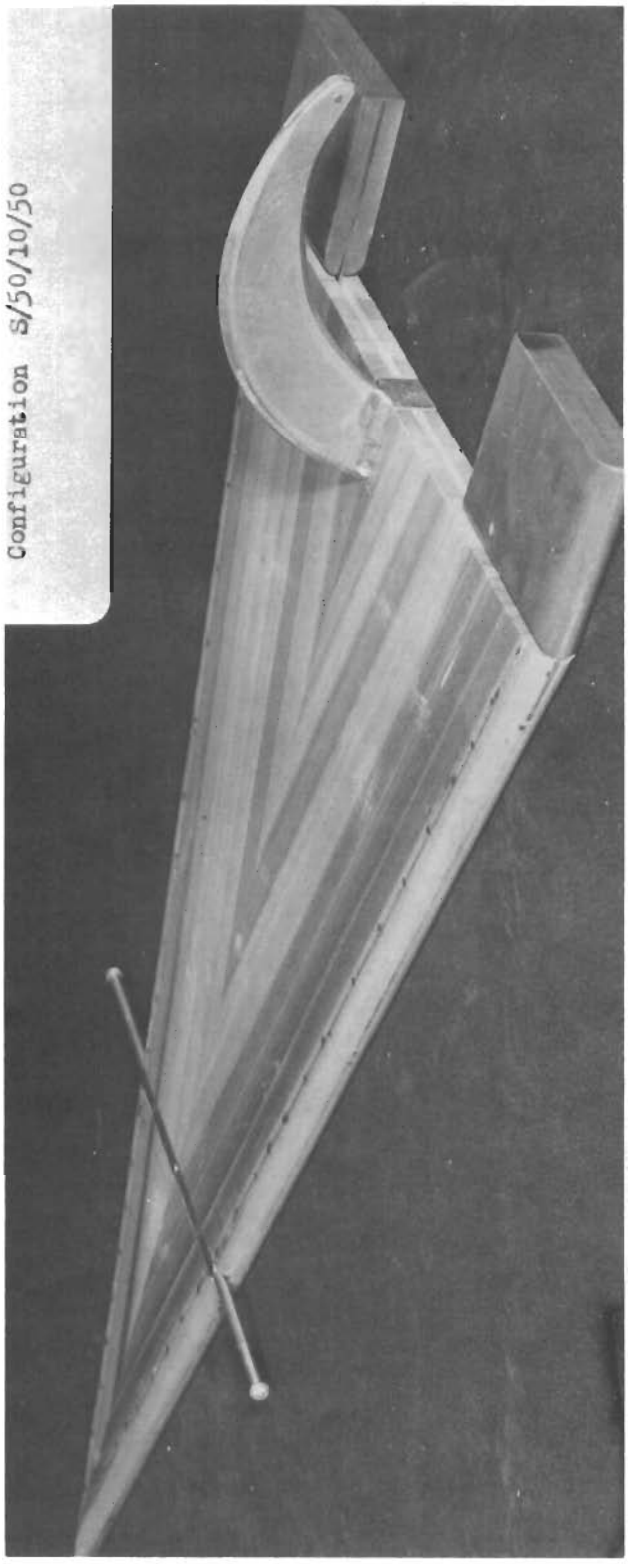


Figure 7. (Continued)

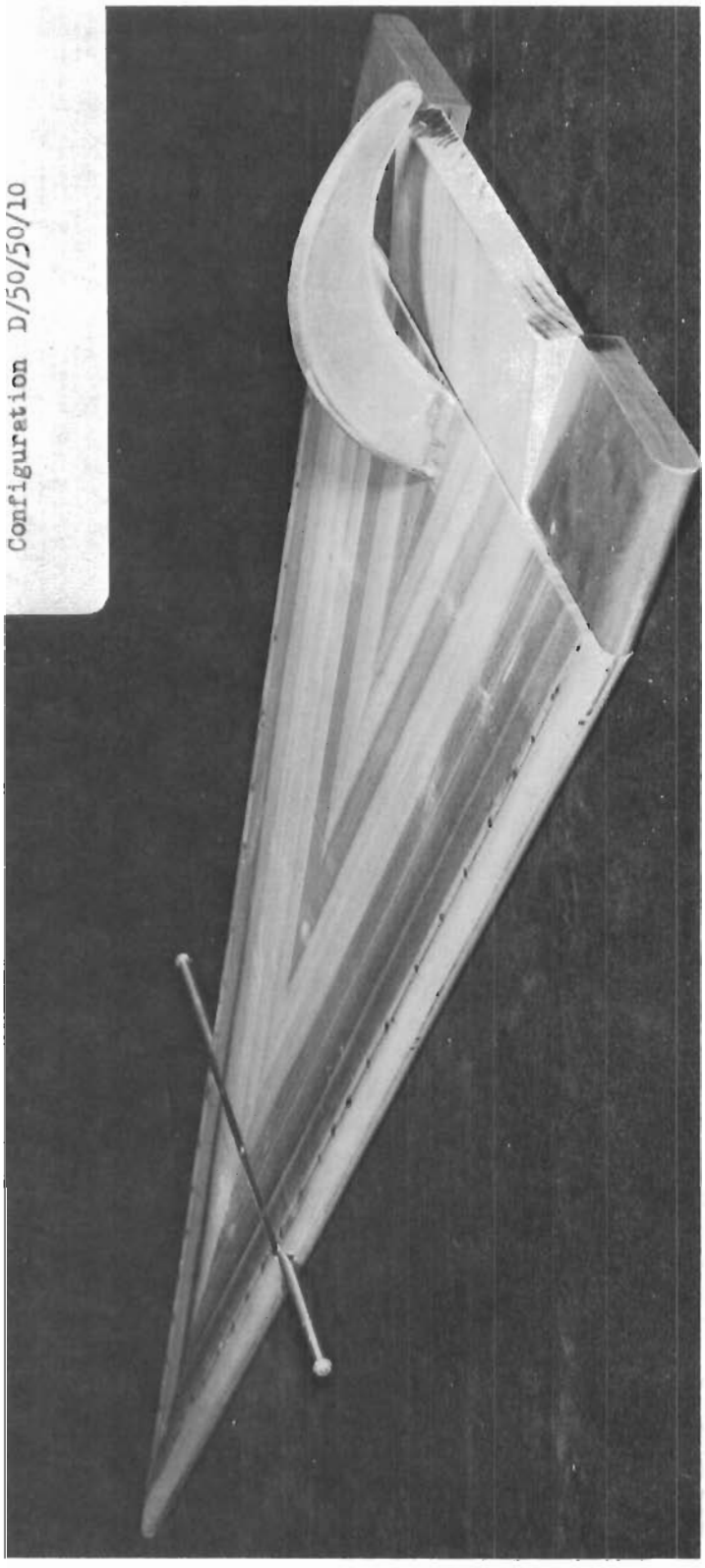


Figure 7. (Continued)

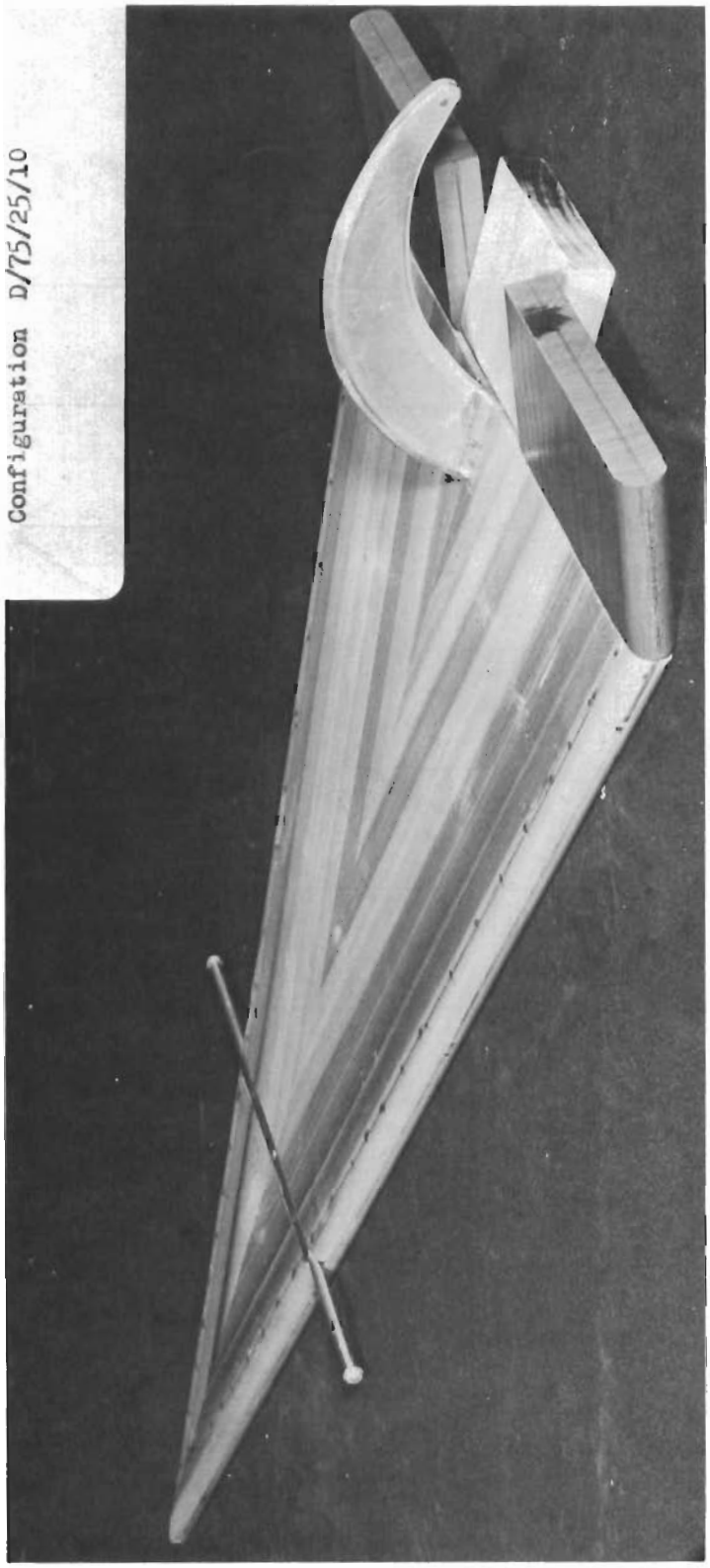


Figure 7. (Concluded)

| RUN | SYMBOL |
|---|---|
| 1 | ○ |
| 19 | Δ |
| 32 | + |
| 45 | x |

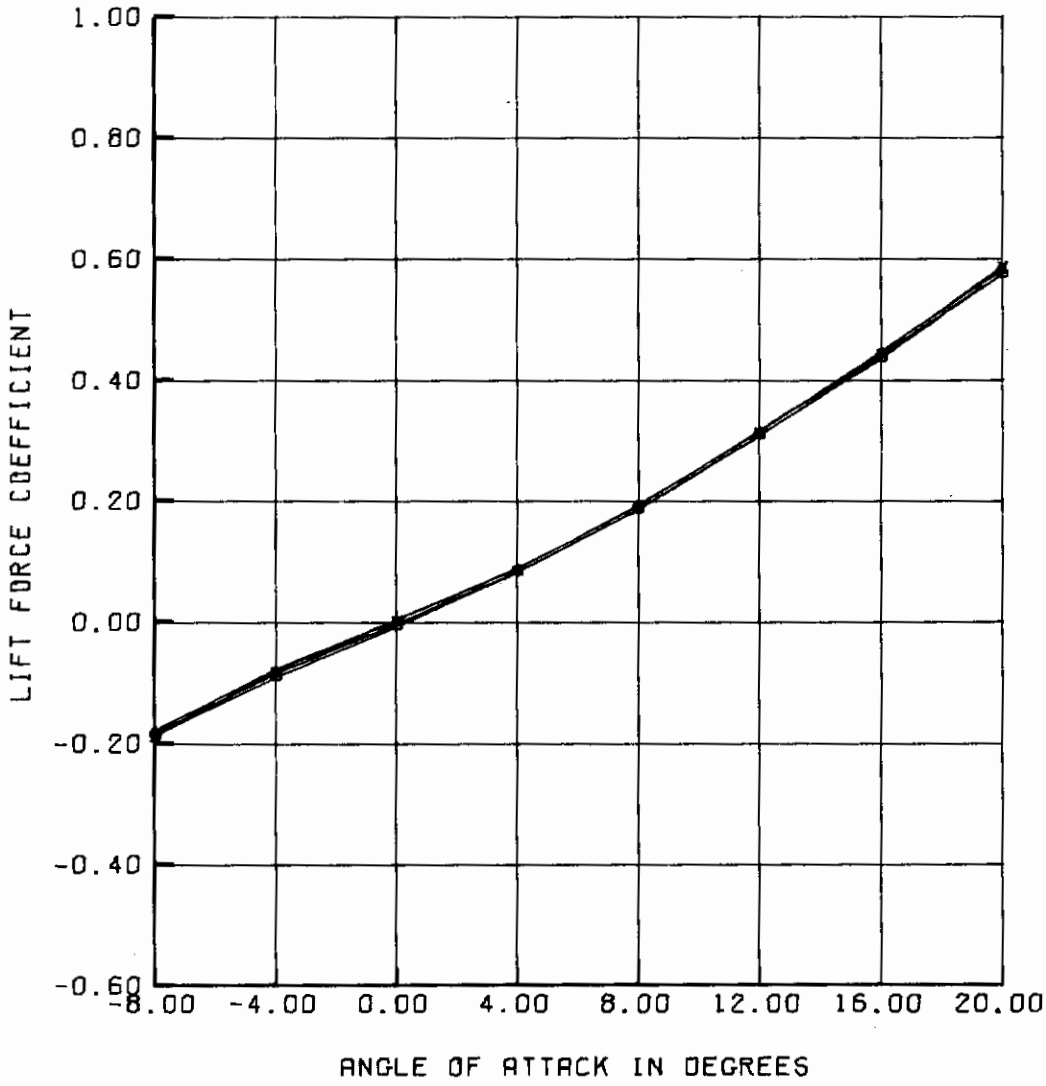


Figure 8. Data Repeatability, Basic Wing Model

| RUN | SYMBOL |
|---|---|
| 1 | ○ |
| 19 | Δ |
| 32 | + |
| 45 | x |

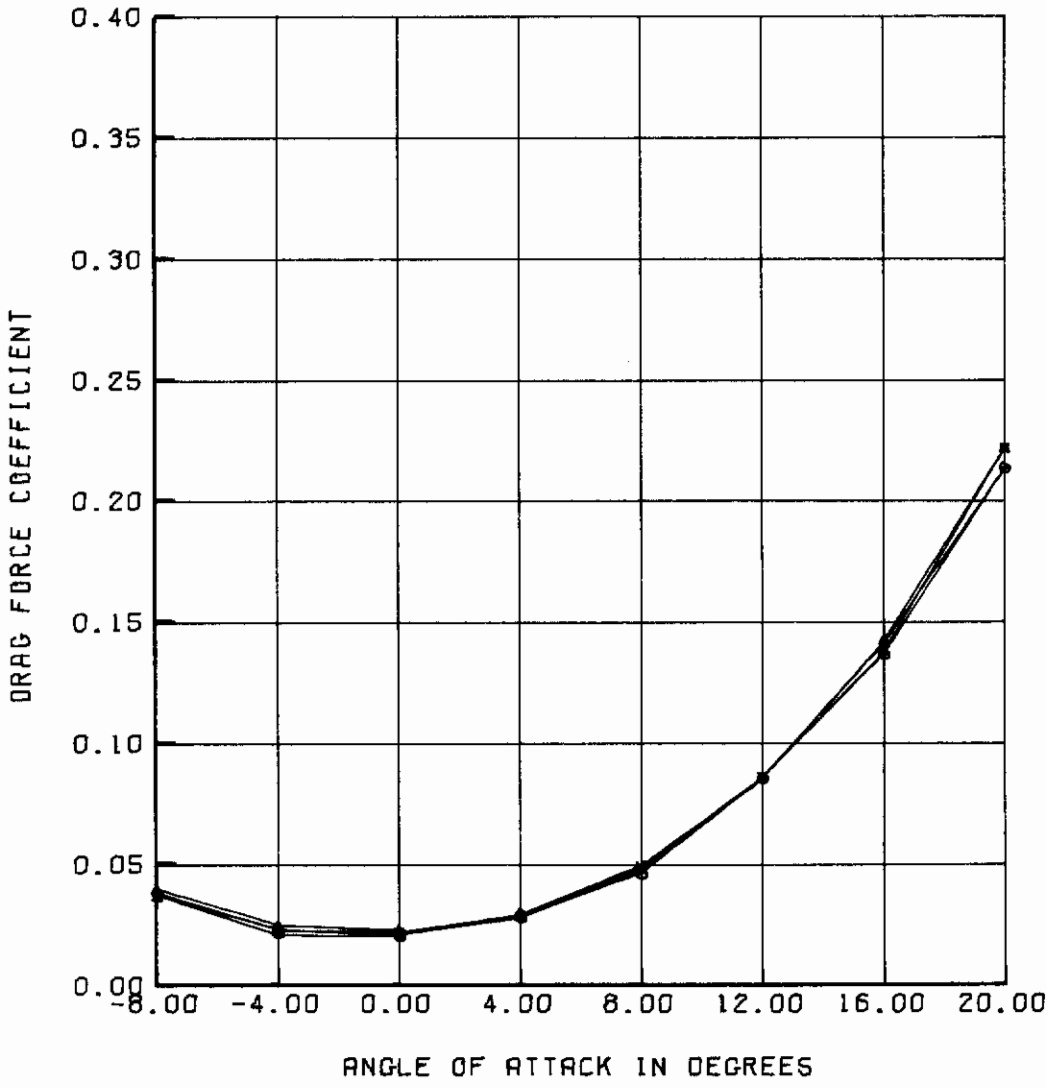


Figure 8. (Continued)

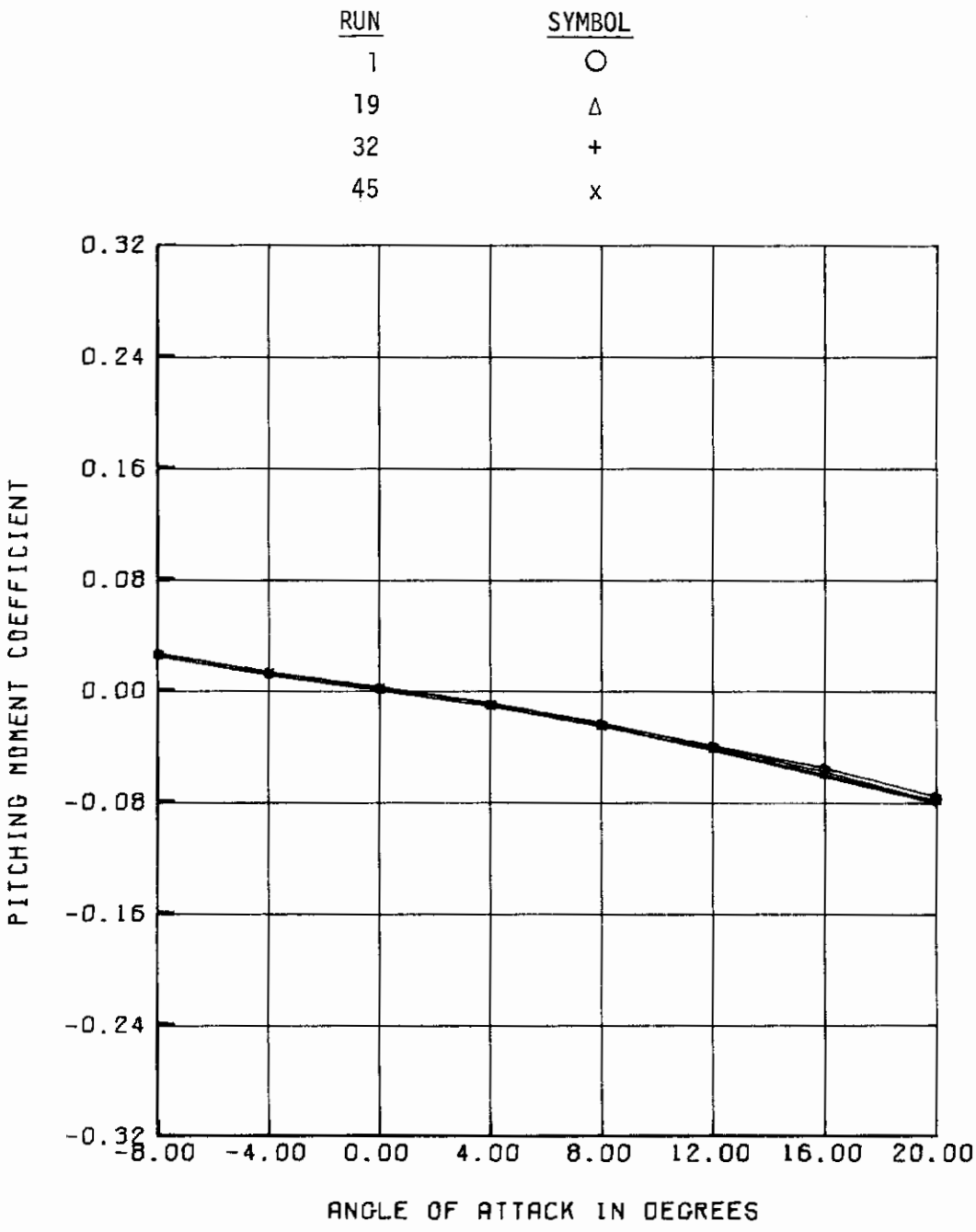


Figure 8. (Continued)

| RUN | SYMBOL |
|---|---|
| 1 | ○ |
| 19 | △ |
| 32 | + |
| 45 | x |

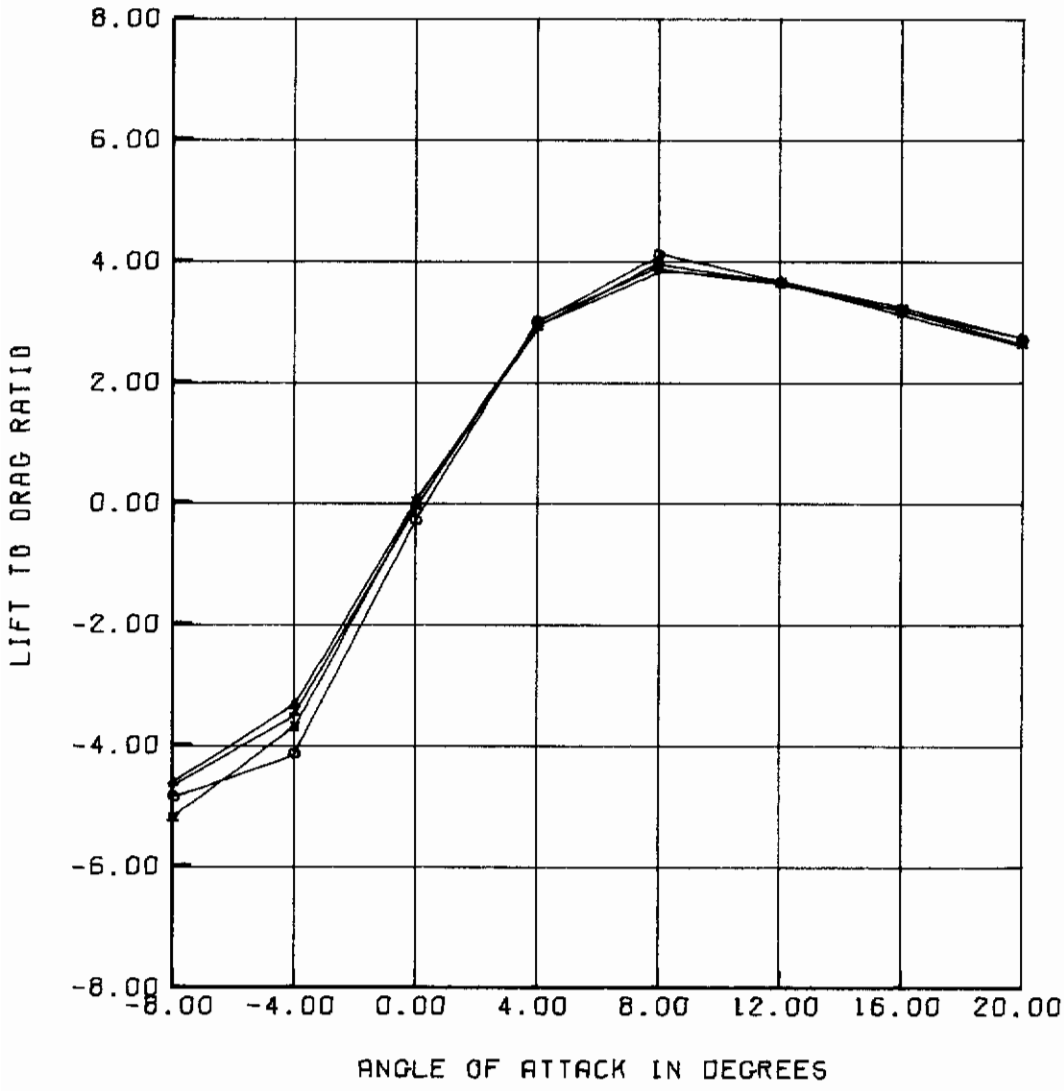


Figure 8. (Concluded)

| SYMBOL | FLAP DEFLECTION, DEG |
|---|---|
| ○ | 10 |
| △ | 0 |
| + | -10 |
| x | -20 |

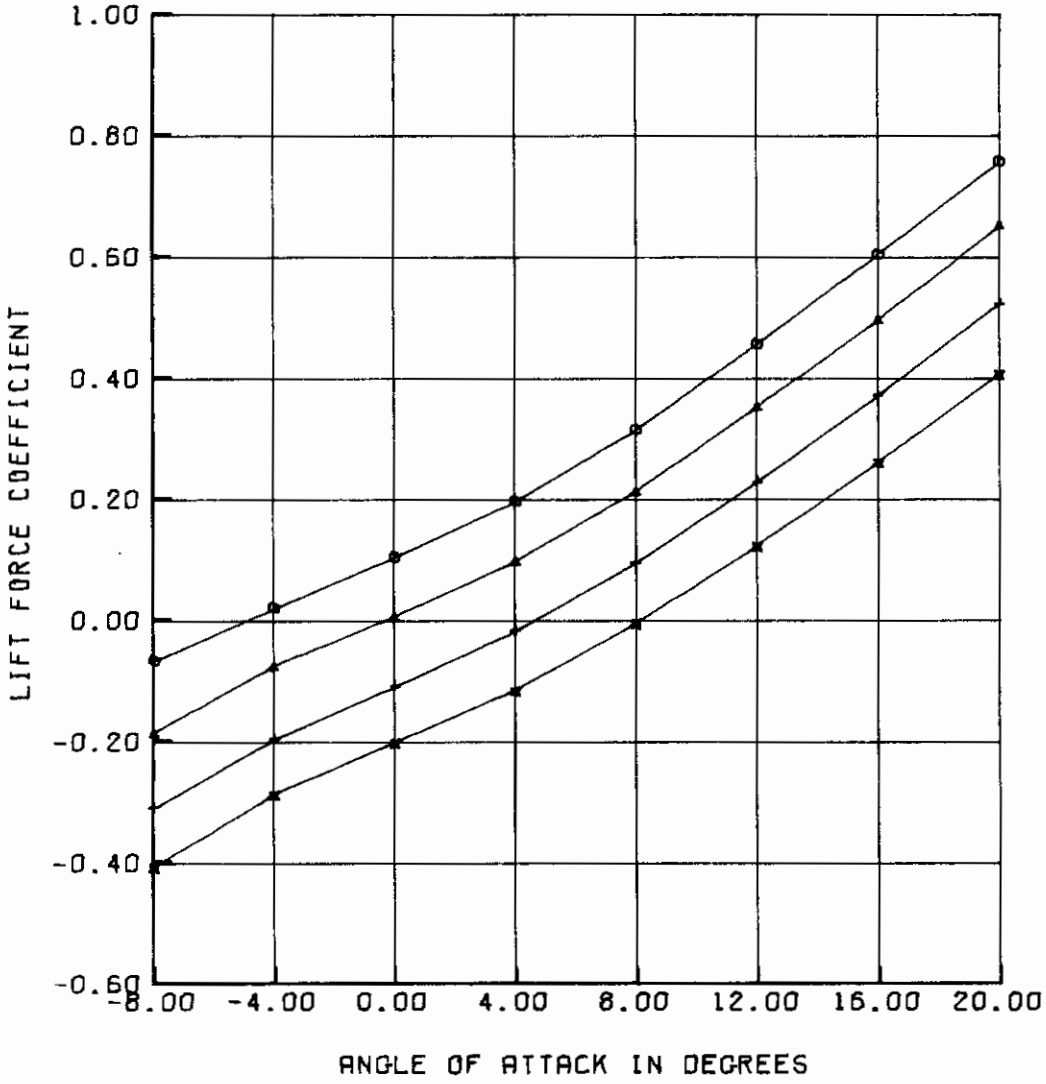


Figure 9. Control Surface Effects for Configuration S/100/5/0

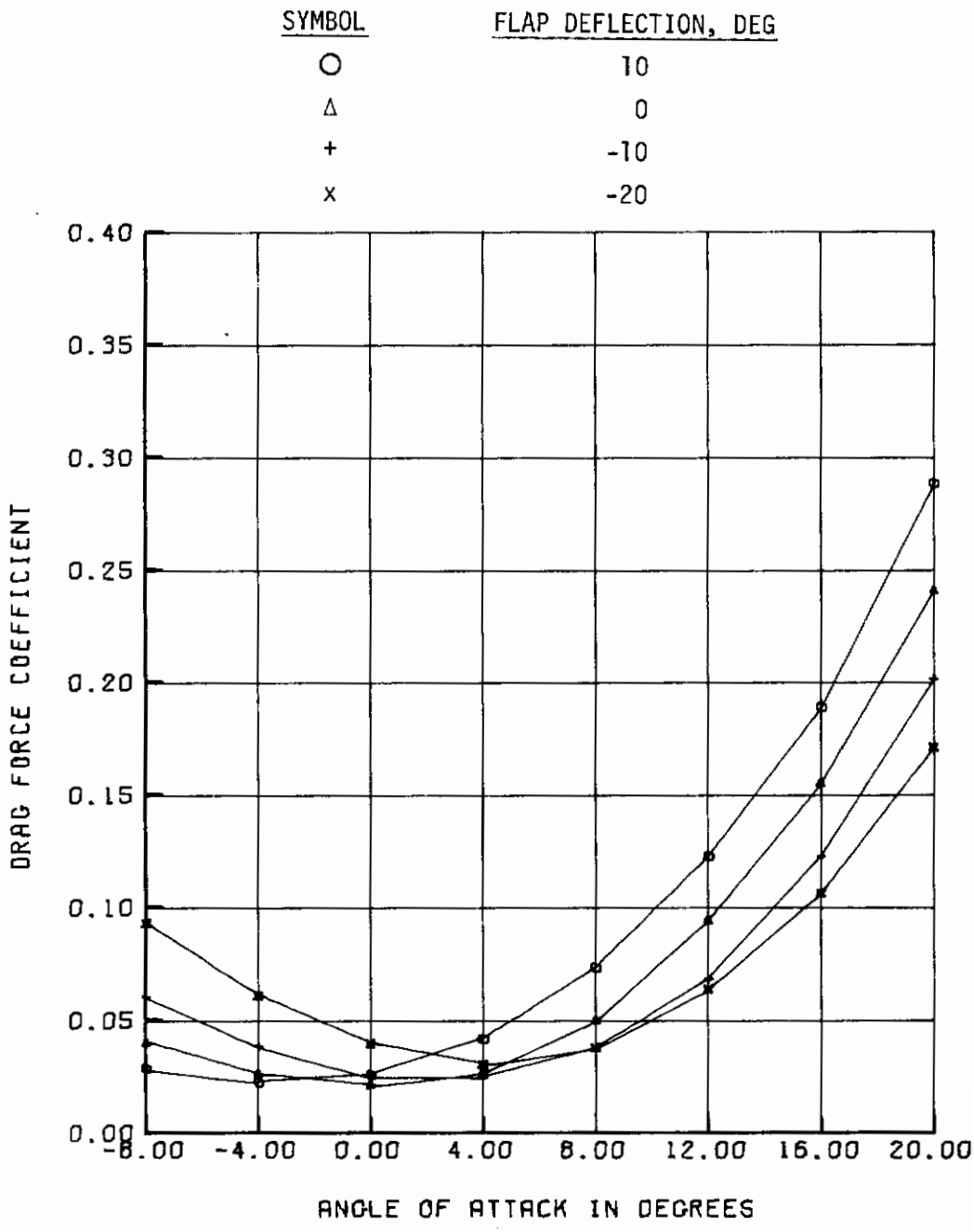


Figure 9. (Continued)

| SYMBOL | FLAP DEFLECTION, DEG |
|---|---|
| ○ | 10 |
| Δ | 0 |
| + | -10 |
| x | -20 |

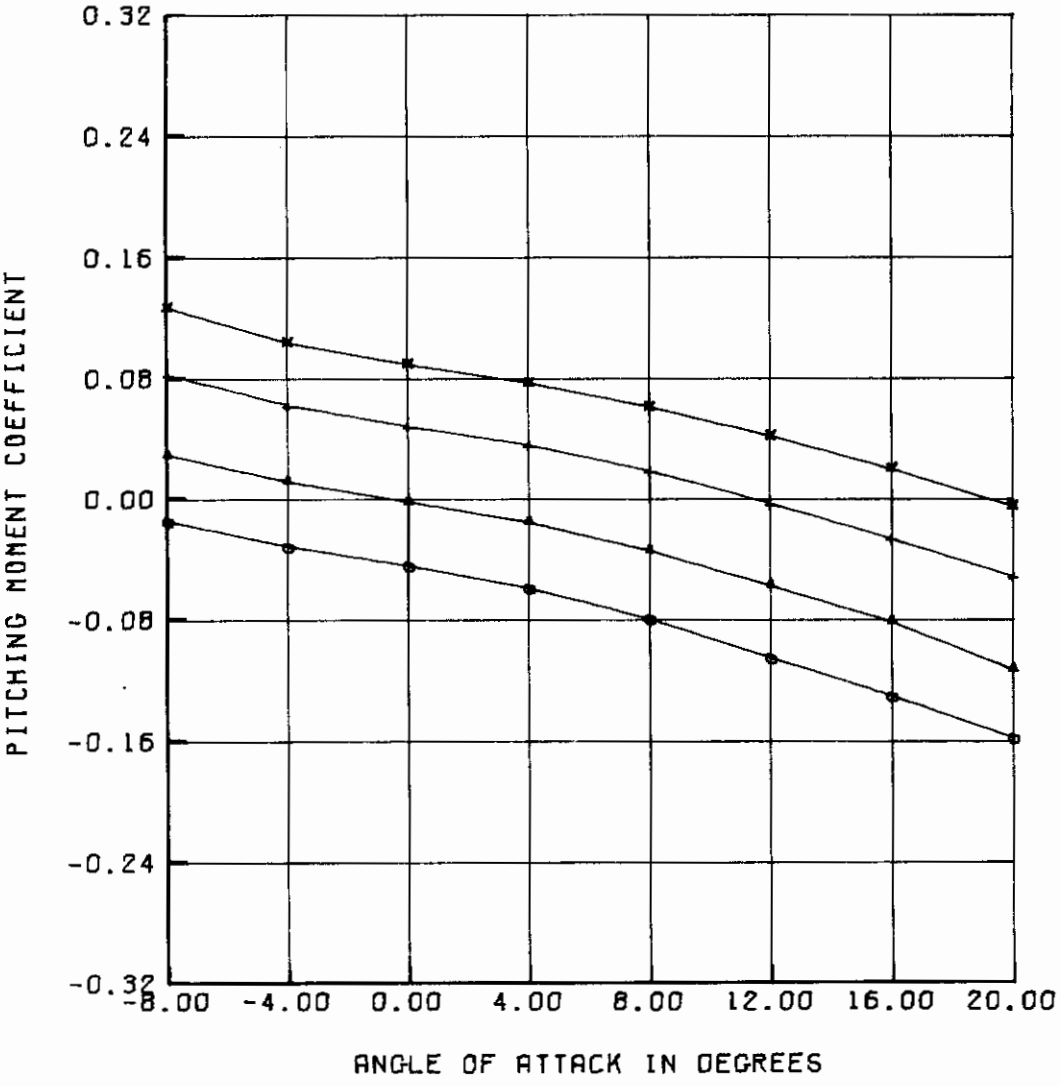


Figure 9. (Continued)

| SYMBOL | FLAP DEFLECTION, DEG |
|---|---|
| ○ | 10 |
| Δ | 0 |
| + | -10 |
| x | -20 |

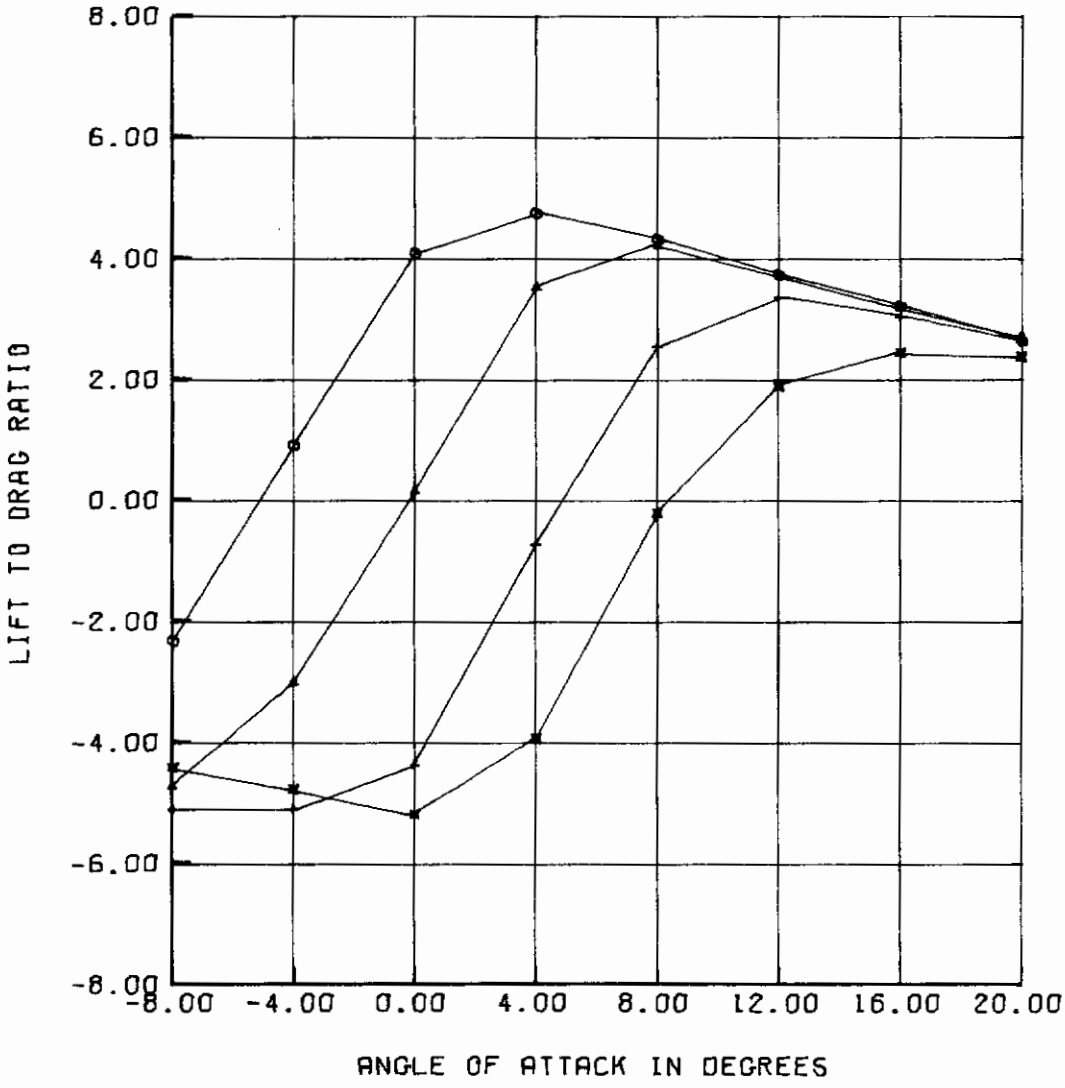


Figure 9. (Concluded)

| SYMBOL | FLAP DEFLECTION, DEG |
|---|---|
| ○ | 10 |
| △ | 0 |
| + | -10 |
| x | -20 |

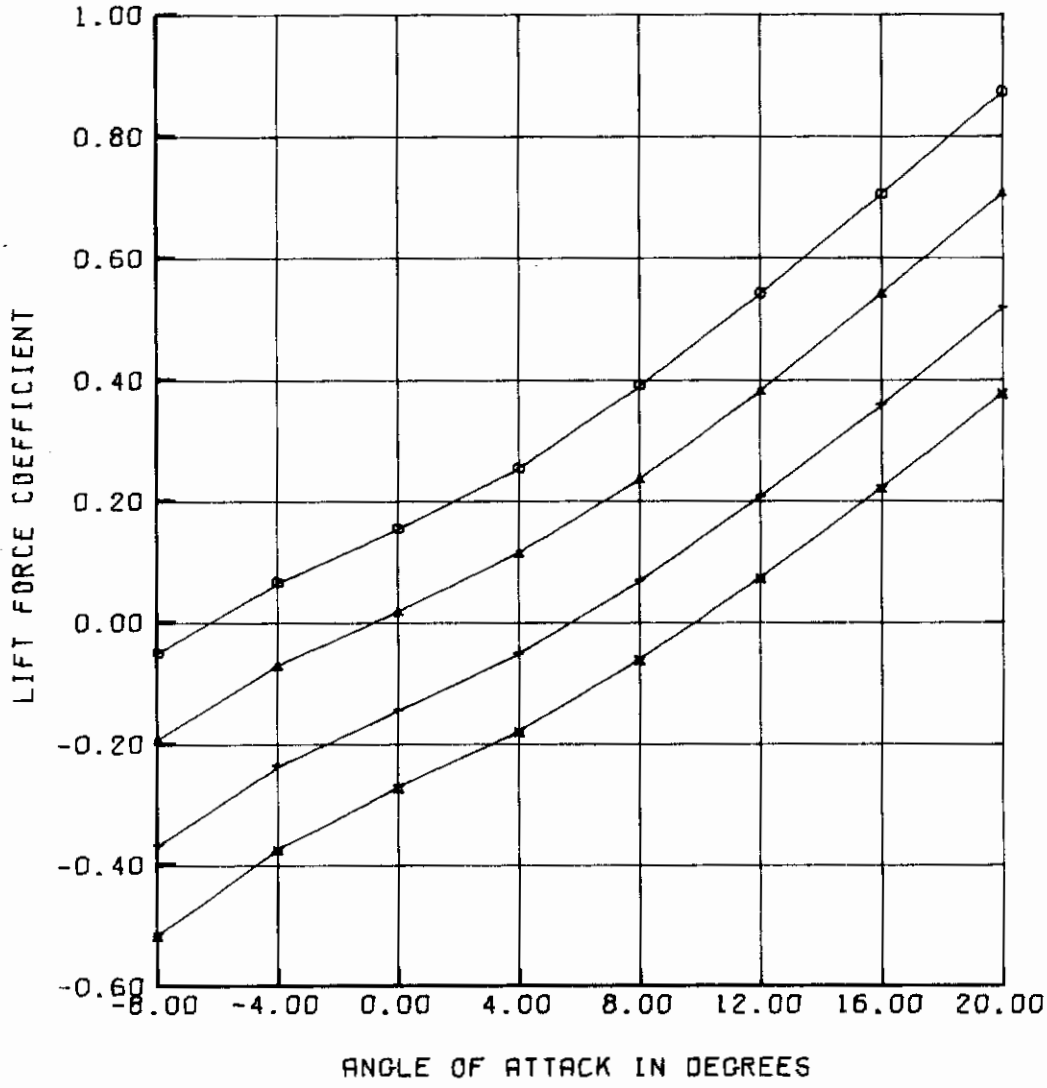


Figure 10. Control Surface Effects for Configuration S/100/10/0

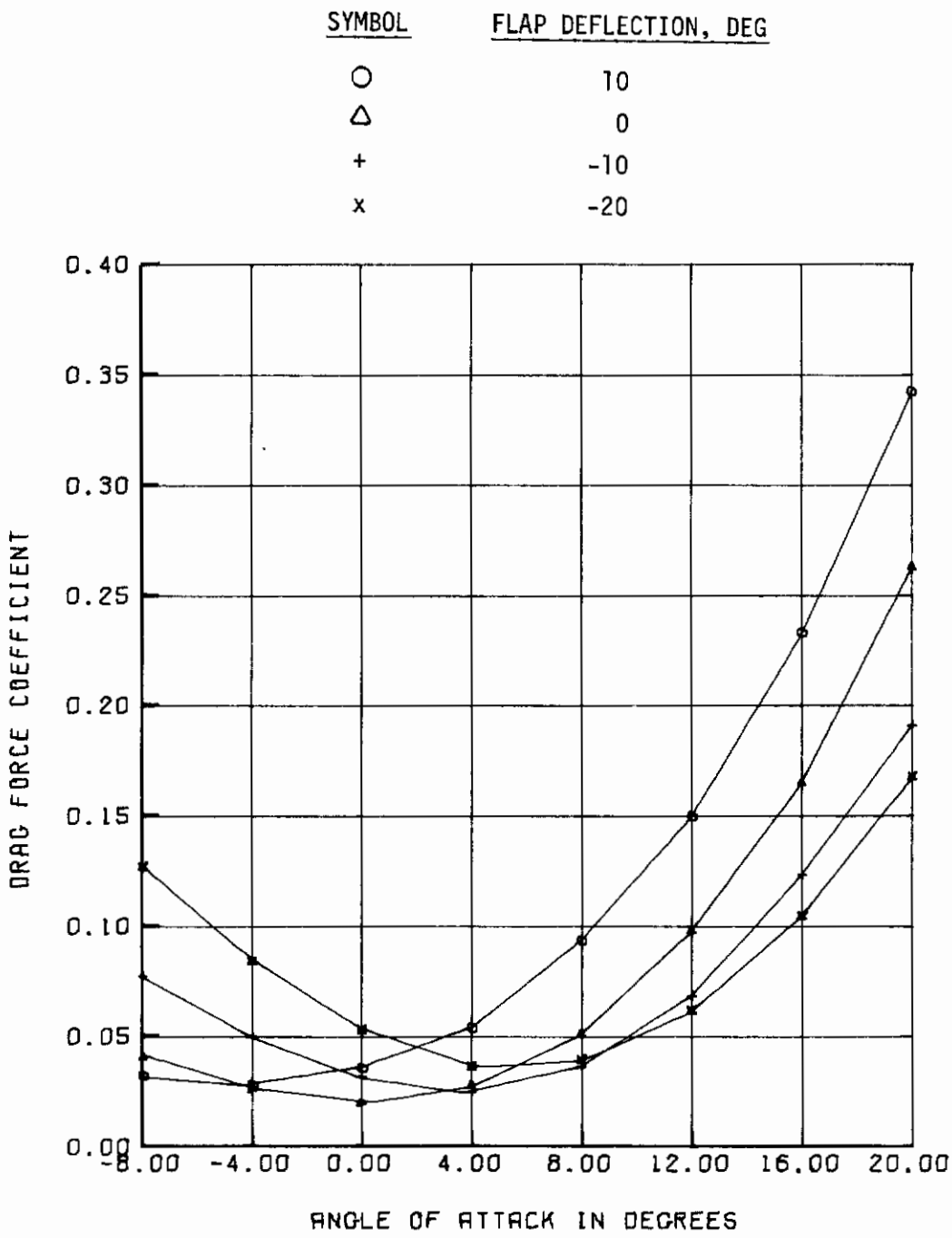


Figure 10. (Continued)

| SYMBOL | FLAP DEFLECTION, DEG |
|---|---|
| ○ | 10 |
| △ | 0 |
| + | -10 |
| x | -20 |

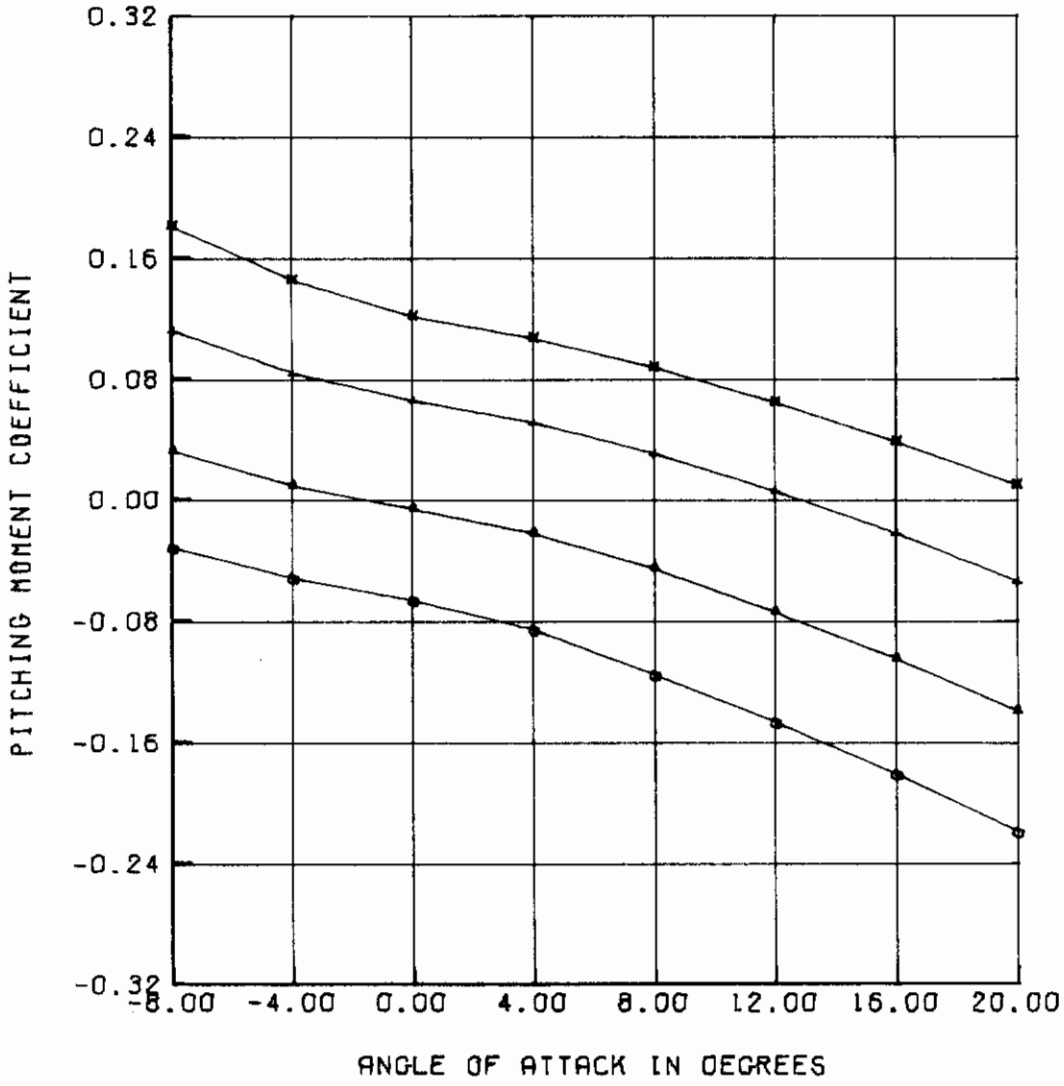


Figure 10. (Continued)

| SYMBOL | FLAP DEFLECTION, DEG |
|---|---|
| ○ | 10 |
| △ | 0 |
| + | -10 |
| x | -20 |

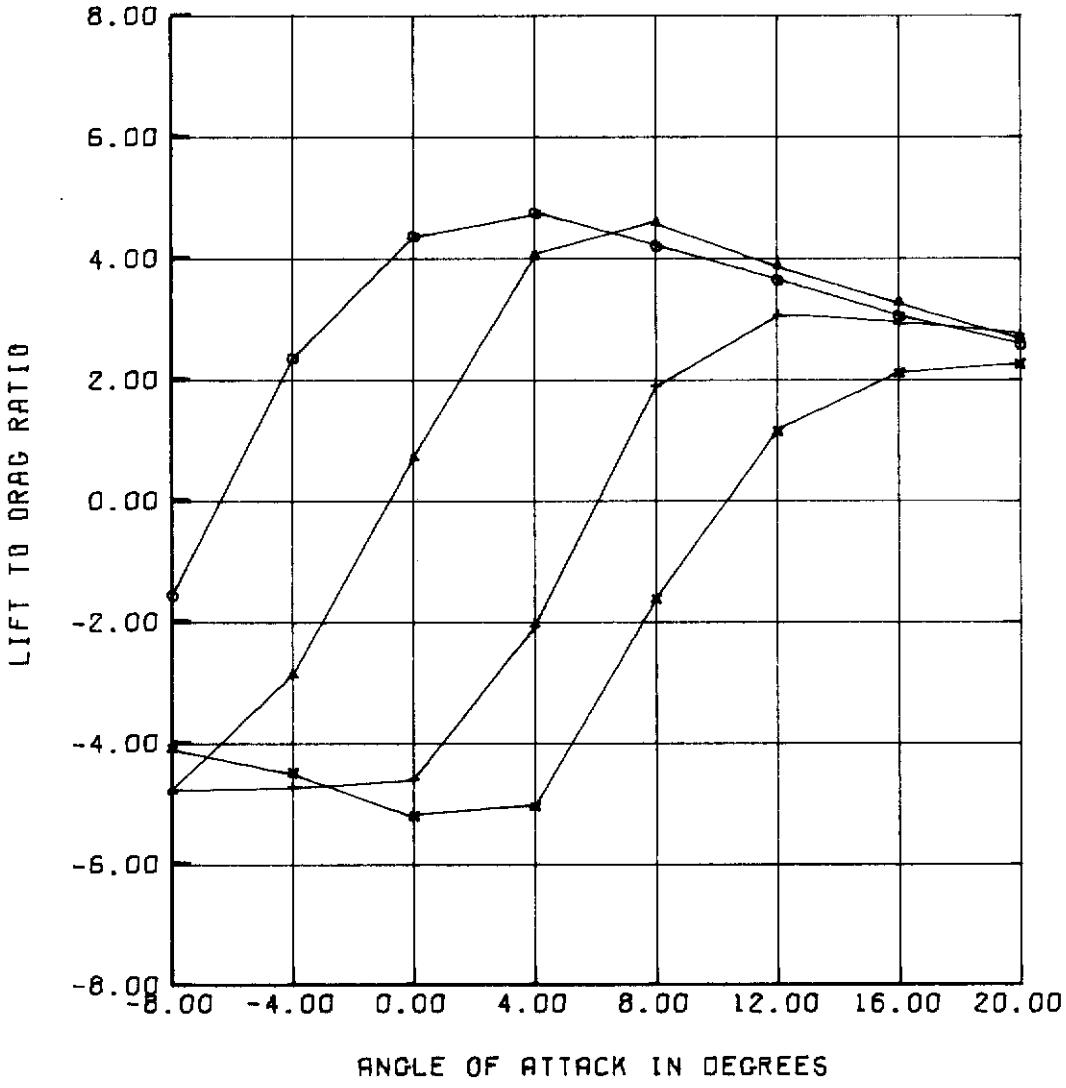


Figure 10. (Concluded)

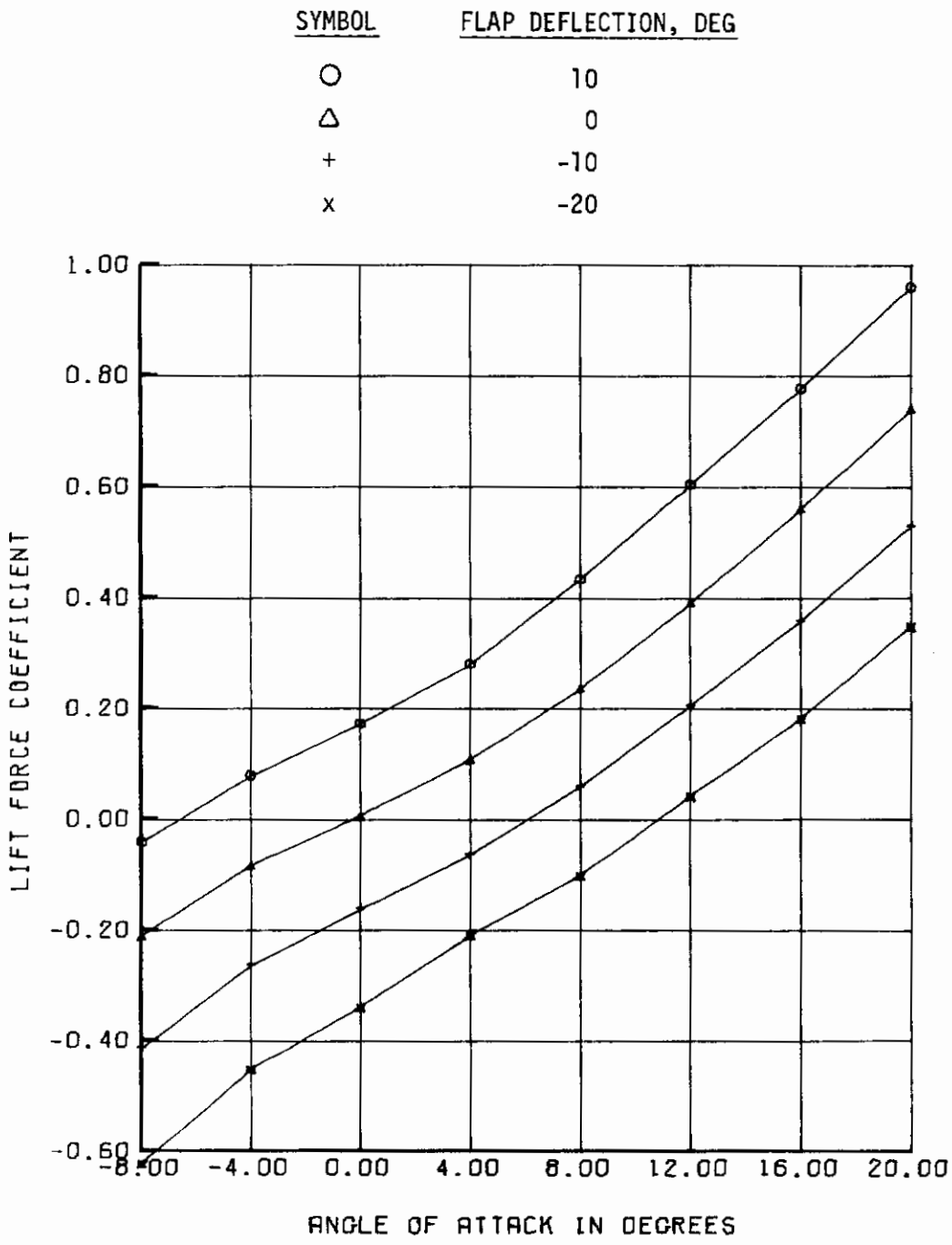


Figure 11. Control Surface Effects for Configuration S/100/15/0

| SYMBOL | FLAP DEFLECTION, DEG |
|---|---|
| ○ | 10 |
| △ | 0 |
| + | -10 |
| x | -20 |

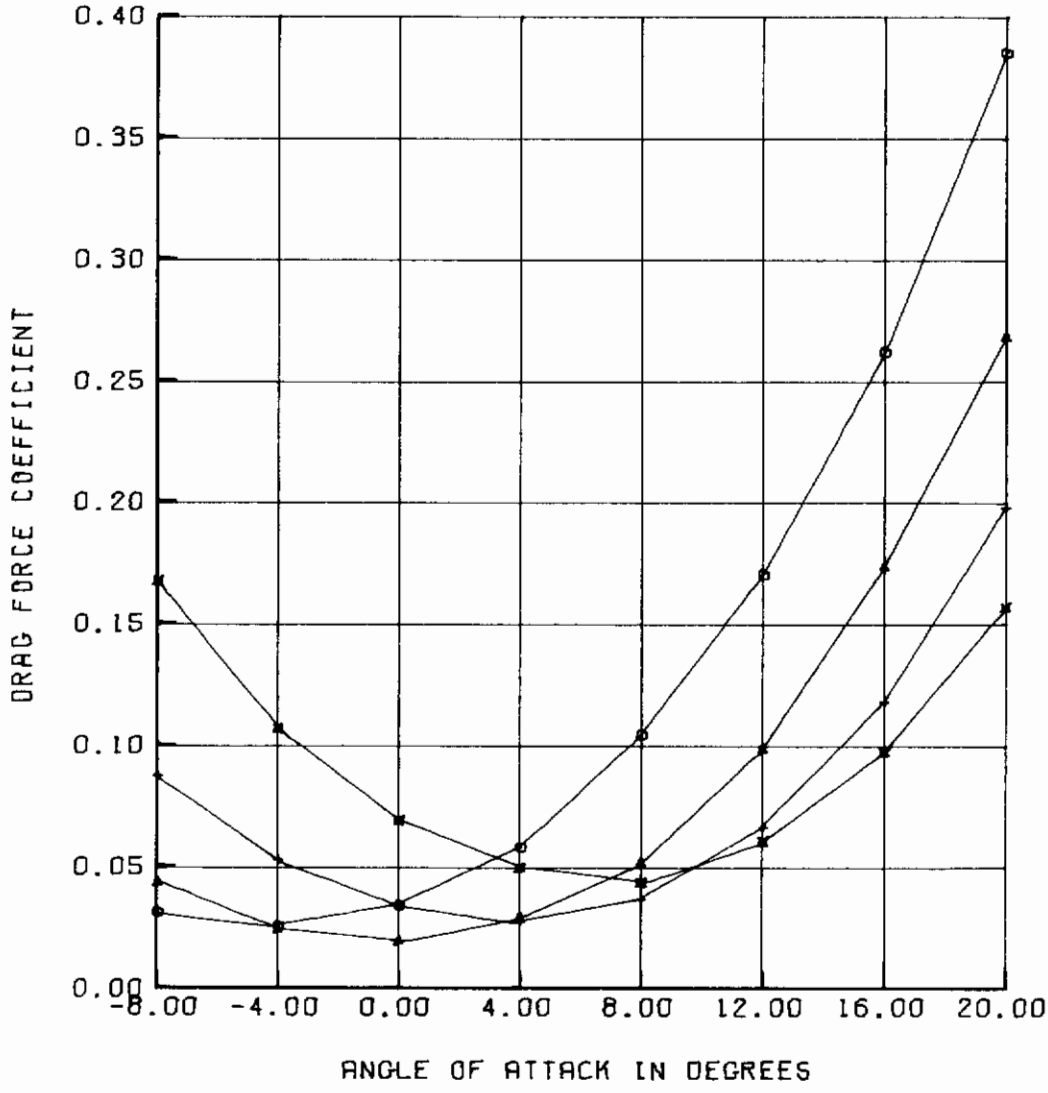


Figure 11. (Continued)

| SYMBOL | FLAP DEFLECTION, DEG |
|---|---|
| ○ | 10 |
| △ | 0 |
| + | -10 |
| x | -20 |

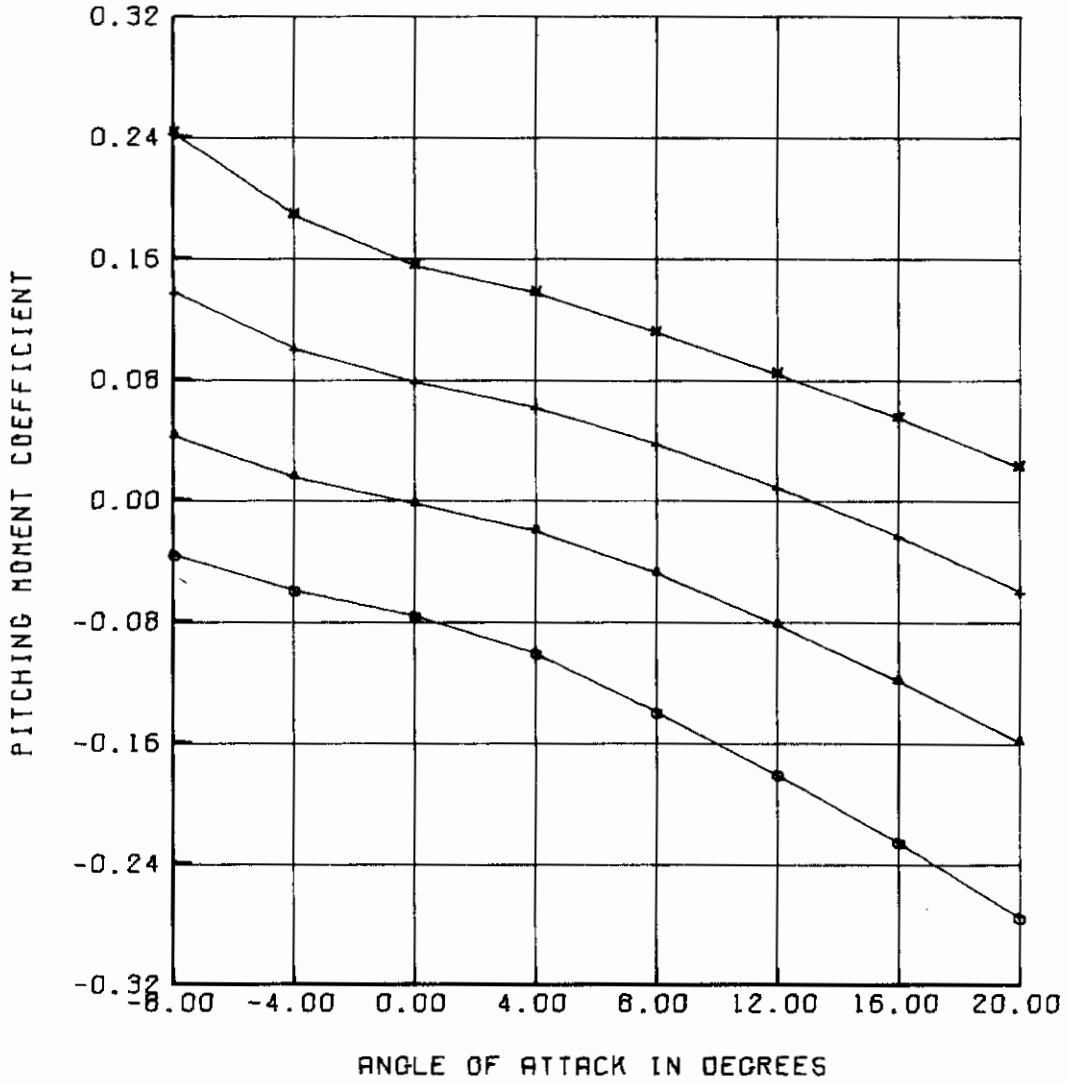


Figure 11. (Continued)

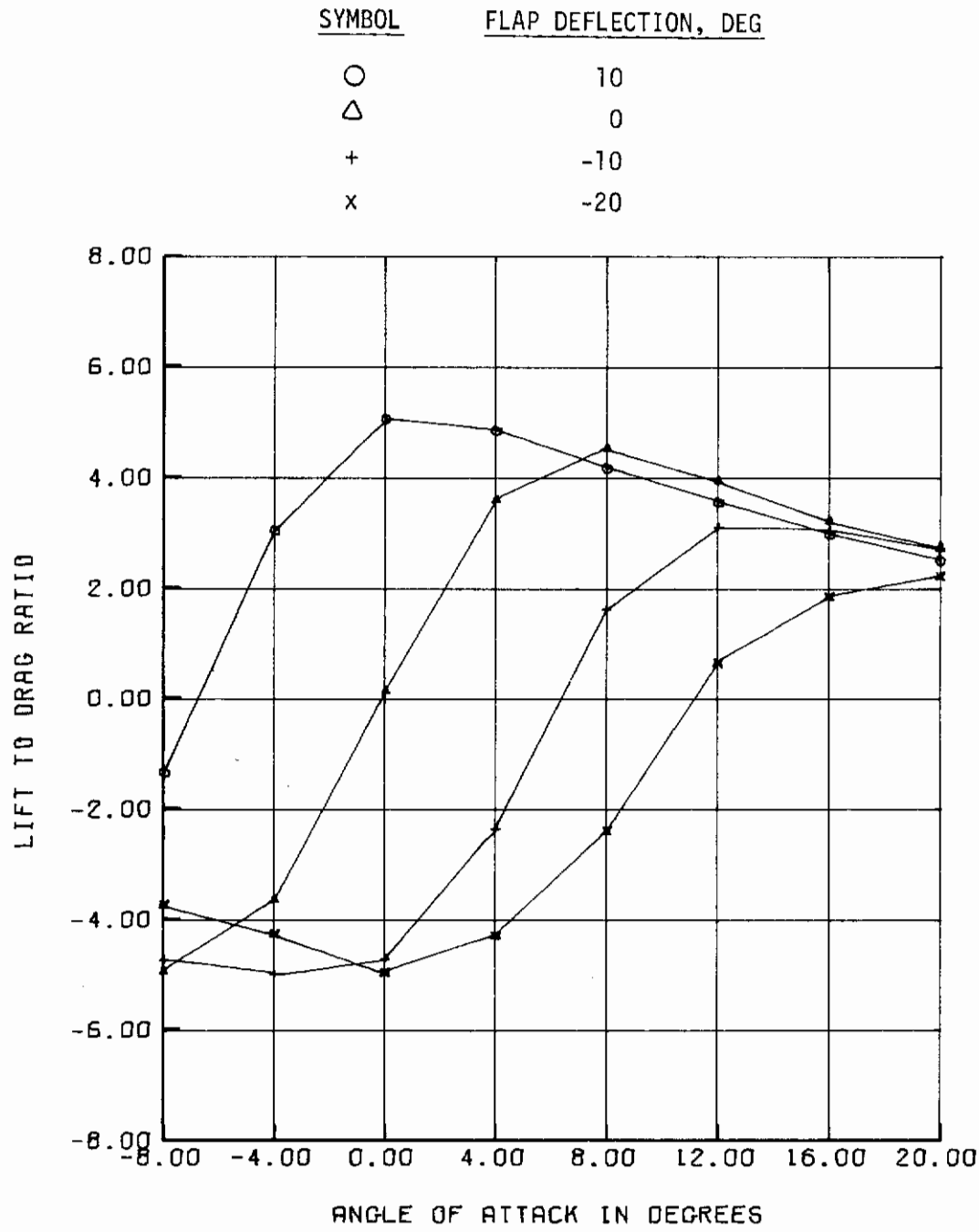


Figure 11. (Concluded)

| SYMBOL | FLAP DEFLECTION, DEG |
|---|---|
| ○ | 10 |
| △ | 0 |
| + | -10 |
| x | -20 |

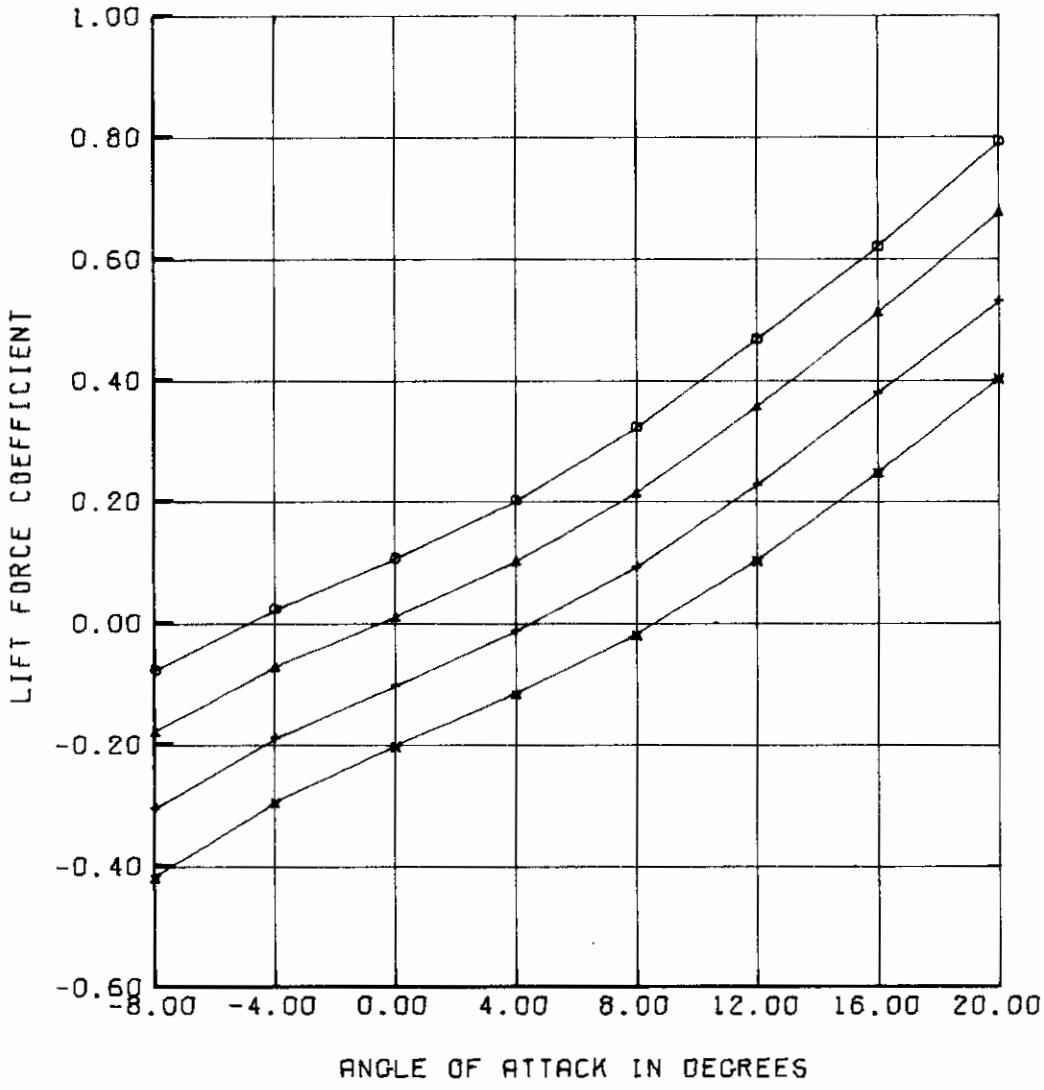


Figure 12. Control Surface Effects for Configuration S/75/10/0

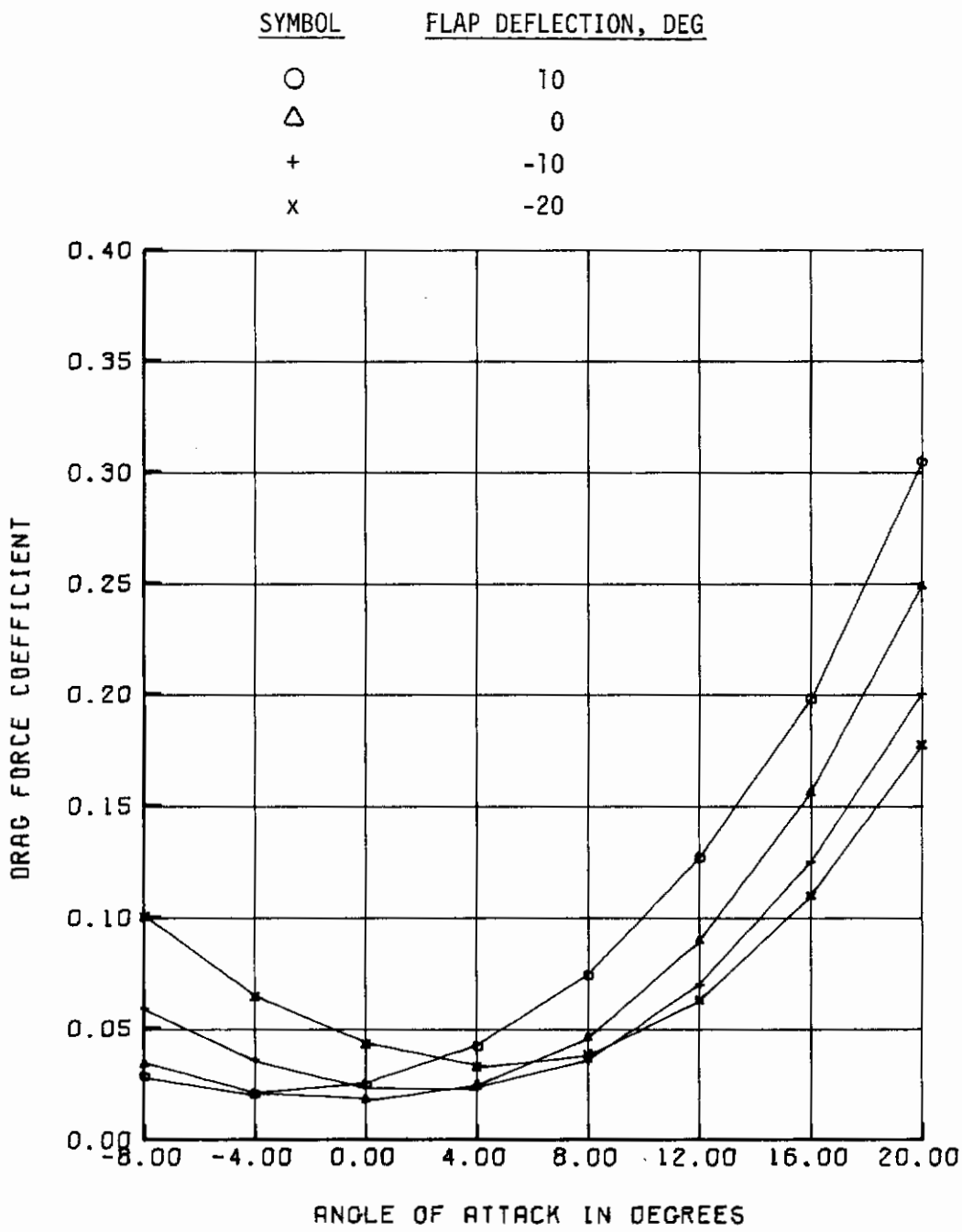


Figure 12. (Continued)

| SYMBOL | FLAP DEFLECTION, DEG |
|---|---|
| ○ | 10 |
| △ | 0 |
| + | -10 |
| x | -20 |

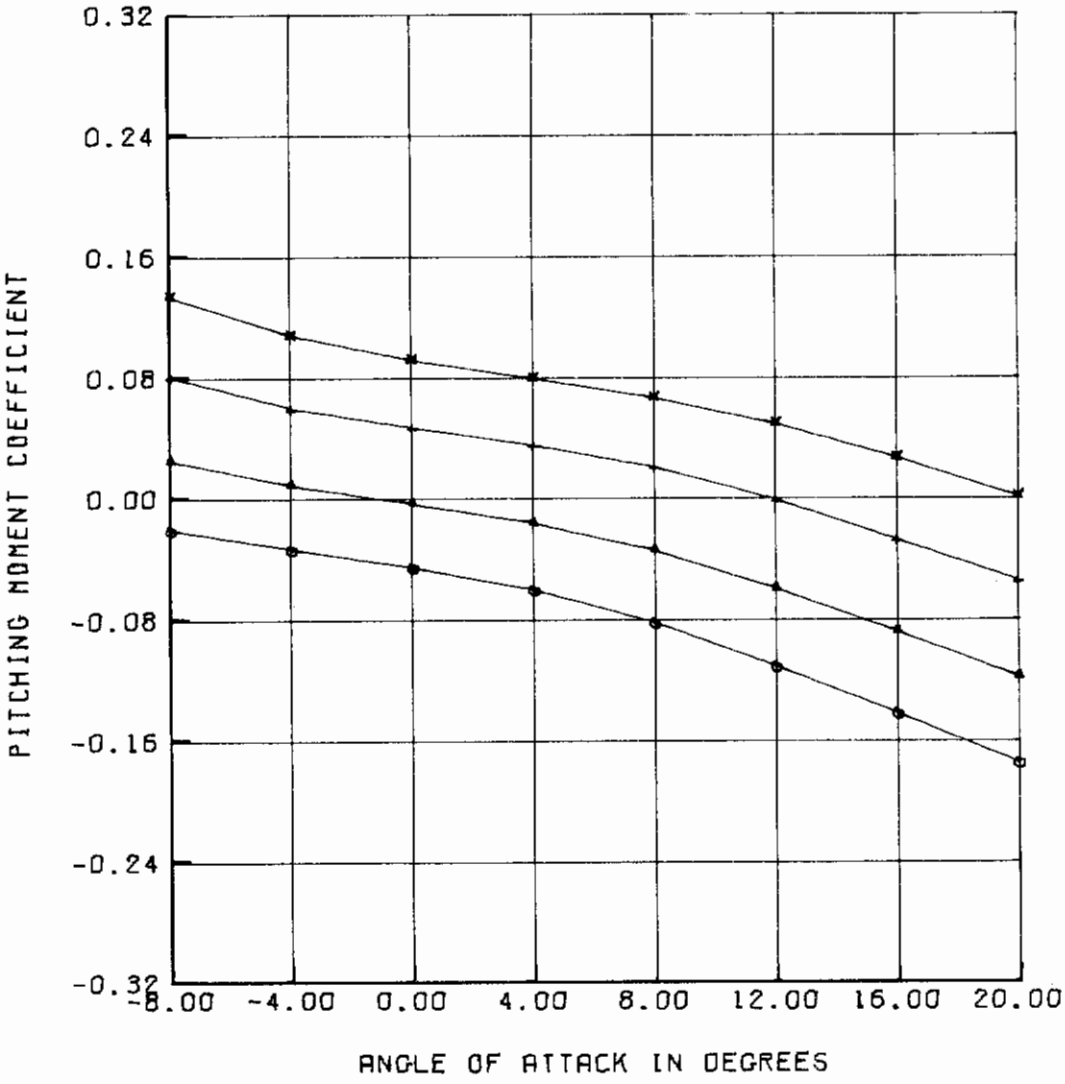


Figure 12. (Continued)

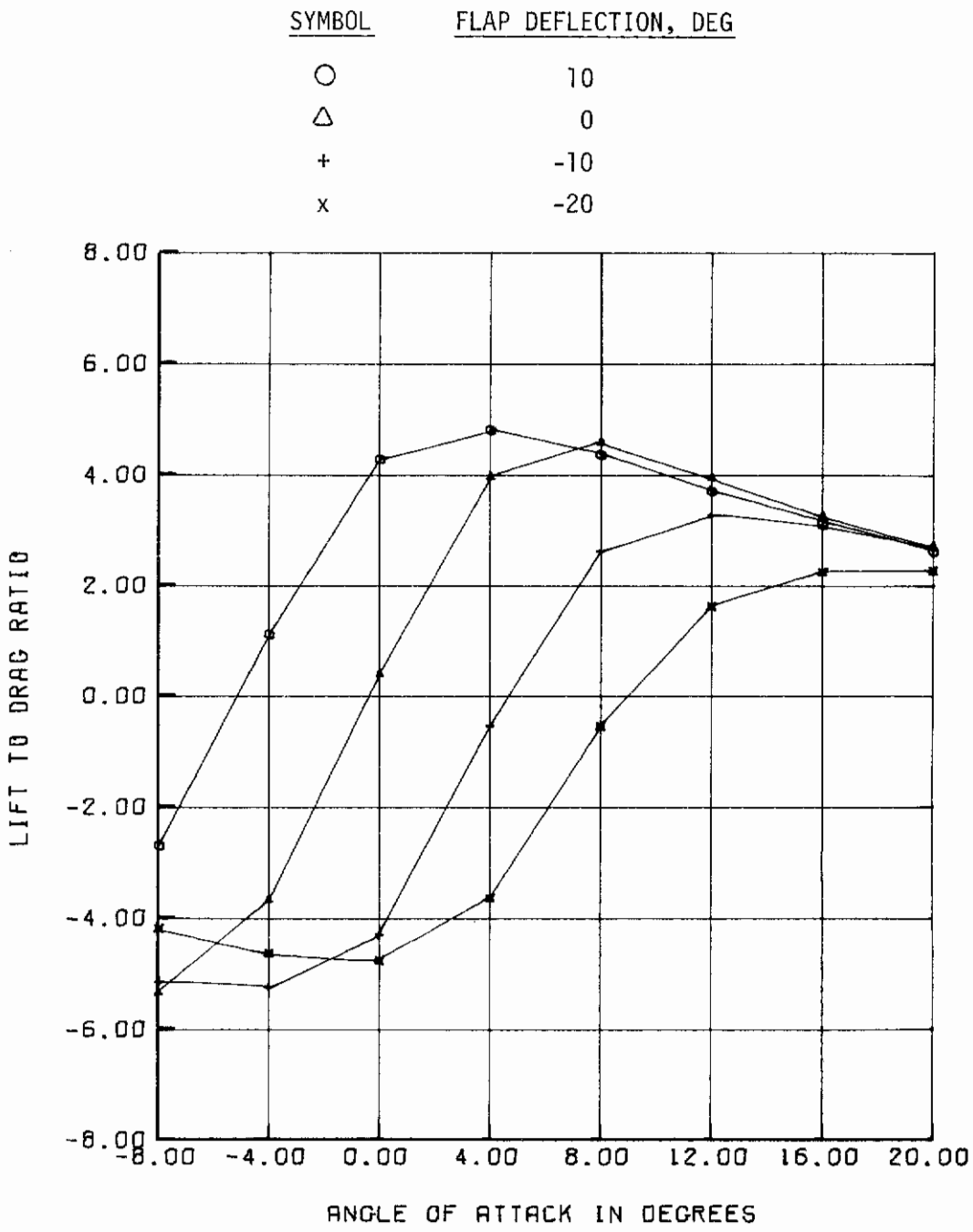


Figure 12. (Concluded)

| SYMBOL | FLAP DEFLECTION, DEG |
|---|---|
| ○ | 10 |
| △ | 0 |
| + | -10 |
| x | -20 |

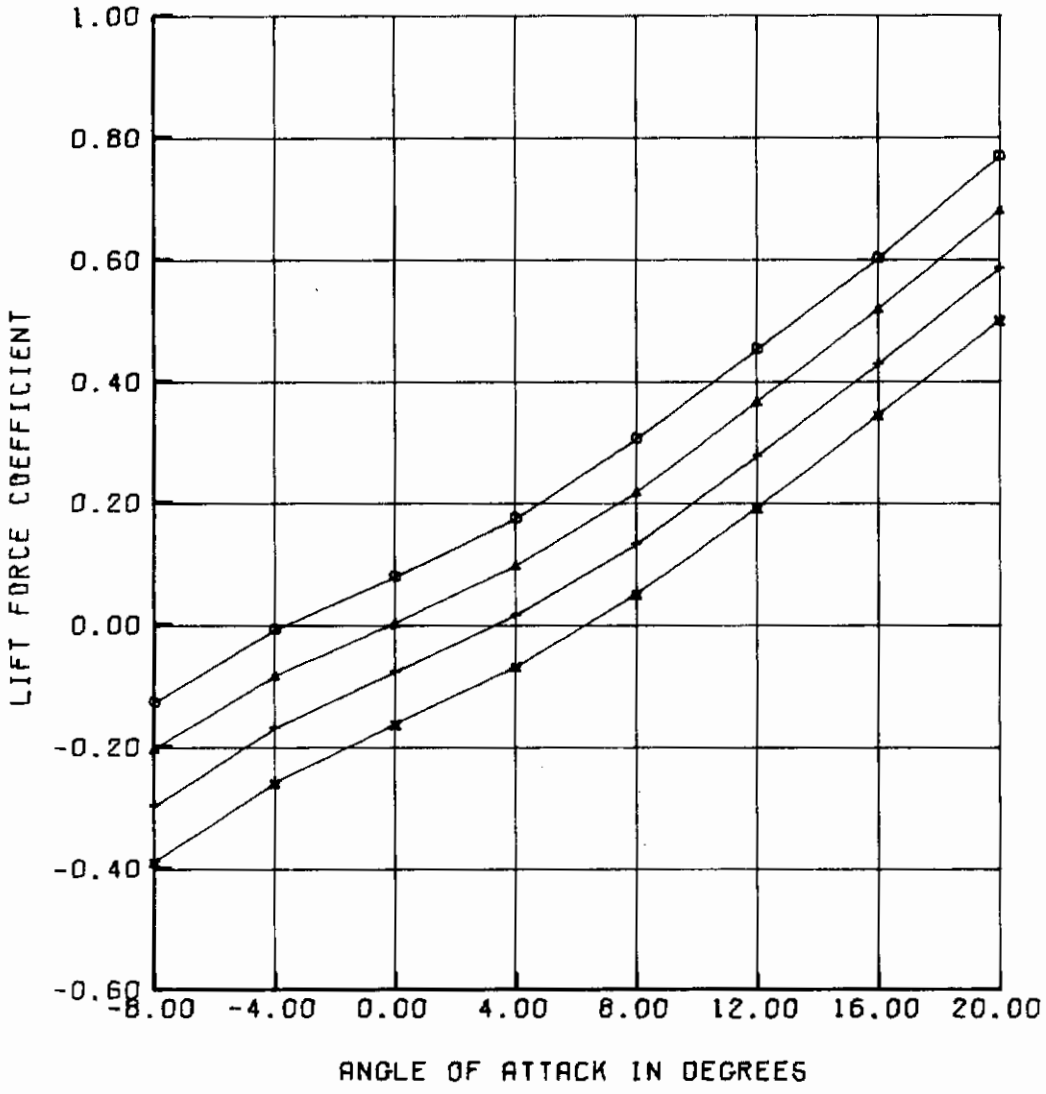


Figure 13. Control Surface Effects for Configuration S/75/10/25

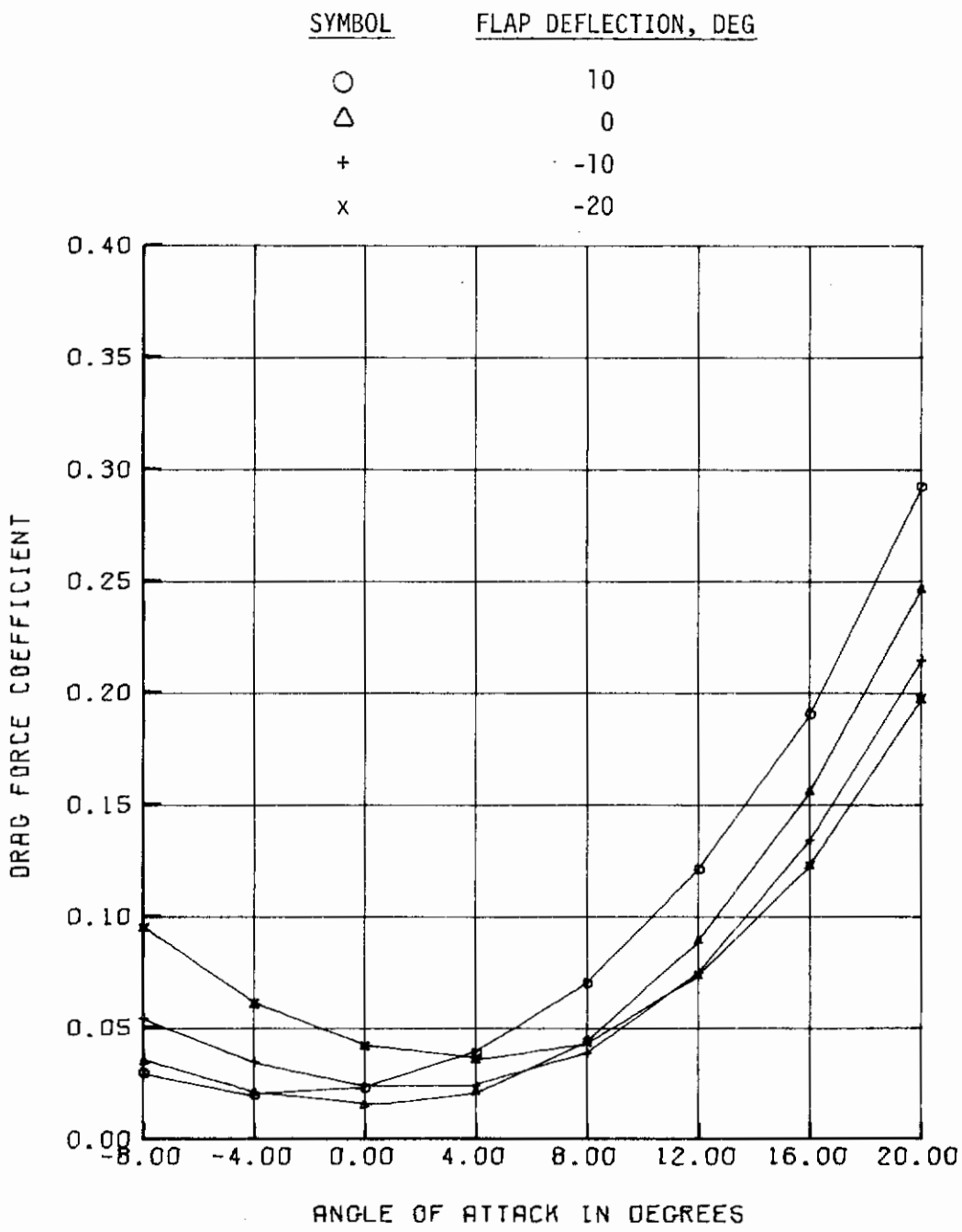


Figure 13. (Continued)

| SYMBOL | FLAP DEFLECTION, DEG |
|---|---|
| ○ | 10 |
| △ | 0 |
| + | -10 |
| x | -20 |

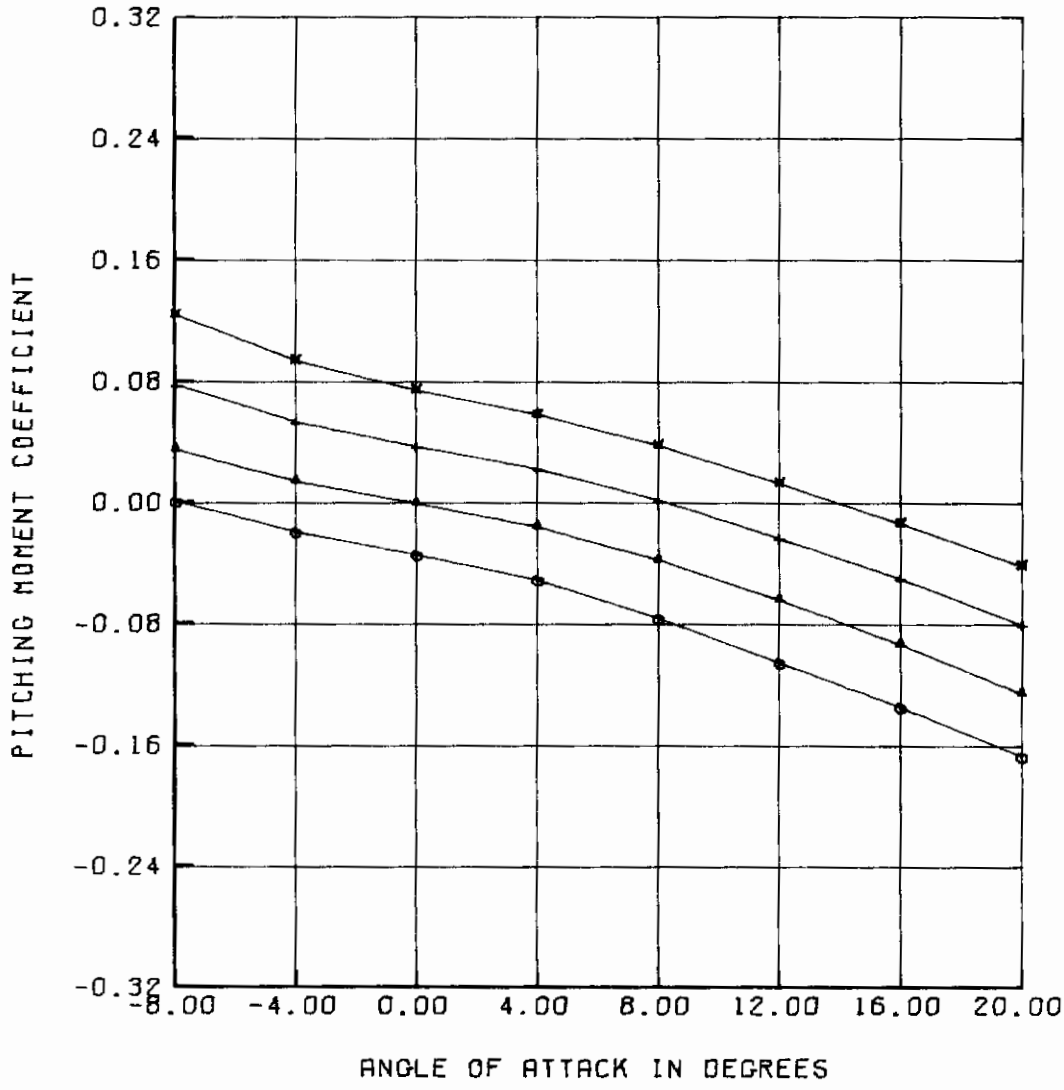


Figure 13. (Continued)

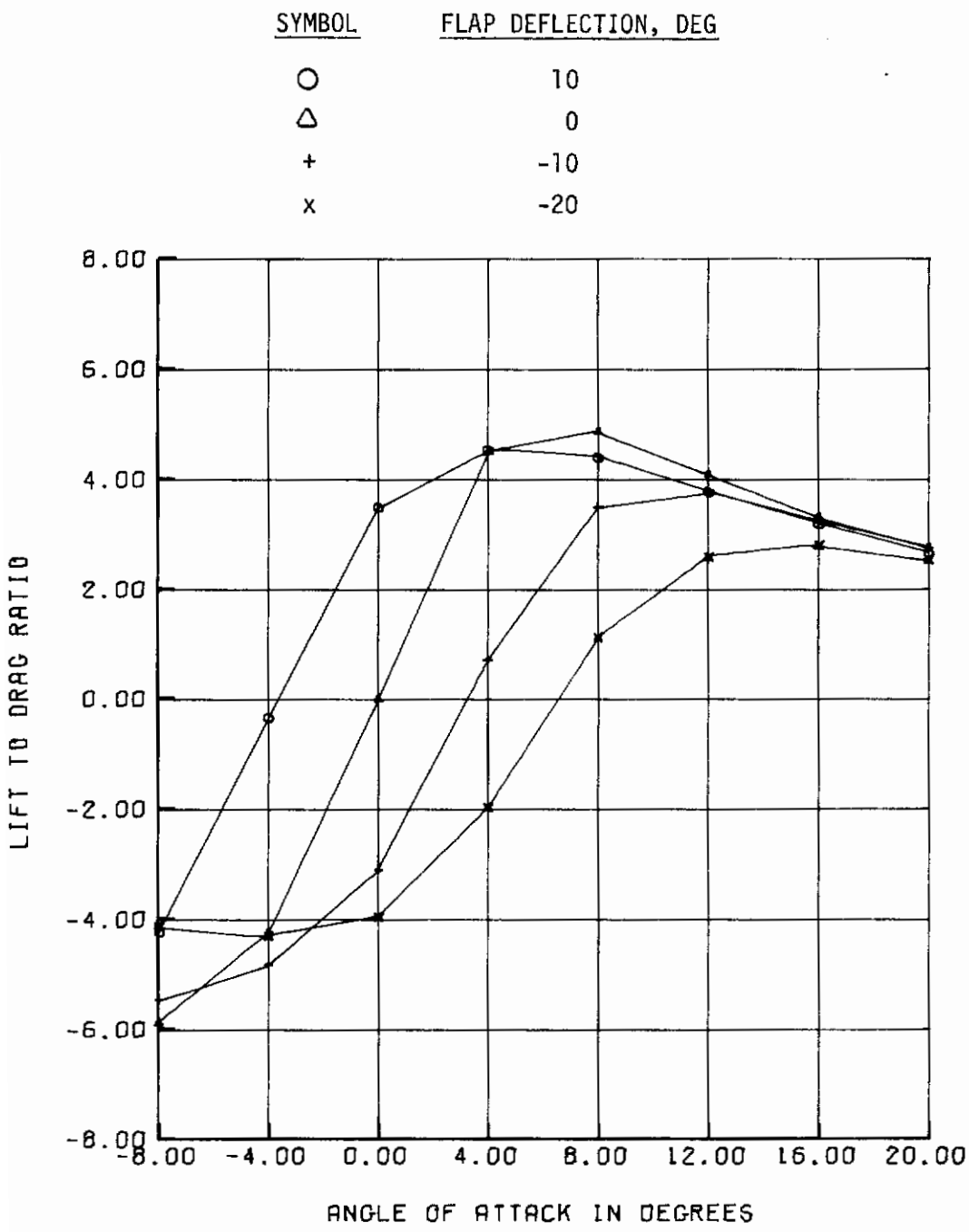


Figure 13. (Concluded)

| SYMBOL | FLAP DEFLECTION, DEG |
|---|---|
| ○ | 10 |
| △ | 0 |
| + | -10 |
| x | -20 |

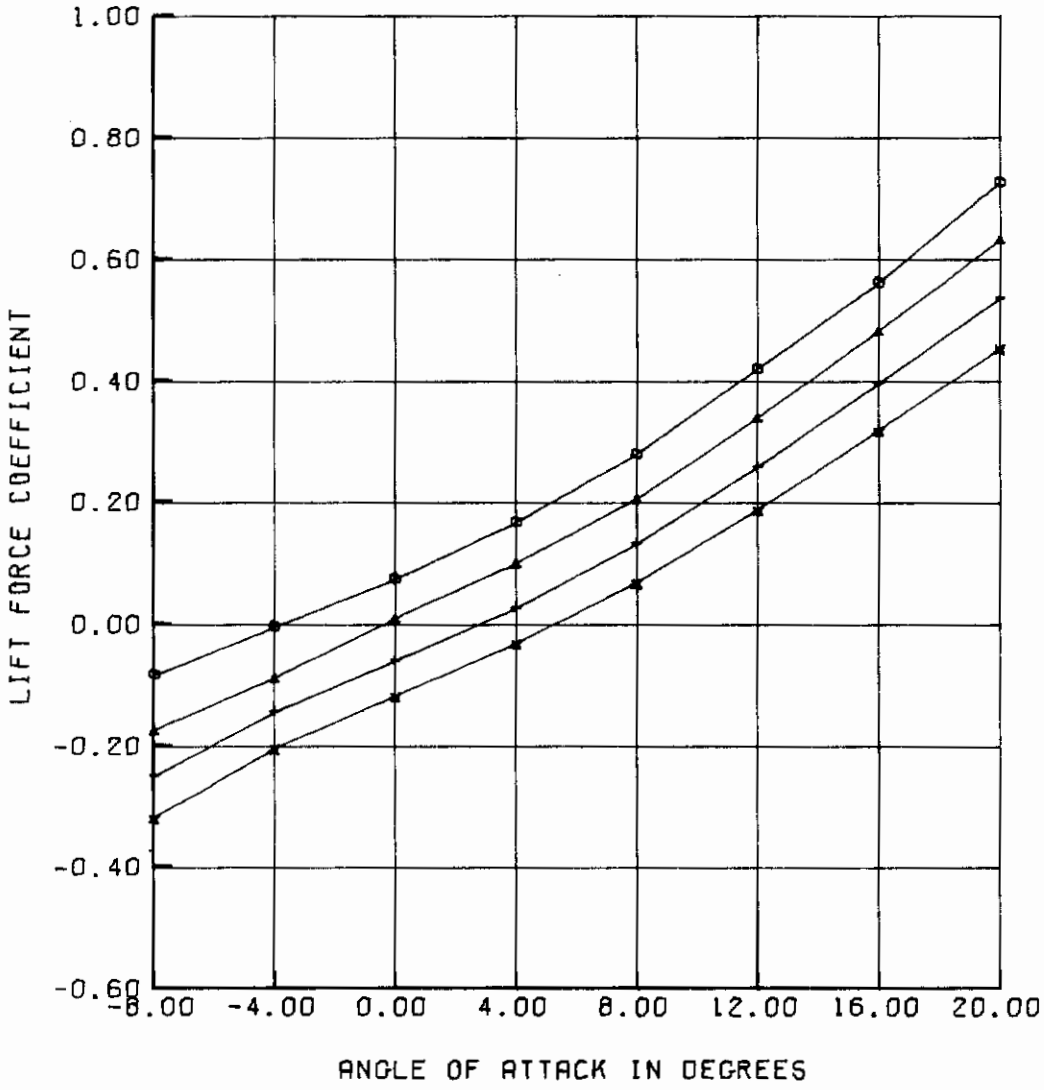


Figure 14. Control Surface Effects for Configuration S/50/10/0

| SYMBOL | FLAP DEFLECTION, DEG |
|---|---|
| ○ | 10 |
| △ | 0 |
| + | -10 |
| x | -20 |

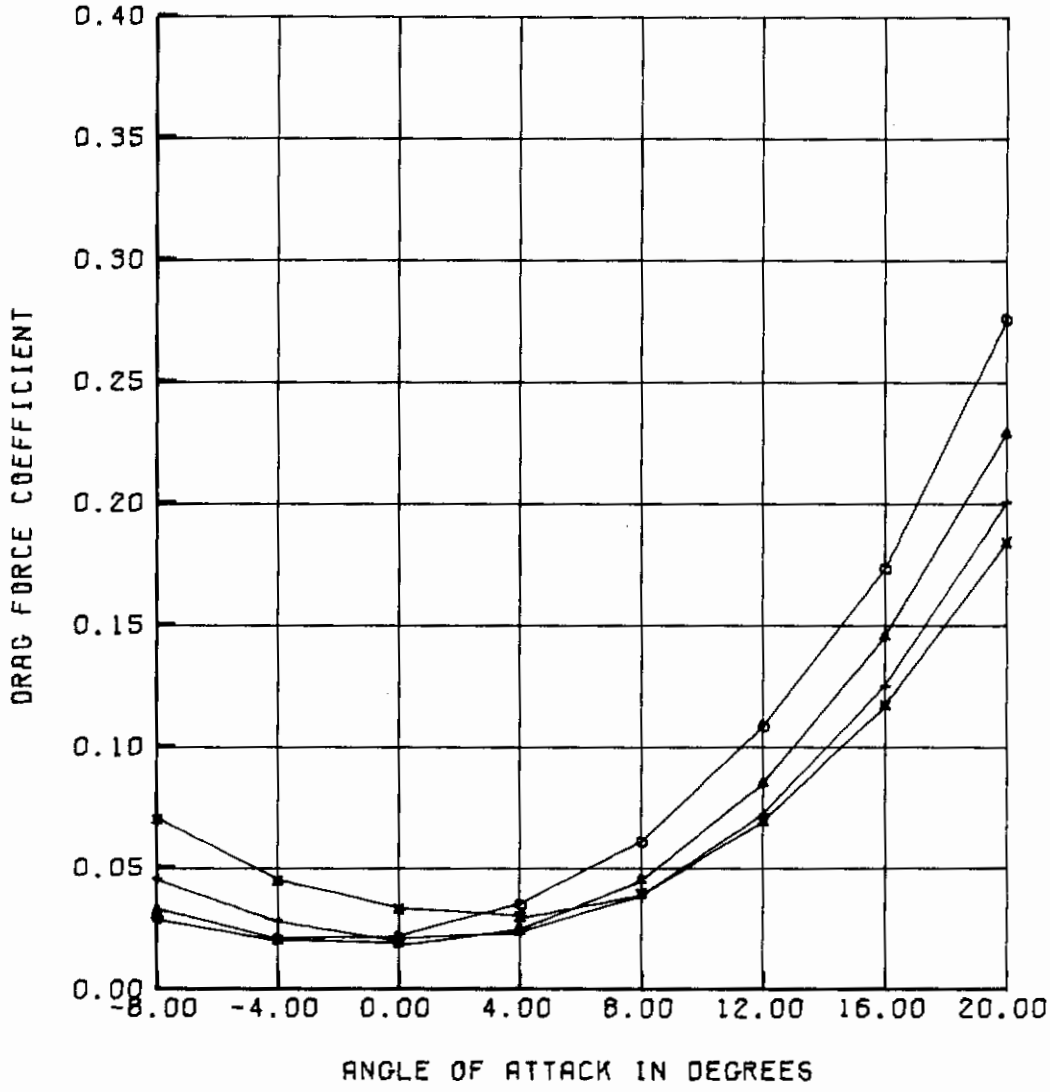


Figure 14. (Continued)

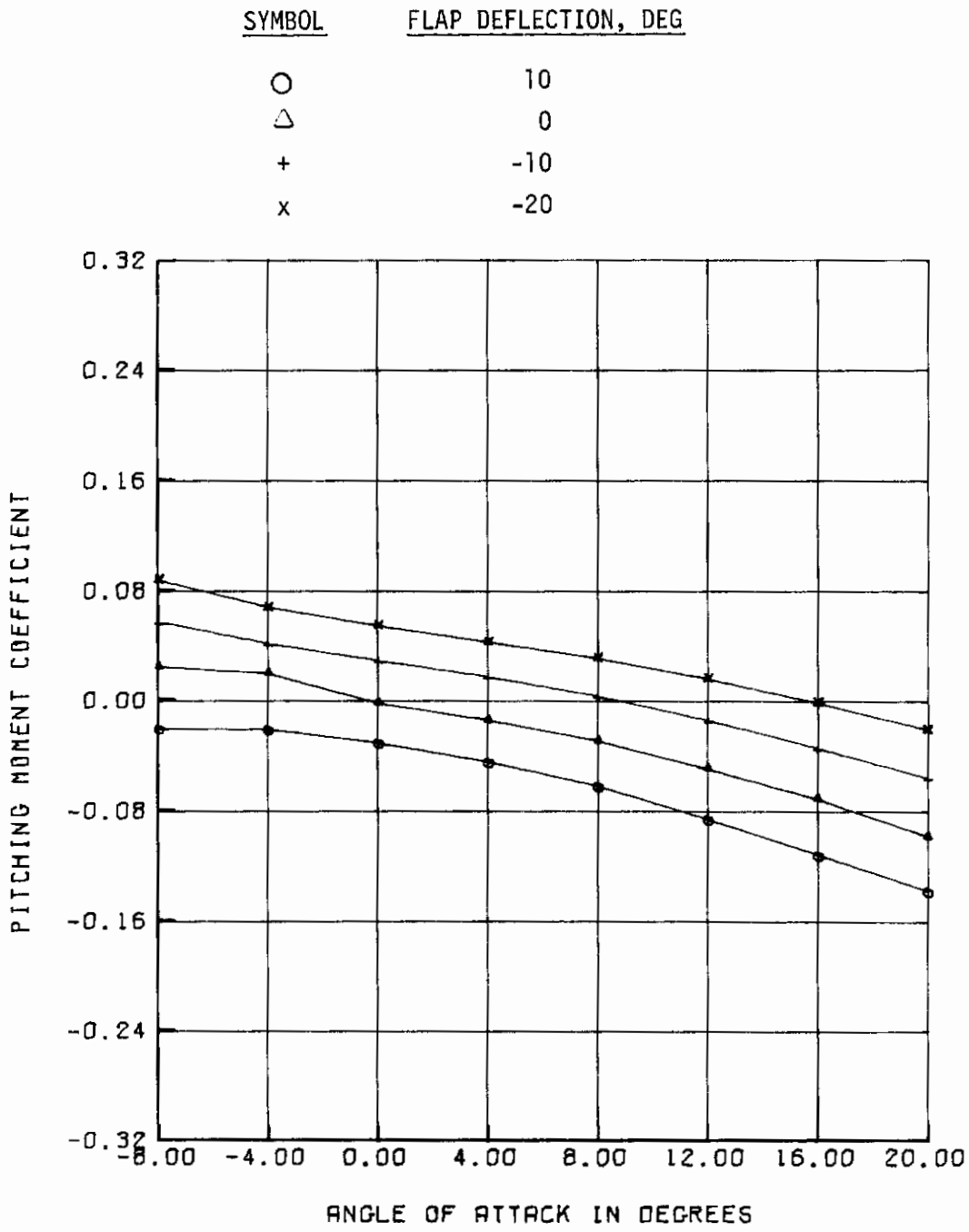


Figure 14. (Continued)

| SYMBOL | FLAP DEFLECTION, DEG |
|---|---|
| ○ | 10 |
| △ | 0 |
| + | -10 |
| x | -20 |

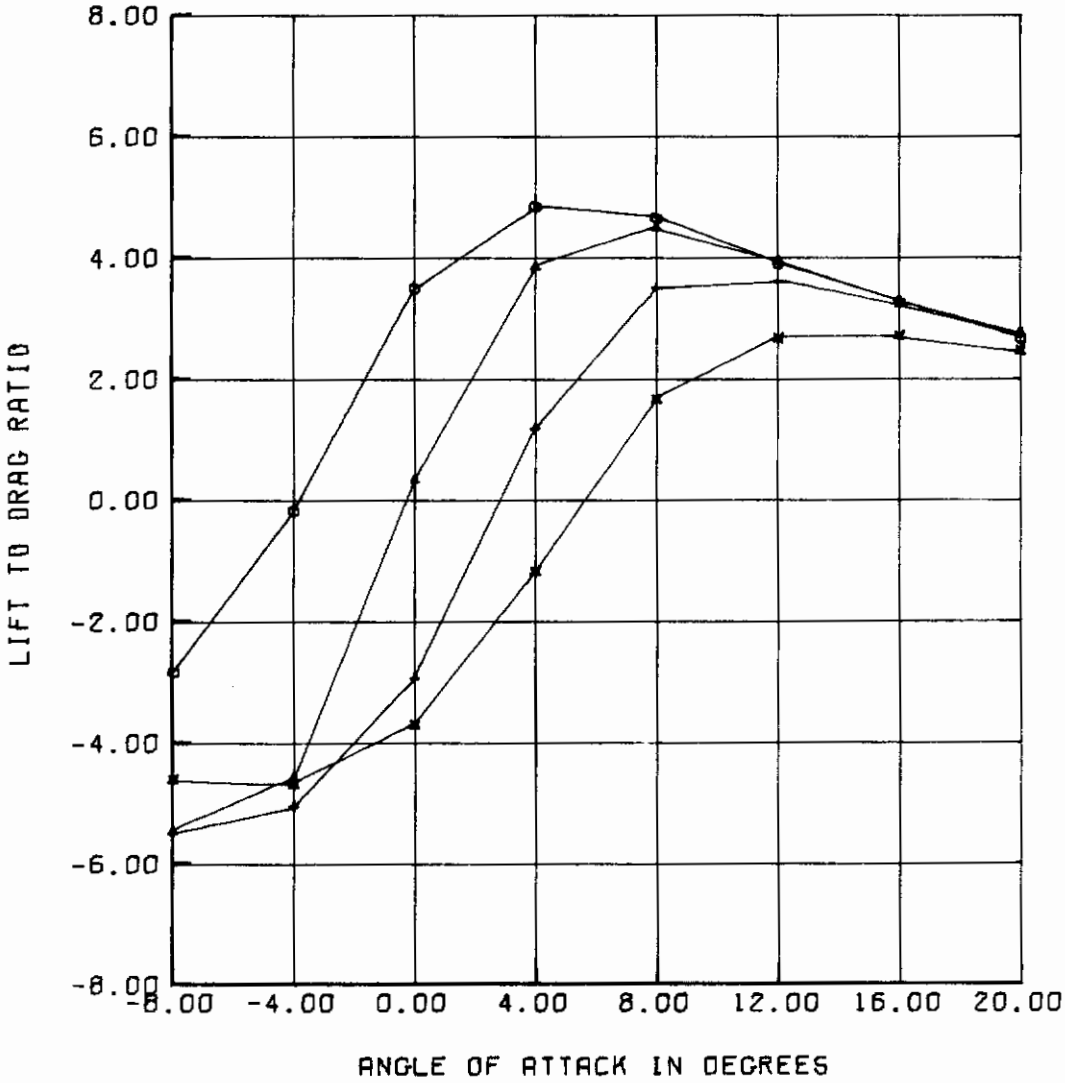


Figure 14. (Concluded)

| SYMBOL | FLAP DEFLECTION, DEG |
|---|---|
| ○ | 10 |
| △ | 0 |
| + | -10 |
| x | -20 |

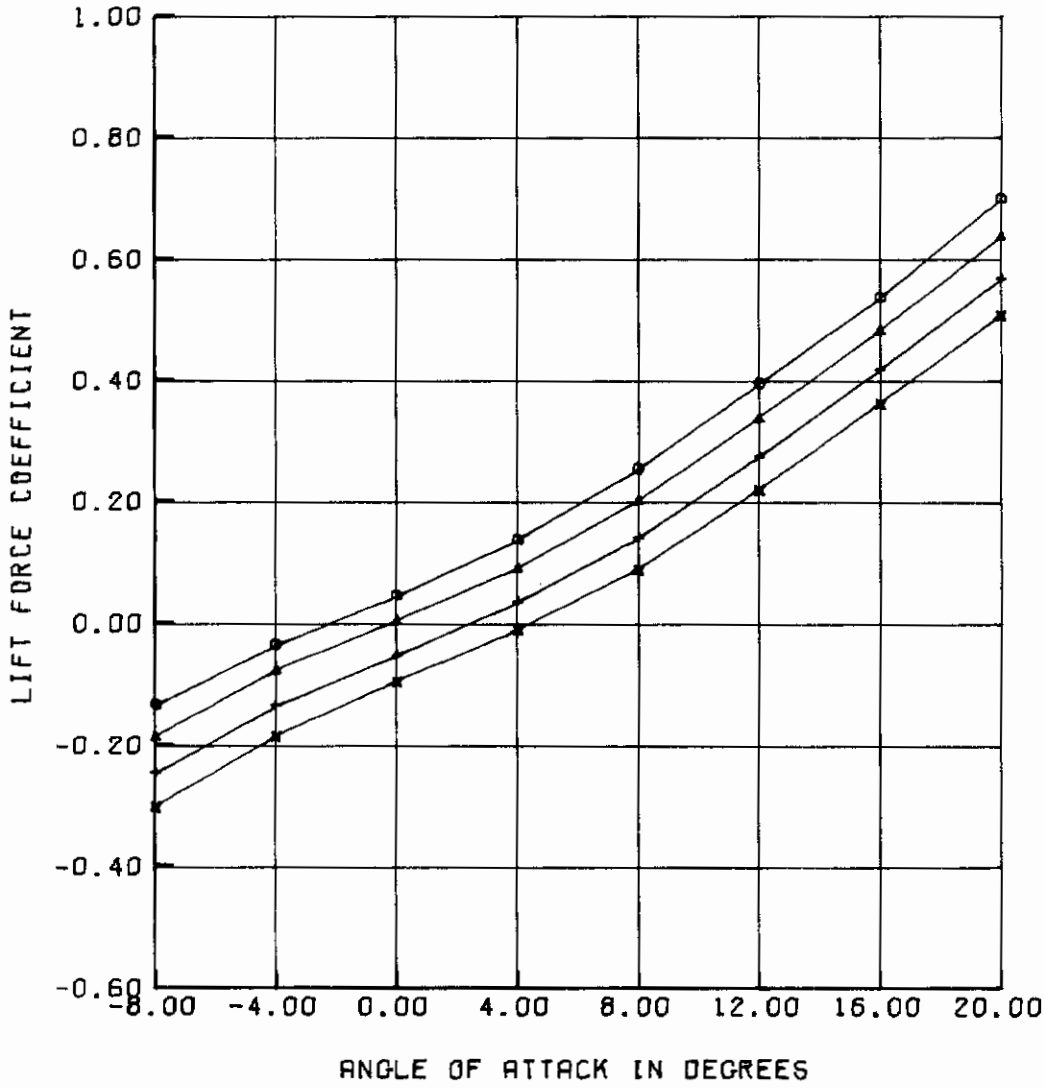


Figure 15. Control Surface Effects for Configuration S/50/10/25

| SYMBOL | FLAP DEFLECTION, DEG |
|---|---|
| ○ | 10 |
| △ | 0 |
| + | -10 |
| x | -20 |

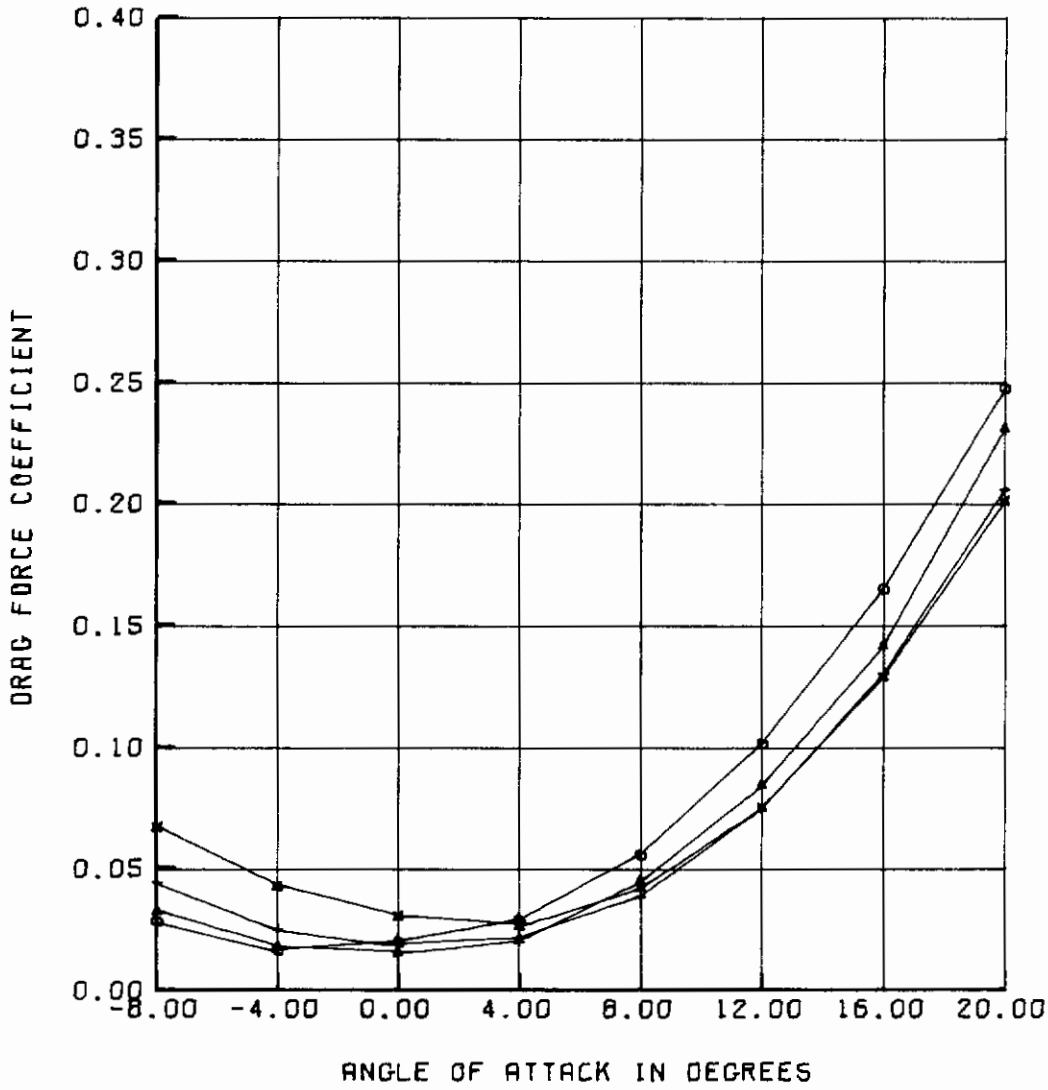


Figure 15. (Continued)

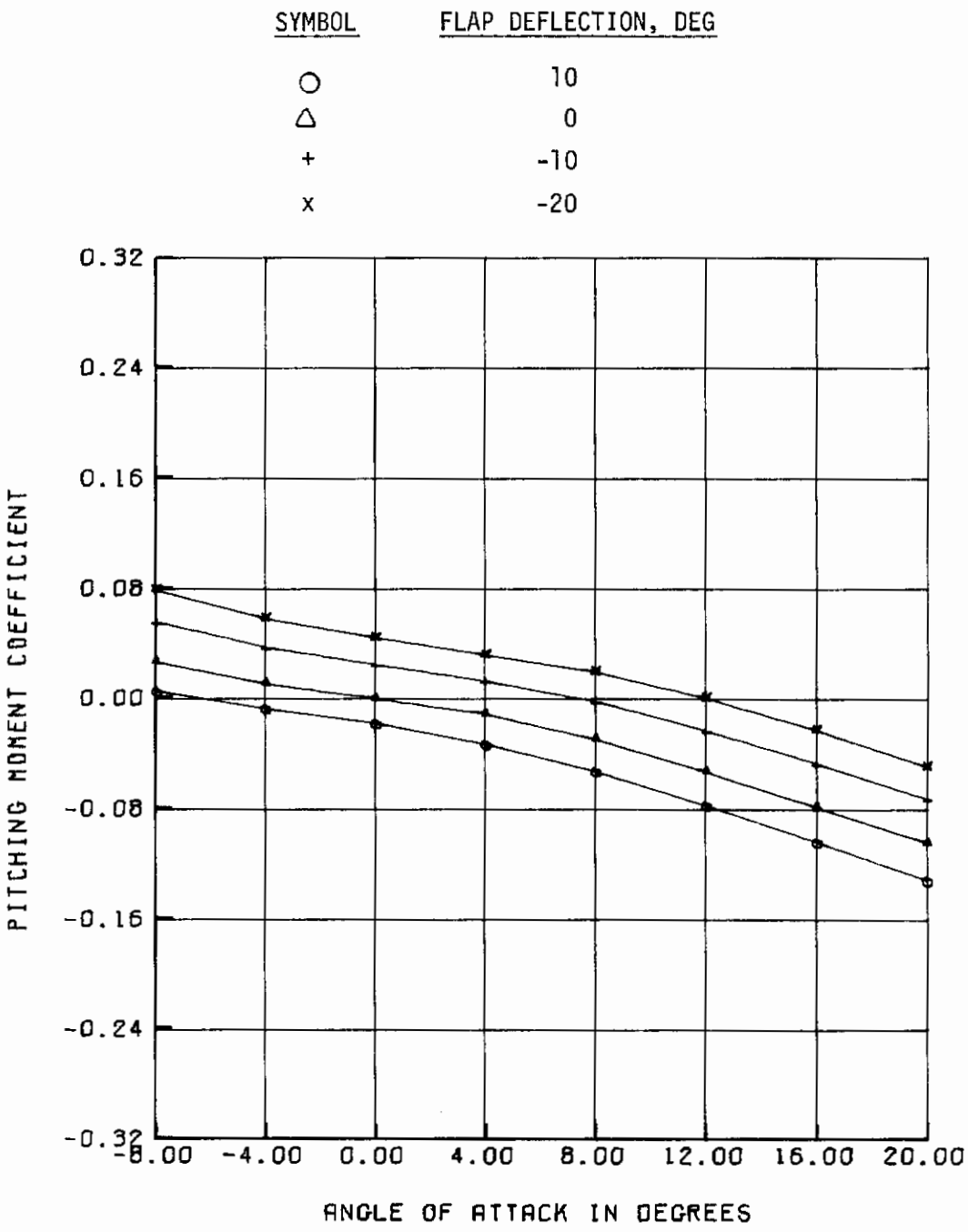


Figure 15. (Continued)

| SYMBOL | FLAP DEFLECTION, DEG |
|---|---|
| ○ | 10 |
| △ | 0 |
| + | -10 |
| x | -20 |

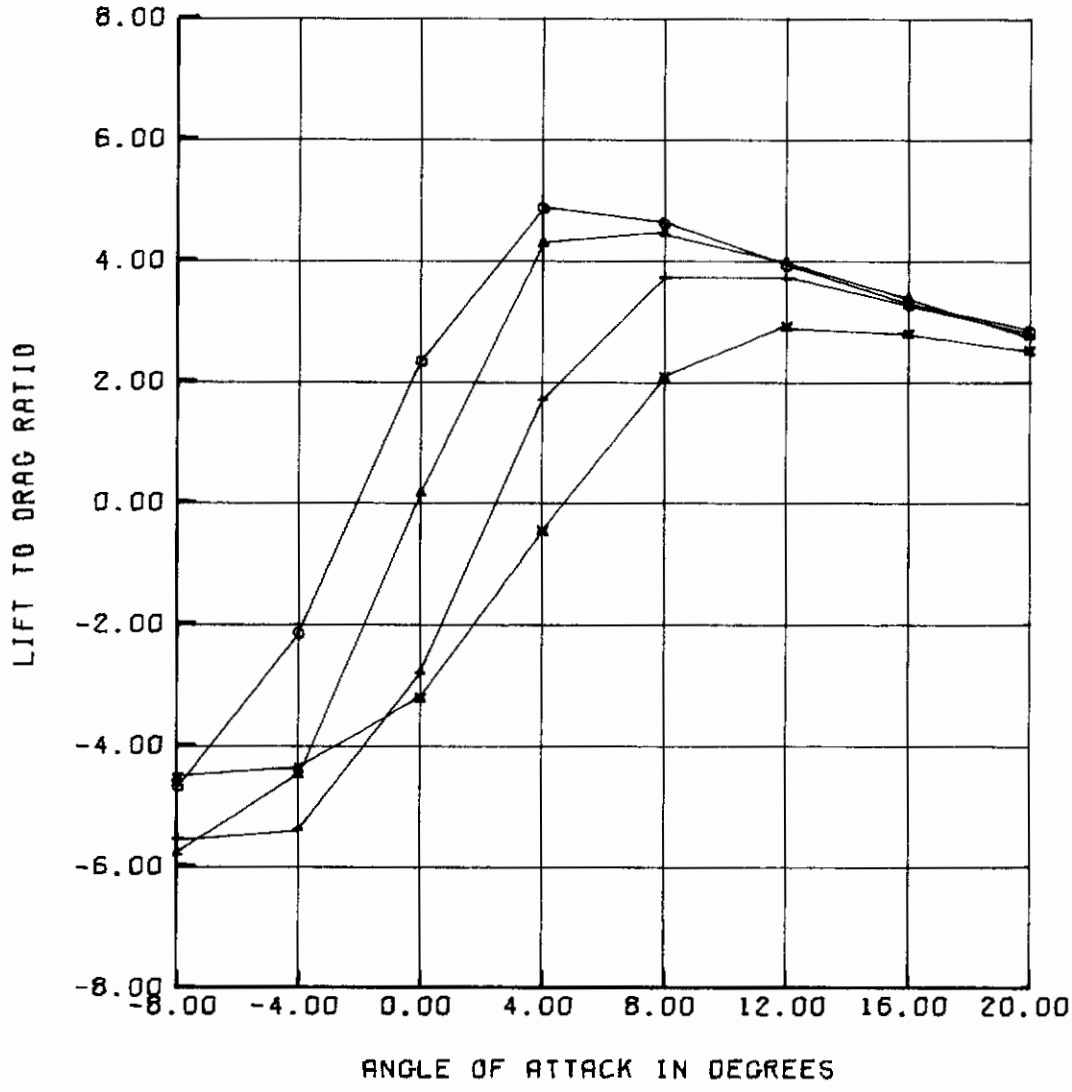


Figure 15. (Concluded)

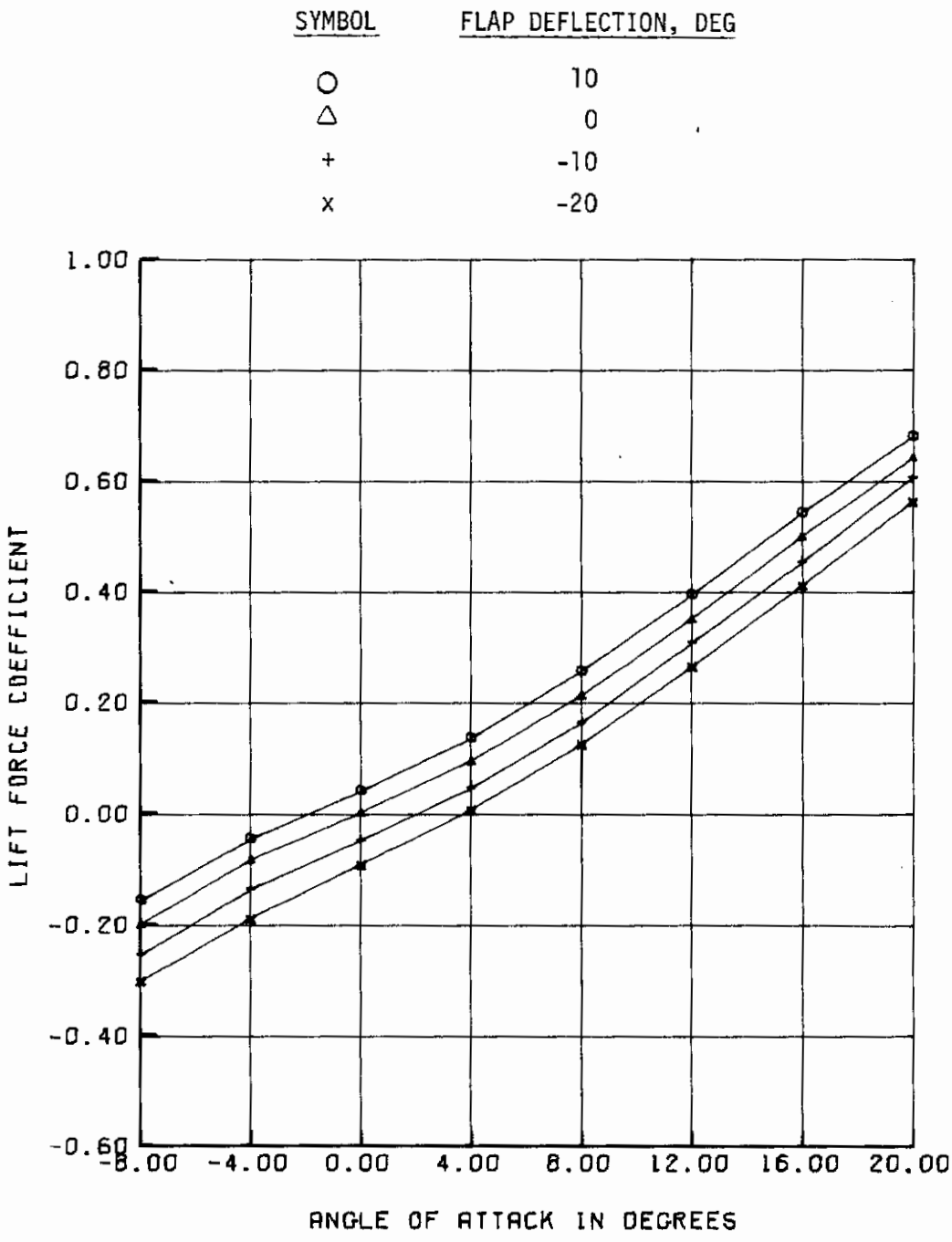


Figure 16. Control Surface Effects for Configuration S/50/10/50

| SYMBOL | FLAP DEFLECTION, DEG |
|---|---|
| ○ | 10 |
| △ | 0 |
| + | -10 |
| x | -20 |

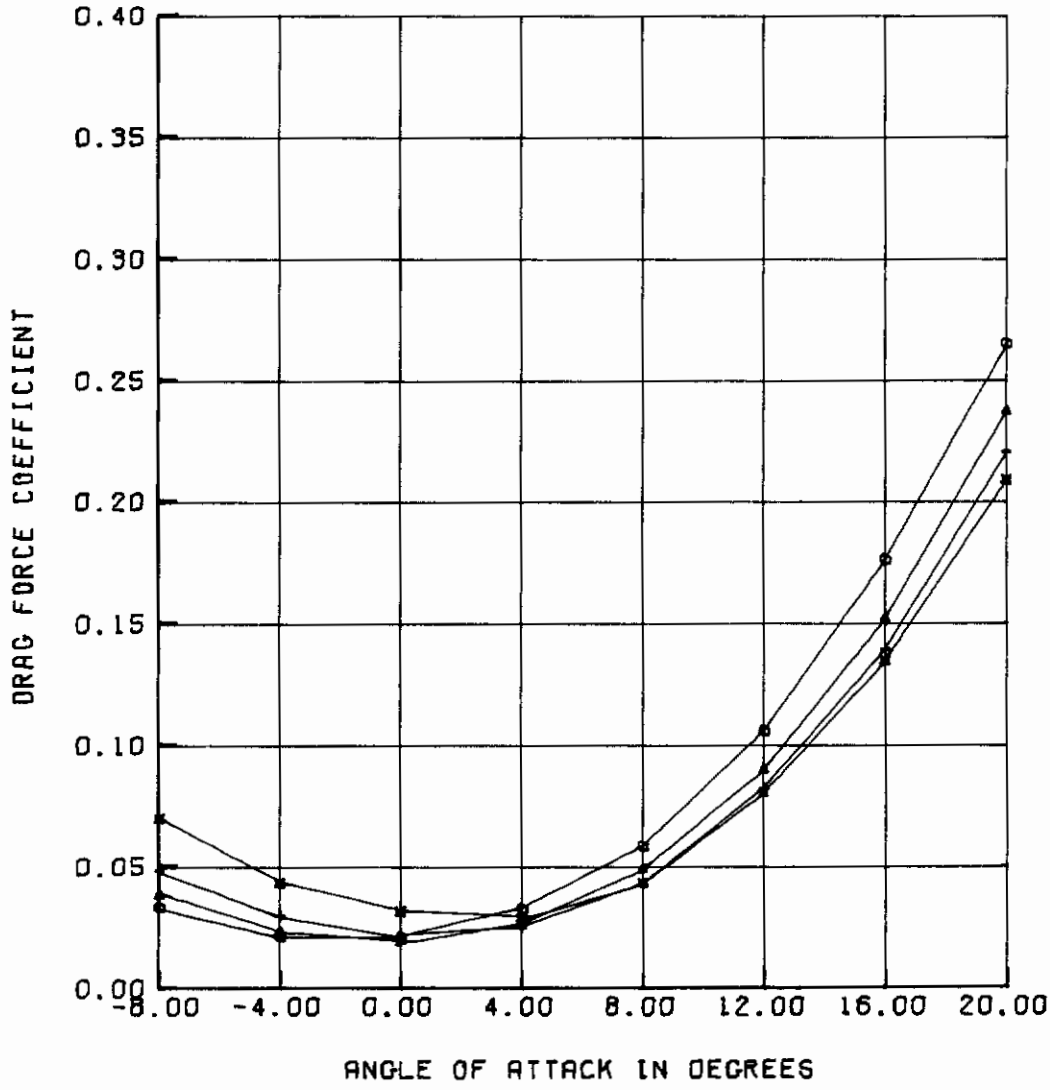


Figure 16. (Continued)

| SYMBOL | FLAP DEFLECTION, DEG |
|---|---|
| ○ | 10 |
| △ | 0 |
| + | -10 |
| x | -20 |

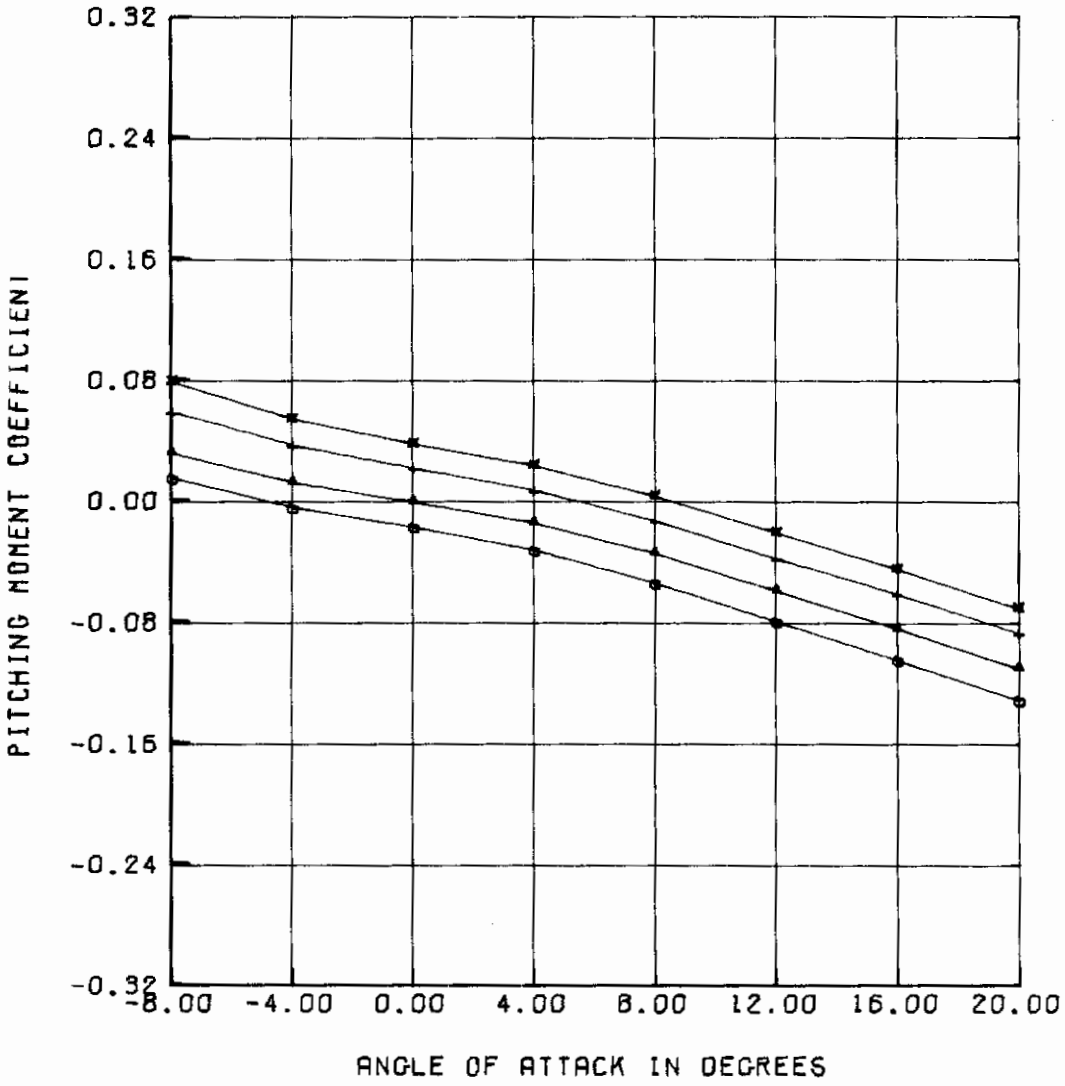


Figure 16. (Continued)

| SYMBOL | FLAP DEFLECTION, DEG |
|---|---|
| ○ | 10 |
| △ | 0 |
| + | -10 |
| x | -20 |

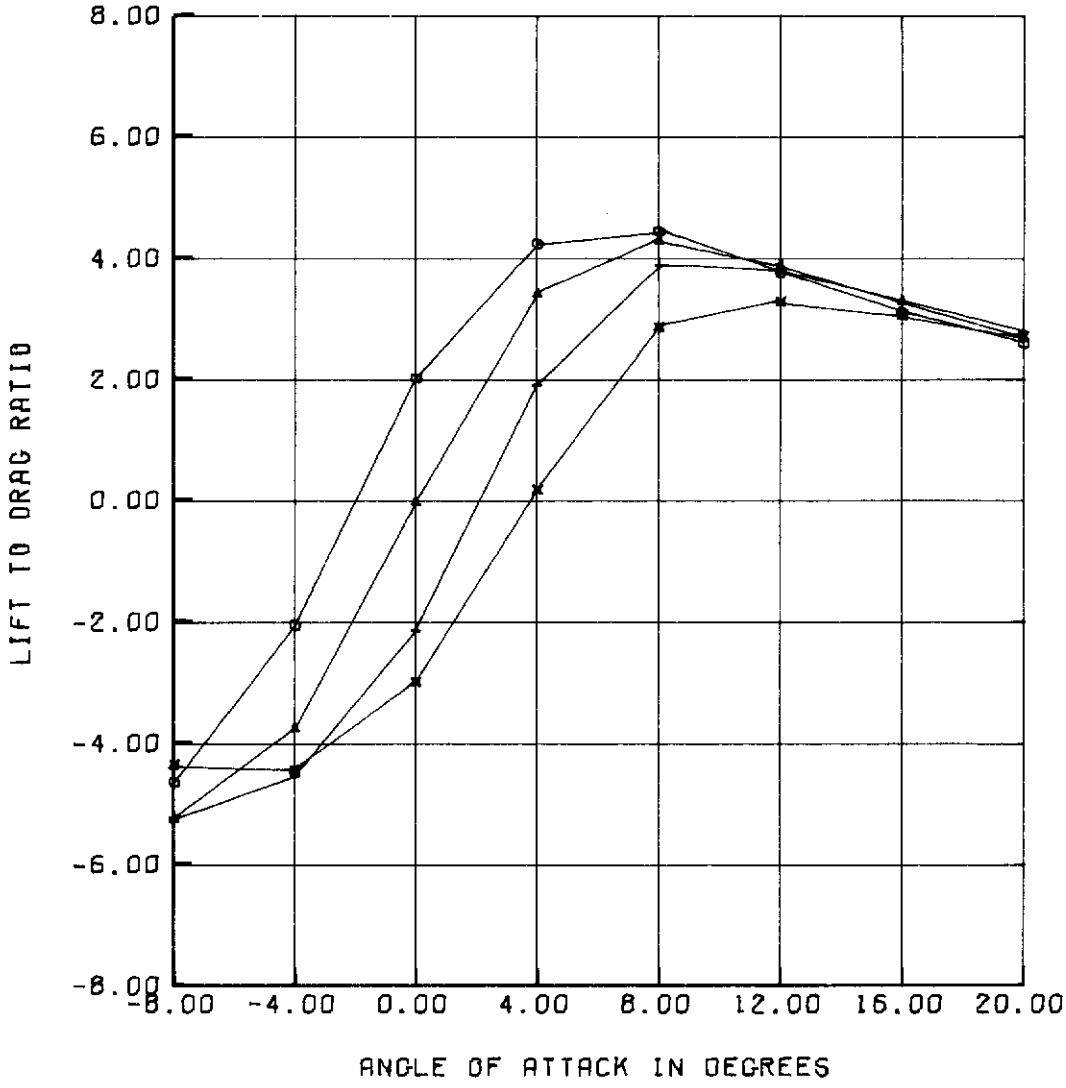


Figure 16. (Concluded)

| SYMBOL | FLAP DEFLECTION, DEG |
|---|---|
| ○ | 10 |
| △ | 0 |
| + | -10 |
| x | -20 |

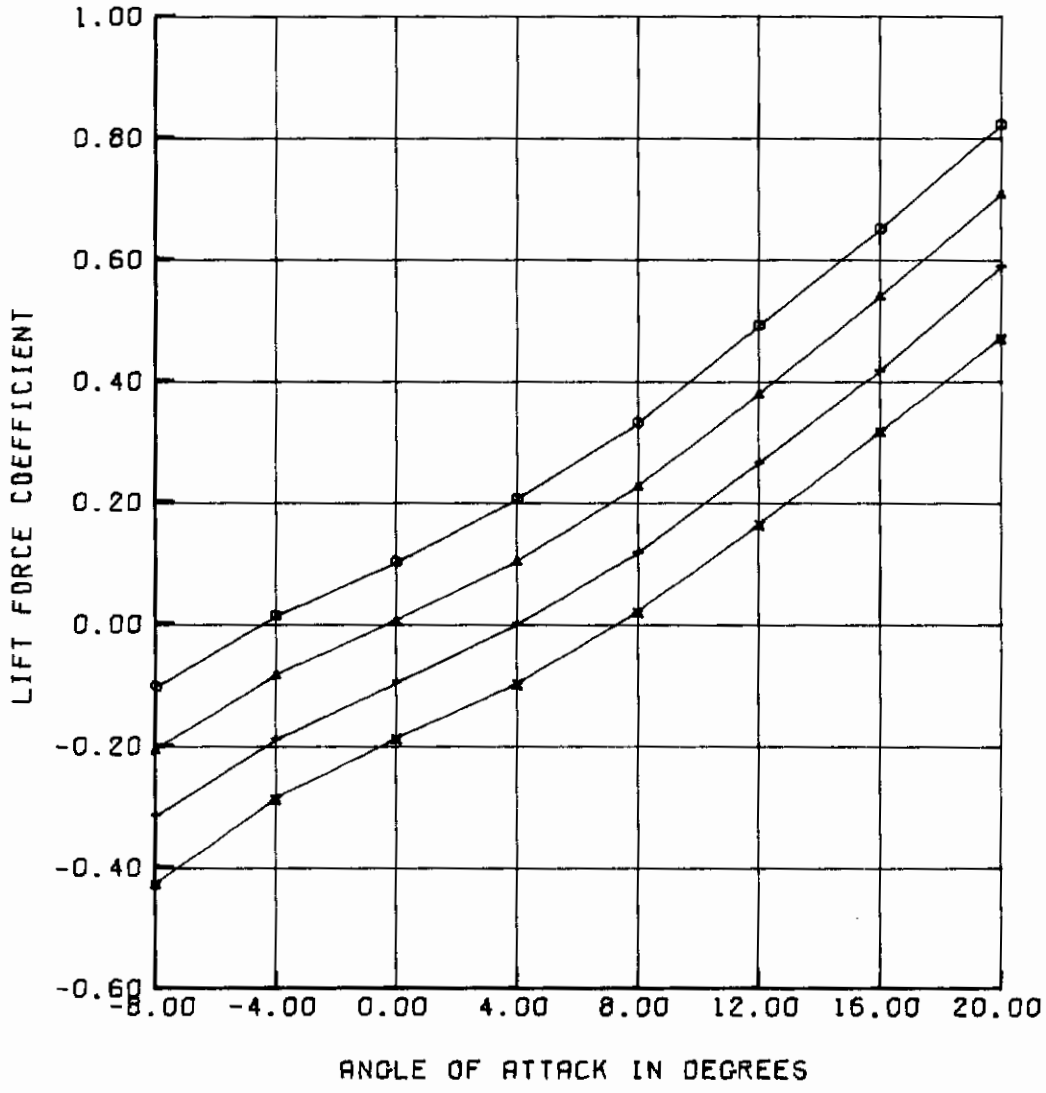


Figure 17. Control Surface Effects for Configuration D/75/25/10, Inner Flap Fixed

| SYMBOL | FLAP DEFLECTION, DEG |
|---|---|
| ○ | 10 |
| △ | 0 |
| + | -10 |
| x | -20 |

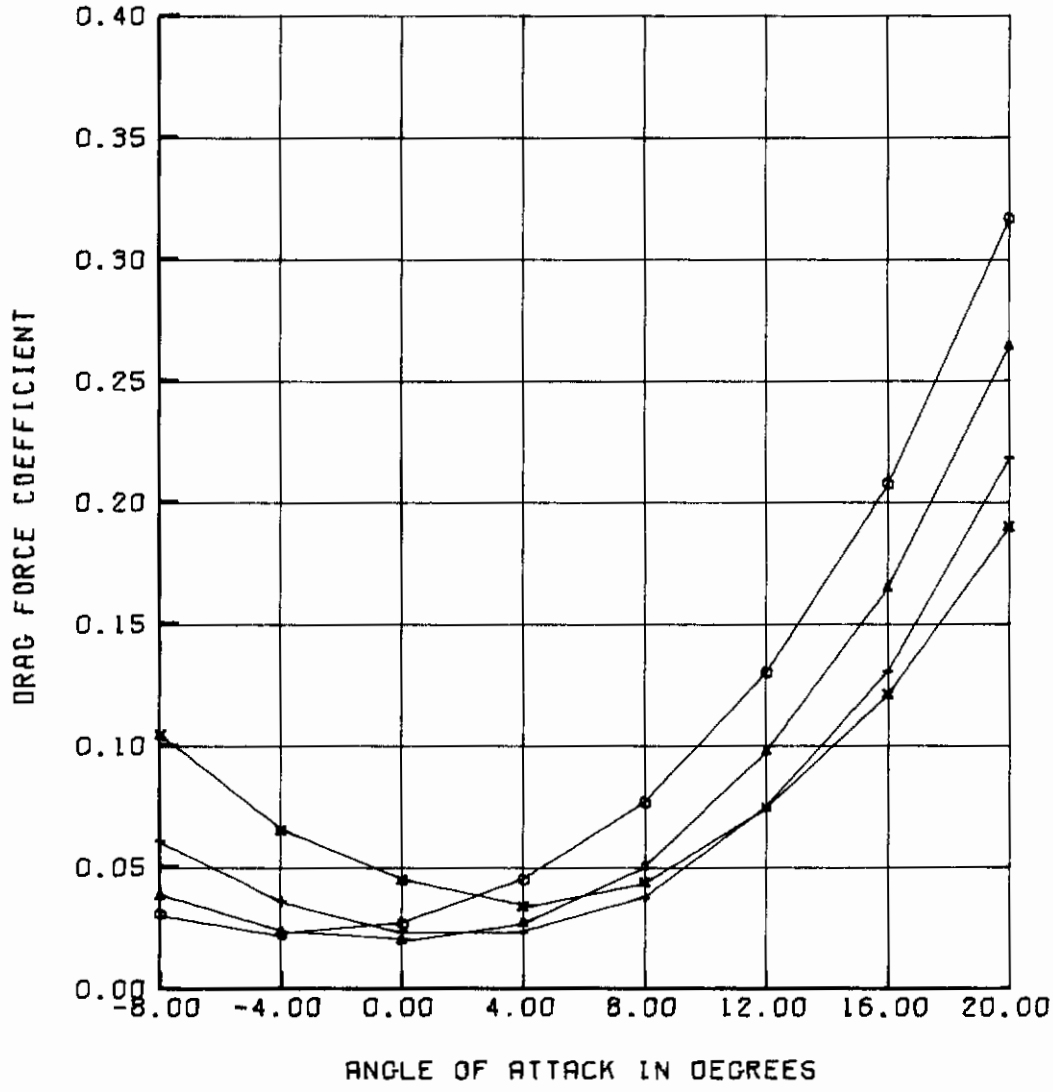


Figure 17. (Continued)

| SYMBOL | FLAP DEFLECTION, DEG |
|---|---|
| ○ | 10 |
| △ | 0 |
| + | -10 |
| x | -20 |

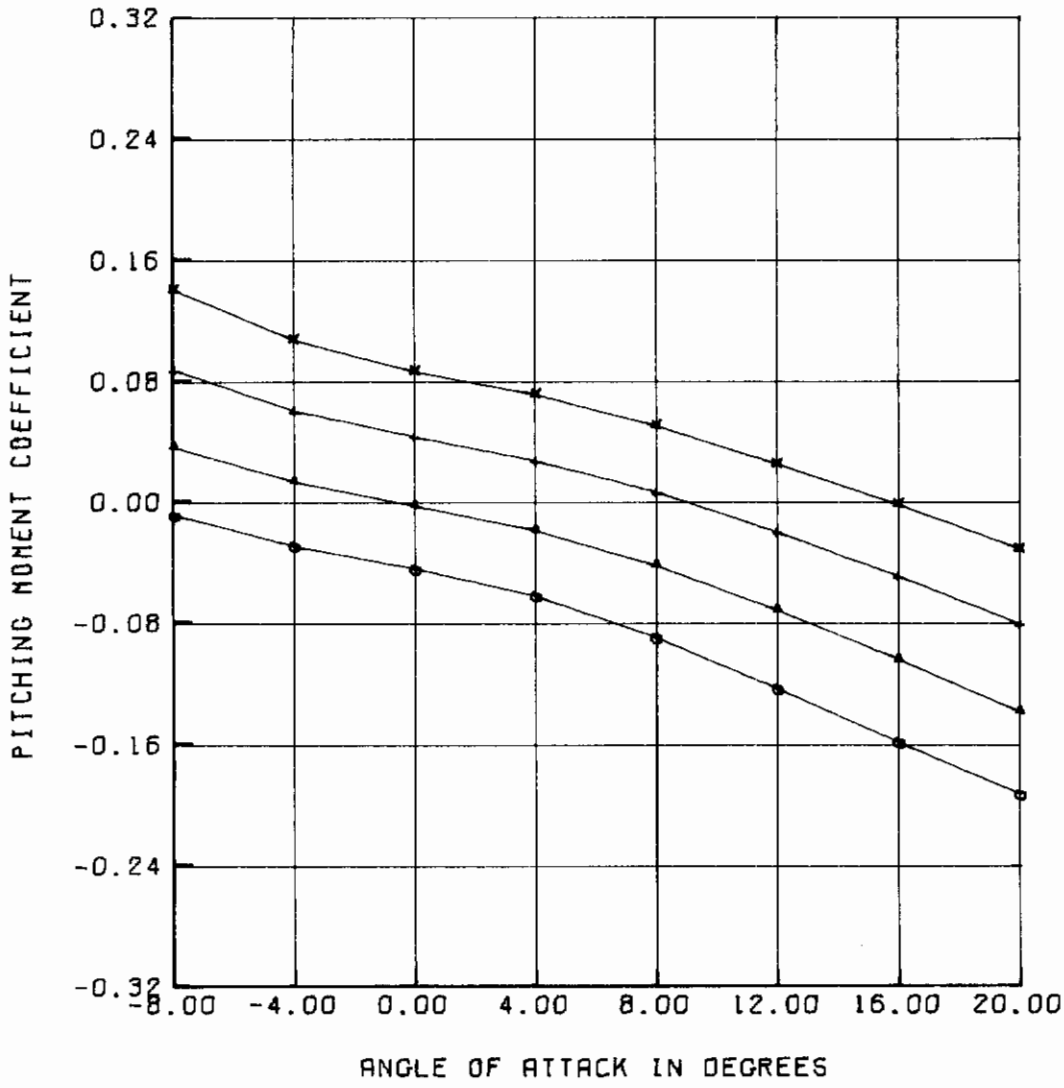


Figure 17. (Continued)

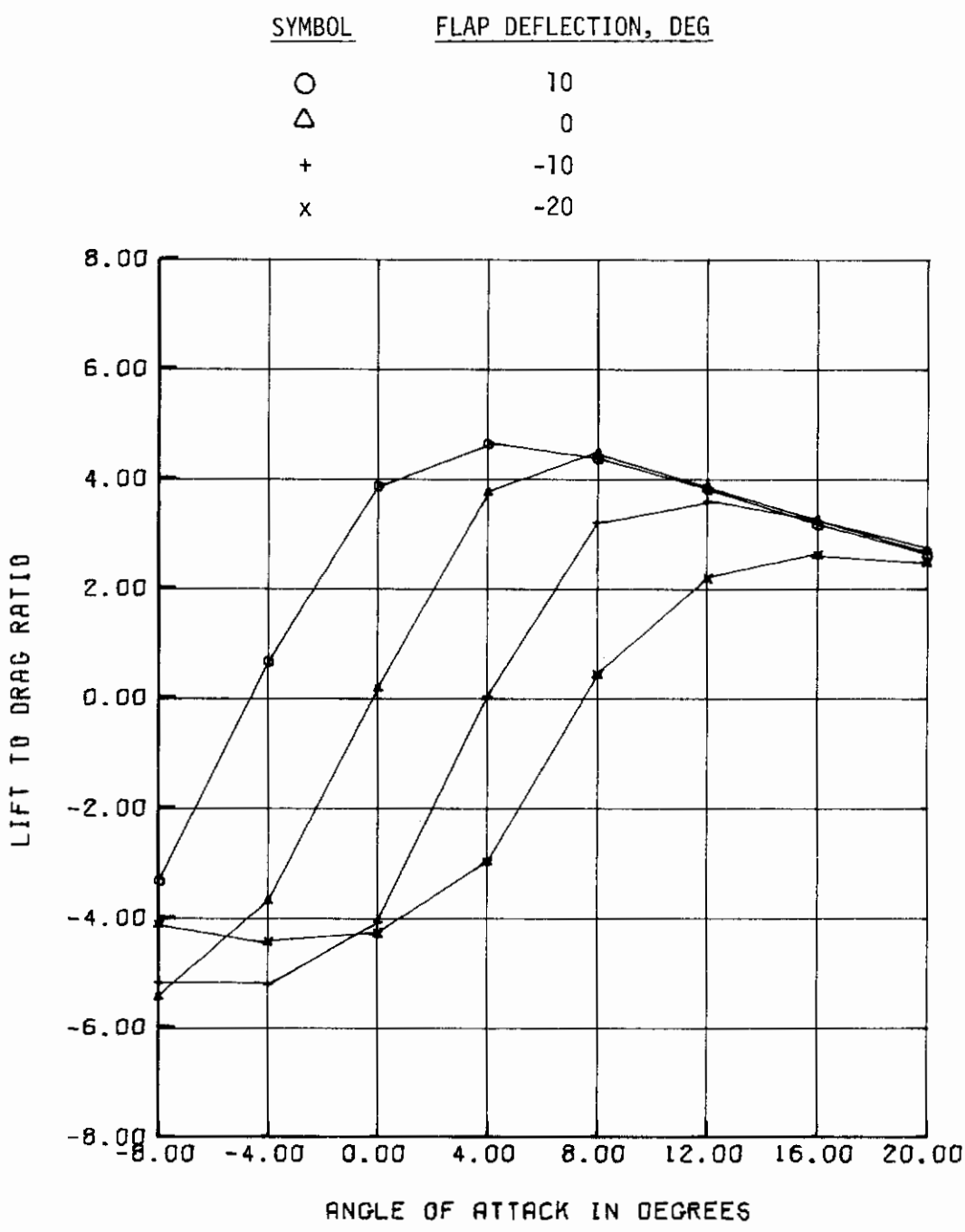


Figure 17. (Concluded)

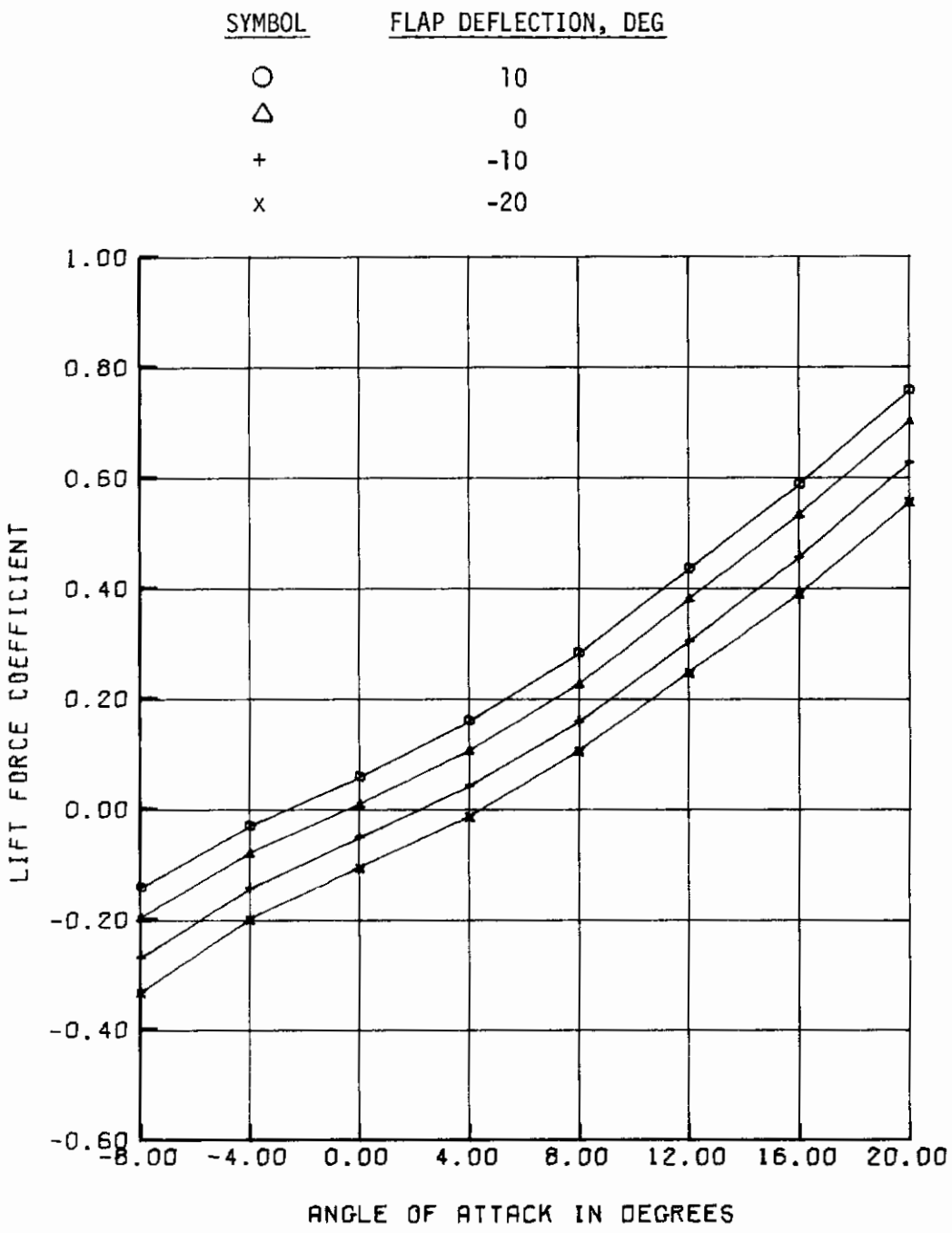


Figure 18. Control Surface Effects for Configuration D/50/50/10, Inner Flap Fixed

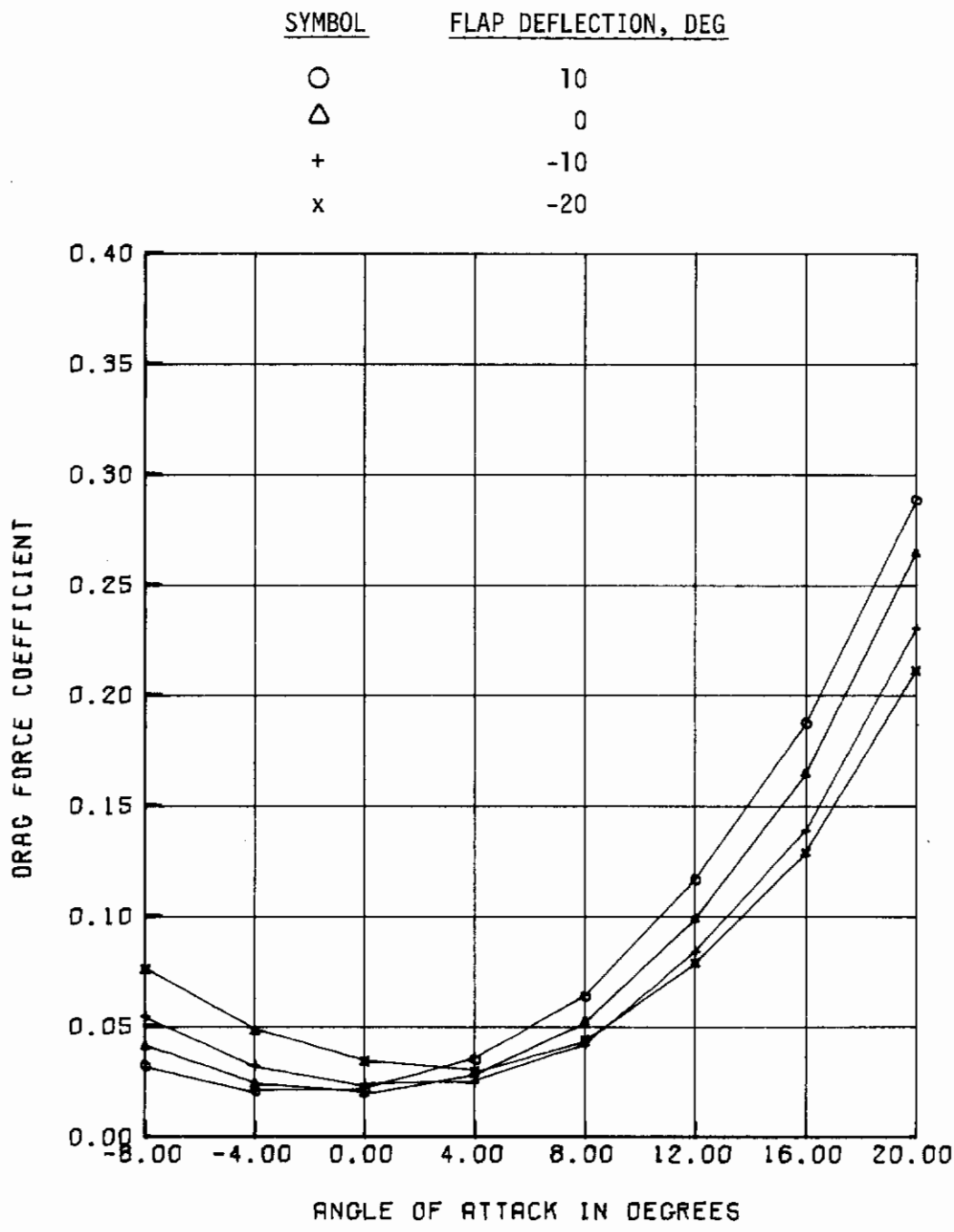


Figure 18. (Continued)

| SYMBOL | FLAP DEFLECTION, DEG |
|---|---|
| ○ | 10 |
| △ | 0 |
| + | -10 |
| x | -20 |

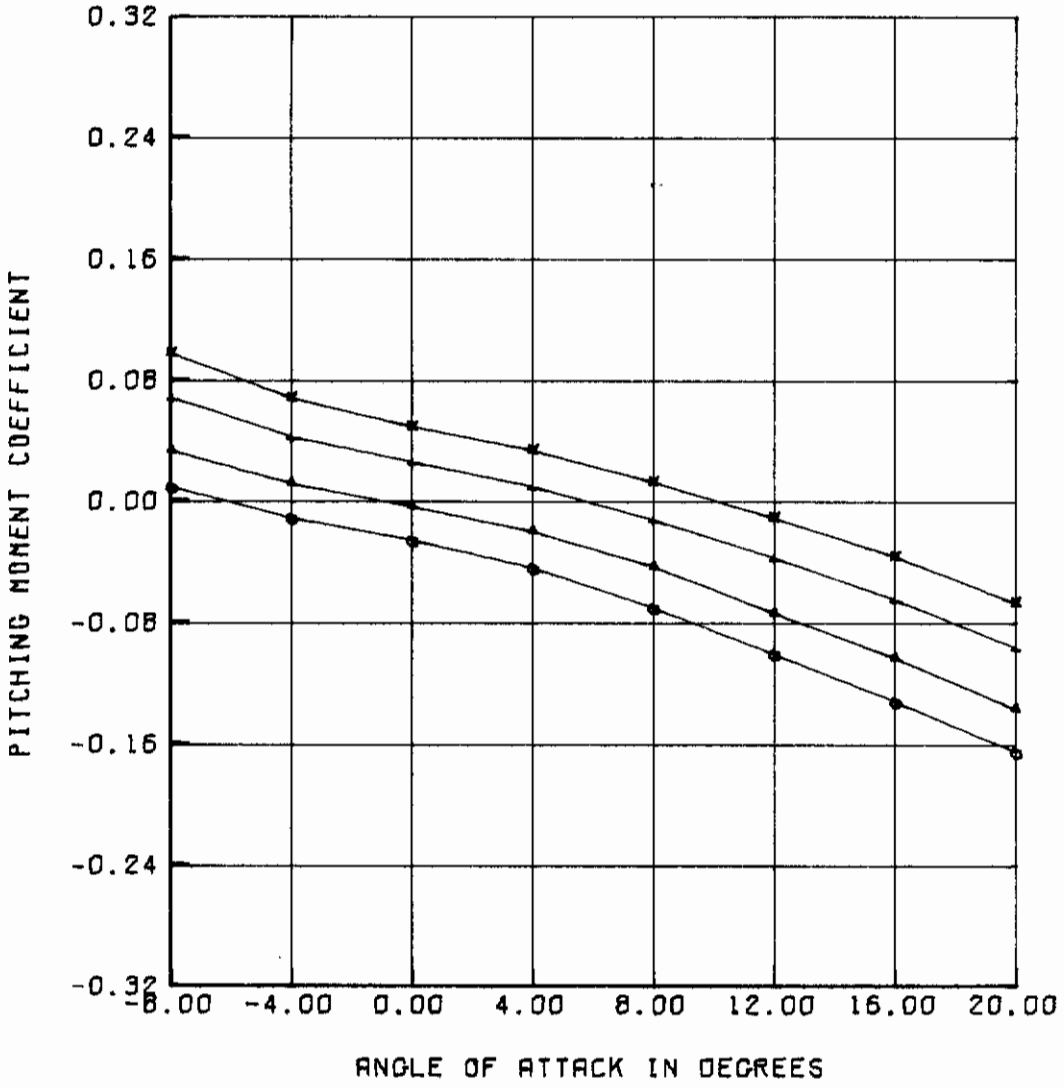


Figure 18. (Continued)

| SYMBOL | FLAP DEFLECTION, DEG |
|---|---|
| ○ | 10 |
| △ | 0 |
| + | -10 |
| x | -20 |

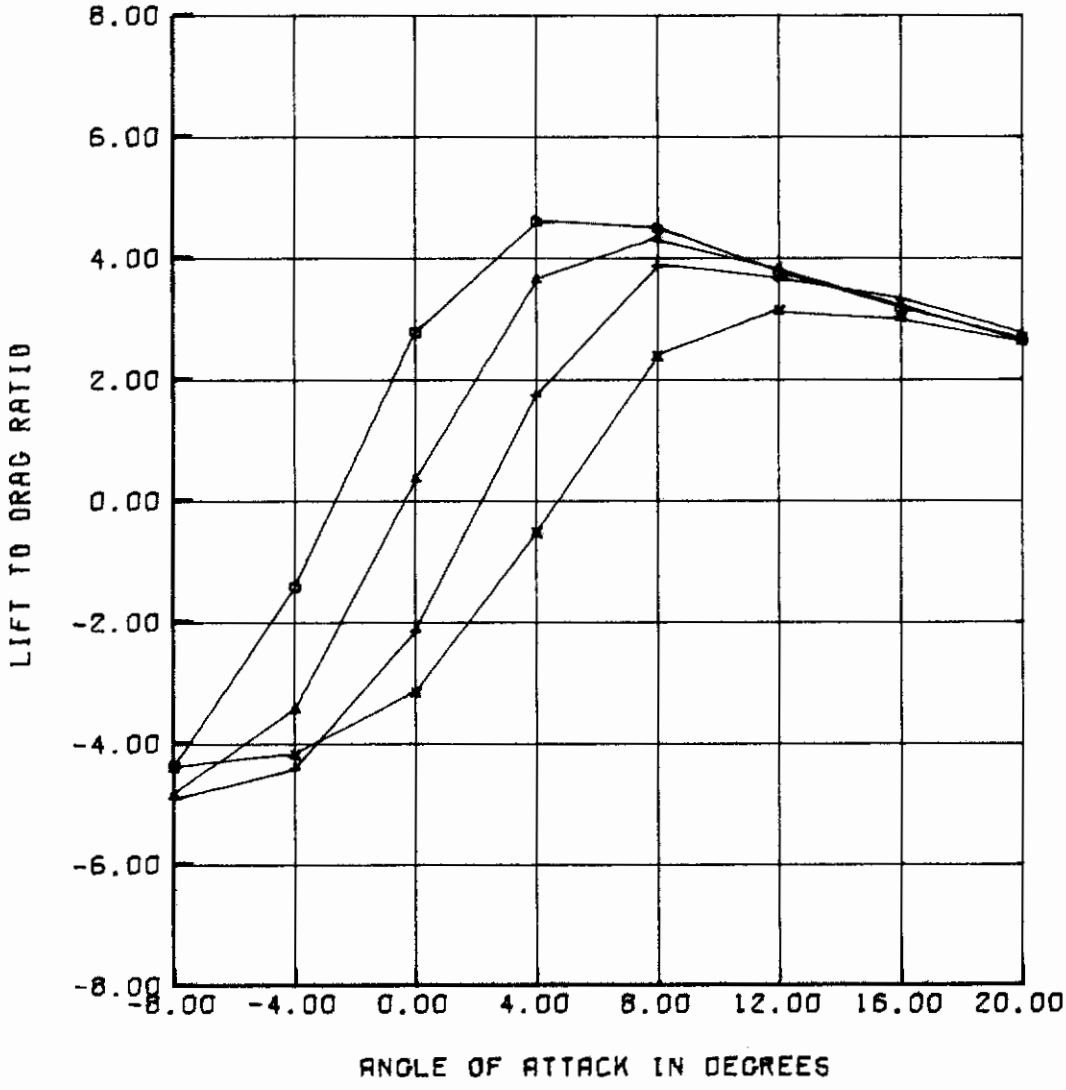


Figure 18. (Concluded)

| SYMBOL | FLAP DEFLECTION, DEG |
|---|---|
| ○ | 10 |
| △ | 0 |
| + | -10 |
| x | -20 |

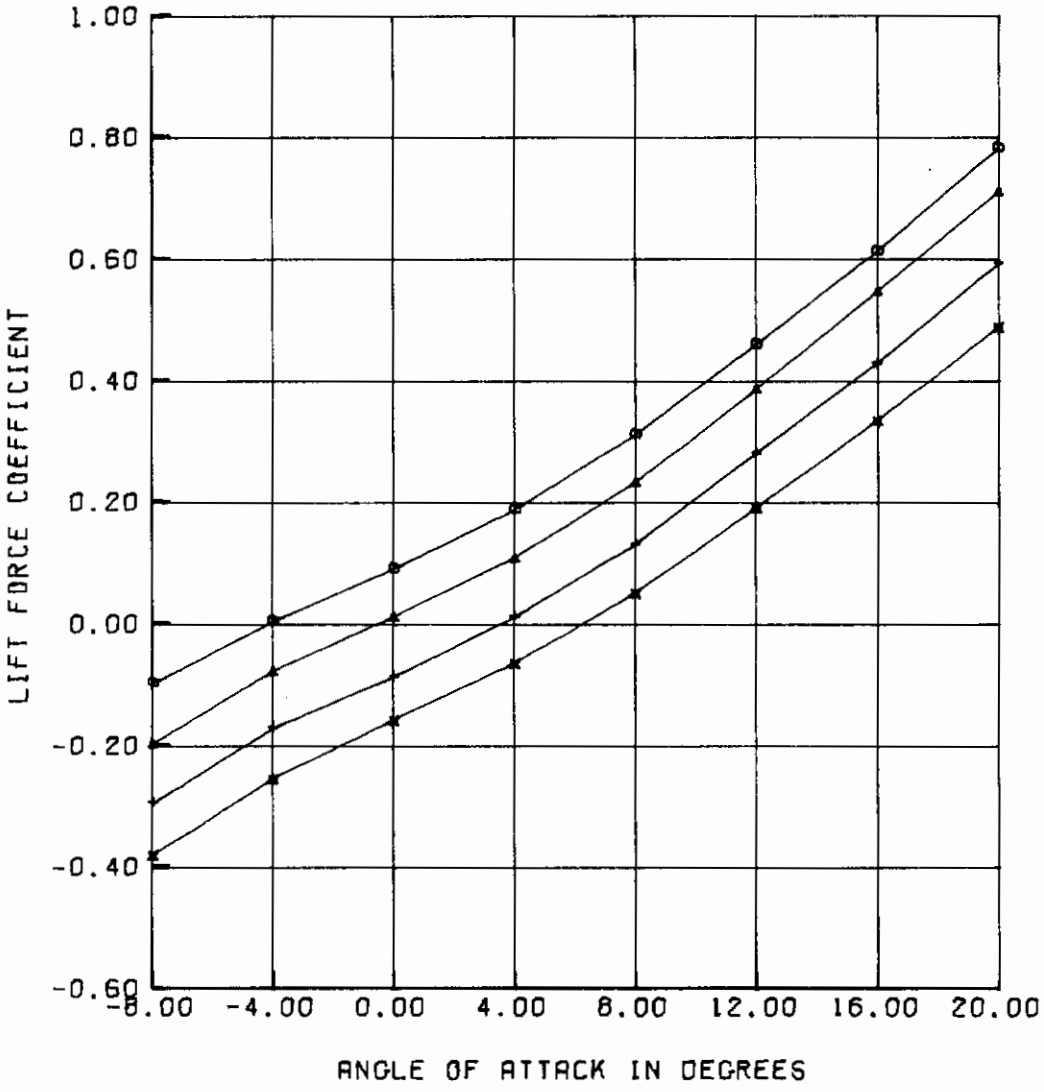


Figure 19. Control Surface Effects for Configuration D/50/50/10, Outer Flap Fixed

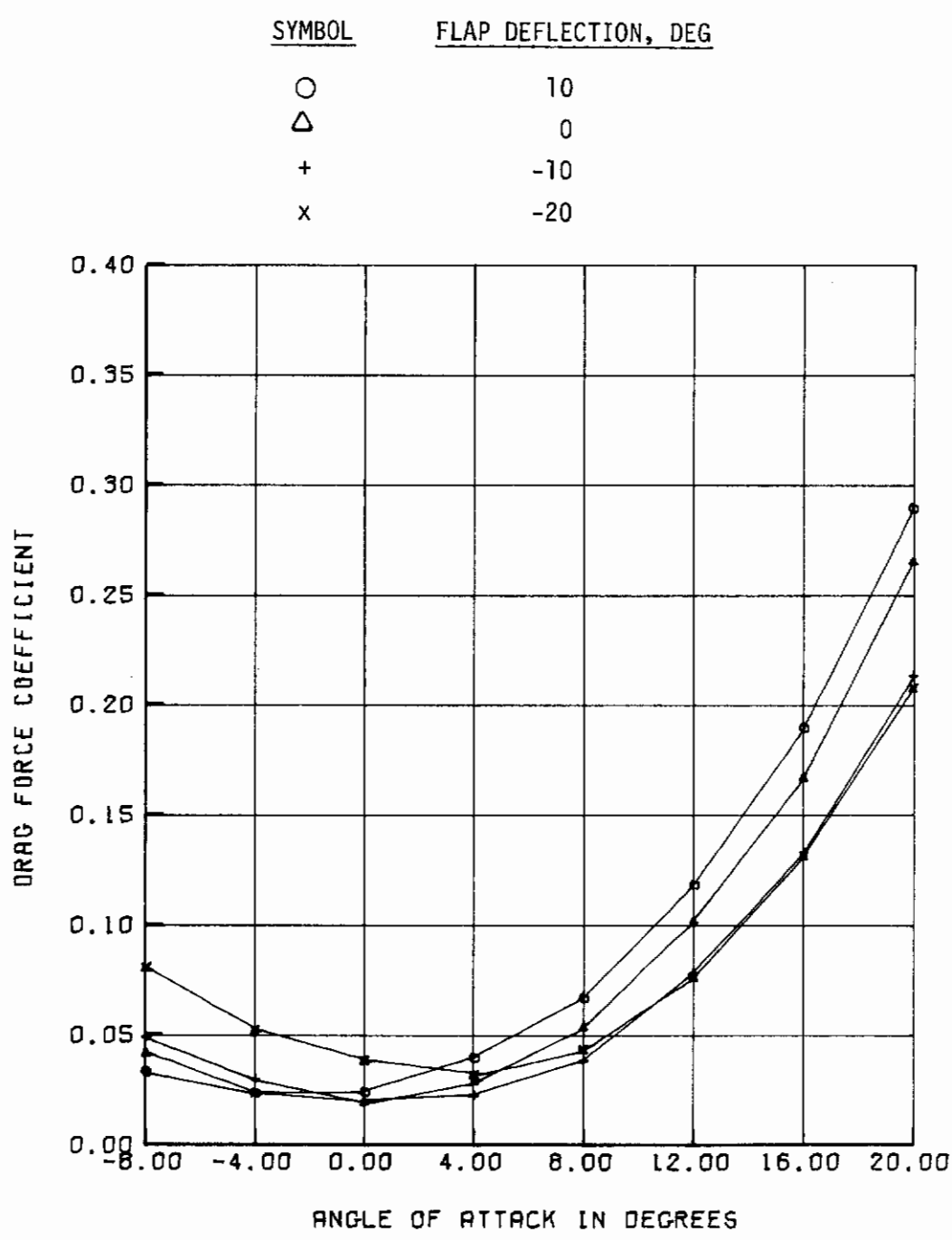


Figure 19. (Continued)

| SYMBOL | FLAP DEFLECTION, DEG |
|---|---|
| ○ | 10 |
| △ | 0 |
| + | -10 |
| x | -20 |

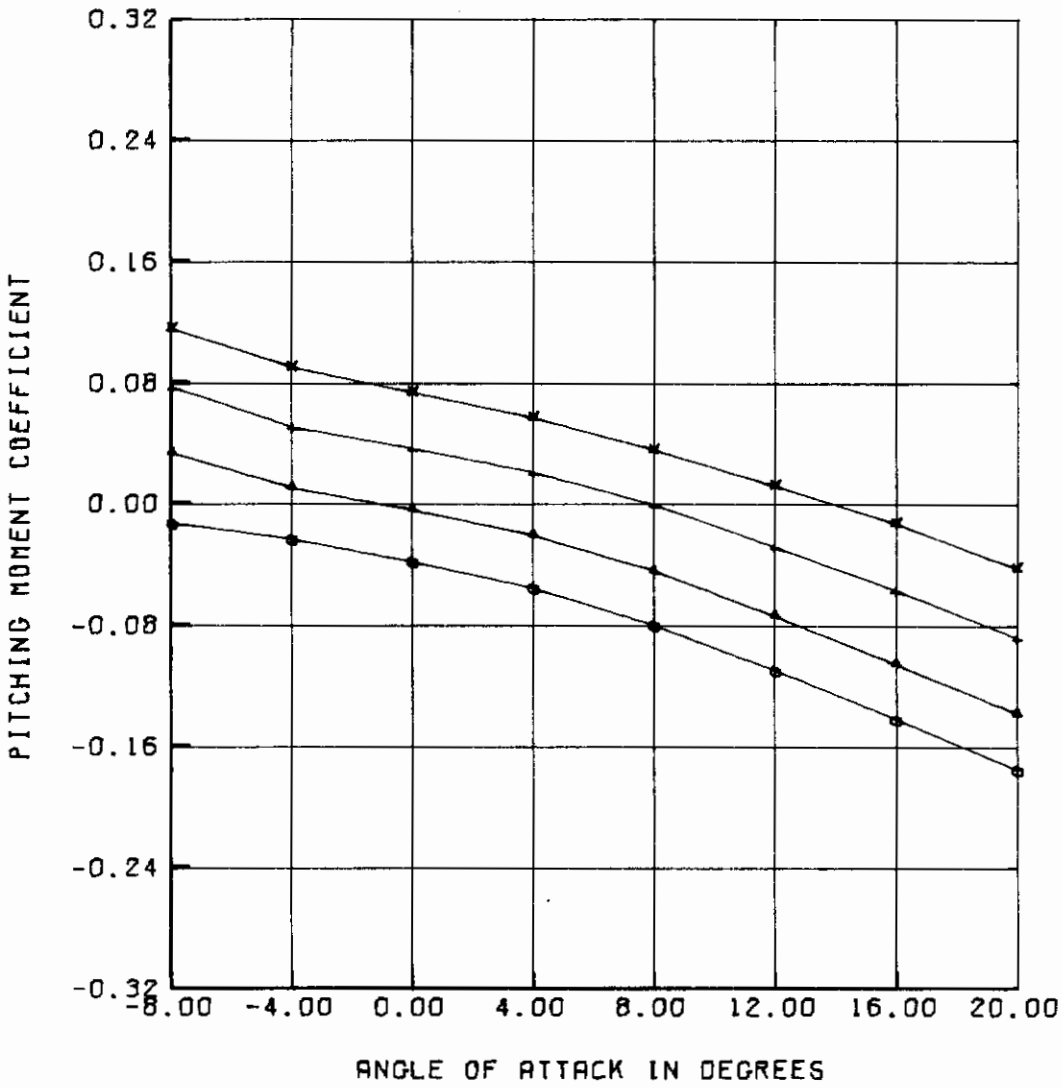


Figure 19. (Continued)

| SYMBOL | FLAP DEFLECTION, DEG |
|---|---|
| ○ | 10 |
| △ | 0 |
| + | -10 |
| x | -20 |

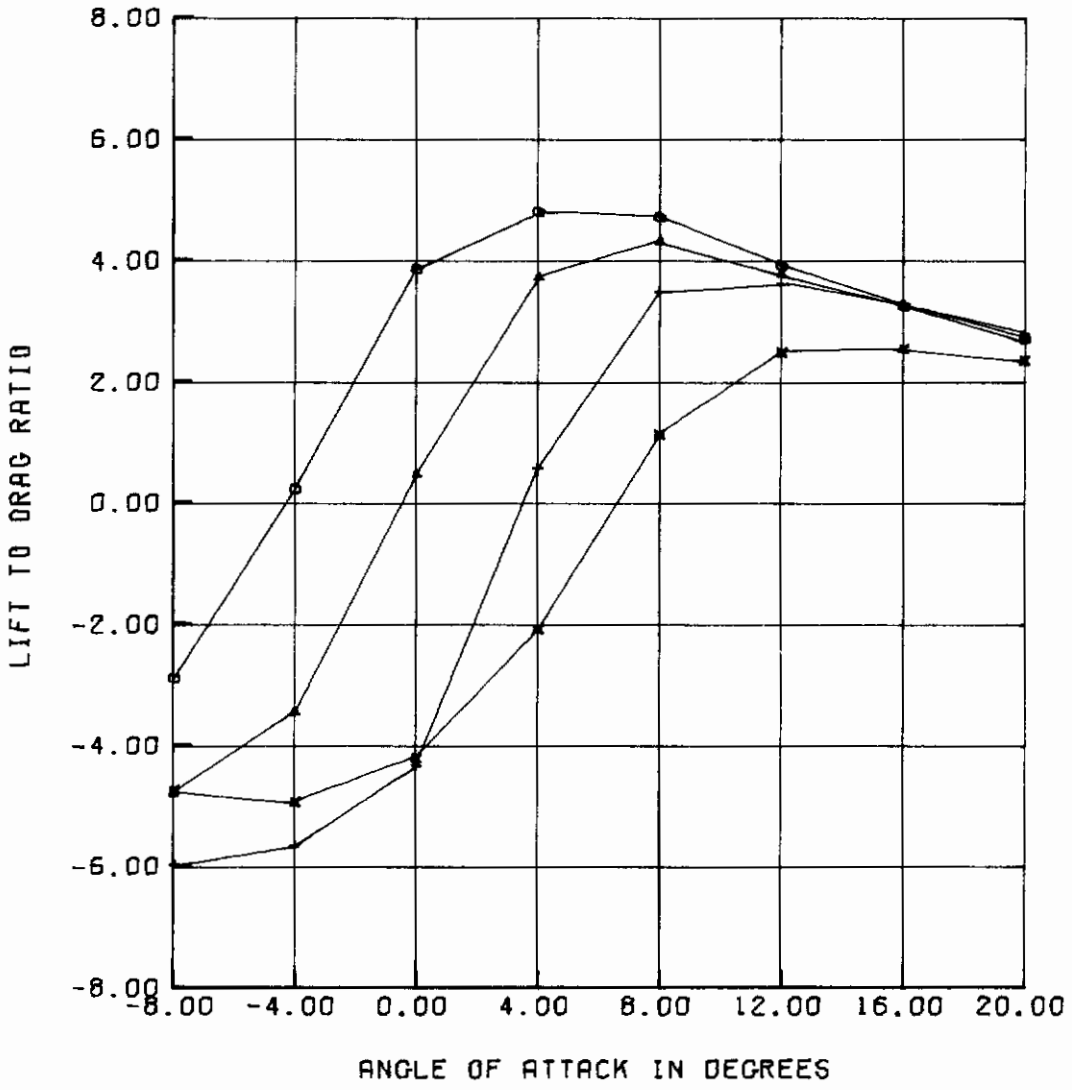


Figure 19. (Concluded)

| CONFIGURATION | FLAP DEFLECTION, DEG | |
|---|---|---|
| | 0° | -20° |
| S/100/5/0 | ○ | △ |
| S/100/10/0 | + | x |
| S/100/15/0 | * | □ |

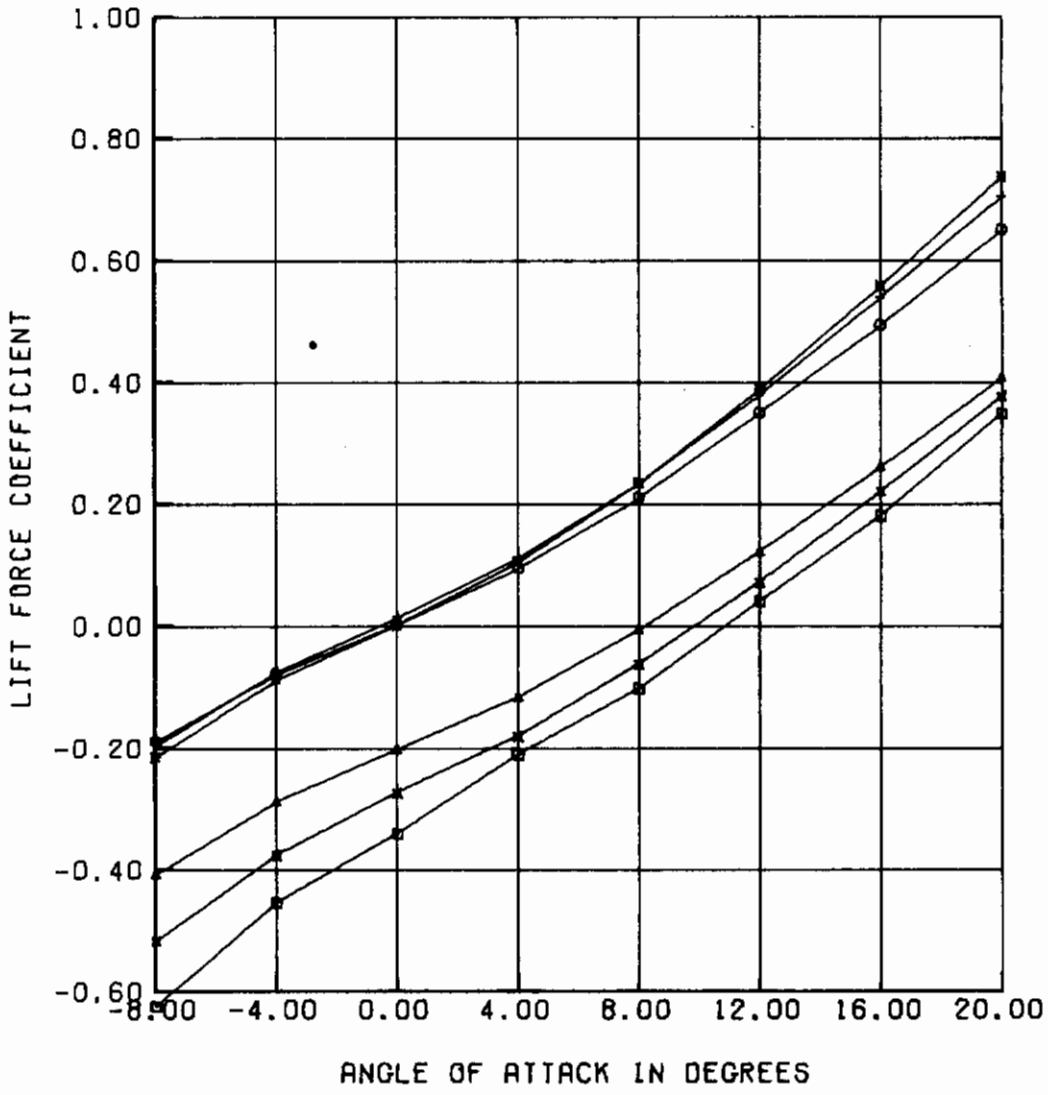


Figure 20. Effects of Control Surface Chord for Configurations With Constant Span

| CONFIGURATION | FLAP DEFLECTION, DEG | |
|---|---|---|
| | 0° | -20° |
| S/100/5/0 | ○ | △ |
| S/100/10/0 | + | x |
| S/100/15/0 | * | □ |

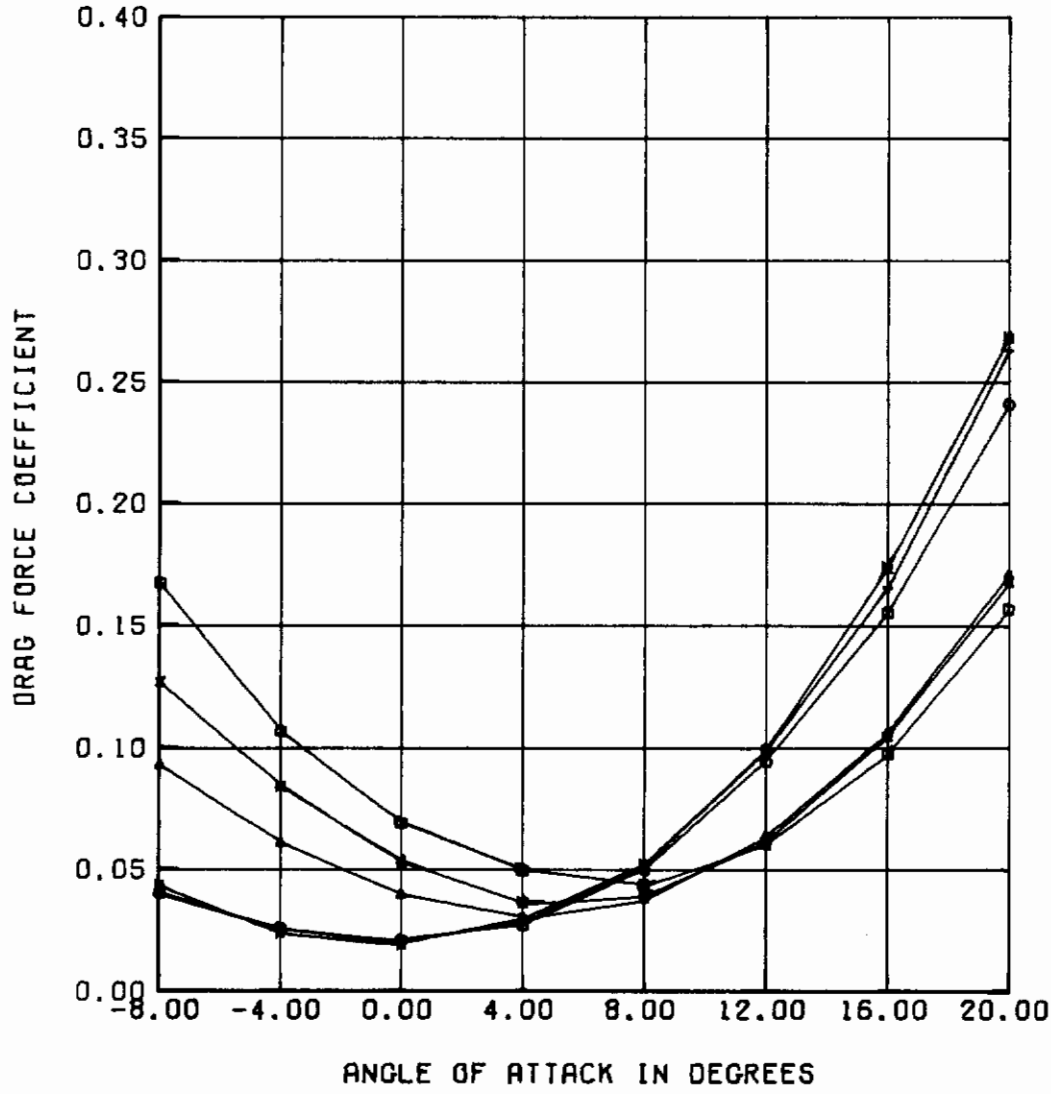


Figure 20. (Continued)

| CONFIGURATION | FLAP DEFLECTION, DEG | |
|---|---|---|
| | 0° | -20° |
| S/100/5/0 | ○ | △ |
| S/100/10/0 | + | x |
| S/100/15/0 | * | □ |

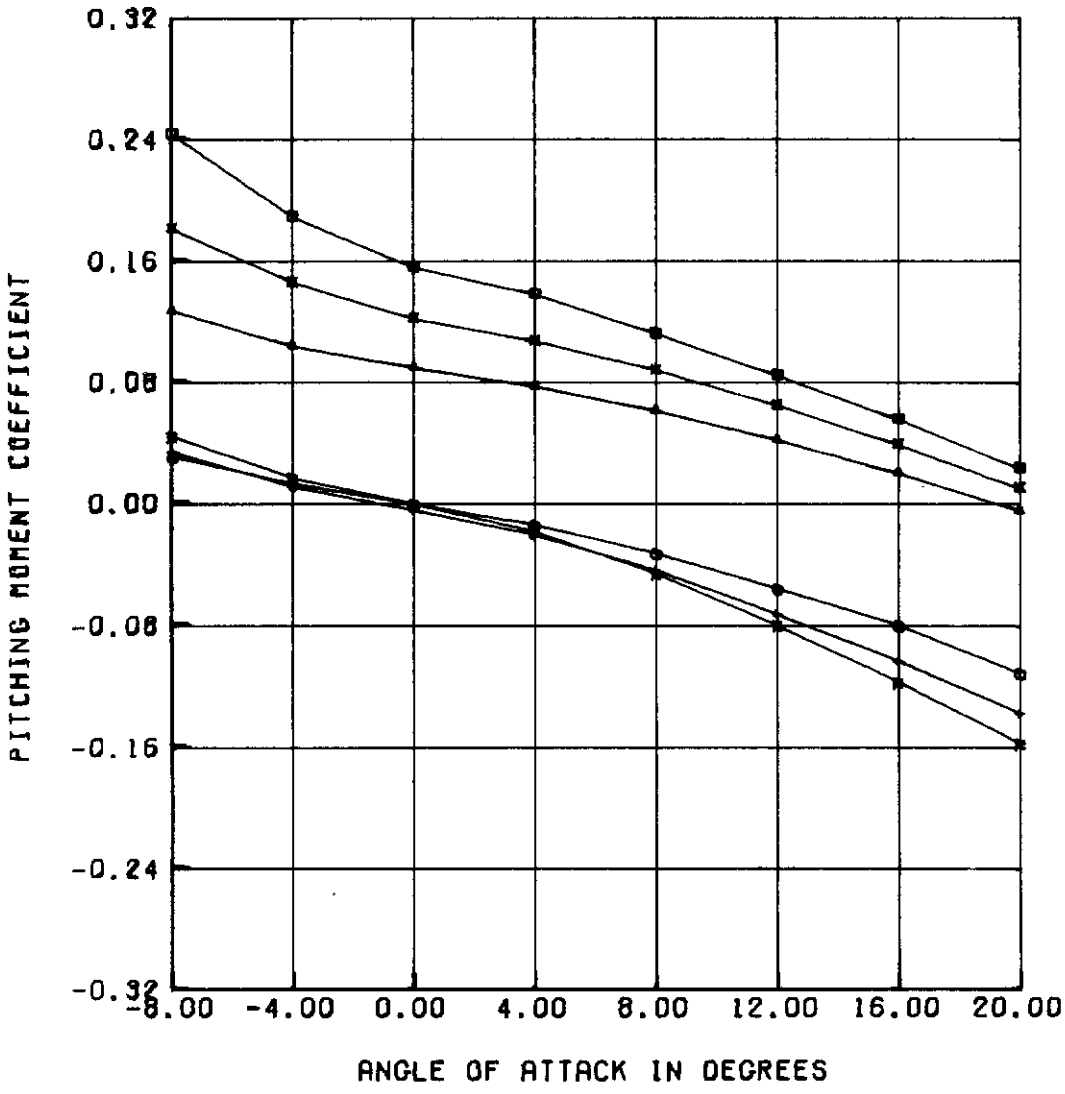


Figure 20. (Continued)

| CONFIGURATION | FLAP DEFLECTION, DEG | |
|---|---|---|
| | 0° | -20° |
| S/100/5/0 | ○ | △ |
| S/100/10/0 | + | x |
| S/100/15/0 | * | □ |

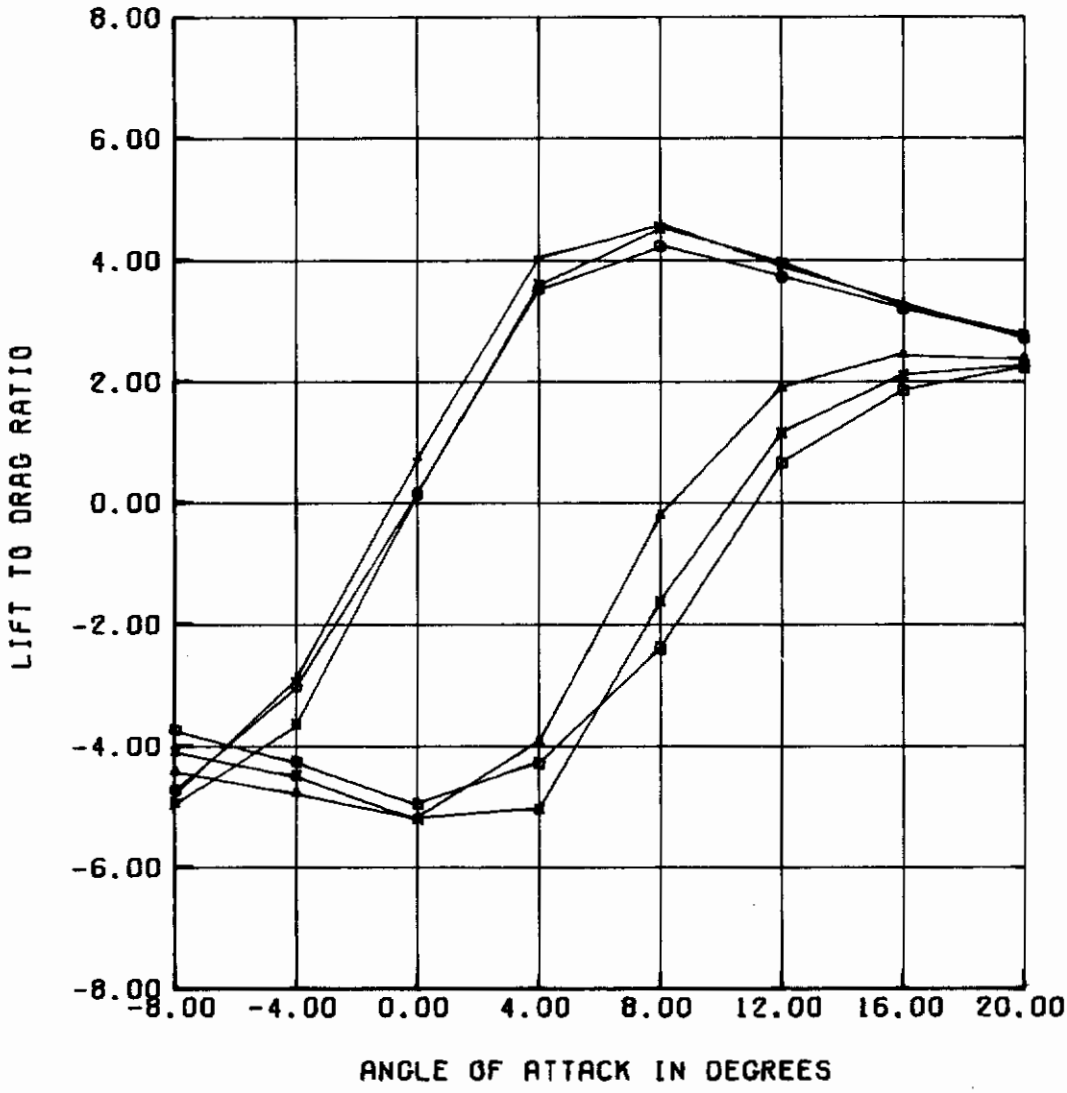


Figure 20. (Concluded)

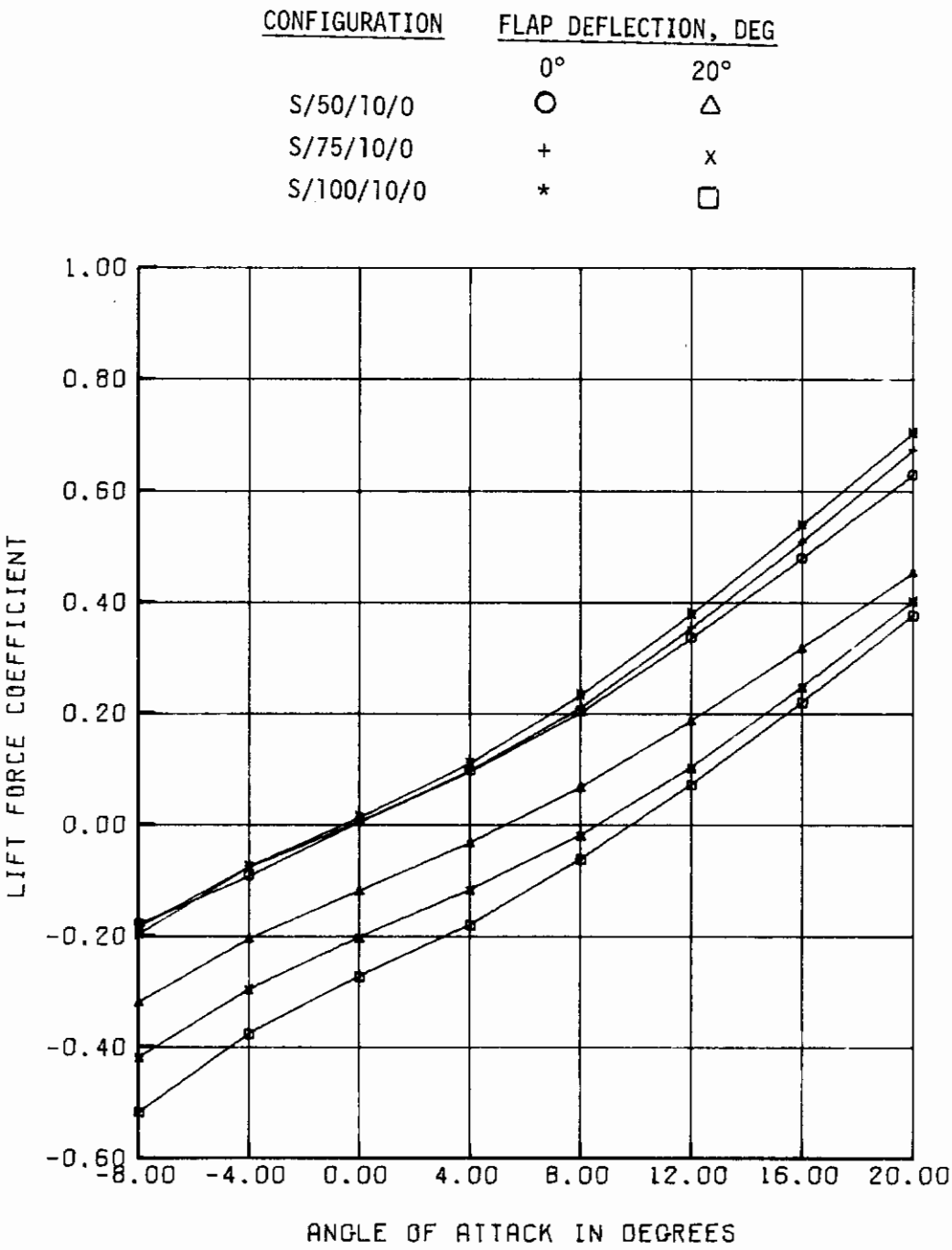


Figure 21. Effects of Control Surface Span for Configurations With Constant Chord

| CONFIGURATION | FLAP DEFLECTION, DEG | |
|---|---|---|
| | 0° | 20° |
| S/50/10/0 | ○ | △ |
| S/75/10/0 | + | x |
| S/100/10/0 | * | □ |

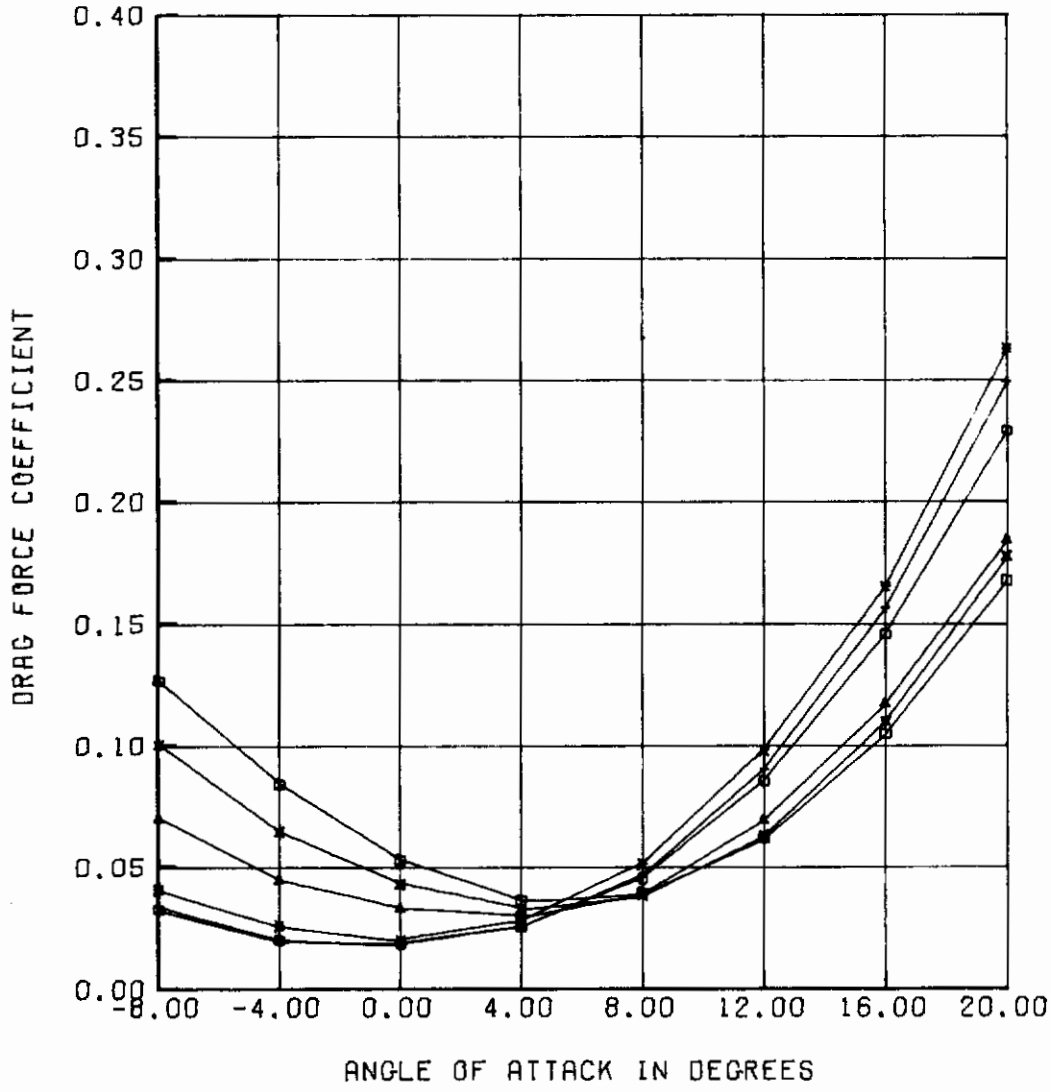


Figure 21. (Continued)

| CONFIGURATION | FLAP DEFLECTION, DEG | |
|---|---|---|
| | 0° | 20° |
| S/50/10/0 | ○ | △ |
| S/75/10/0 | + | x |
| S/100/10/0 | * | □ |

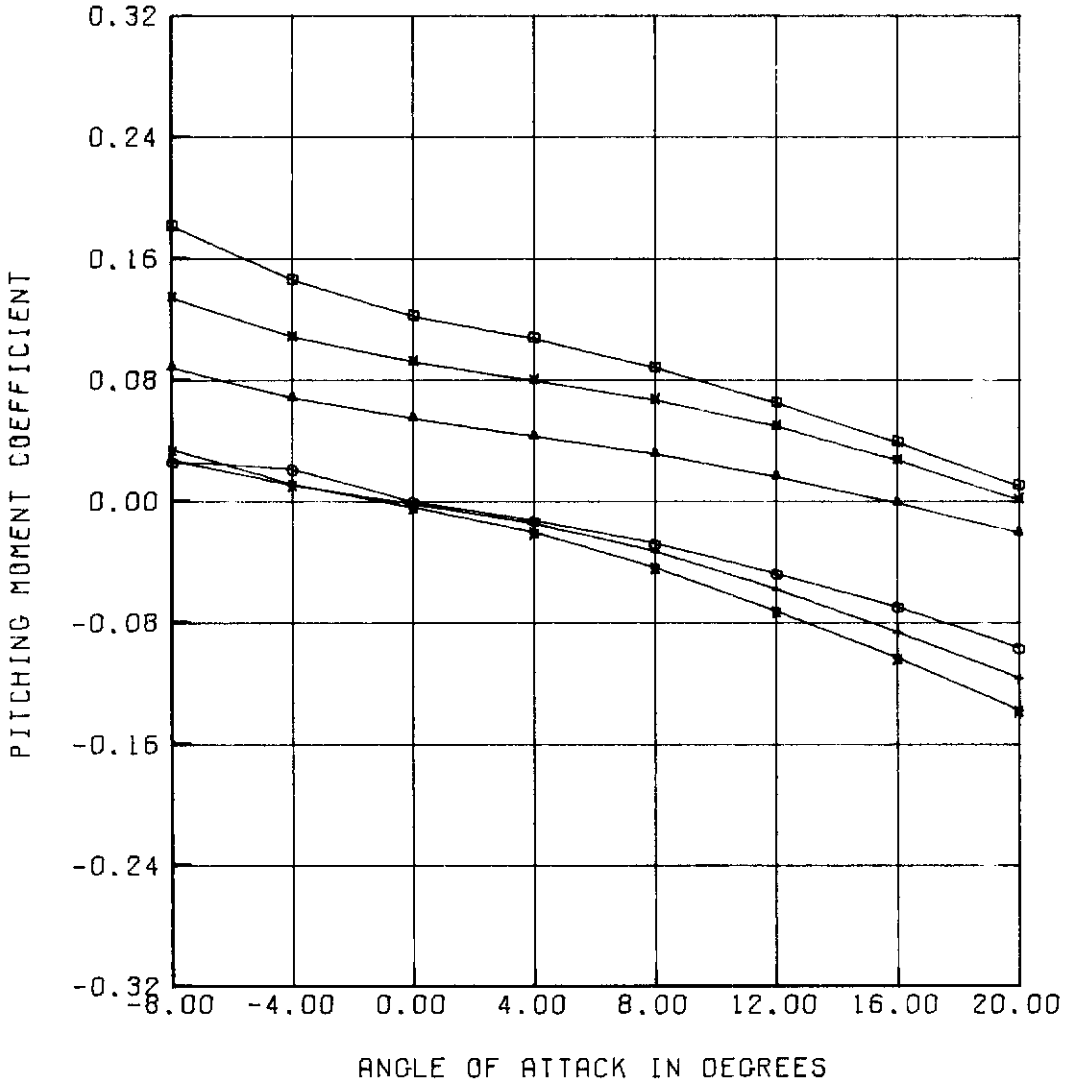


Figure 21. (Continued)

| CONFIGURATION | FLAP DEFLECTION, DEG | |
|---|---|---|
| | 0° | 20° |
| S/50/10/0 | ○ | △ |
| S/75/10/0 | + | x |
| S/100/10/0 | * | □ |

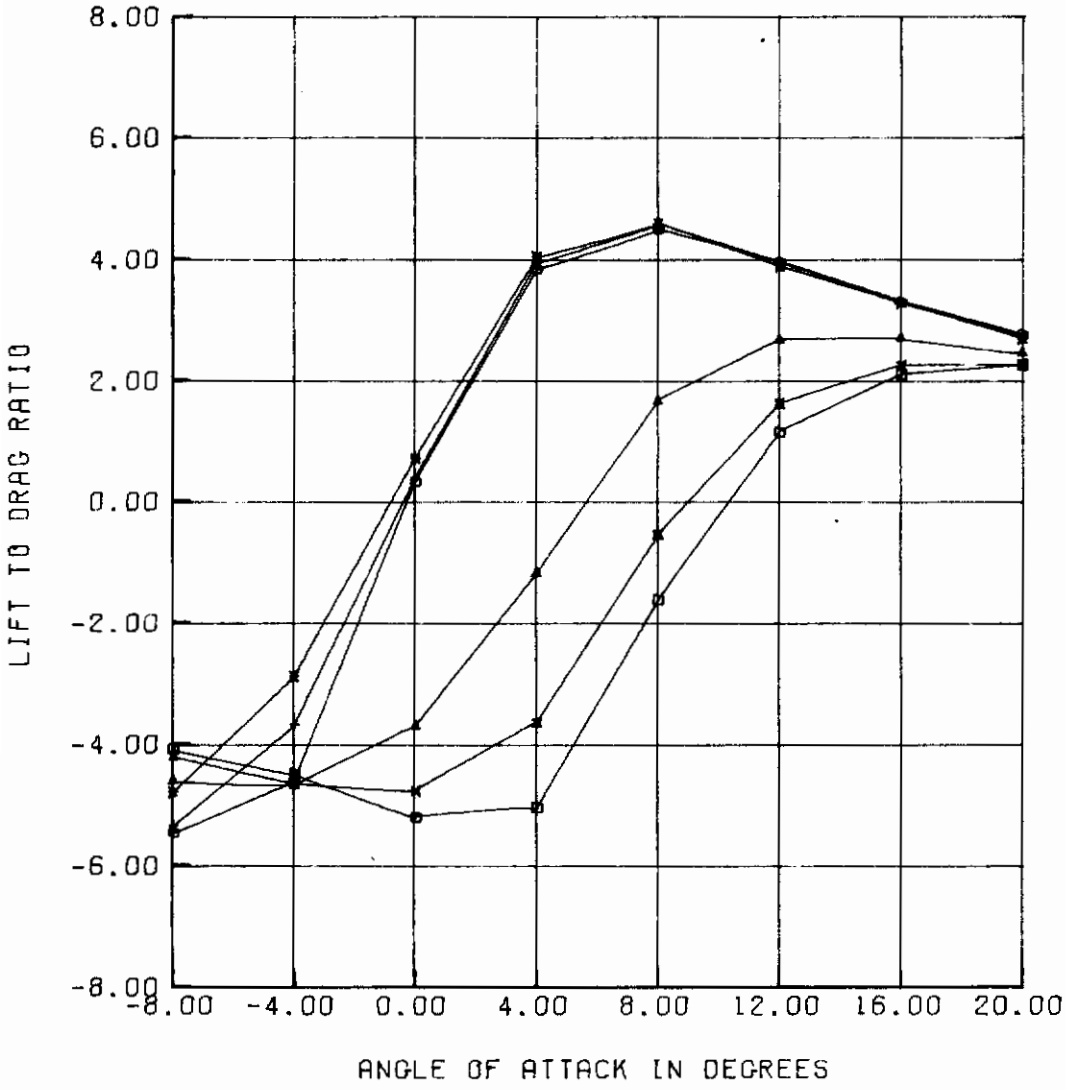


Figure 21. (Concluded)

| CONFIGURATION | FLAP DEFLECTION, DEG | |
|---|---|---|
| | 0° | -20° |
| S/75/10/25 | ○ | △ |
| S/75/10/0 | + | x |

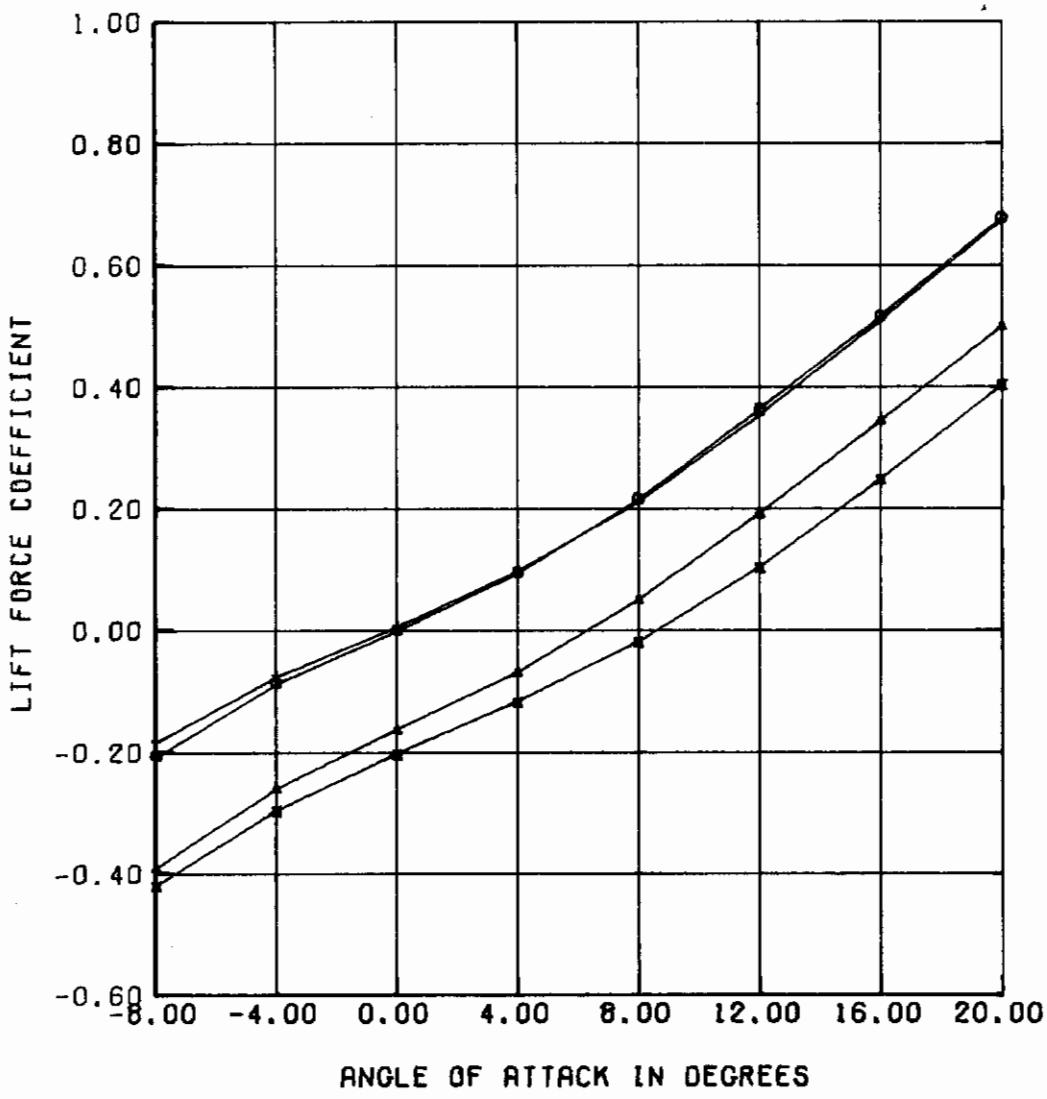


Figure 22. Effects of Control Surface Spacing for Configurations With 75% b Span

| CONFIGURATION | FLAP DEFLECTION, DEG | |
|---|---|---|
| | 0° | -20° |
| S/75/10/25 | ○ | △ |
| S/75/10/0 | + | x |

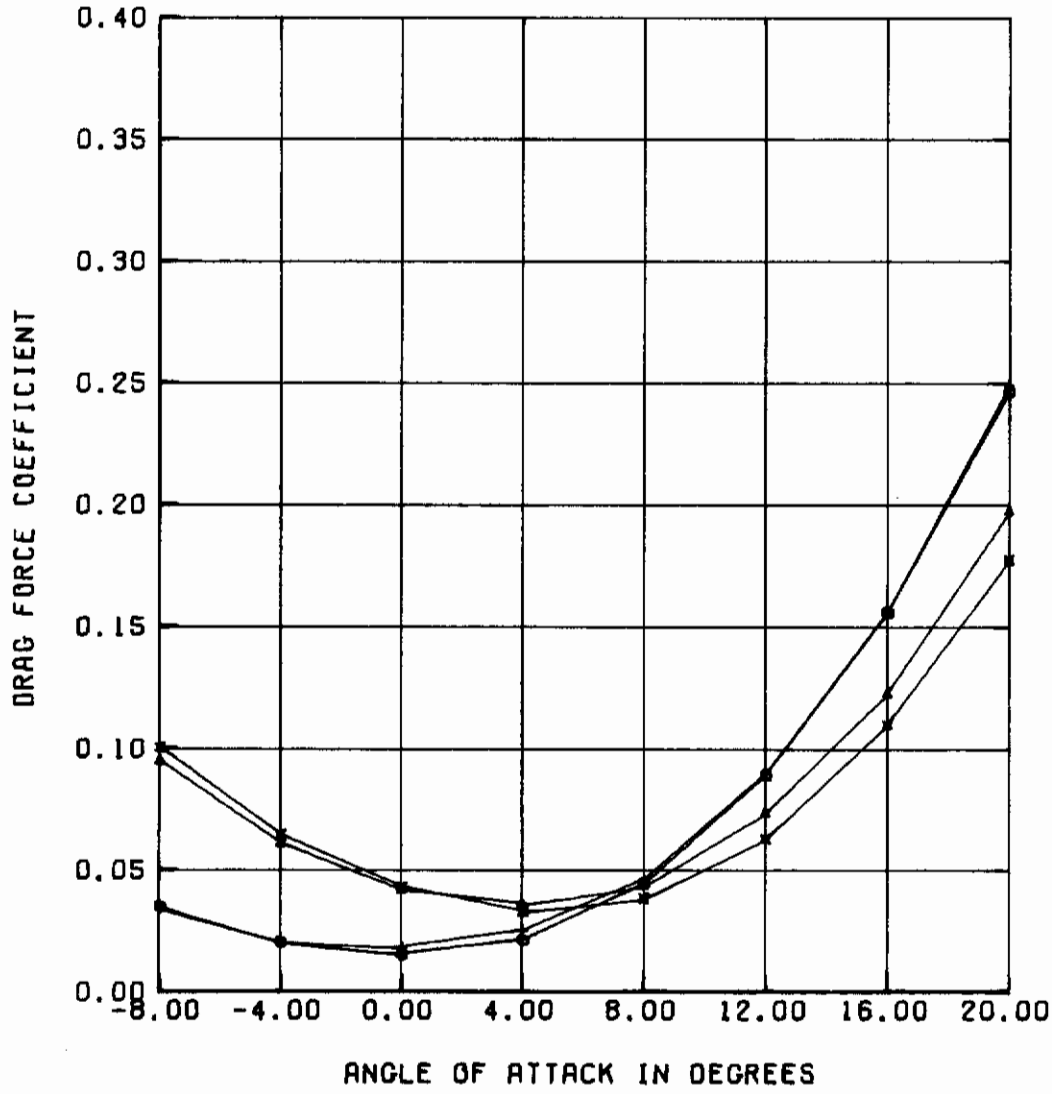


Figure 22. (Continued)

| CONFIGURATION | FLAP DEFLECTION, DEG | |
|---|---|---|
| | 0° | -20° |
| S/75/10/25 | ○ | △ |
| S/75/10/0 | + | x |

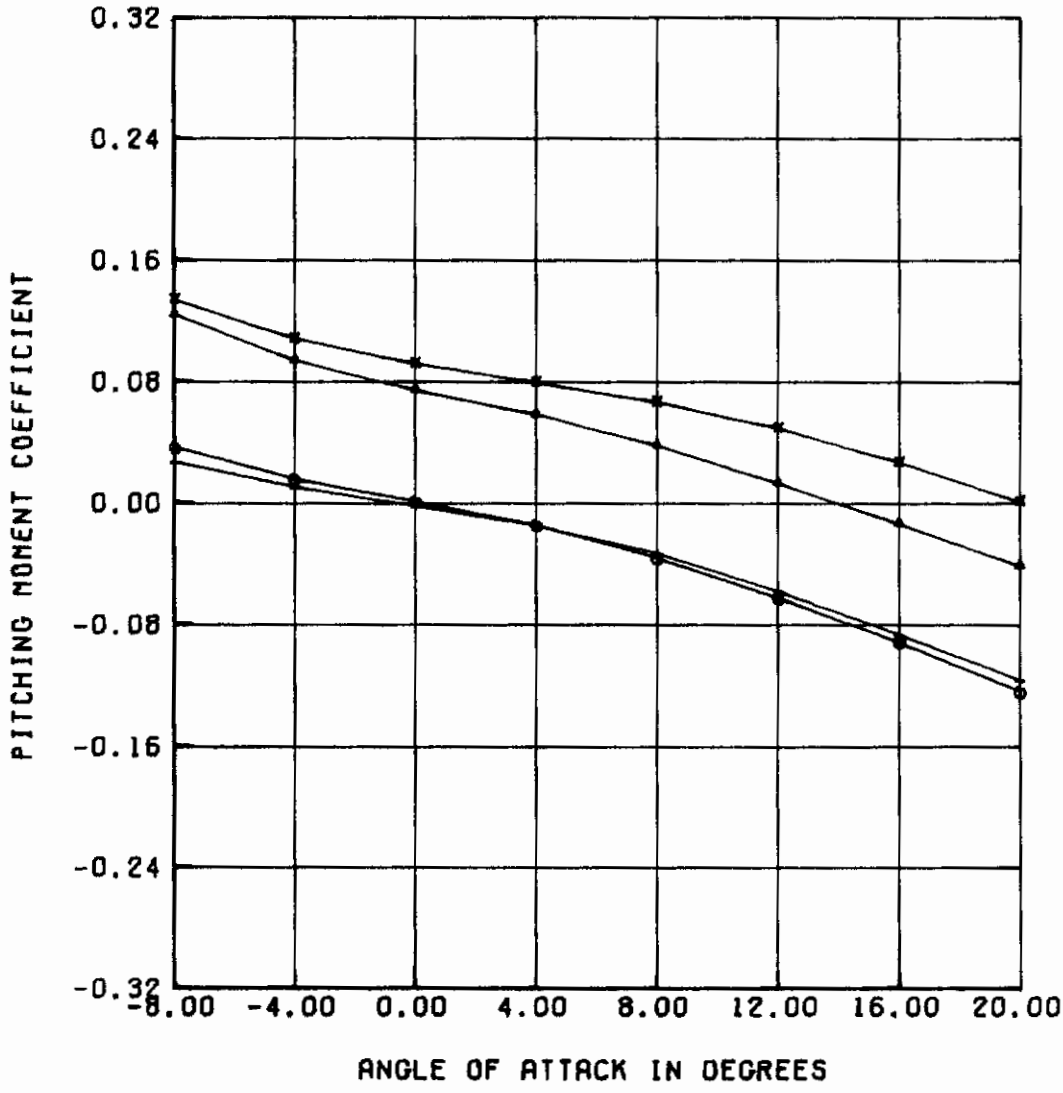


Figure 22. (Continued)

| CONFIGURATION | FLAP DEFLECTION, DEG | |
|---|---|---|
| | 0° | -20° |
| S/75/10/25 | ○ | △ |
| S/75/10/0 | + | x |

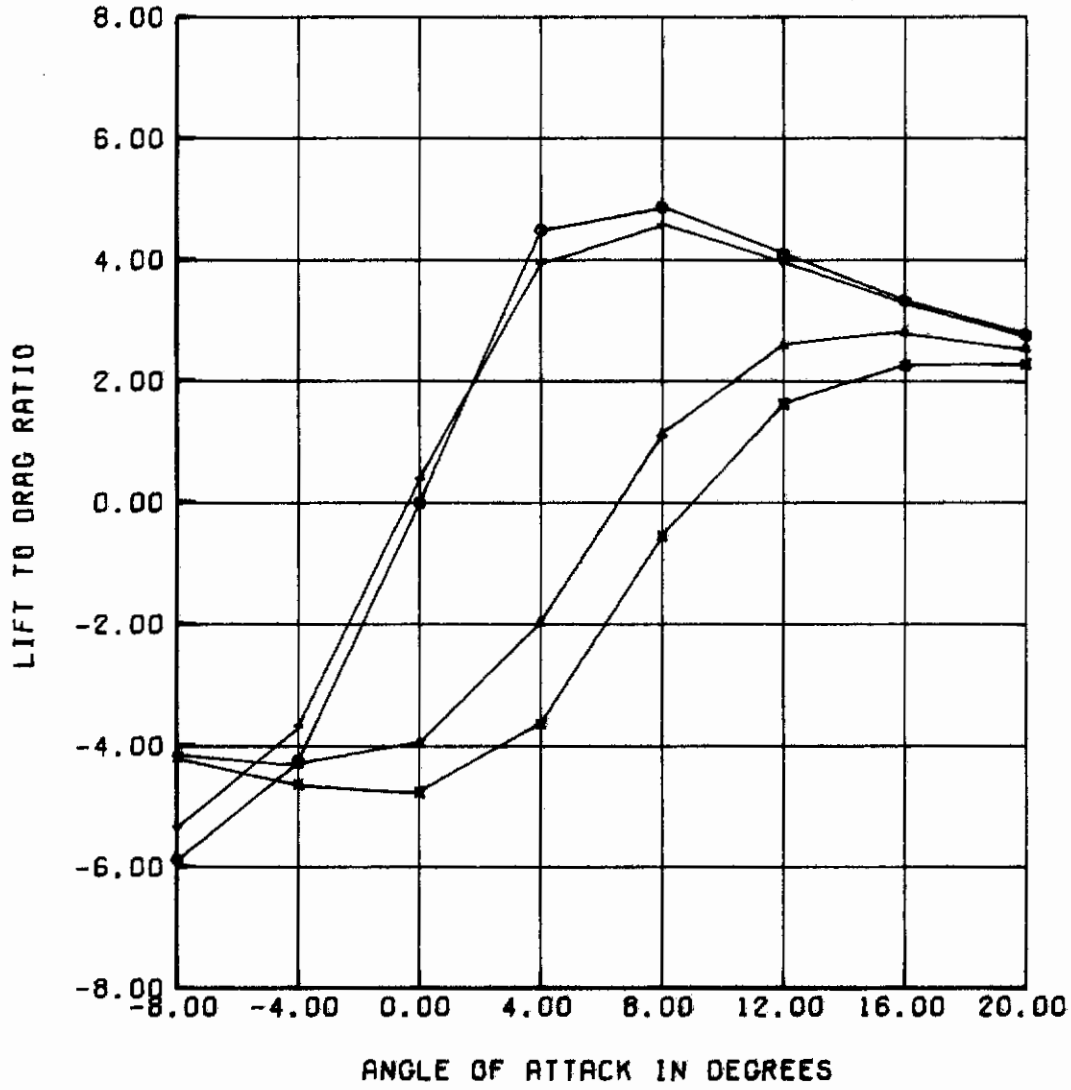


Figure 22. (Concluded)

| CONFIGURATION | FLAP DEFLECTION, DEG | |
|---|---|---|
| | 0° | -20° |
| S/50/10/50 | ○ | △ |
| S/50/10/25 | + | x |
| S/50/10/0 | * | □ |

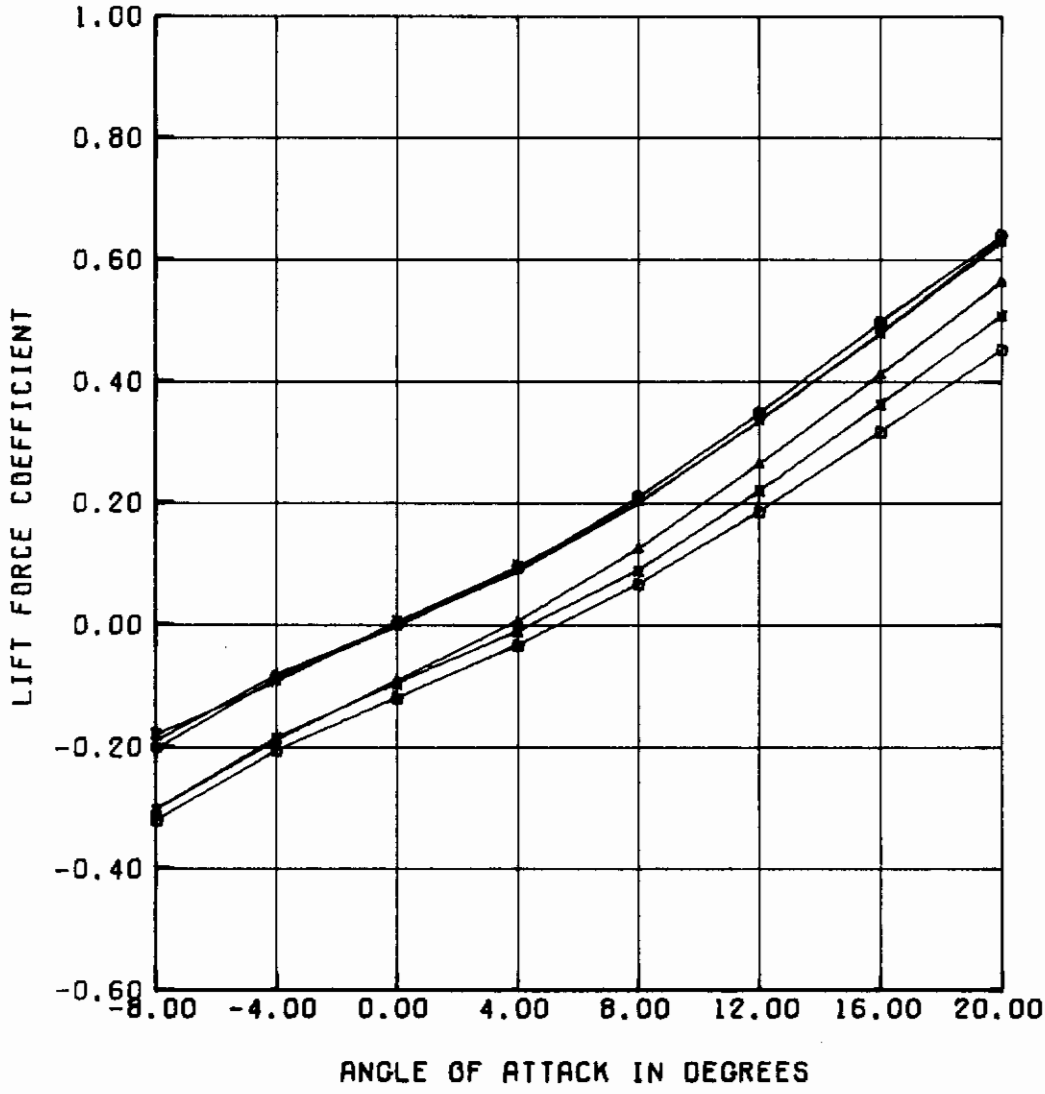


Figure 23. Effects of Control Surface Spacing for Configurations With 50% b Span

| CONFIGURATION | FLAP DEFLECTION, DEG | |
|---|---|---|
| | 0° | -20° |
| S/50/10/50 | ○ | △ |
| S/50/10/25 | + | x |
| S/50/10/0 | * | □ |

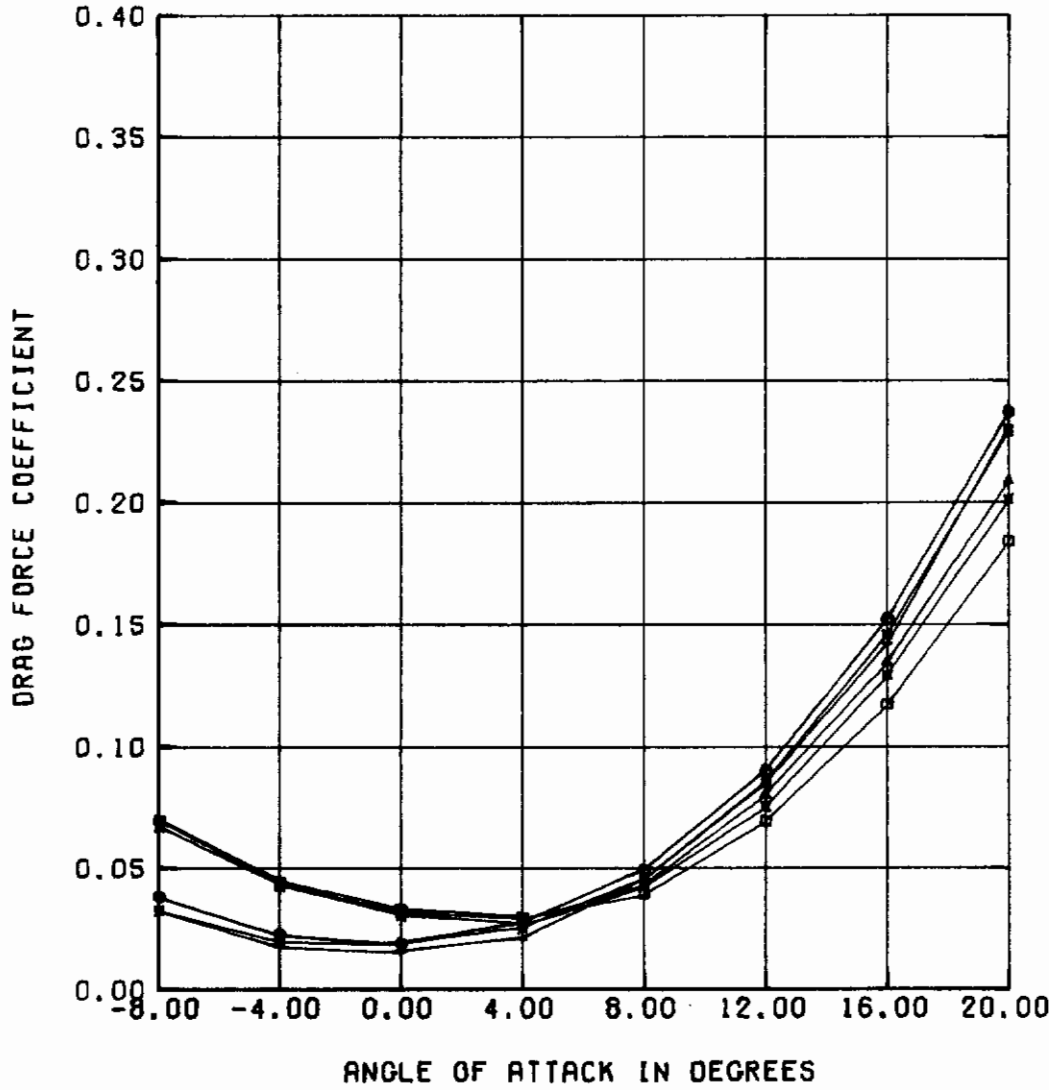


Figure 23. (Continued)

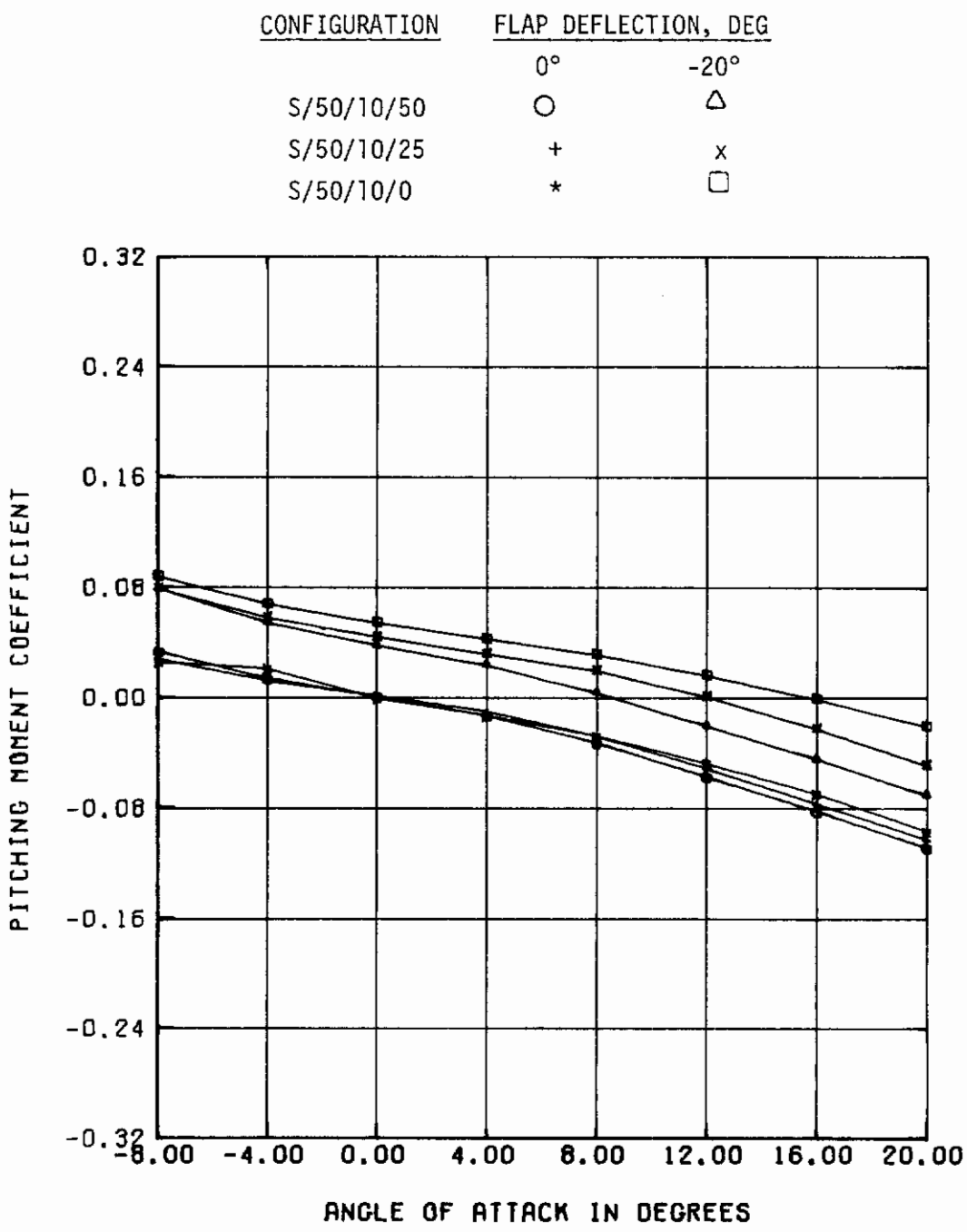


Figure 23. (Continued)

| CONFIGURATION | FLAP DEFLECTION, DEG | |
|---|---|---|
| | 0° | -20° |
| S/50/10/50 | ○ | △ |
| S/50/10/25 | + | x |
| S/50/10/0 | * | □ |

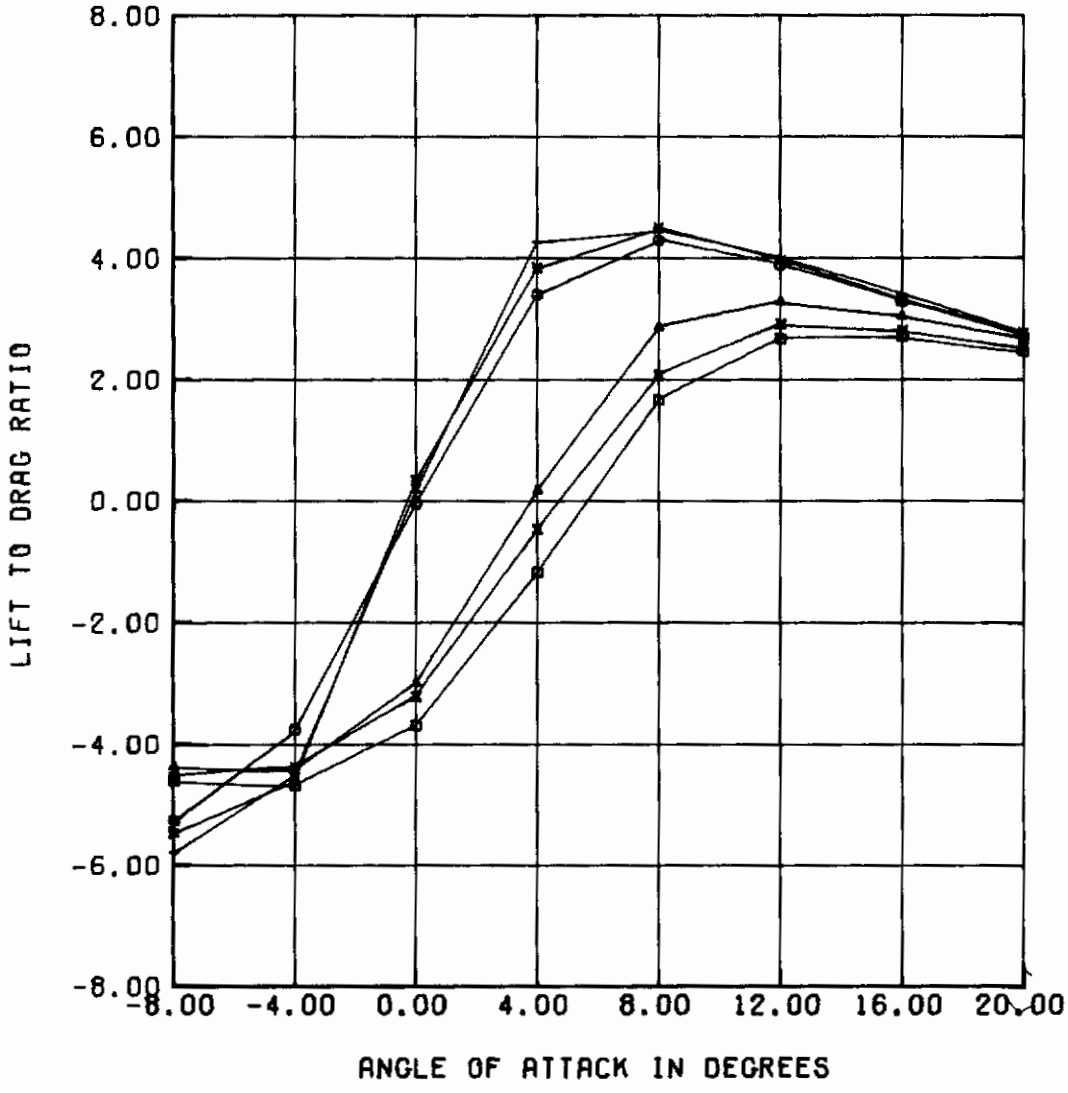


Figure 23. (Concluded)

| CONFIGURATION | FLAP DEFLECTION, DEG | |
|---|---|---|
| | 0° | -20° |
| S/75/10/25 | ○ | △ |
| D/75/25/10 (INNER FLAP FIXED) | + | x |

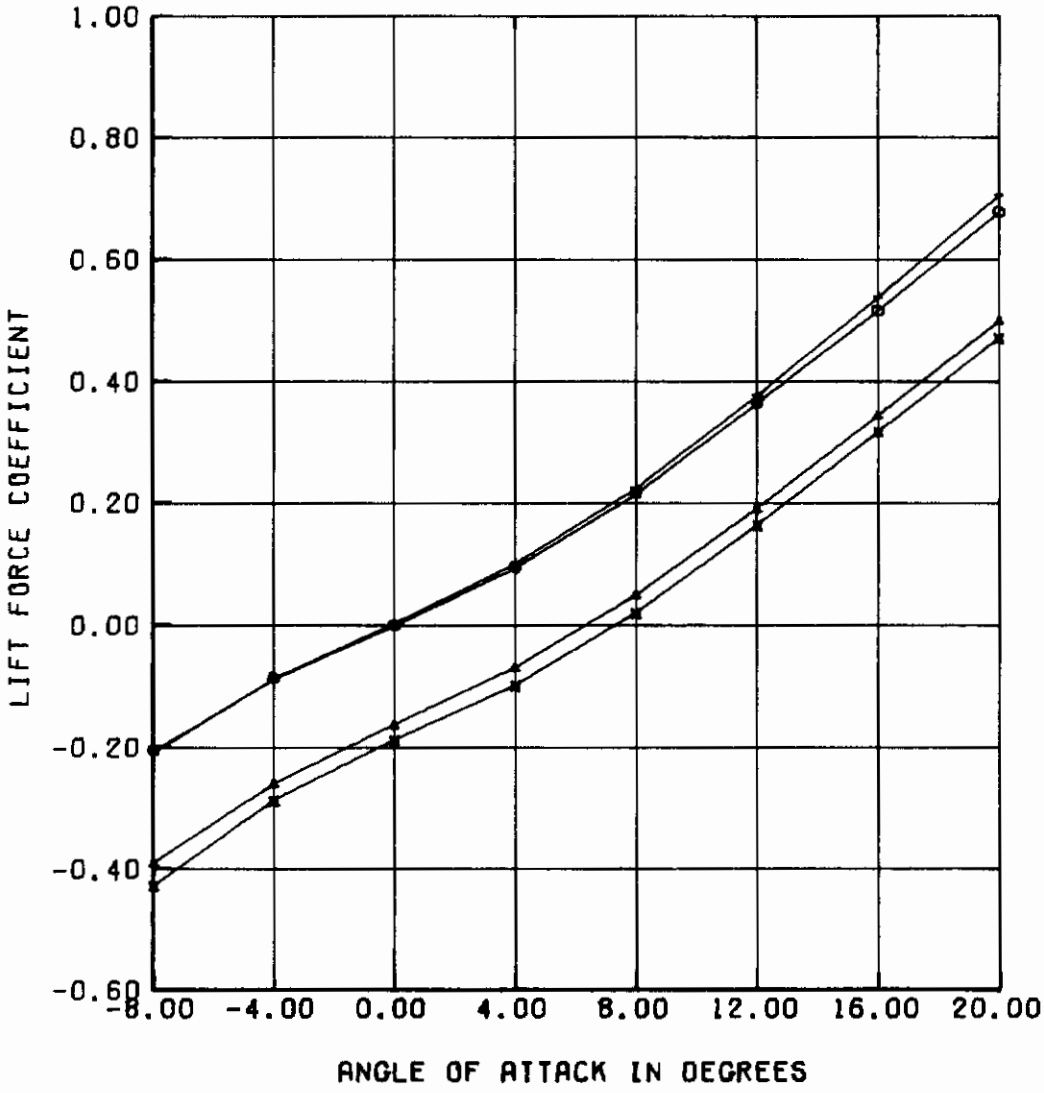


Figure 24. Effects of A Fixed Center Flap on A 75% b Flap Configuration

| CONFIGURATION | FLAP DEFLECTION, DEG | |
|---|---|---|
| | 0° | -20° |
| S/75/10/25 | ○ | △ |
| D/75/25/10 (INNER FLAP FIXED) | + | x |

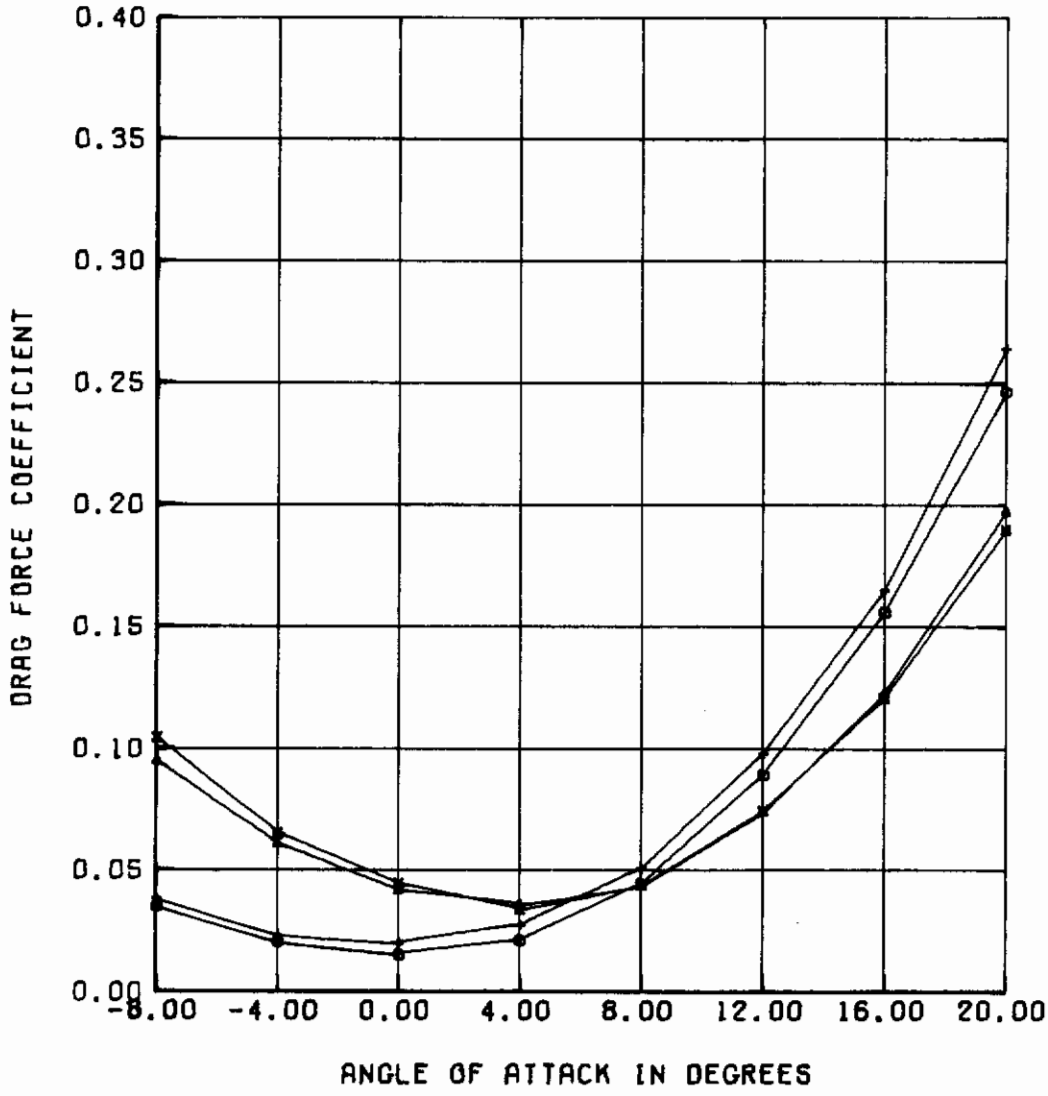


Figure 24. (Continued)

| CONFIGURATION | FLAP DEFLECTION, DEG | |
|---|---|---|
| | 0° | -20° |
| S/75/10/25 | ○ | △ |
| D/75/25/10 (INNER FLAP FIXED) | + | x |

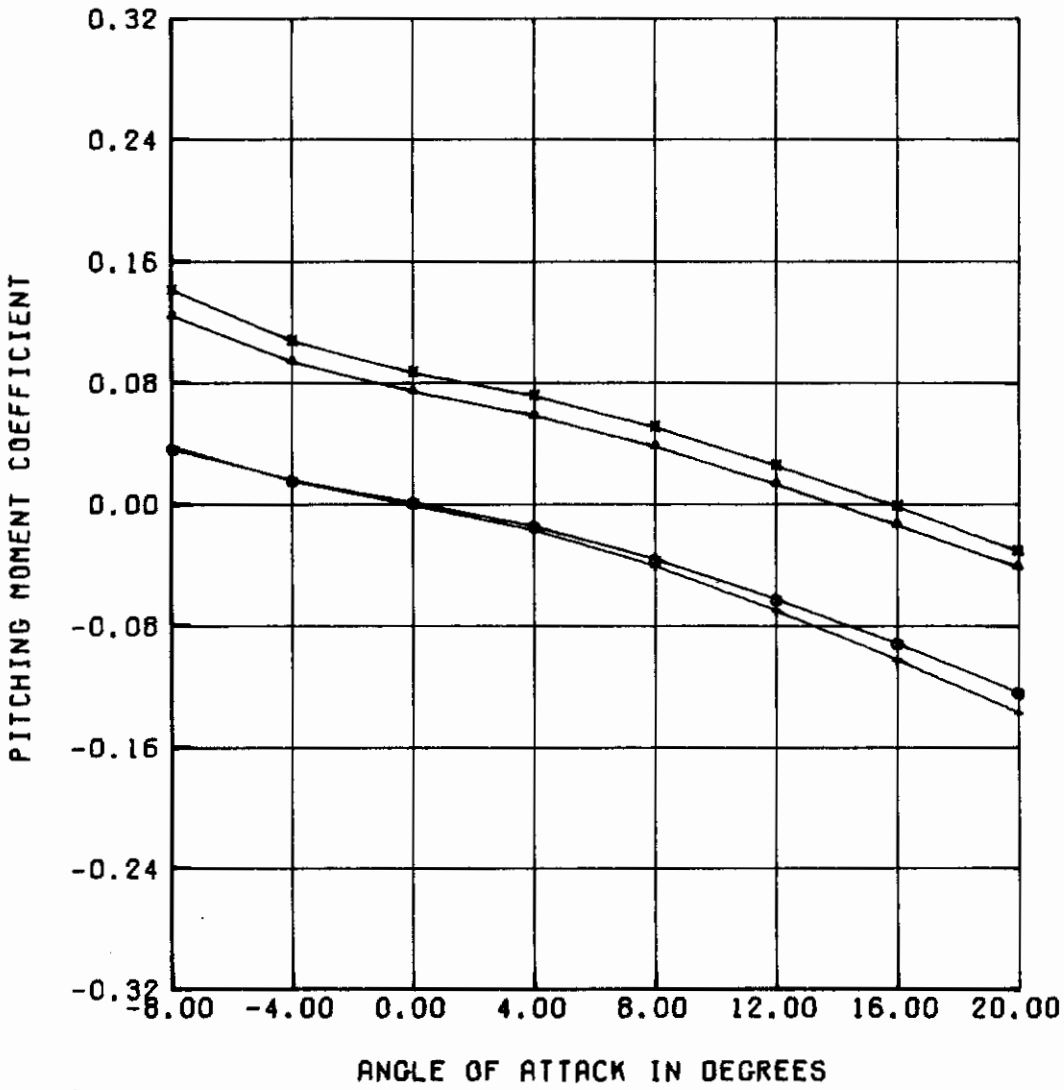


Figure 24. (Continued)

| CONFIGURATION | FLAP DEFLECTION, DEG | |
|---|---|---|
| | 0° | -20° |
| S/75/10/25 | ○ | △ |
| D/75/25/10 (INNER FLAP FIXED) | + | x |

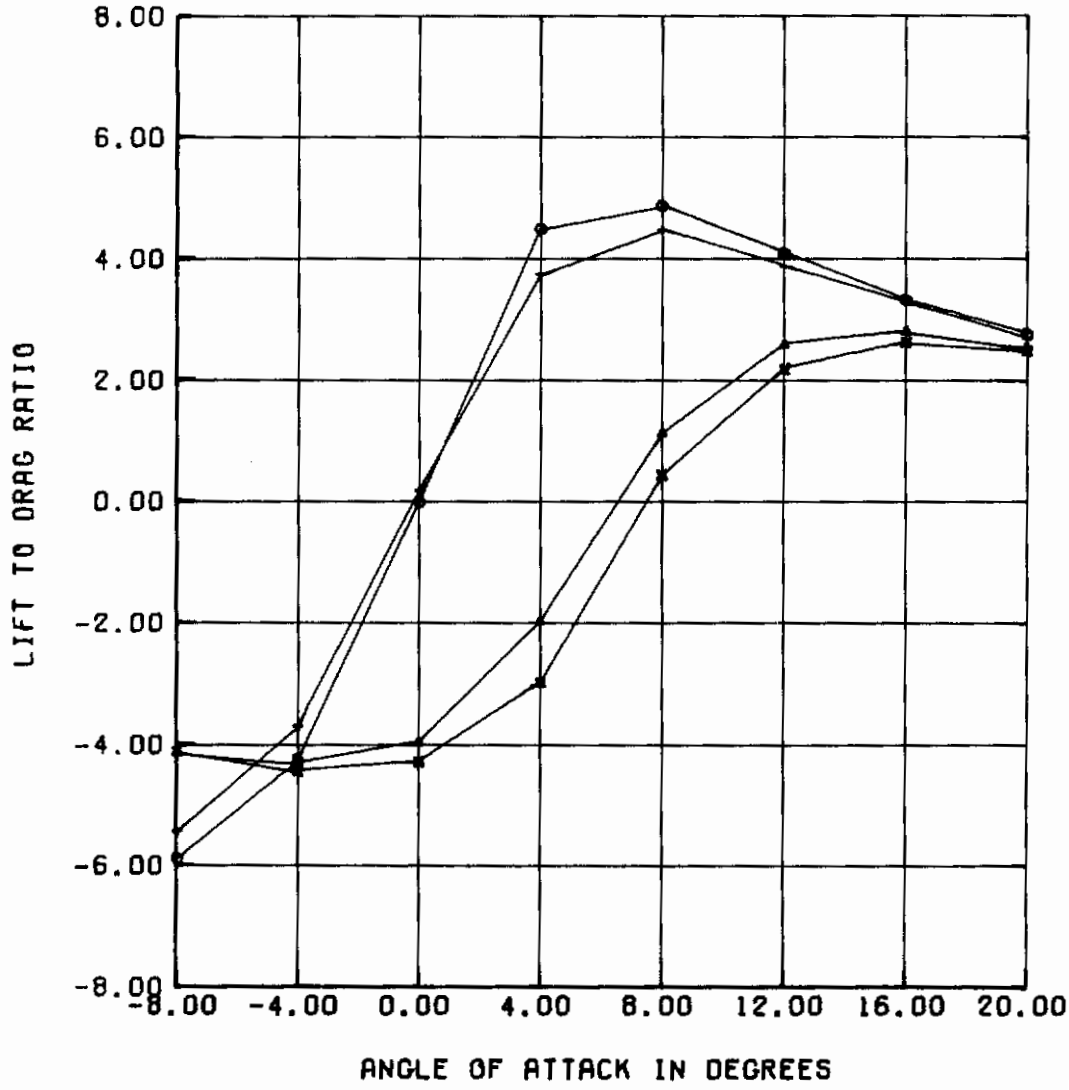


Figure 24. (Concluded)

| CONFIGURATION | FLAP DEFLECTION, DEG | |
|---|---|---|
| | 0° | -20° |
| S/50/10/50 | ○ | △ |
| D/50/50/10 (INNER FLAP FIXED) | + | x |

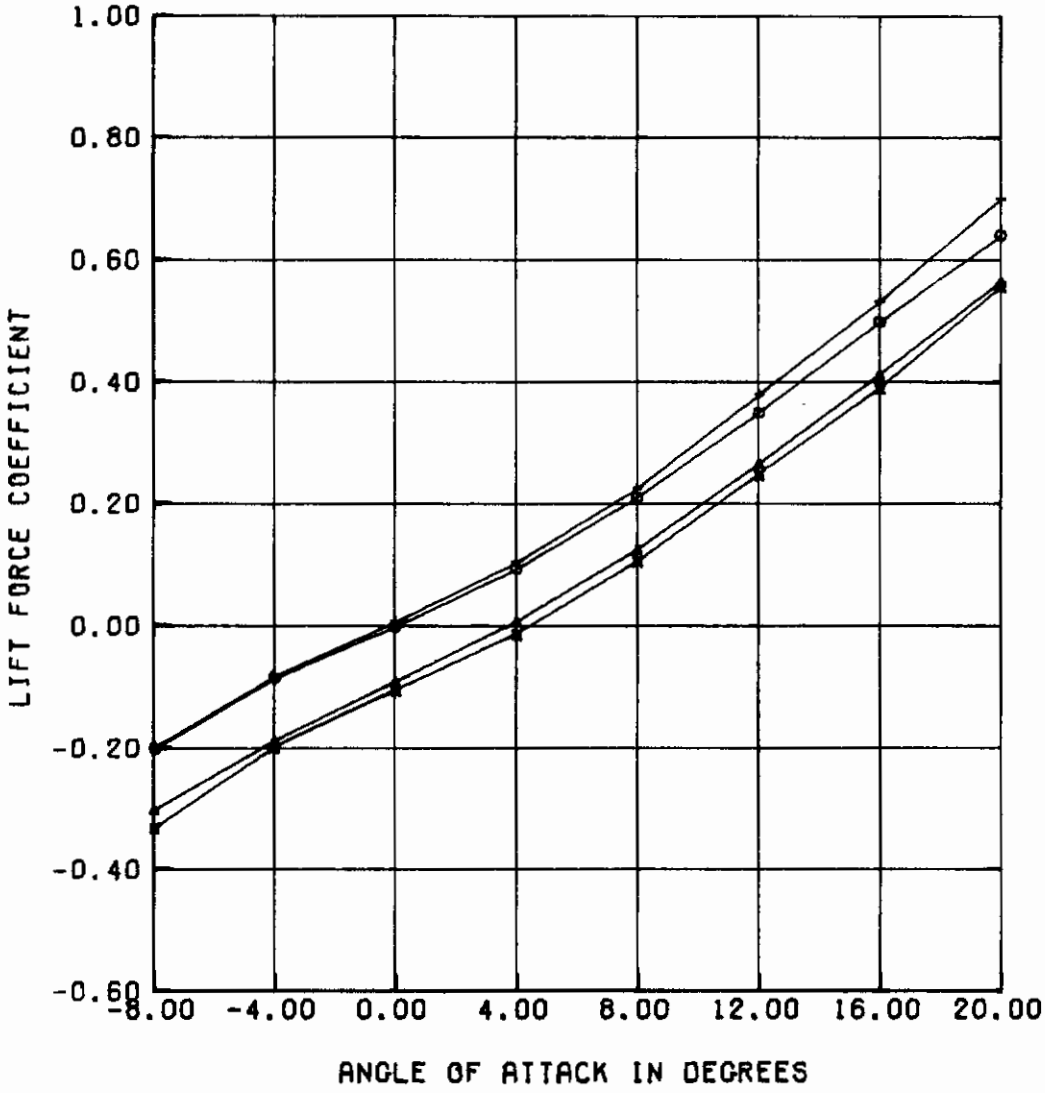


Figure 25. Effects of A Fixed Center Flap on A 50% b Flap Configuration

| CONFIGURATION | FLAP DEFLECTION, DEG | |
|---|---|---|
| | 0° | -20° |
| S/50/10/50 | ○ | △ |
| D/50/50/10 (INNER FLAP FIXED) | + | x |

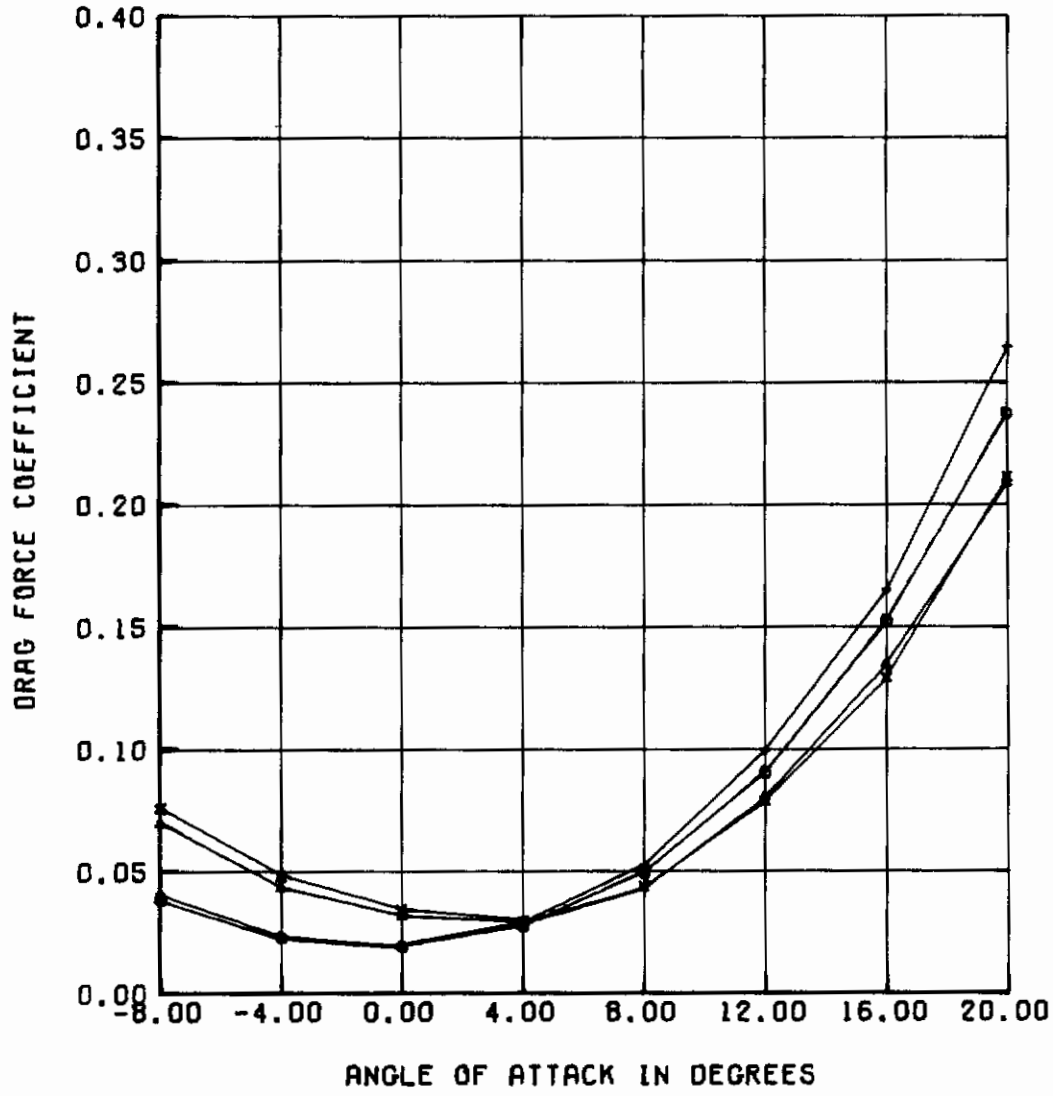


Figure 25. (Continued)

| CONFIGURATION | FLAP DEFLECTION, DEG | |
|---|---|---|
| | 0° | -20° |
| S/50/10/50 | ○ | △ |
| D/50/50/10 (INNER FLAP FIXED) | + | x |

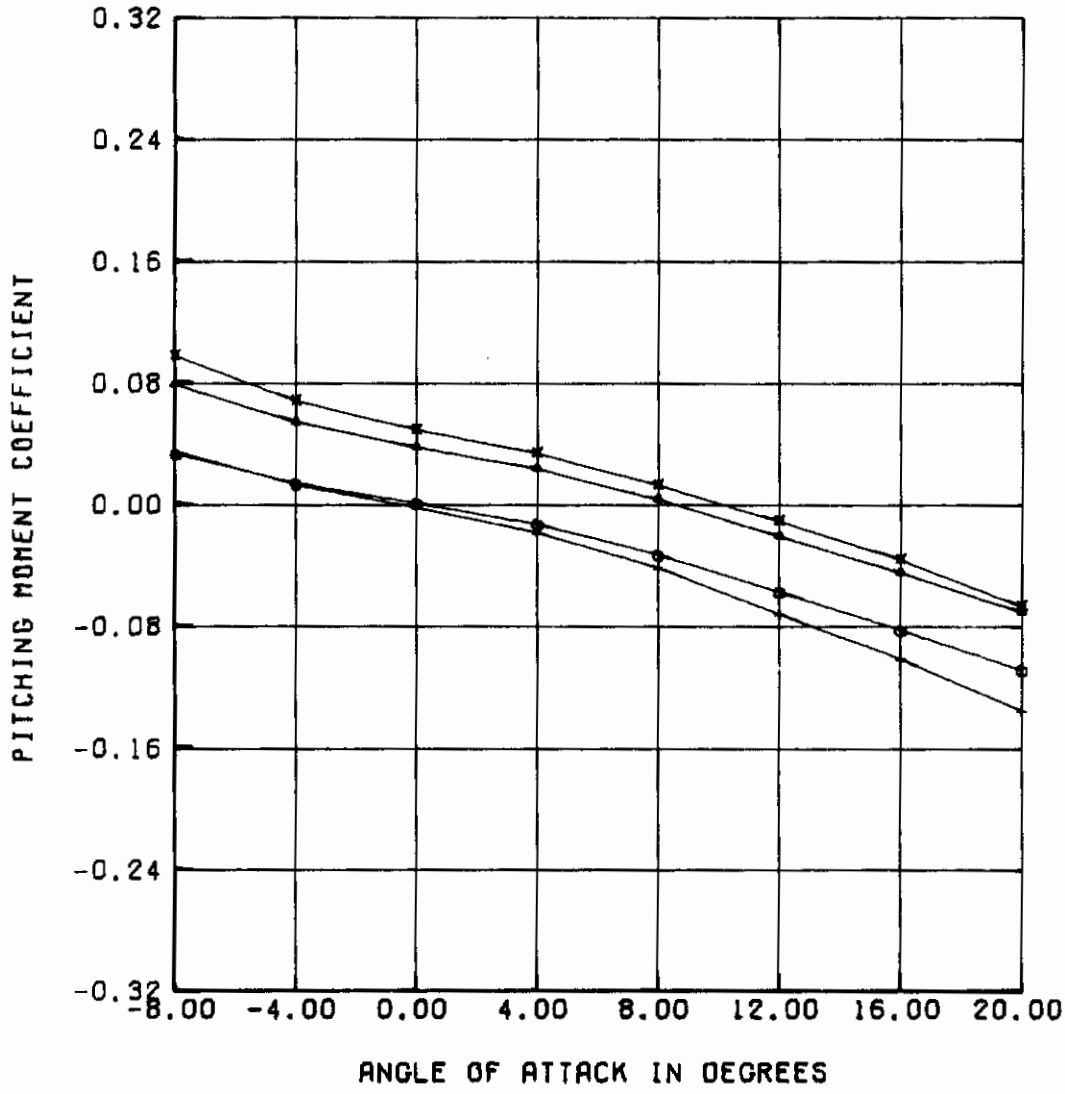


Figure 25. (Continued)

| CONFIGURATION | FLAP DEFLECTION, DEG | |
|---|---|---|
| | 0° | -20° |
| S/50/10/50 | ○ | △ |
| D/50/50/10 (INNER FLAP FIXED) | + | x |

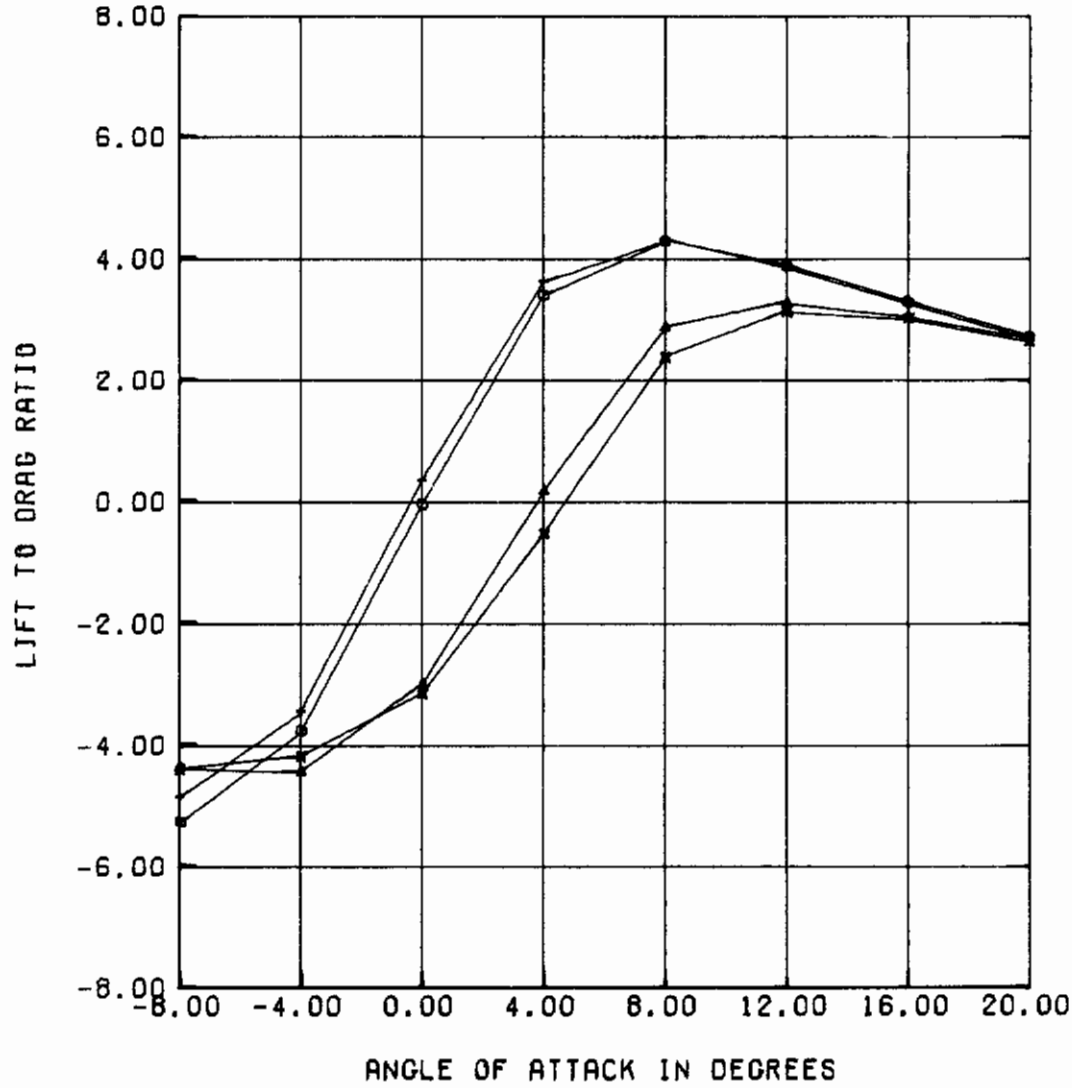


Figure 25. (Concluded)

| CONFIGURATION | FLAP DEFLECTION, DEG | |
|---|---|---|
| | 0° | -20° |
| D/50/50/10 (INNER FLAP FIXED) | O | △ |
| D/50/50/10 (OUTER FLAP FIXED) | + | x |

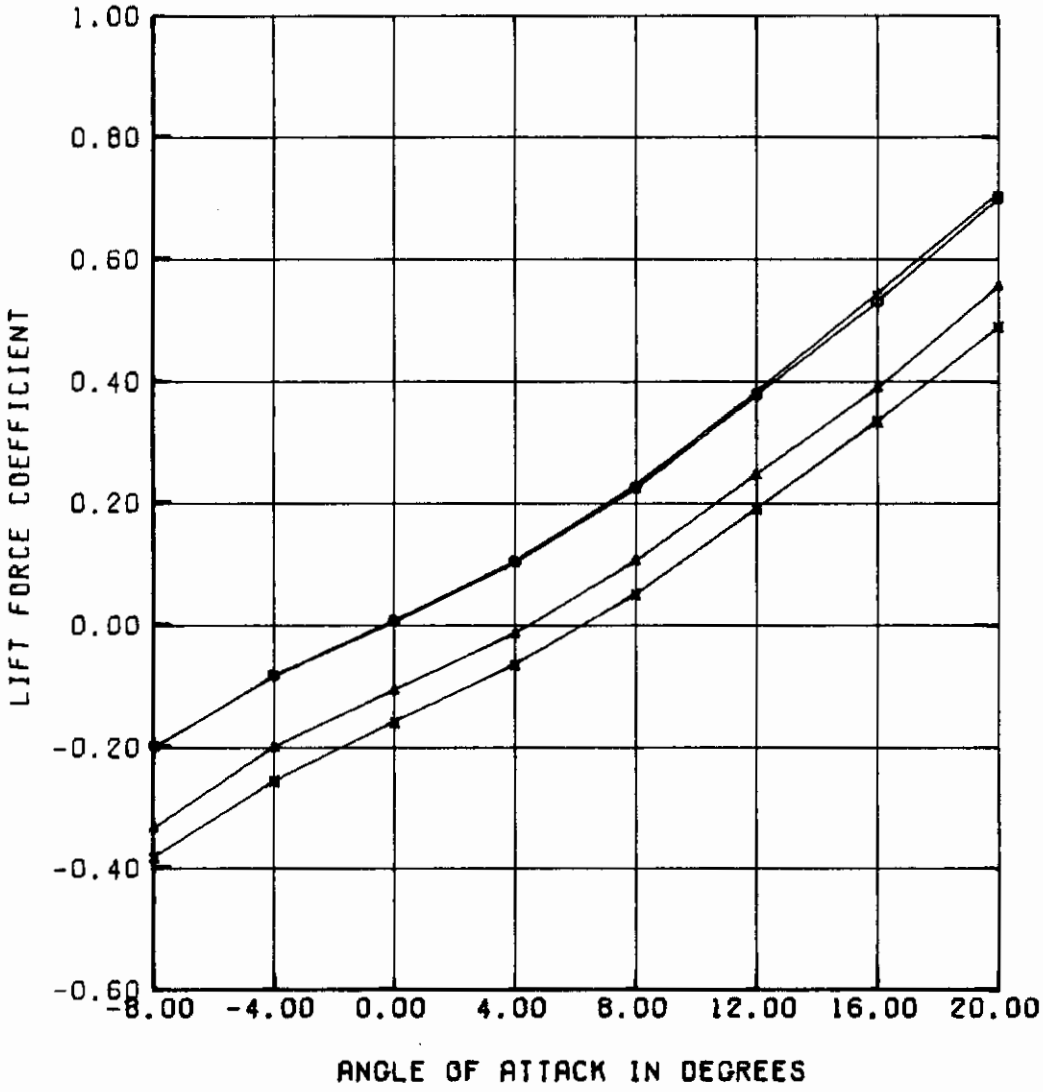


Figure 26. Comparison of Center and Outboard Control Surface Effectiveness for a Dual Flap Configuration

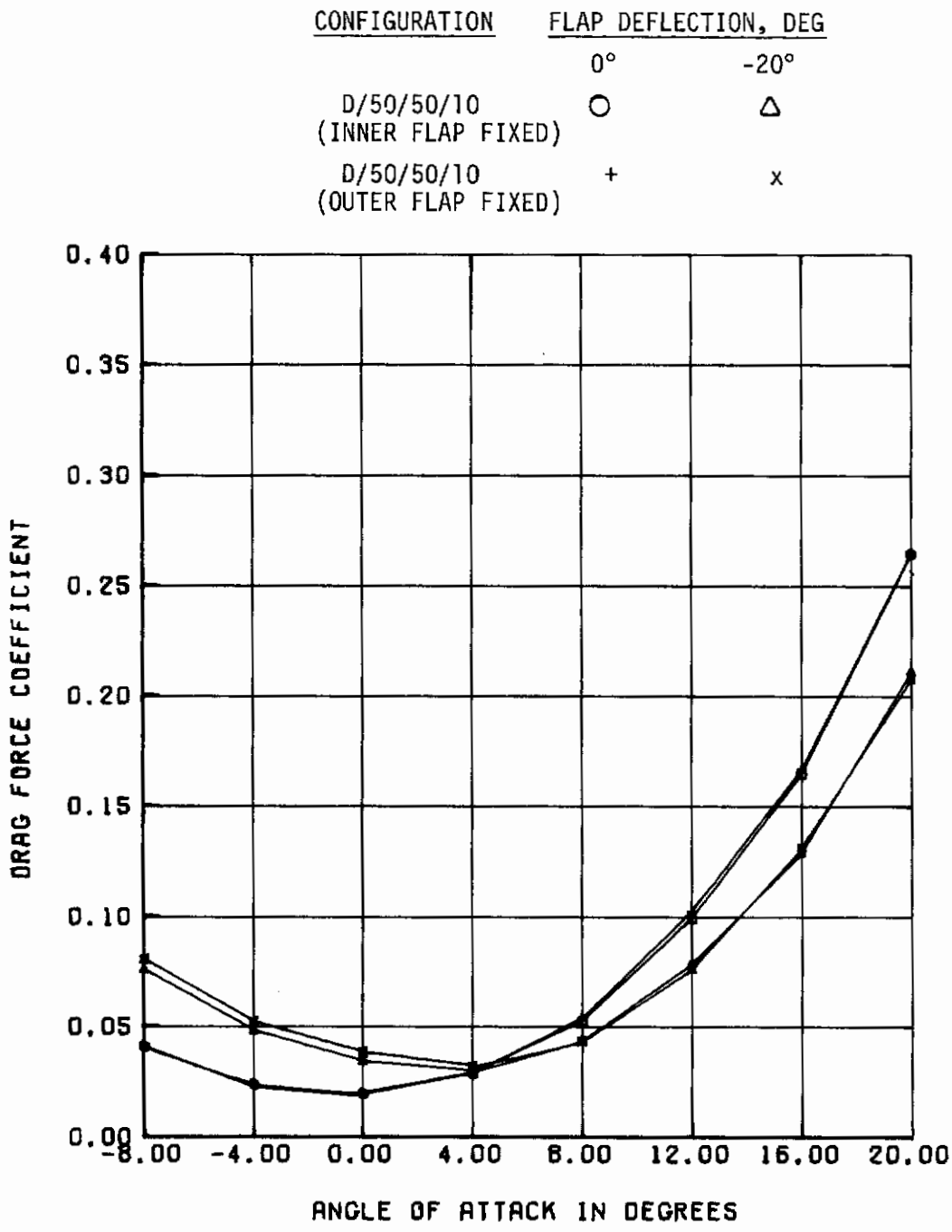


Figure 26. (Continued)

| CONFIGURATION | FLAP DEFLECTION, DEG | |
|---|---|---|
| | 0° | -20° |
| D/50/50/10 (INNER FLAP FIXED) | ○ | △ |
| D/50/50/10 (OUTER FLAP FIXED) | + | x |

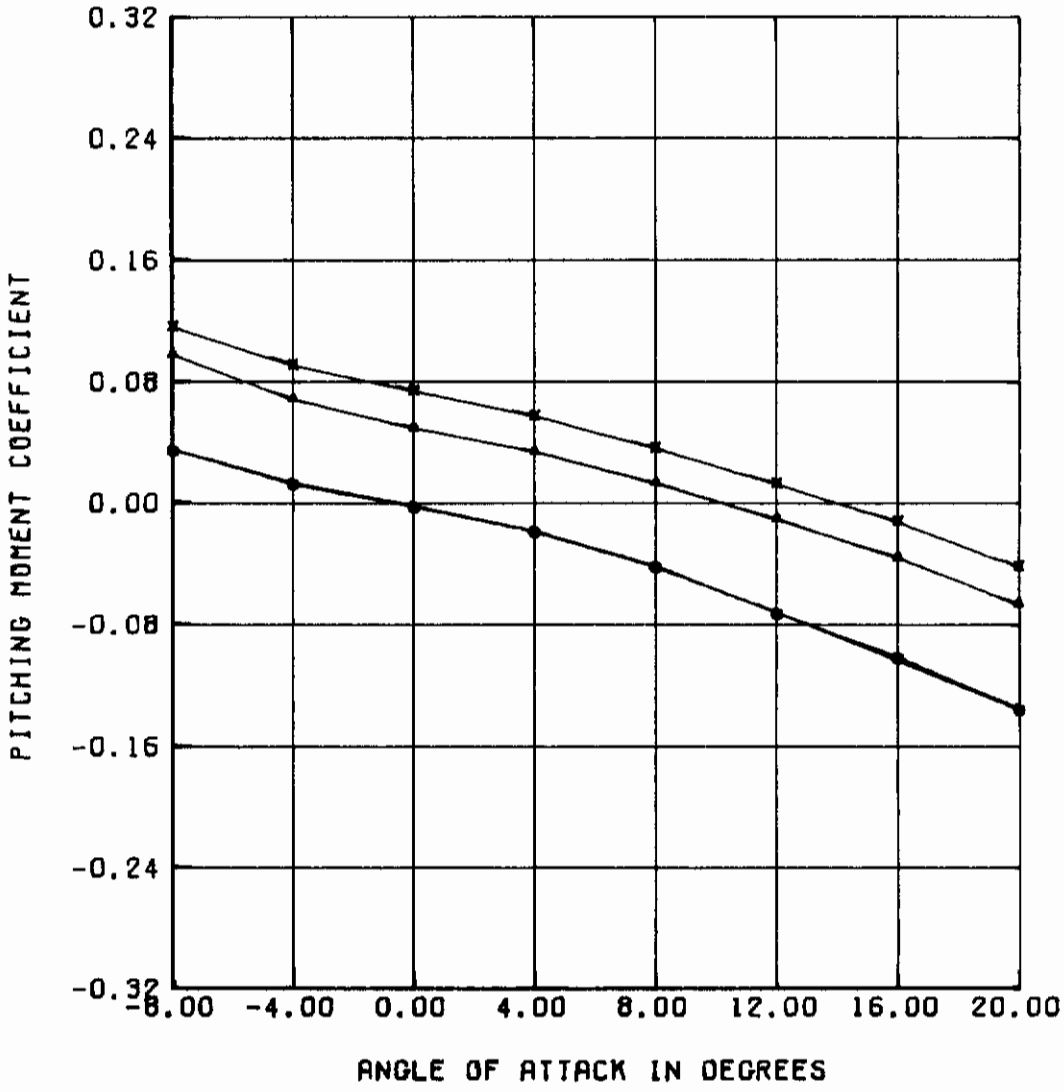


Figure 26. (Continued)

| CONFIGURATION | FLAP DEFLECTION, DEG | |
|---|---|---|
| | 0° | -20° |
| D/50/50/10 (INNER FLAP FIXED) | ○ | △ |
| D/50/50/10 (OUTER FLAP FIXED) | + | x |

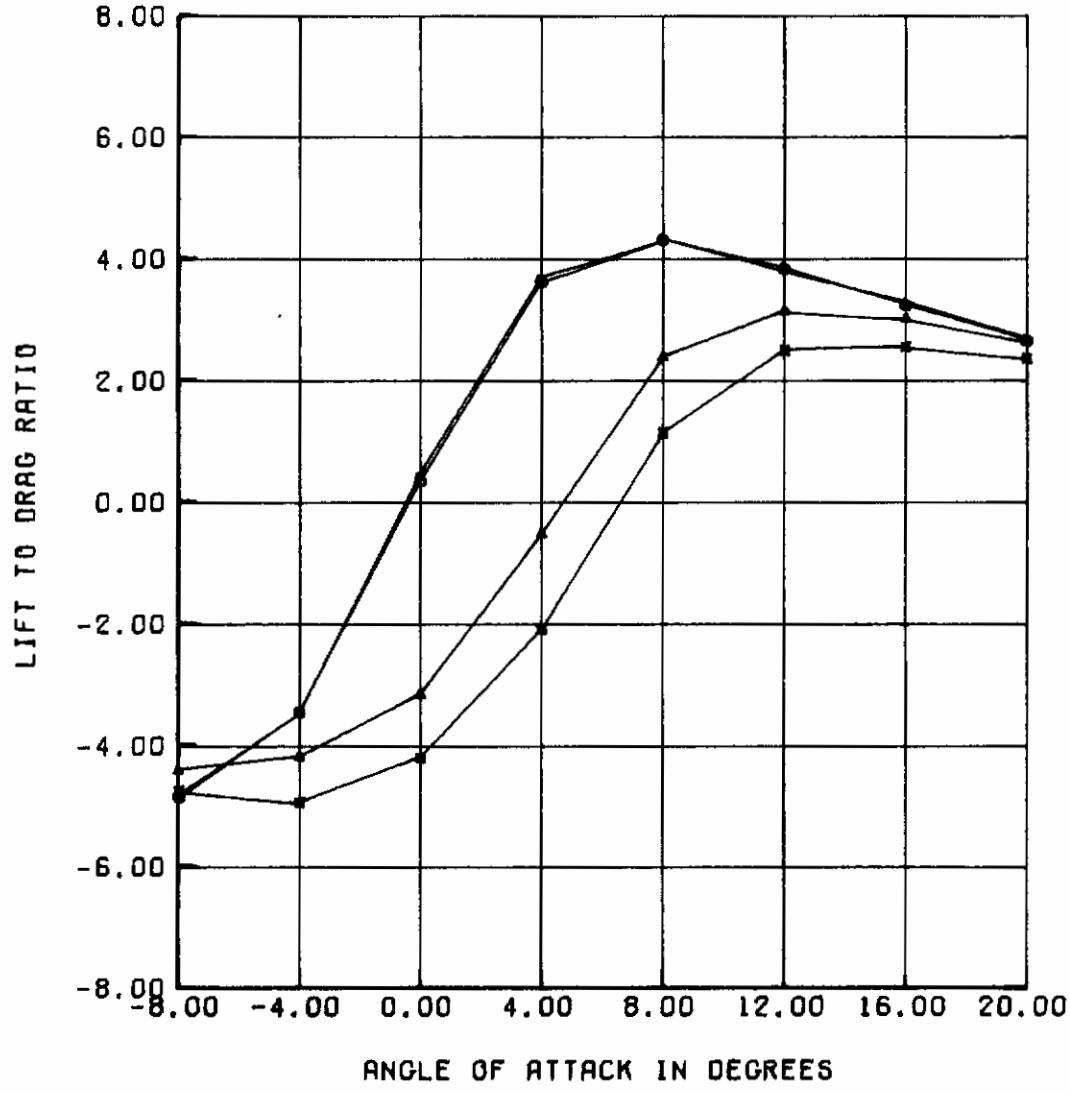


Figure 26. (Concluded)

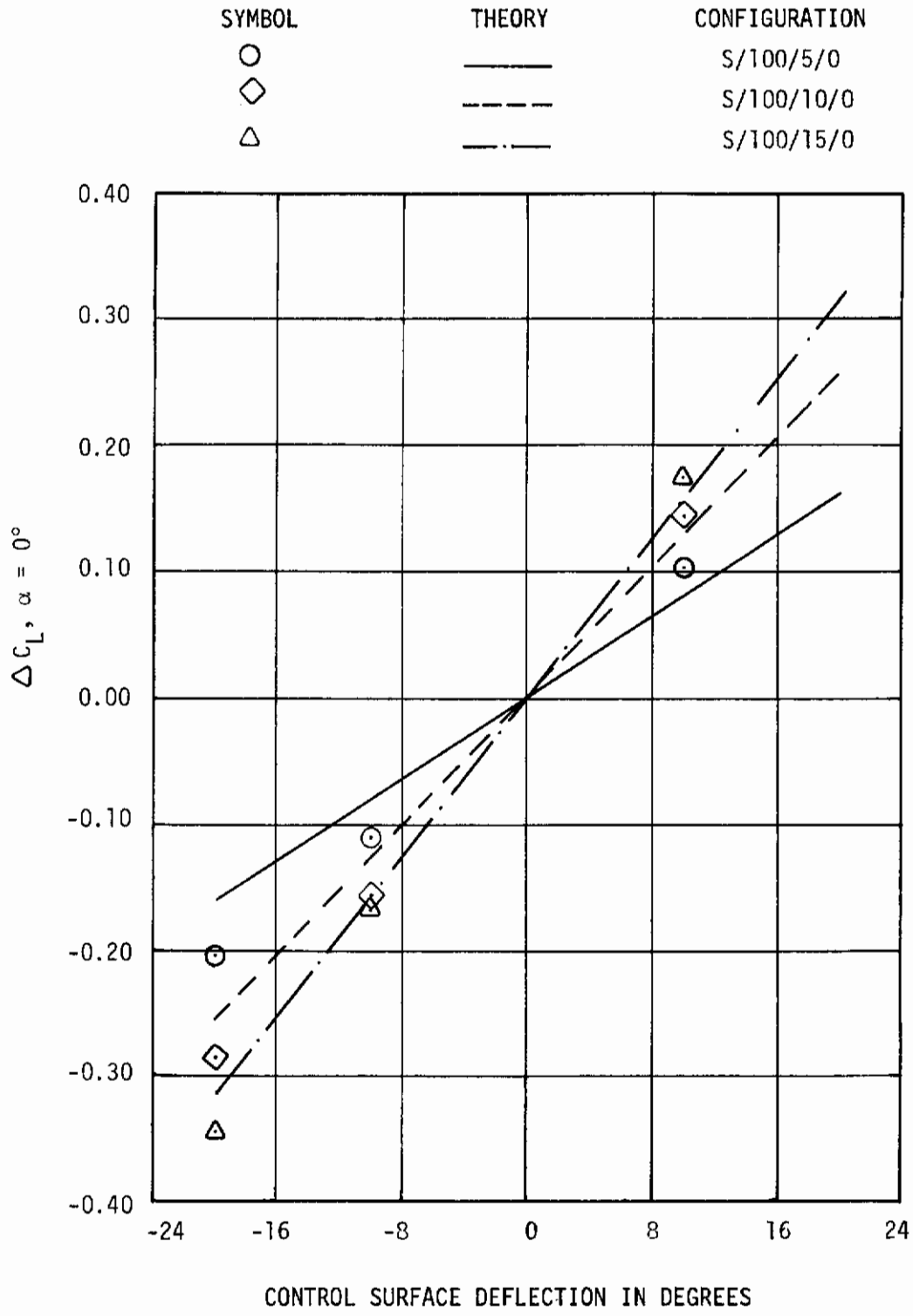


Figure 27. Comparison of Measured and Calculated Incremental Control Surface Effects for Various Flap Chords at Constant Span Using the Isolated Wing Concept

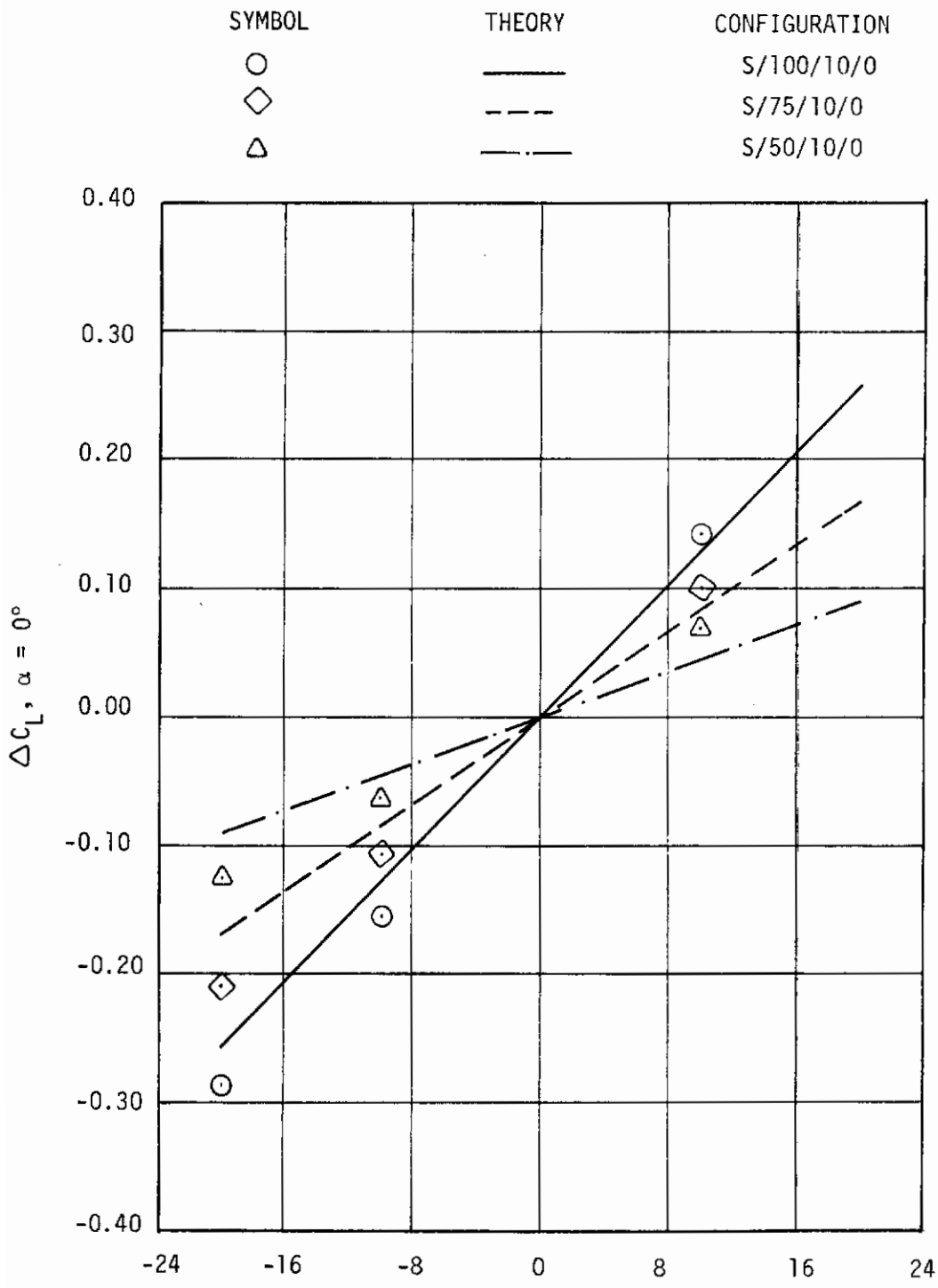


Figure 28. Comparison of Measured and Calculated Incremental Control Surface Effects for Various Span Configurations Using the Isolated Wing Concept

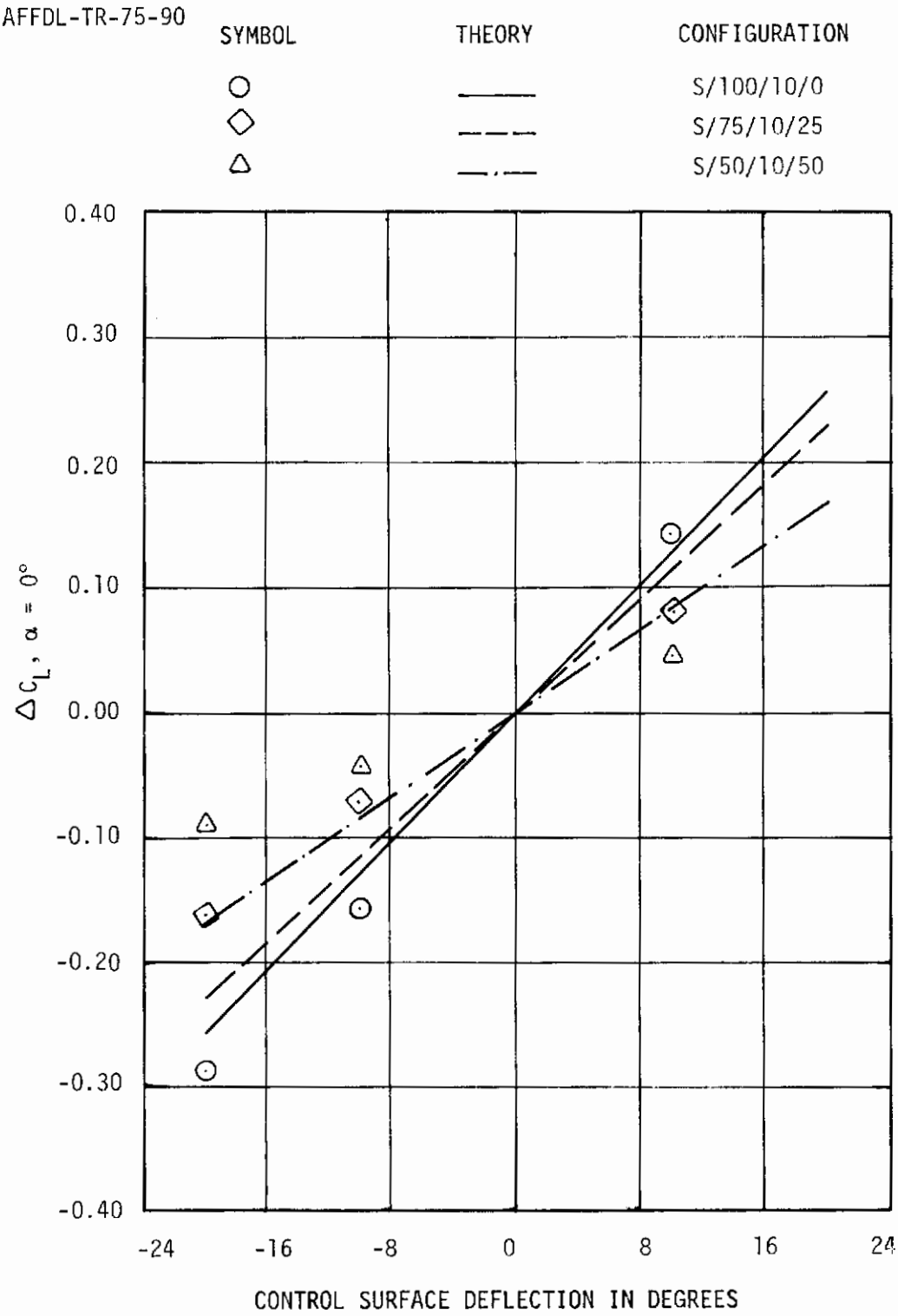


Figure 29. Comparison of Measured and Calculated Incremental Control Surface Effects for Various Span Configurations With Separated Flaps Using the Isolated Wing Concept

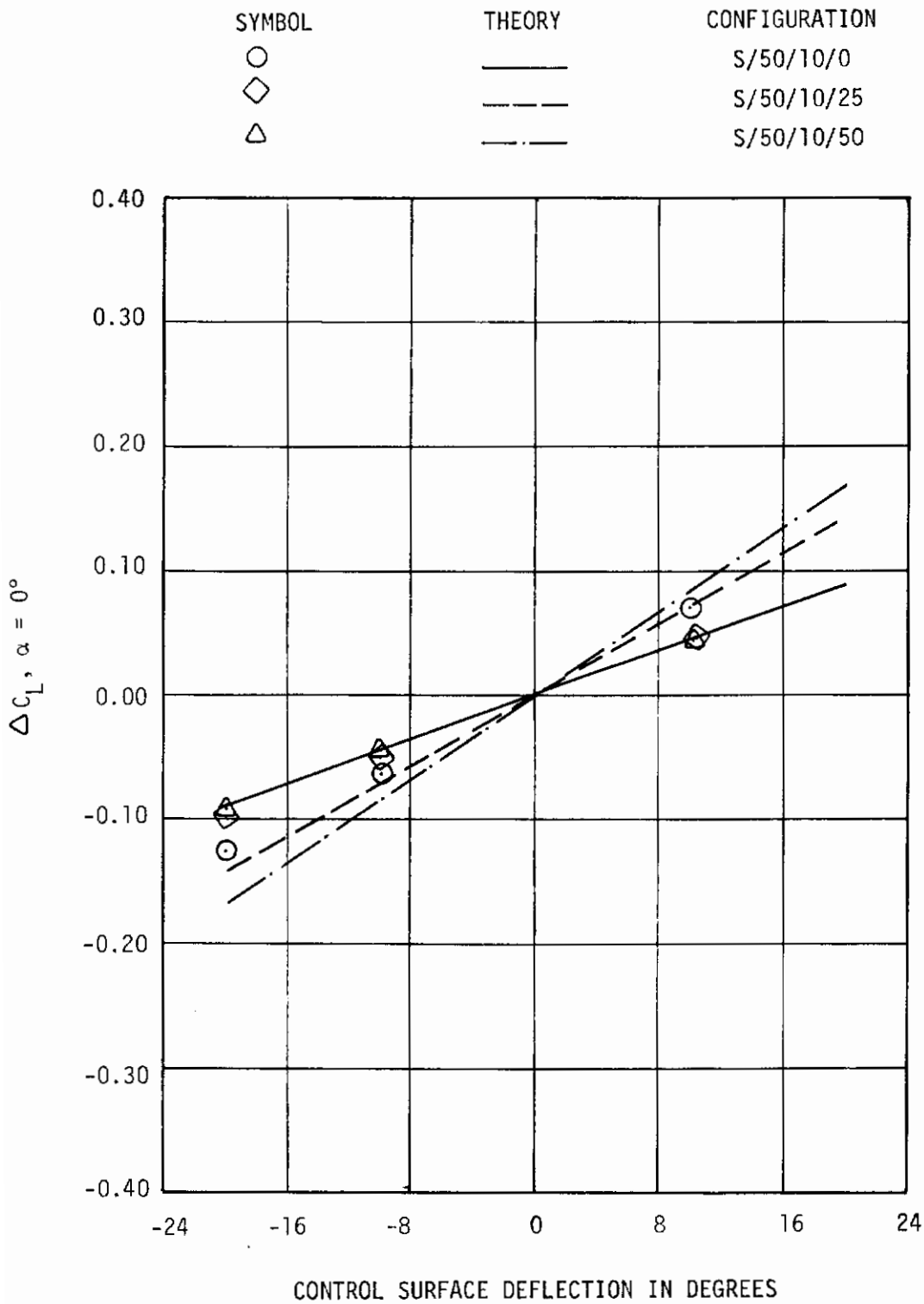


Figure 30. Comparison of Measured and Calculated Incremental Control Surface Effects for Various Separation Distances Using the Isolated Wing Concept

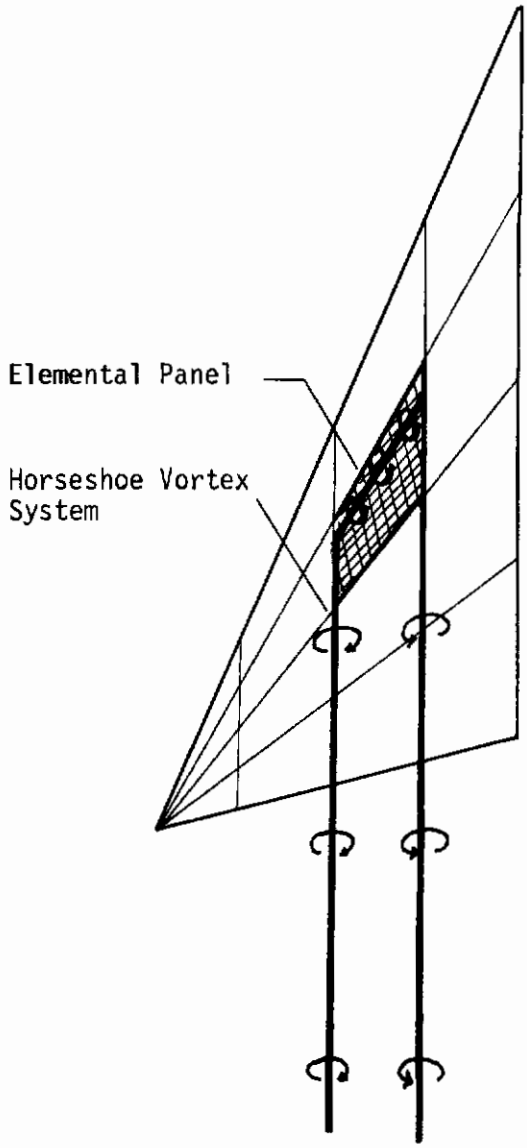


Figure 31. Typical Horseshoe Vortex System

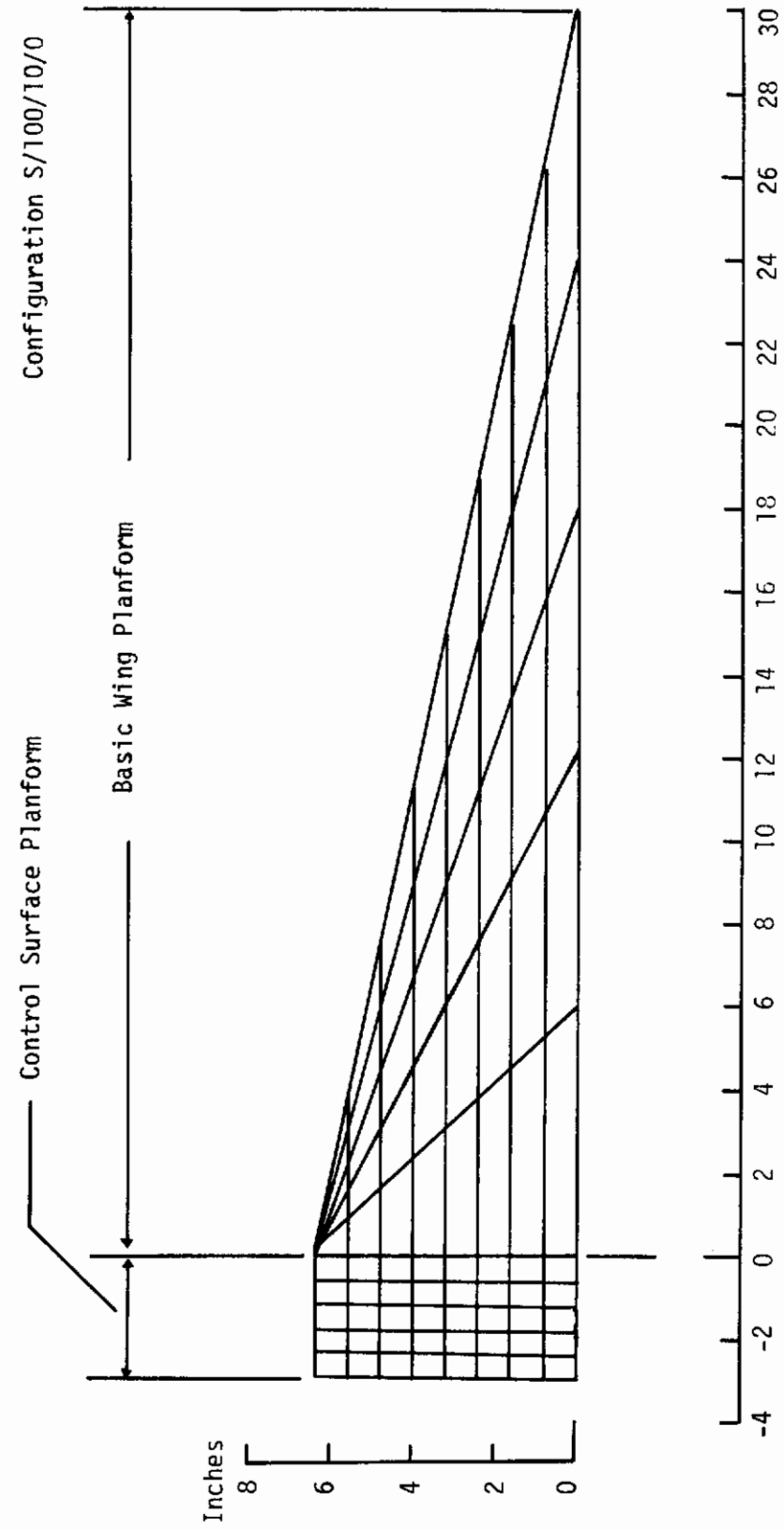


Figure 32. Panel Element Breakdown for a Typical Two Planform Configuration

| SYMBOL | THEORY | CONFIGURATION |
|---|---|---|
| ○ | ——— | S/100/5/0 |
| ◇ | – – – | S/100/10/0 |
| △ | —·— | S/100/15/0 |

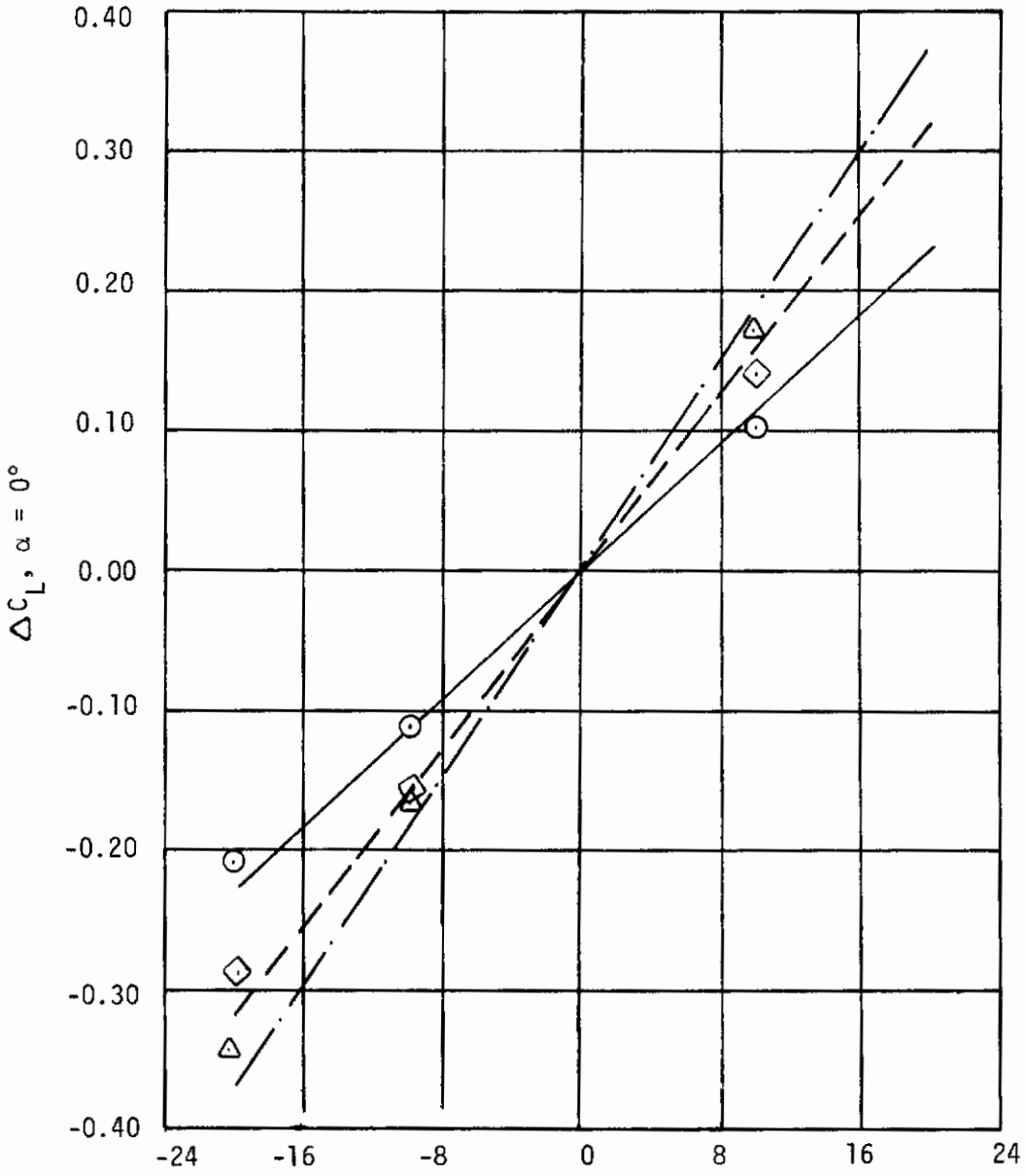


Figure 33. Comparison of Measured and Calculated Incremental Control Surface Effects for Various Flap Chords at Constant Span Using the Vortex Lattice Method

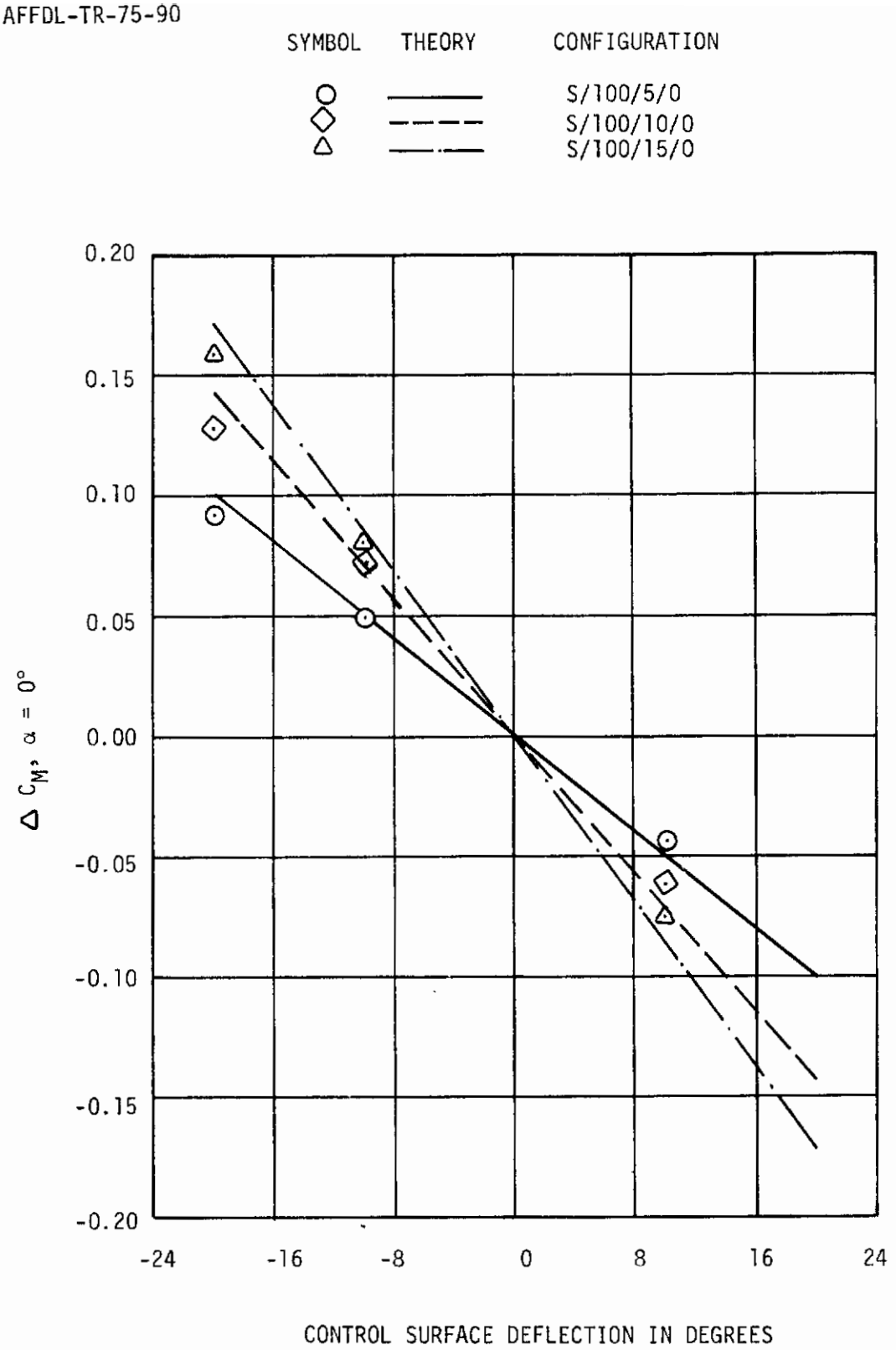


Figure 33 . (Concluded)

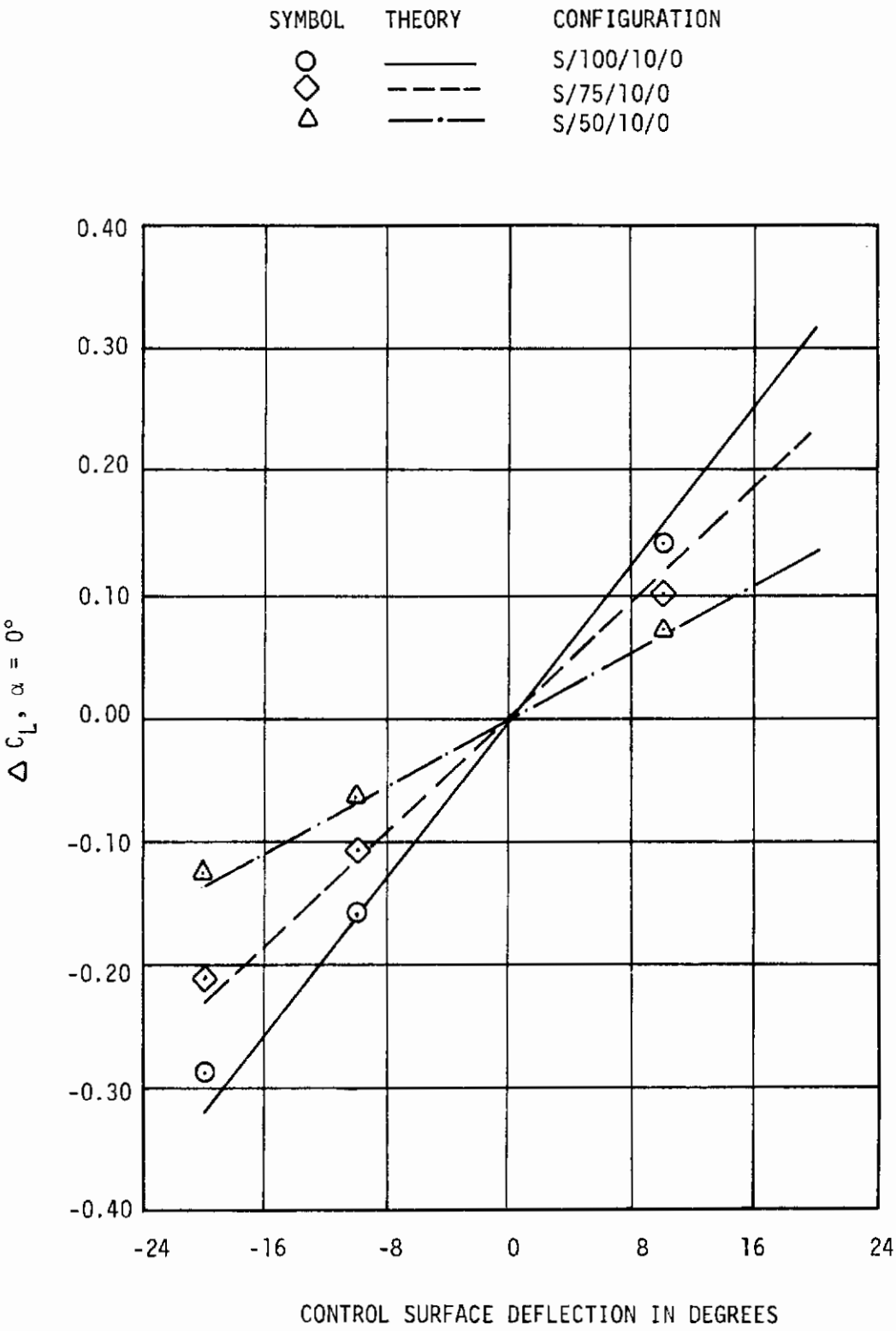


Figure 34. Comparison of Measured and Calculated Incremental Control Surface Effects for Various Span Configurations Using the Vortex Lattice Method

| SYMBOL | THEORY | CONFIGURATION |
|---|---|---|
| ○ | ——— | S/100/10/0 |
| ◇ | – – – | S/75/10/0 |
| △ | —·— | S/50/10/0 |

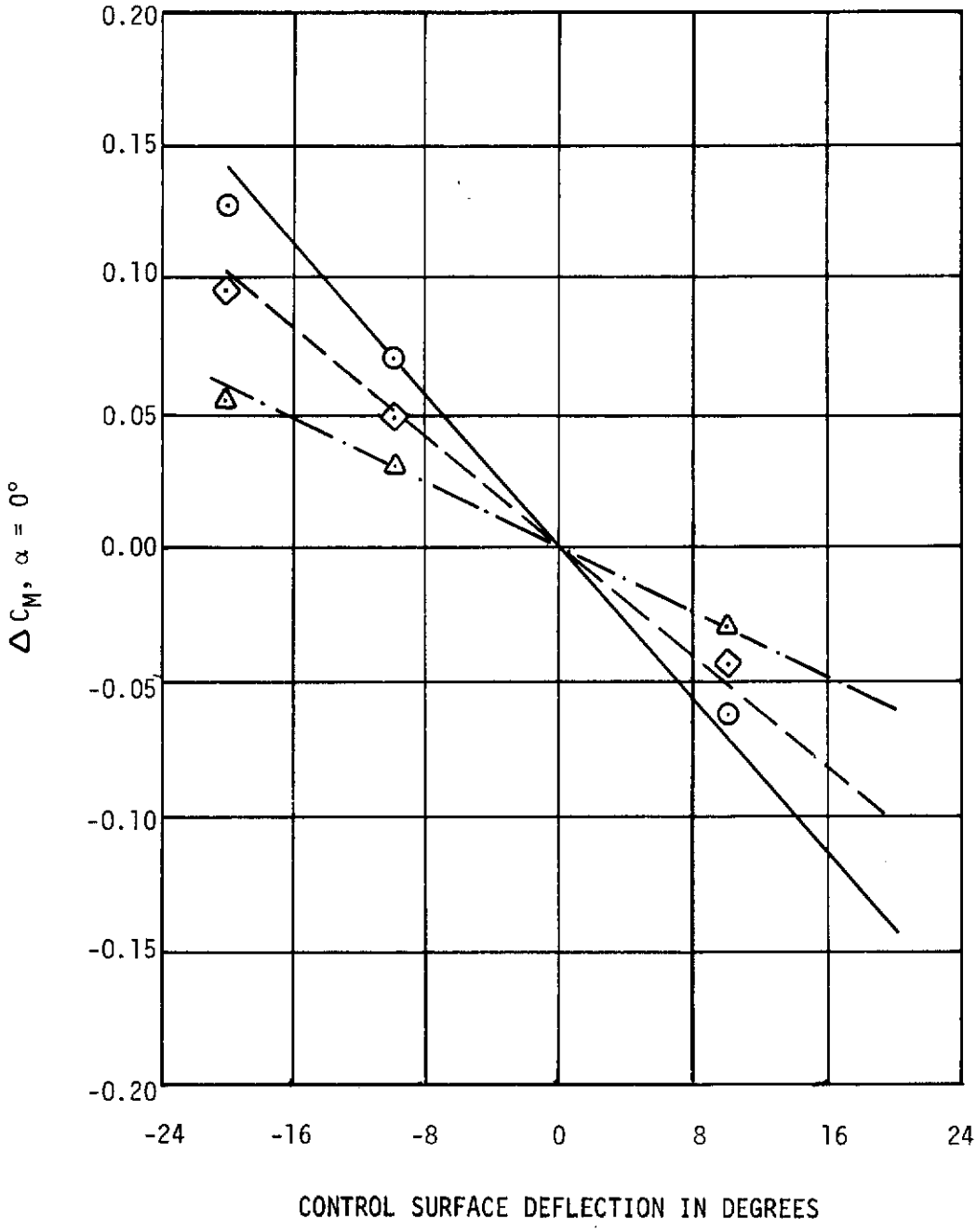


Figure 34 . (Concluded)

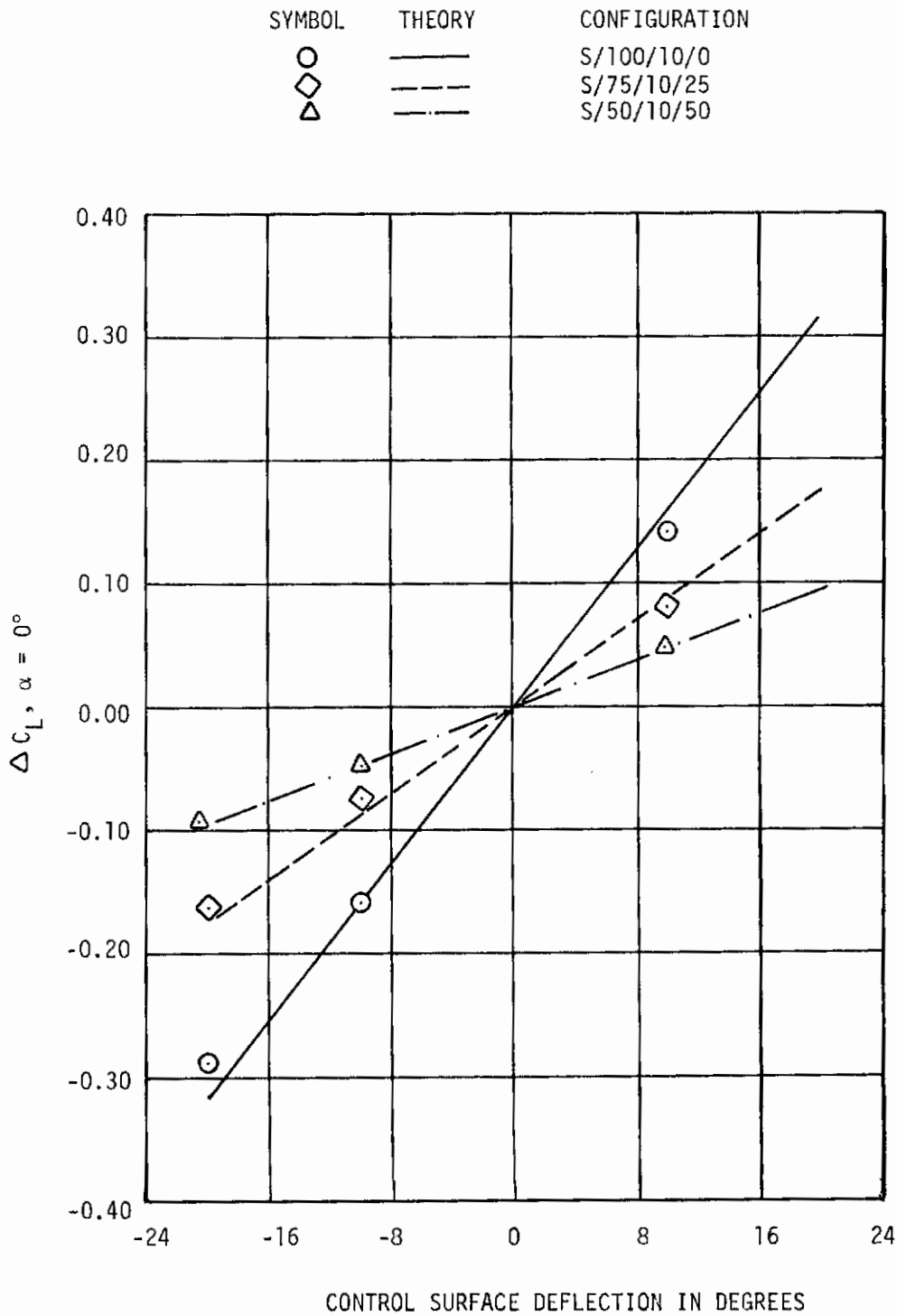


Figure 35. Comparison of Measured and Calculated Incremental Control Surface Effects for Various Span Configurations with Separated Flaps Using the Vortex Lattice Method

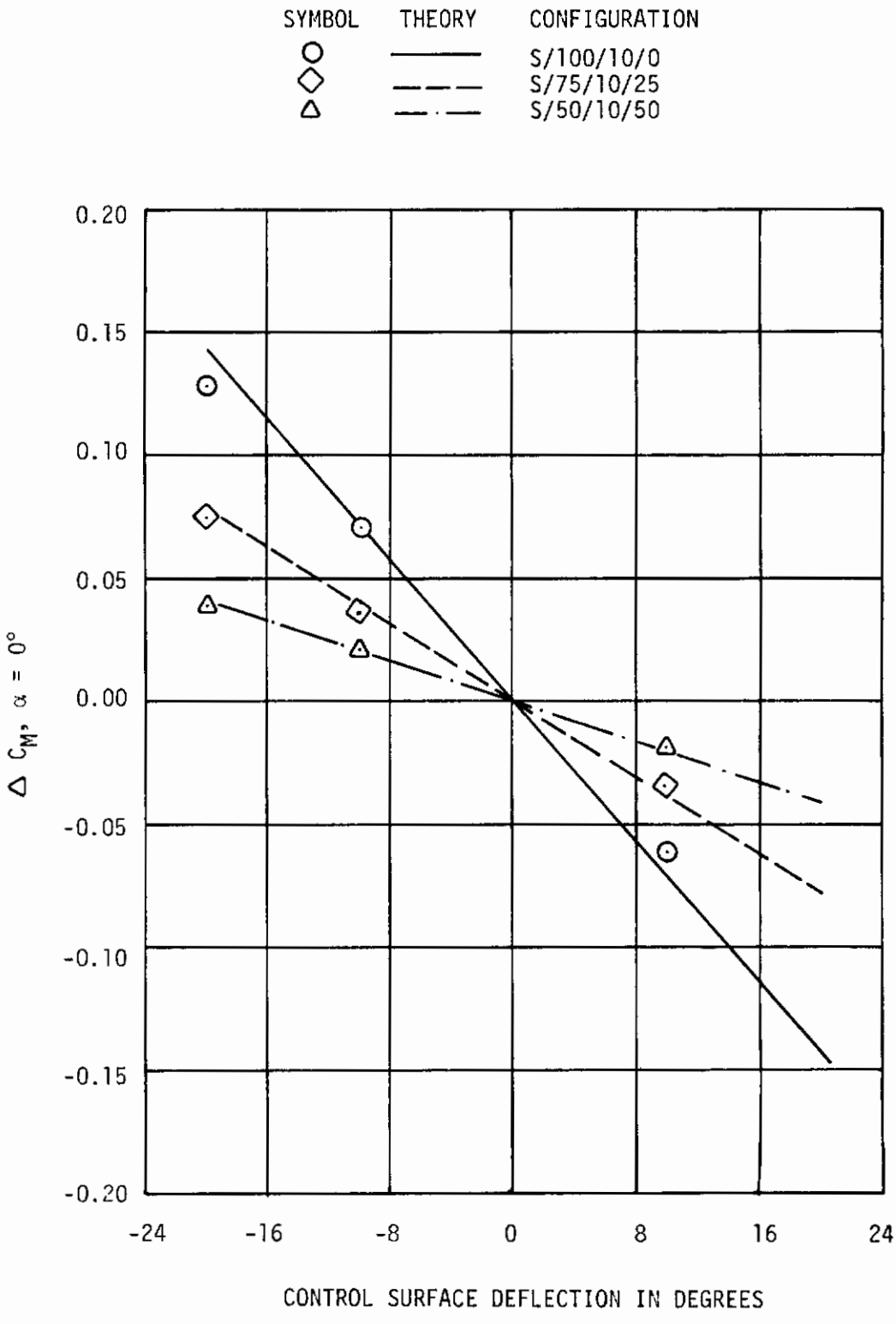


Figure 35 . (Concluded)

| SYMBOL | THEORY | CONFIGURATION |
|---|---|---|
| ○ | ——— | S/50/10/0 |
| ◇ | — — — | S/50/10/25 |
| △ | — . — | S/50/10/50 |

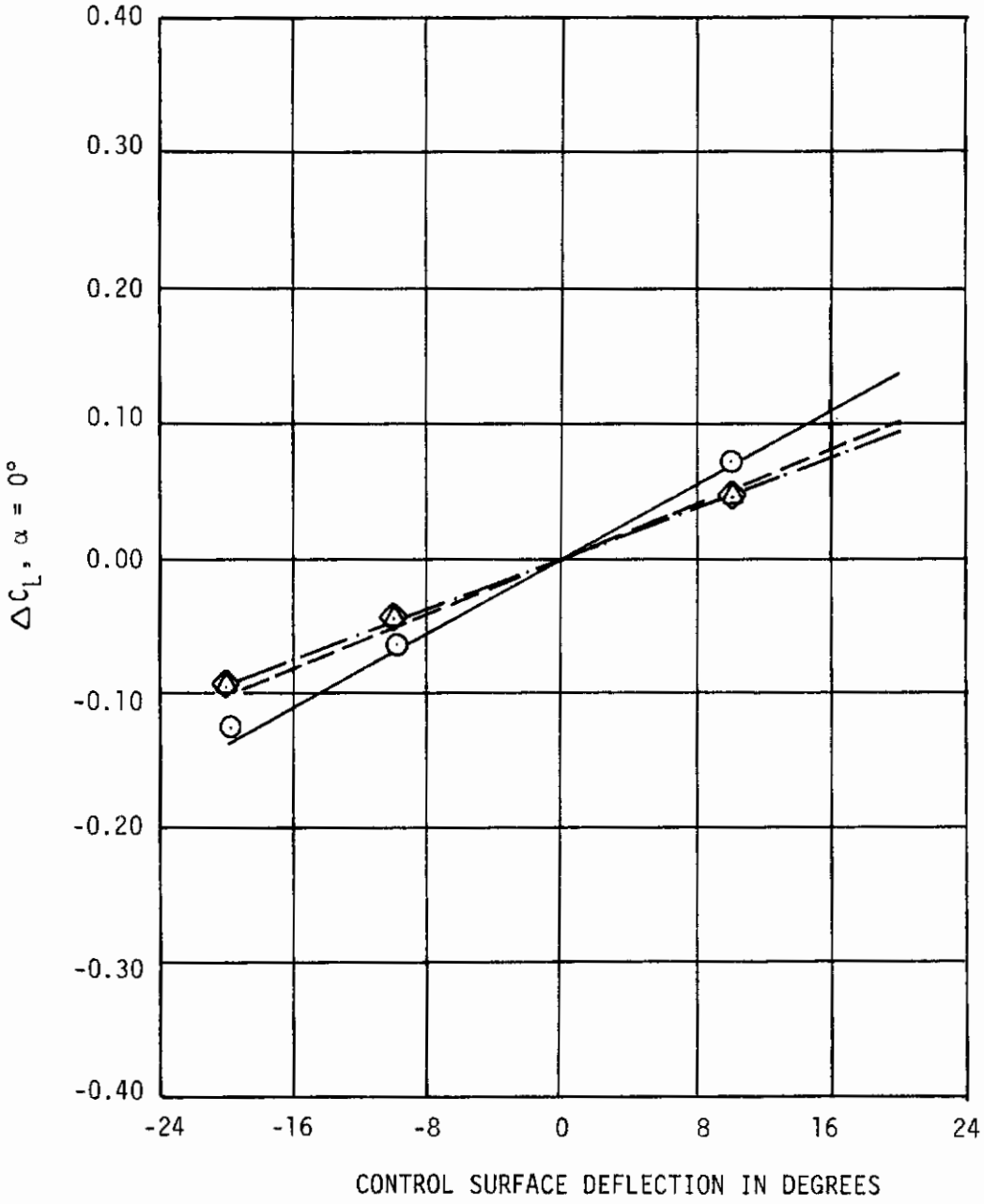


Figure 36. Comparison of Measured and Calculated Incremental Control Surface Effects for Various Separation Distances Using the Vortex Lattice Method

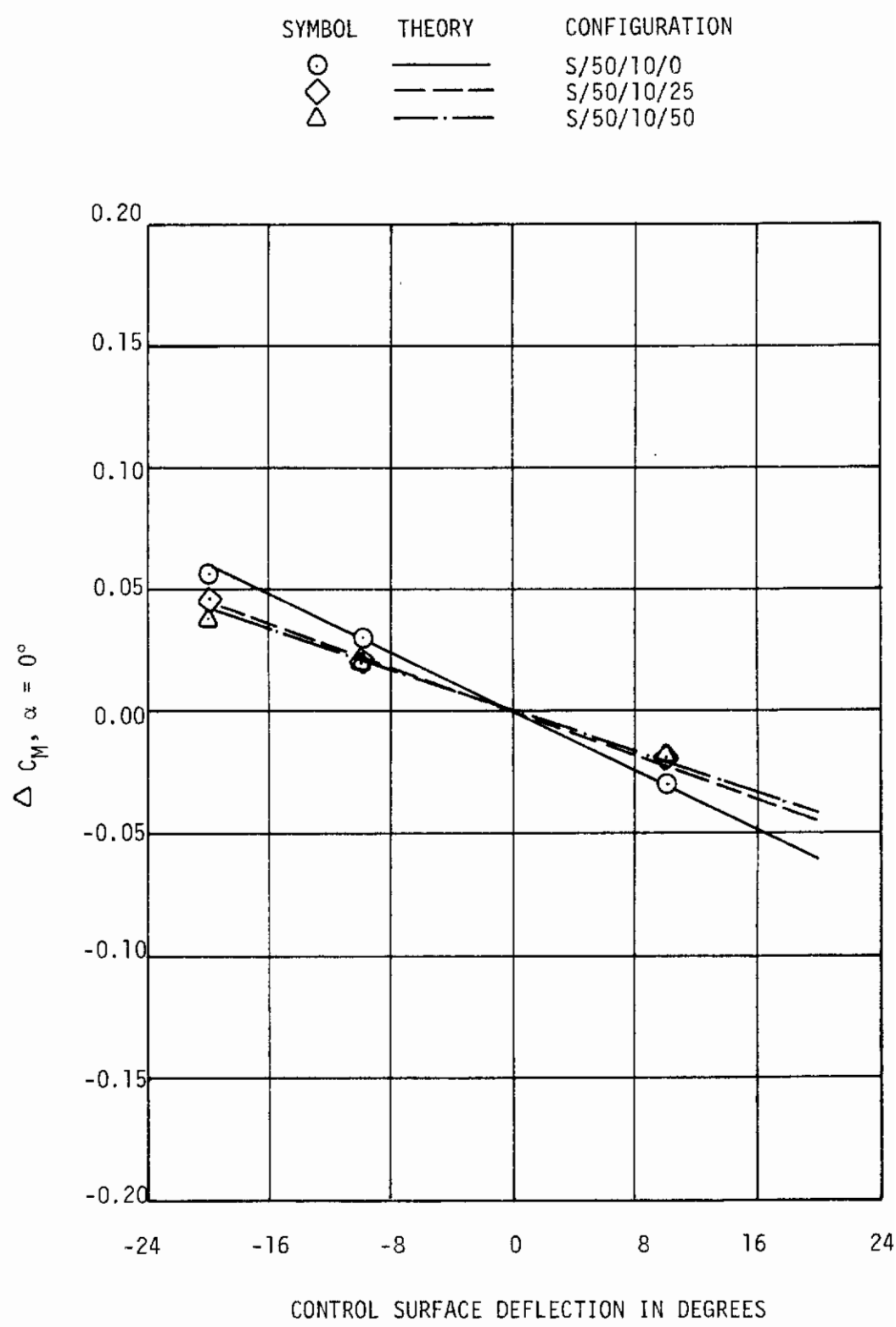


Figure 36 . (Concluded)

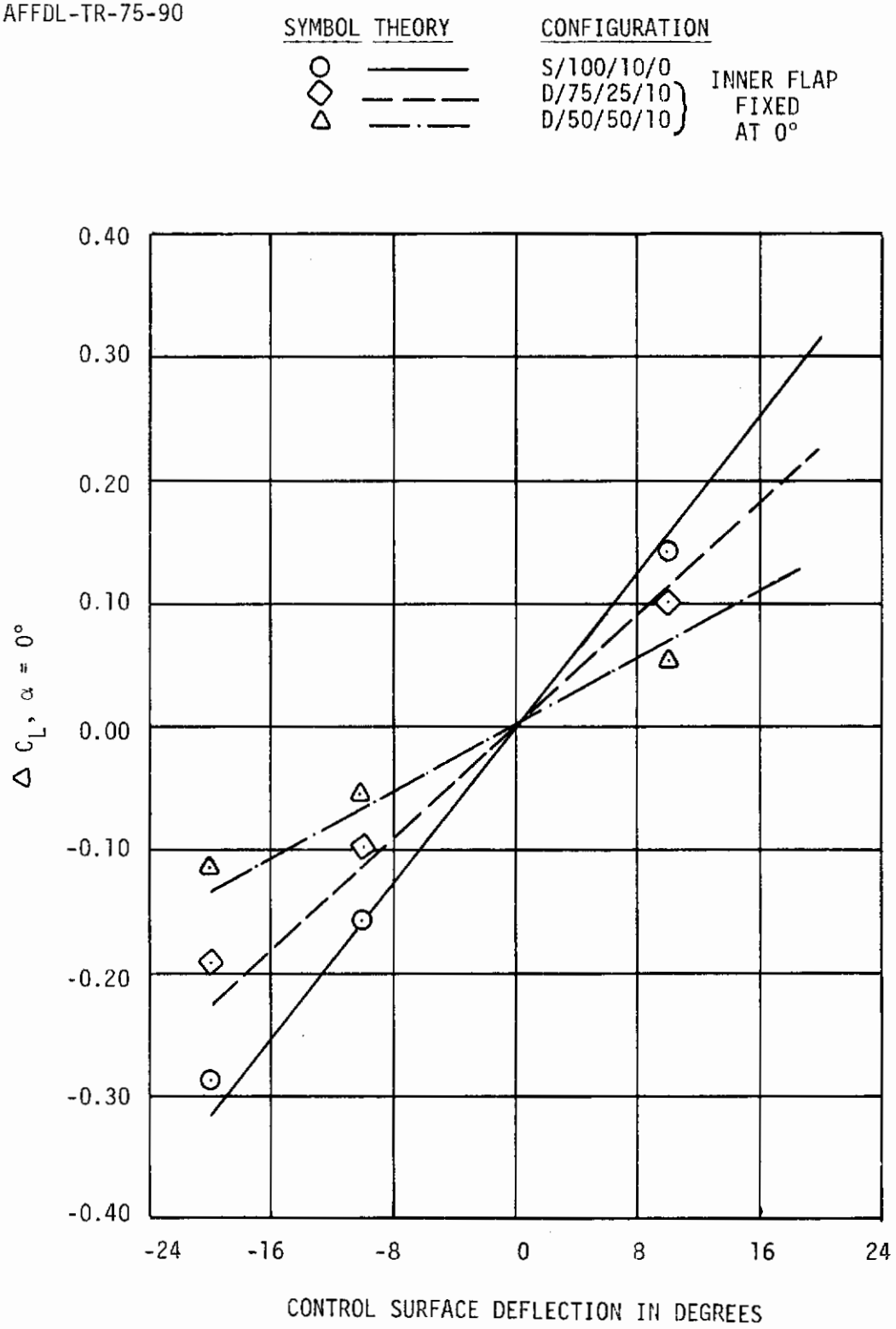


Figure 37. Comparison of Measured and Calculated Incremental Control Surface Effects for Various Span Configurations with Separated Flaps and Fixed Center Flaps Using the Vortex Lattice Method

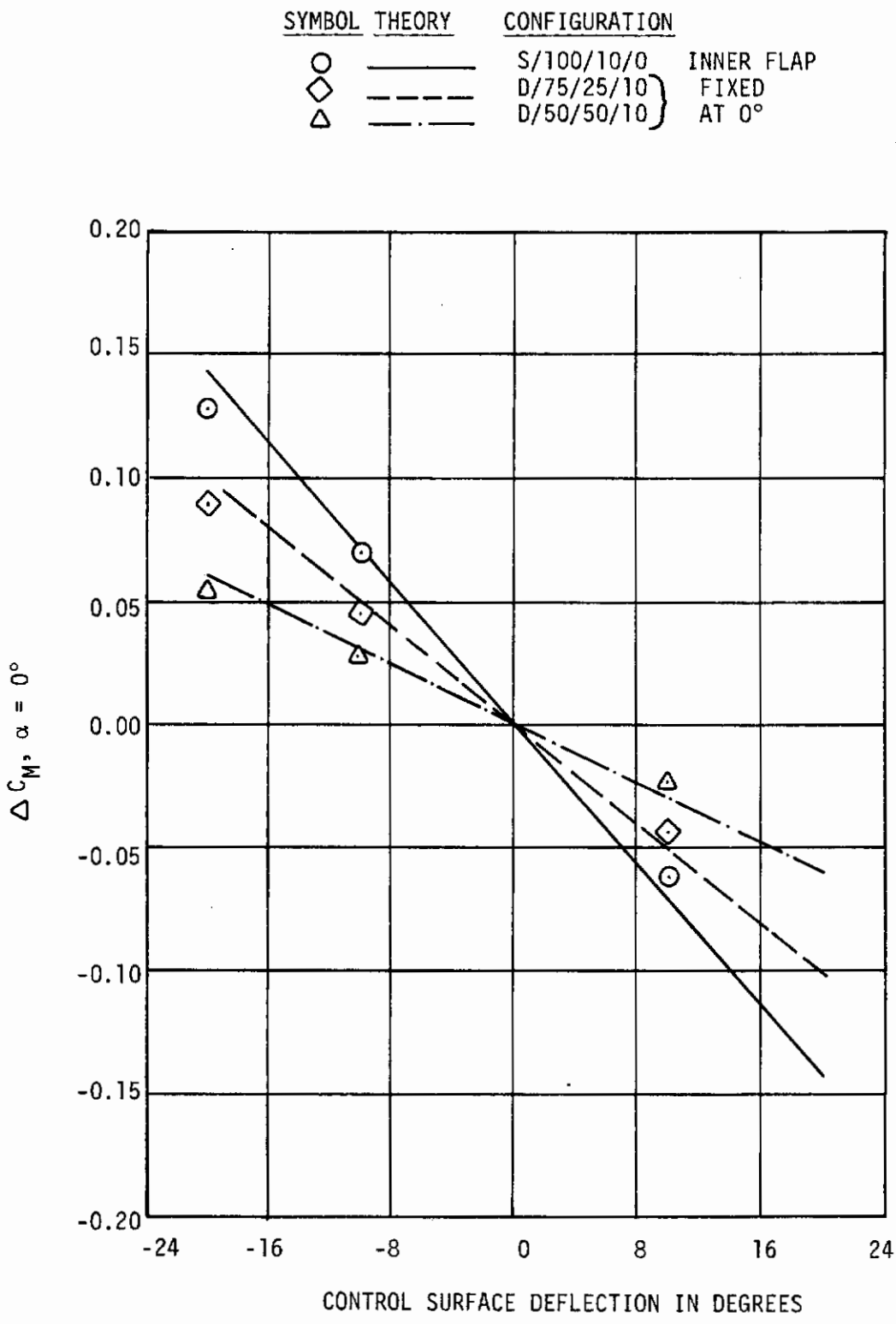


Figure 37 . (Concluded)

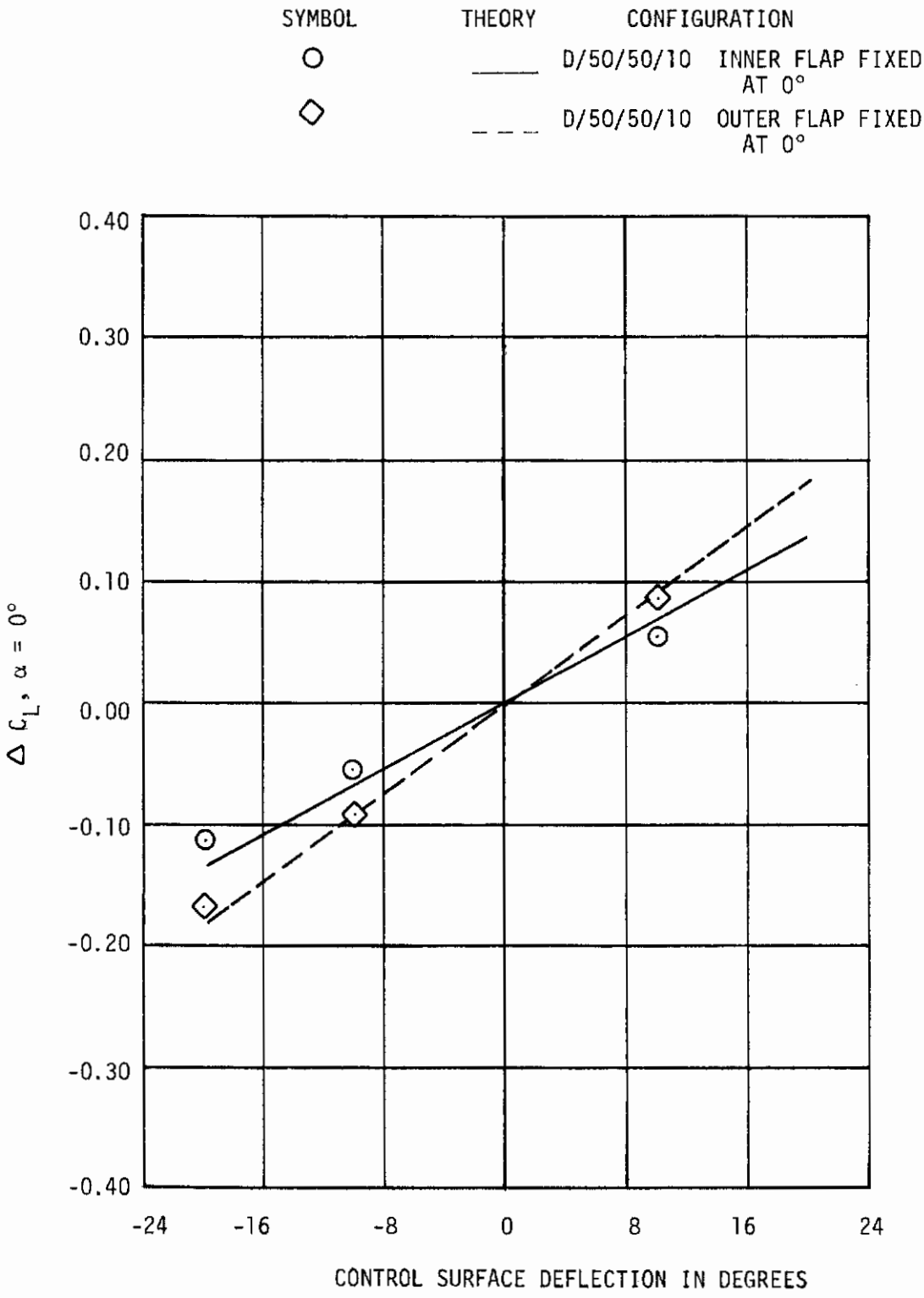


Figure 38. Comparison of Measured and Calculated Incremental Control Surface Effects for a Dual Flap Configuration Using the Vortex Lattice Method

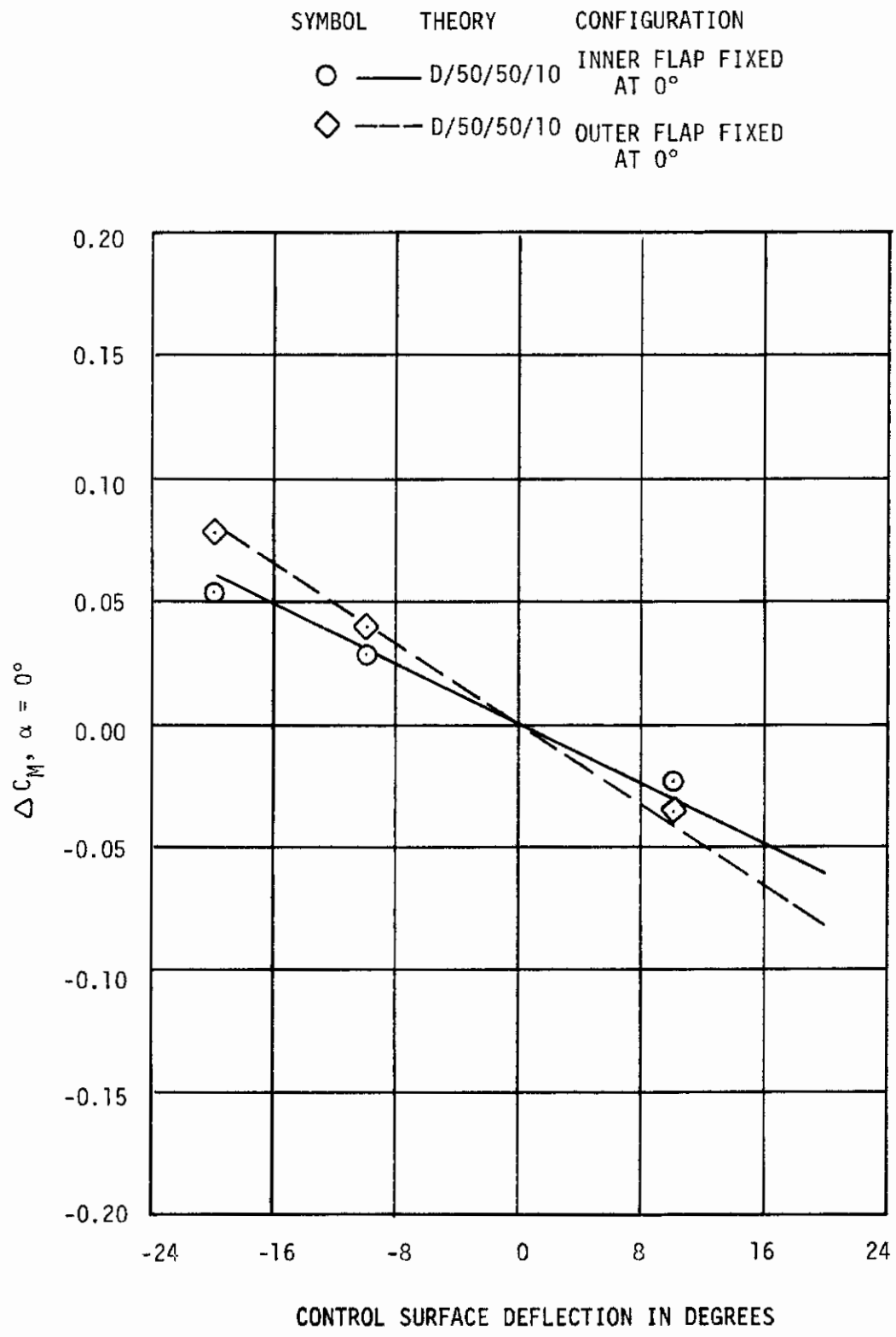


Figure 38 . (Concluded)

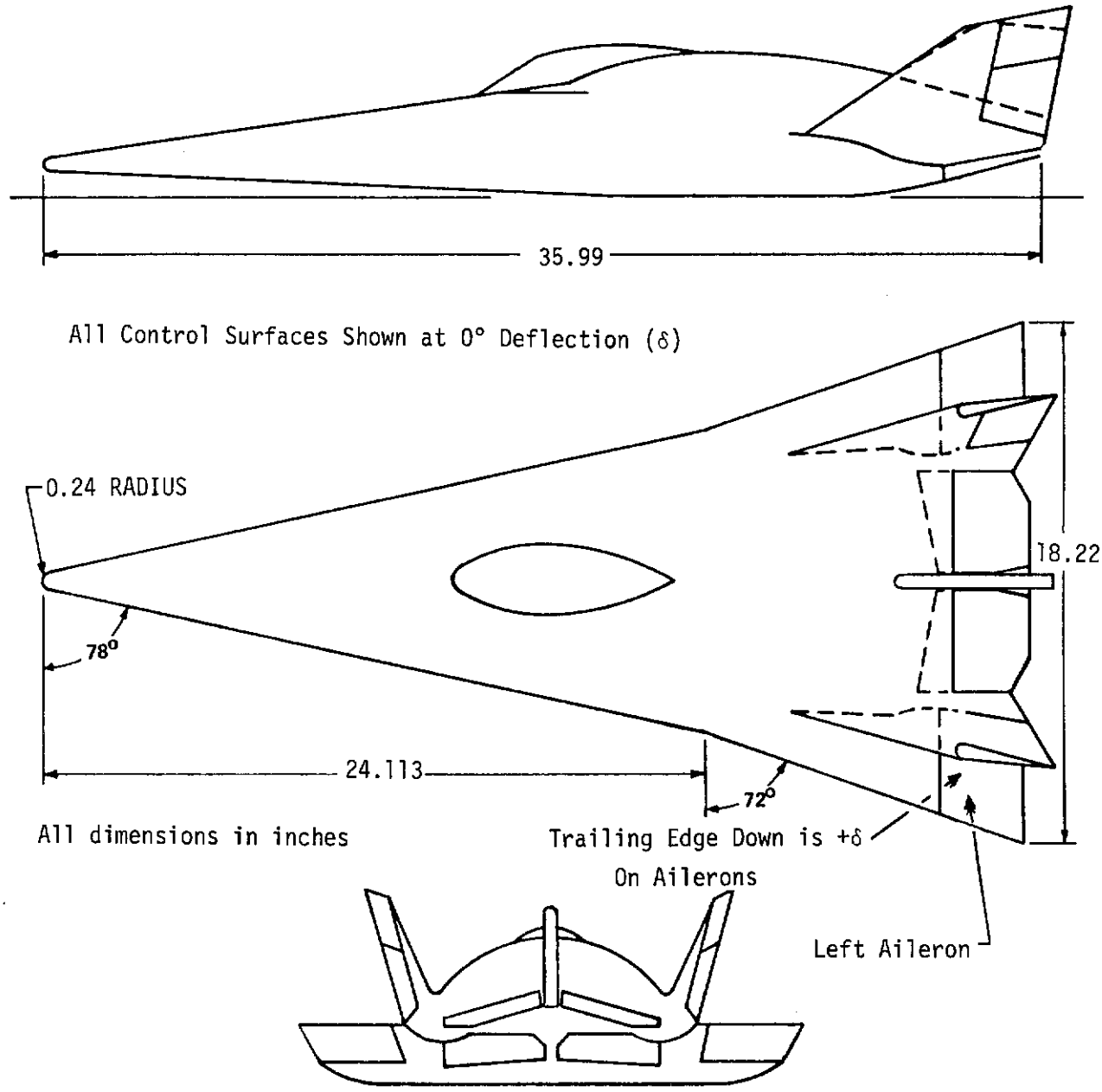


Figure 39. X-24B Configuration

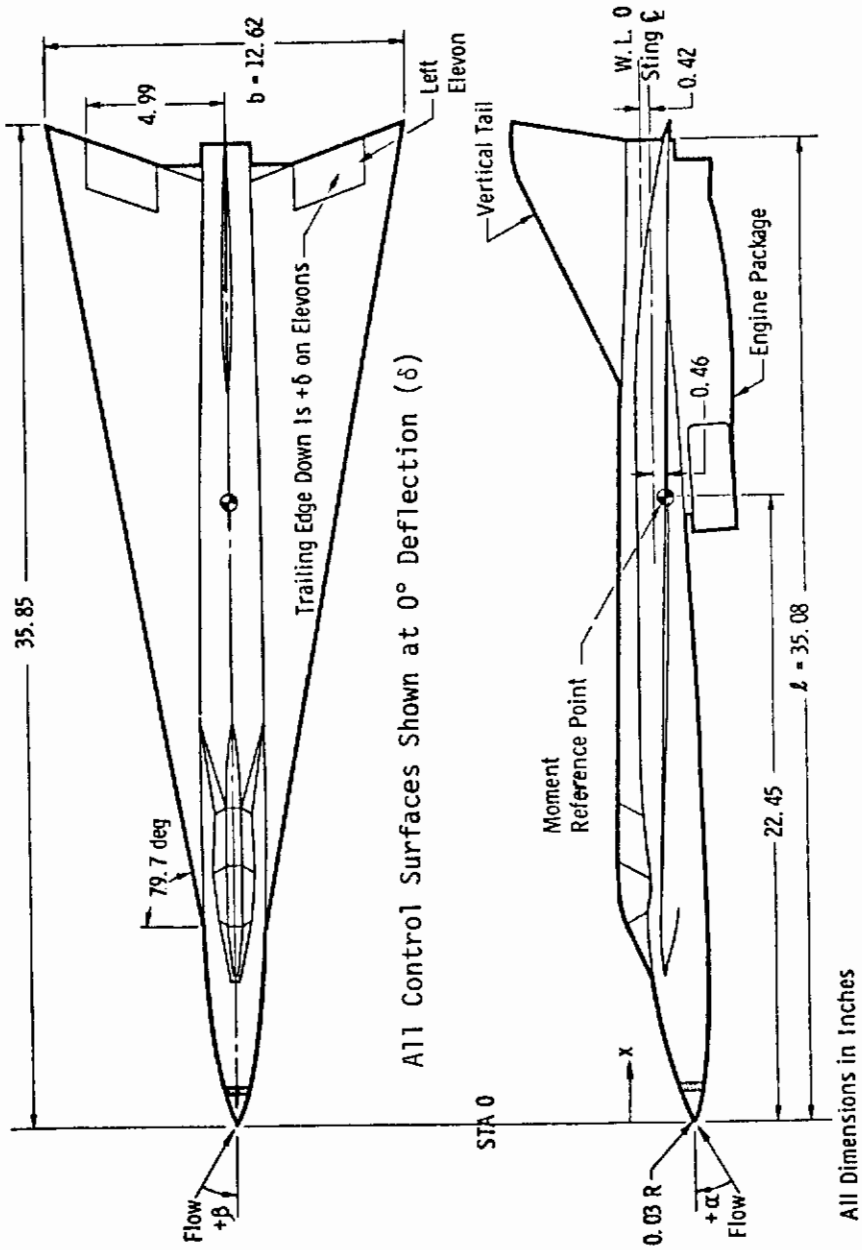


Figure 40. Advanced Air Defense Wing-Body Configuration

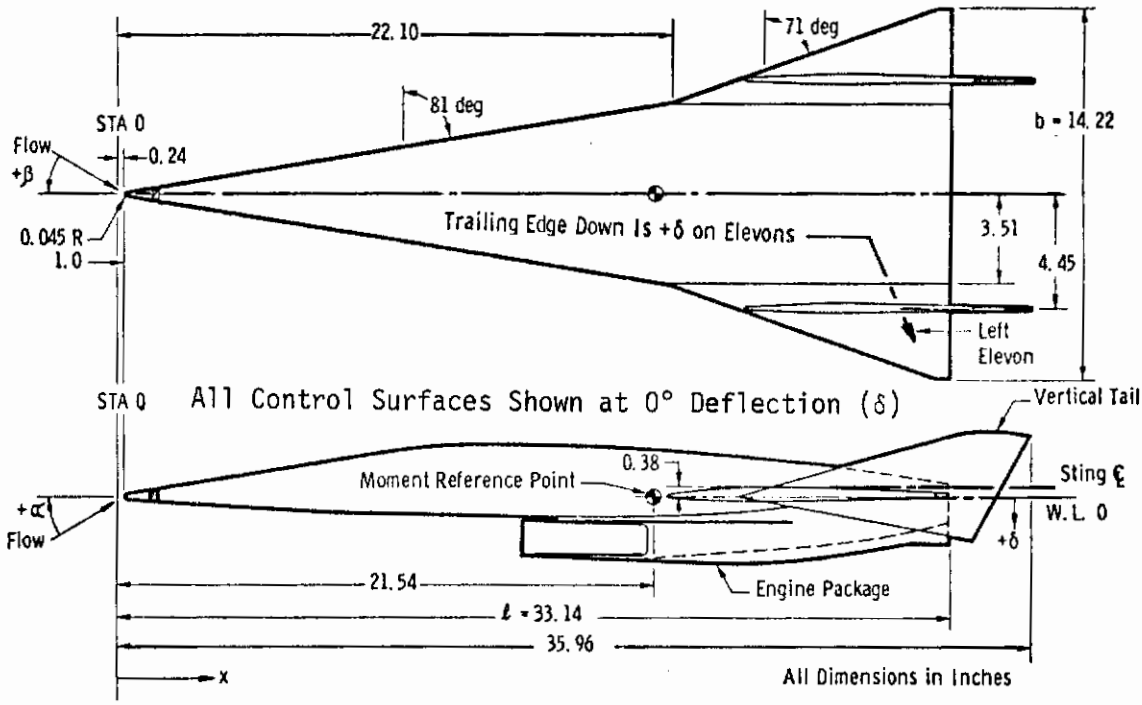


Figure 41. Advanced Air Defense Blended-Body Configuration

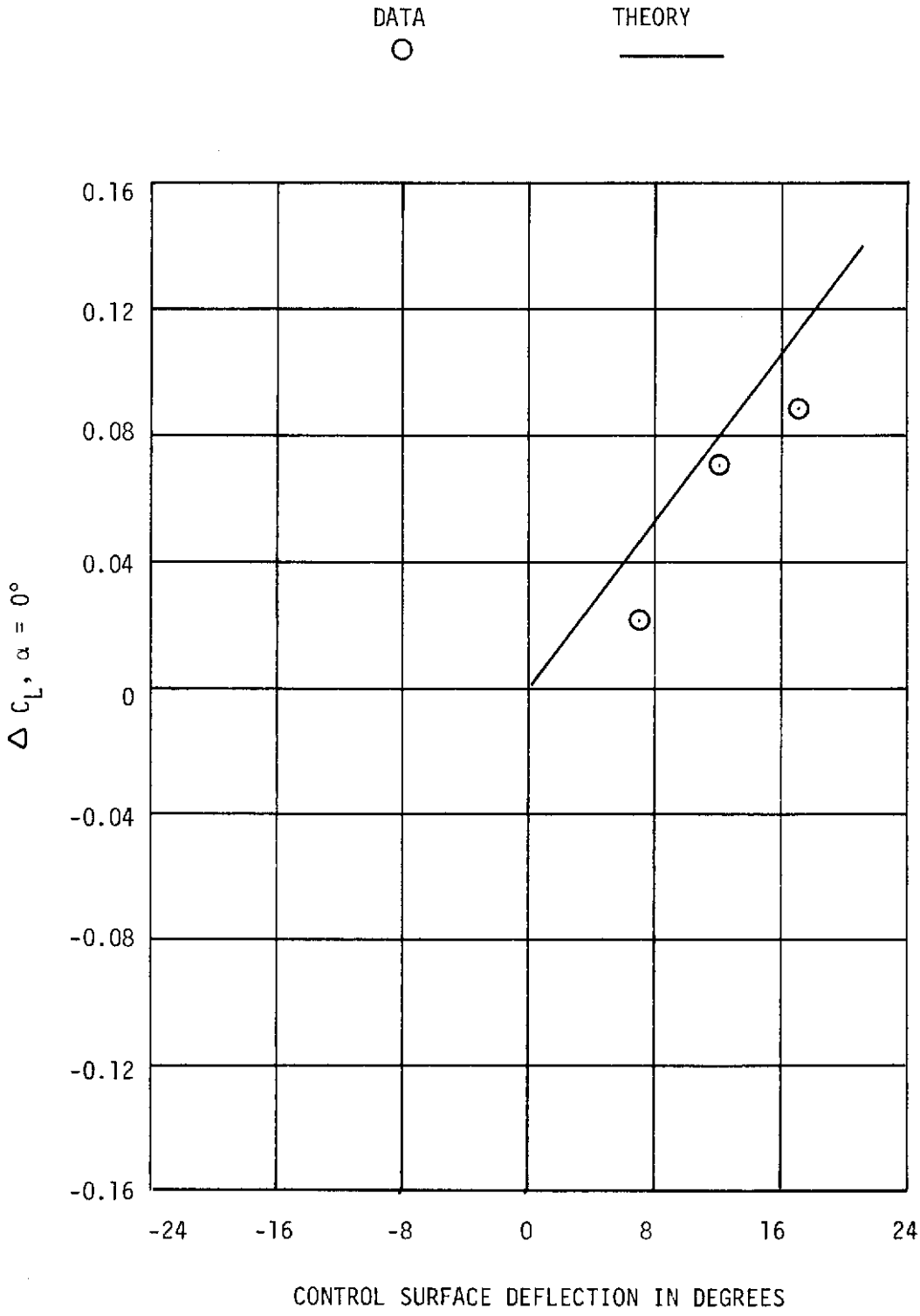


Figure 42. Comparison of Measured and Calculated Incremental Control Surface Effects on an 8% Scale X-24B Model at M=0.6

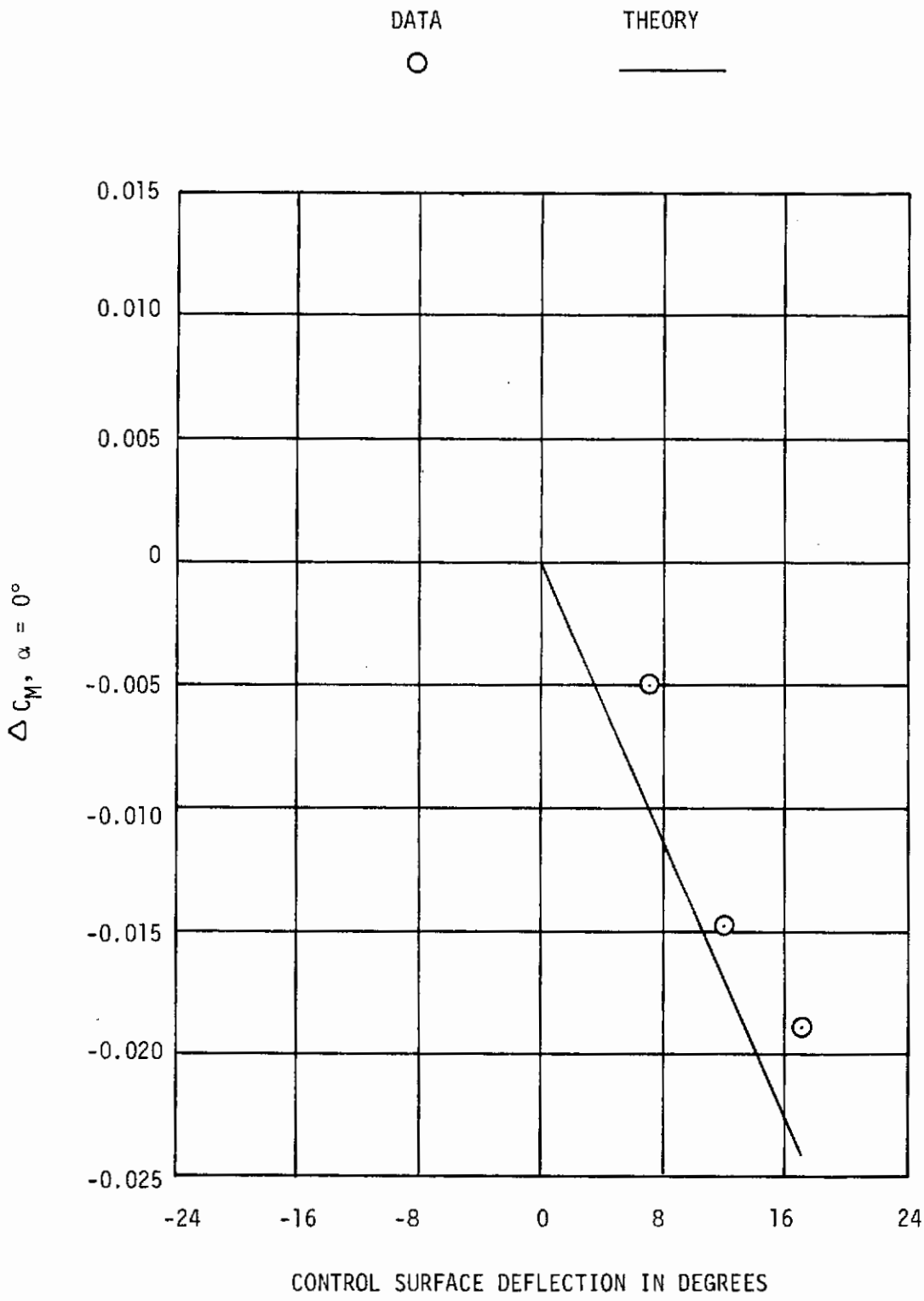


Figure 42 . (Concluded)

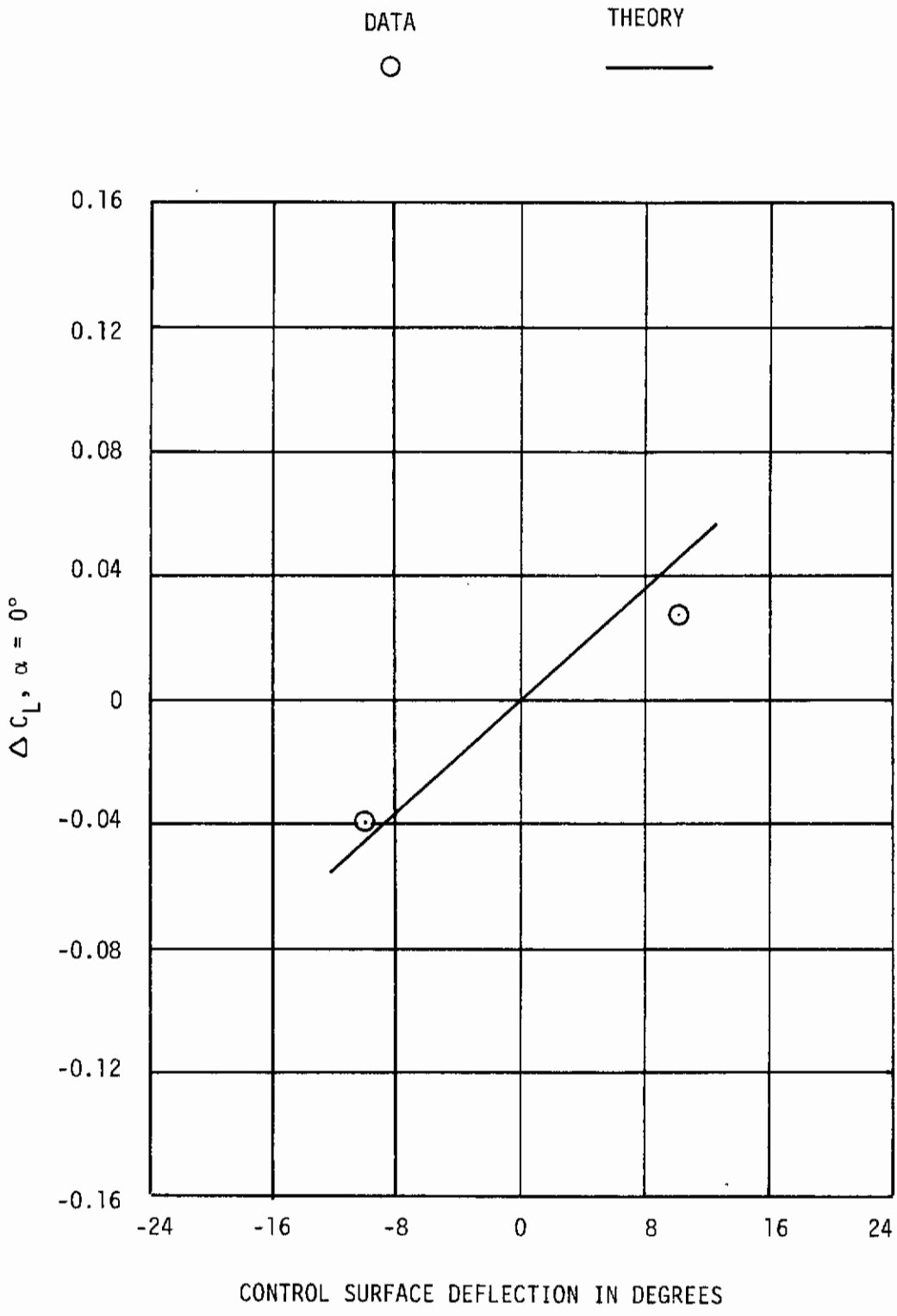


Figure 43. Comparison of Measured and Calculated Incremental Control Surface Effects on an Advanced Air Defense Wing-Body Model at M=0.2

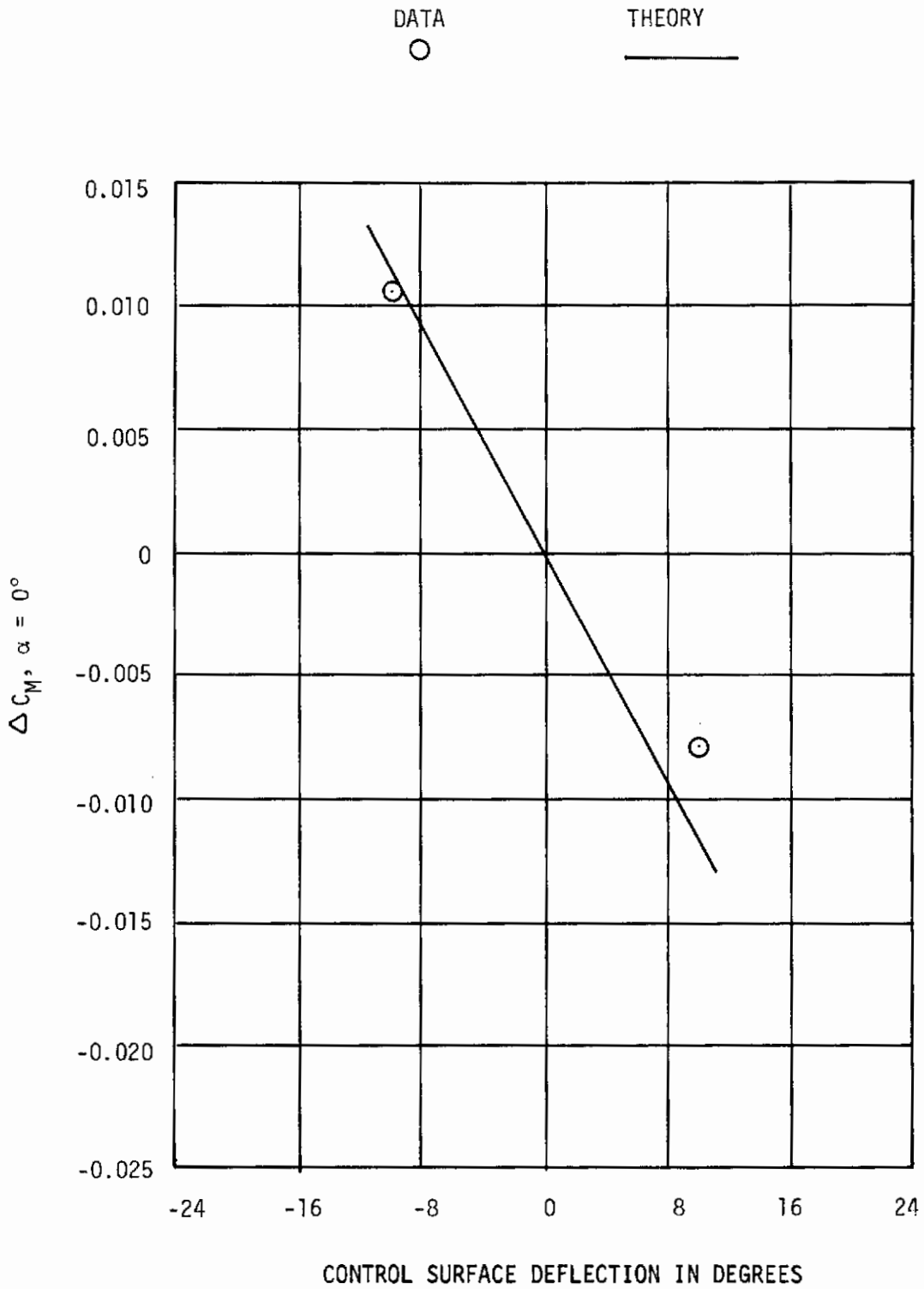


Figure 43. (Concluded)

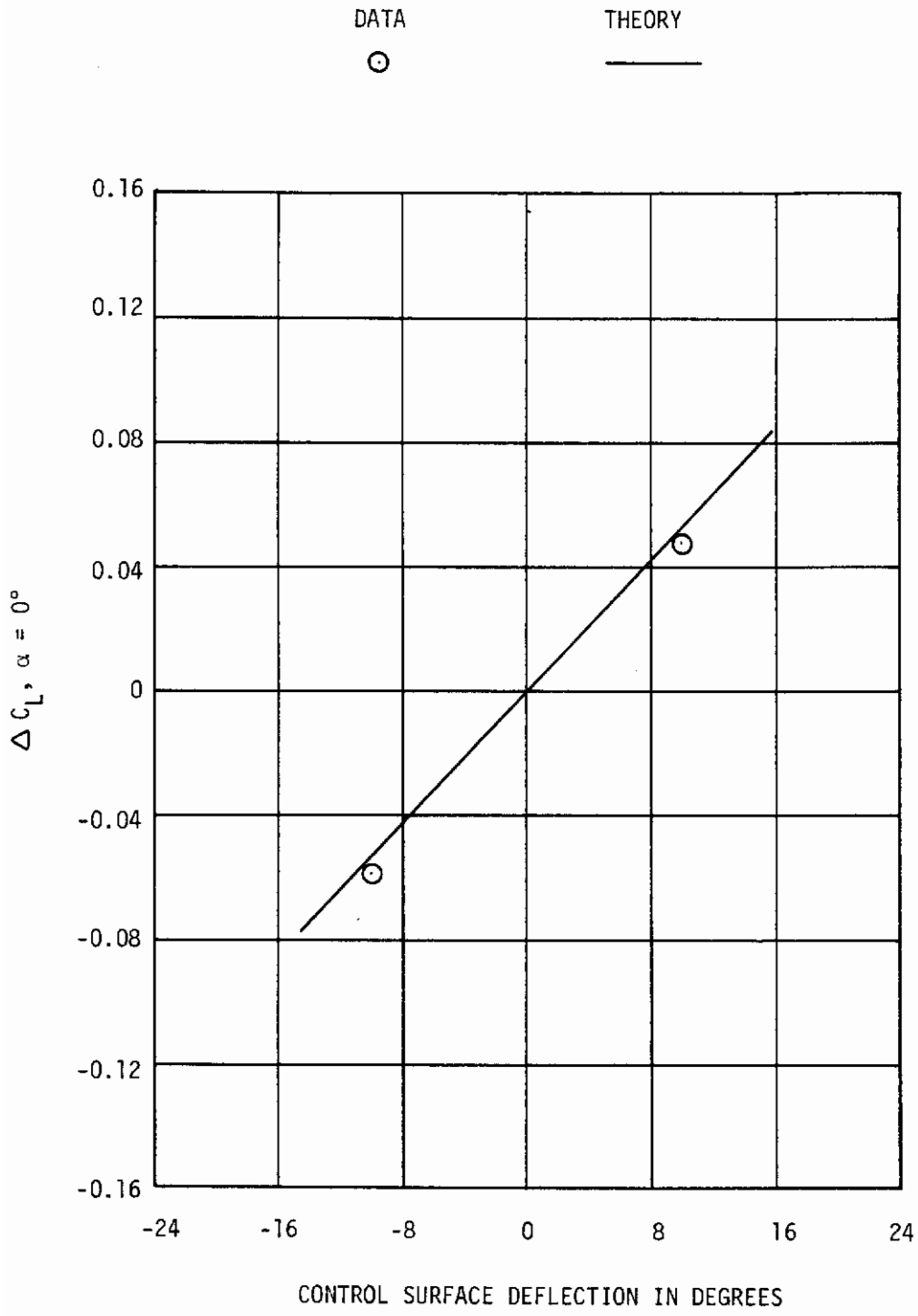


Figure 44. Comparison of Measured and Calculated Incremental Control Surface Effects on an Advanced Air Defense Blended-Body Model at M=0.2

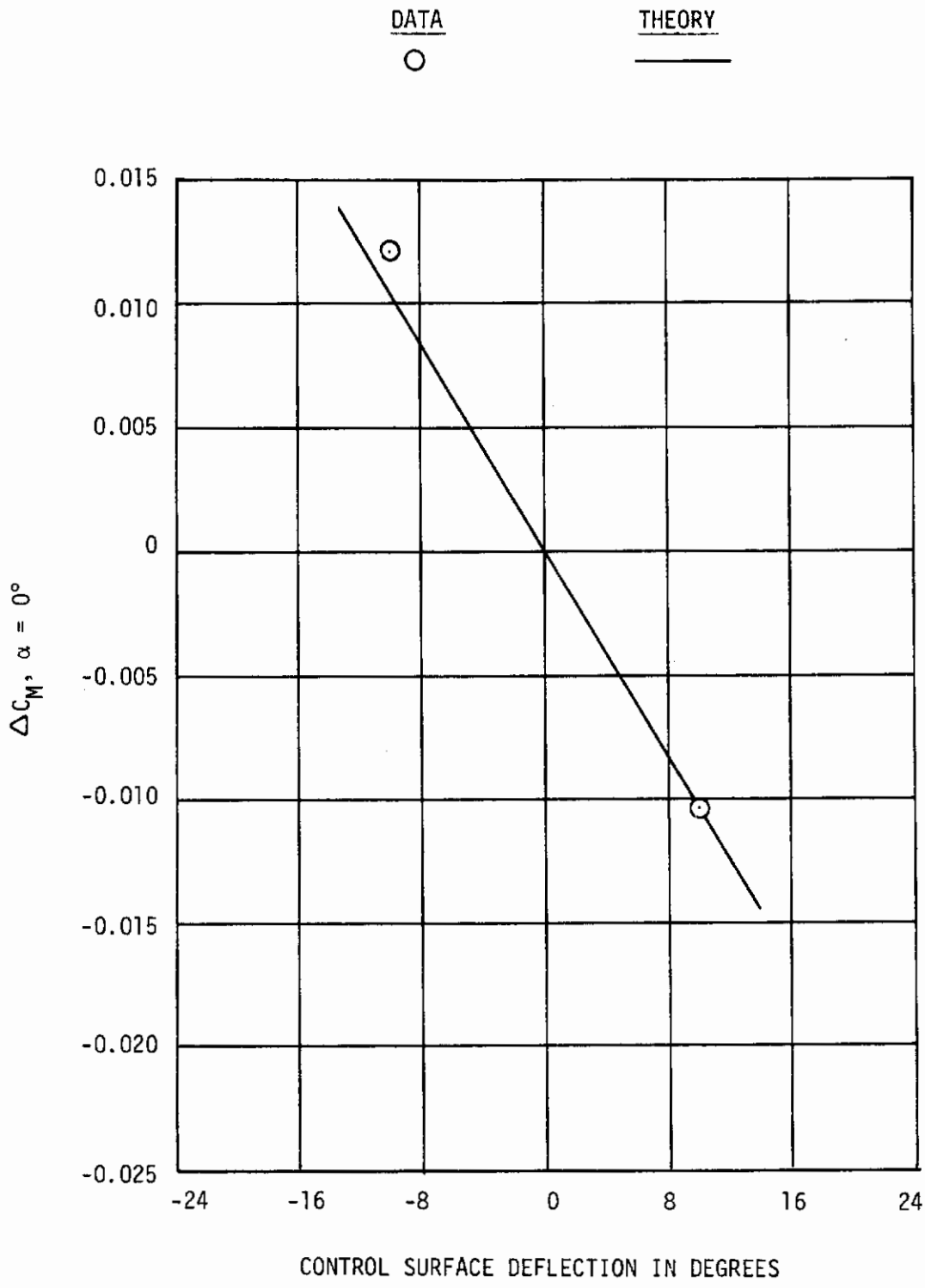


Figure 44. (Concluded)

TABLE I

CONTROL SURFACE IDENTIFICATION

| CONTROL SURFACE CONFIGURATION | OUTER FLAP SYSTEM | | | | INNER FLAP SYSTEM | | | |
|---|---|---|---|---|---|---|---|---|
| | Span % b | Chord % $C_R$ | Area % $S_R$ | Separation Distance % b | Span %b | Chord % $C_R$ | Area % $S_R$ | Separation Distance % b |
| S/100/5/0 | 100 | 5 | 10 | 0 | | | | |
| S/100/10/0 | 100 | 10 | 20 | 0 | | | | |
| S/100/15/0 | 100 | 15 | 30 | 0 | | | | |
| | | | | | | | | |
| S/75/10/0 | 75 | 10 | 15 | 0 | | | | |
| S/75/10/25 | 75 | 10 | 15 | 25 | | | | |
| | | | | | | | | |
| S/50/10/0 | 50 | 10 | 10 | 0 | | | | |
| S/50/10/25 | 50 | 10 | 10 | 25 | | | | |
| S/50/10/50 | 50 | 10 | 10 | 50 | | | | |
| | | | | | | | | |
| D/75/25/10 | 75 | 10 | 15 | 25 | 25 | 10 | 5 | 0 |
| D/50/50/10 | 50 | 10 | 10 | 50 | 50 | 10 | 10 | 0 |

## REFERENCES


1. Popinski, Z. and Ehrlich, C.F., Development Design Methods For Predicting Hypersonic Aerodynamic Control Characteristics, AFFDL-TR-66-85,September 1966.

2. Loptien, George W., Subsonic Wind Tunnel Investigation of Flat Plate Delta and Double Delta Wings, AFFDL FXS TM 71-19, September, 1971.

3. Pope, Alan, Wind Tunnel Testing, Second Edition, John Wiley & Sons, Inc., New York, October 1961.

4. Jones, Robert T., and Cohen, Doris, High Speed Wing Theory, Princeton Aeronautical Paperbacks (Number 6), Princeton University Press, Princeton, New Jersey, pp 96, 1960.

5. Stone, H.N., Aerodynamic Characteristics of Low-Aspect-Ratio Wings with Various Flaps at Subsonic Speeds, Cornell Aeronautical Lab., Report No. AF-743-A-2, January 1952.

6. Glauert, H., The Elements of Aerofoil and Airscrew Theory, Second ed., Cambridge Univ., Press, 1948.

7. Campbell, George S., A Finite-Step Method for the Calculation of Span Loadings of Unusual Plan Forms, NACA RM L50L13, 1951.

8. Margason, Richard J., and Lamar, John E., Vortex-Lattice Fortran Program For Estimating Subsonic Aerodynamic Characteristics of Complex Planforms, NASA TN D-6142, February 1971.

9. Transonic Wind Tunnel Tests On A .08 Scale Model of the FDL-8X Lifting Body, Cornell Aeronautical Laboratory, Report No. AA-4024-W-2, Jan-March 1971.

10. Bland, Verle V. Jr., Low Speed Force and Moment and Nacelle Pressure Tests on Two Advanced Manned Interceptor Models, AFFDL FXG TM 72-14, April 1972.




☆ U. S. GOVERNMENT PRINTING OFFICE: 1976 — 657-630/550